United States
Environmental Protection
Agency

Industrial Environmental Research
Laboratory
Research Triangle Park NC 27711

EPA-600/7-78-214
November 1978

EPA

Performance and Economic Evaluation of a Hot-side Electrostatic Precipitator

Interagency Energy/Environment R&D Program Report

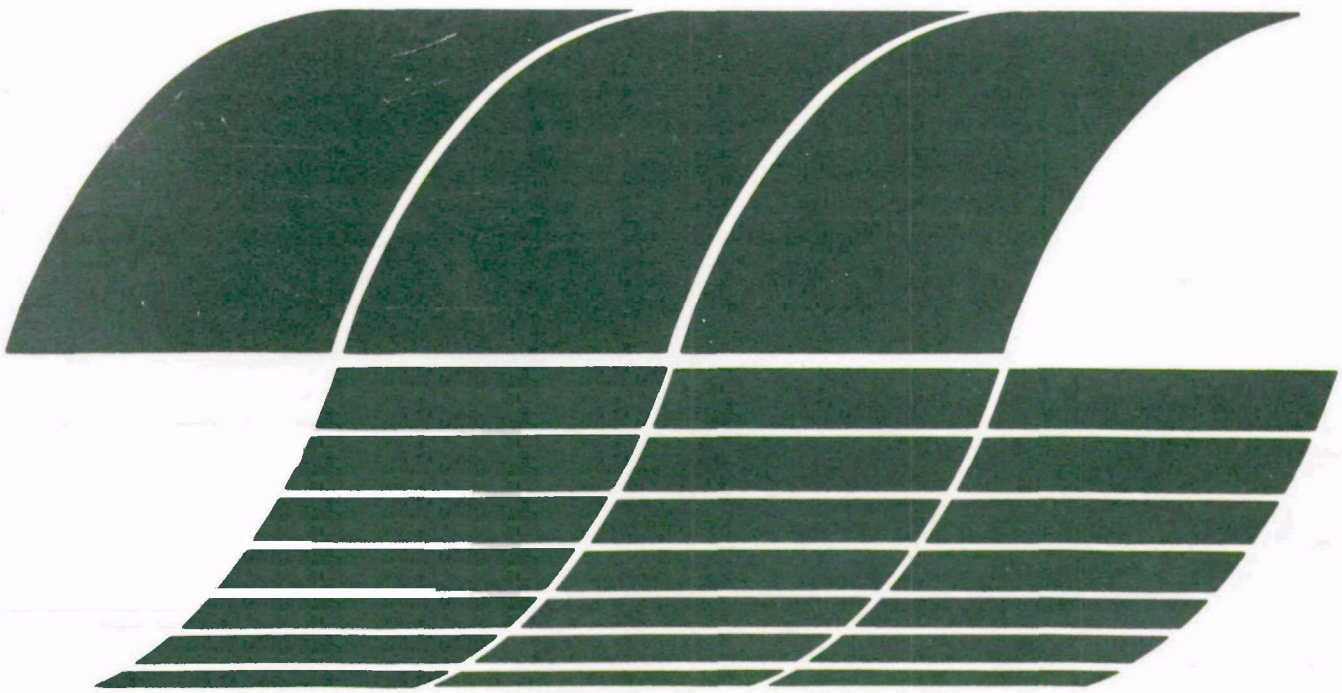

RESEARCH REPORTING SERIES

Research reports of the Office of Research and Development, U.S. Environmental Protection Agency, have been grouped into nine series. These nine broad categories were established to facilitate further development and application of environmental technology. Elimination of traditional grouping was consciously planned to foster technology transfer and a maximum interface in related fields. The nine series are:

1. Environmental Health Effects Research
2. Environmental Protection Technology
3. Ecological Research
4. Environmental Monitoring
5. Socioeconomic Environmental Studies
6. Scientific and Technical Assessment Reports (STAR)
7. Interagency Energy-Environment Research and Development
8. "Special" Reports
9. Miscellaneous Reports

This report has been assigned to the INTERAGENCY ENERGY-ENVIRONMENT RESEARCH AND DEVELOPMENT series. Reports in this series result from the effort funded under the 17-agency Federal Energy/Environment Research and Development Program. These studies relate to EPA's mission to protect the public health and welfare from adverse effects of pollutants associated with energy systems. The goal of the Program is to assure the rapid development of domestic energy supplies in an environmentally-compatible manner by providing the necessary environmental data and control technology. Investigations include analyses of the transport of energy-related pollutants and their health and ecological effects; assessments of, and development of, control technologies for energy systems; and integrated assessments of a wide range of energy-related environmental issues.

EPA REVIEW NOTICE

This report has been reviewed by the participating Federal Agencies, and approved for publication. Approval does not signify that the contents necessarily reflect the views and policies of the Government, nor does mention of trade names or commercial products constitute endorsement or recommendation for use.

This document is available to the public through the National Technical Information Service, Springfield, Virginia 22161.

EPA-600/7-78-214

November 1978

Performance and Economic Evaluation of a Hot-side Electrostatic Precipitator

by

G.H. Marchant Jr. and J.P. Gooch

Southern Research Institute
2000 Ninth Avenue, South
Birmingham, Alabama 35205

Contract No. 68-02-2185
Program Element No. EHE624

EPA Project Officer: Leslie E. Sparks

Industrial Environmental Research Laboratory
Office of Energy, Minerals, and Industry
Research Triangle Park, NC 27711

Prepared for

U.S. ENVIRONMENTAL PROTECTION AGENCY
Office of Research and Development
Washington, DC 20460

ABSTRACT

The report gives results of measurements--to determine the overall mass and fractional collection efficiency of a hot-side electrostatic precipitator (ESP)--across 1 chamber of a 16-chambered ESP. Measurements of fractional efficiency were conducted across the entire ESP. In situ and laboratory resistivity measurements were performed, and voltage-current characteristics of the power supplies were obtained. An engineering analysis was conducted, including an estimate of the specific collecting area required for a cold-side ESP on the same boiler. Results include: (1) voltage waveforms and secondary voltage-current relationships showed characteristics similar to back-corona although fly ash resistivity was 5 x 10 to the 9th power ohm-cm at 350°C (in situ determination); (2) ESP operation was sensitive to resistivity variation in a resistivity region (2 x 10 to the 10th power to 8 x 10 to the 8th power ohm-cm from laboratory determinations) where no sensitivity was expected; (3) overall mass collection efficiency of an isolated chamber was 99.22% for a specific collection area of 52.6 sq m/(cu m/sec), average secondary voltage was 22 kV, and average secondary current density was 40 nA/sq cm; and (4) the turnkey cost of the ESP system was estimated at $34,940,000 ($44/kW) in 1977 dollars.

CONTENTS

Abstract..... ii

Figures..... iv

Tables..... vii

Acknowledgments..... ix

Sections

1 Introduction..... 1

Objective..... 1

Scope of Work..... 1

2 Conclusions..... 2

3 Precipitator Evaluation..... 5

Hot-Side Precipitator Survey and Site Selection..... 5

Description of Facility..... 5

Test Program..... 14

Measurement Techniques..... 15

Test Results..... 20

Theoretical Analysis..... 76

4 Engineering Analysis..... 91

Capital and Operating Costs of Existing Unit... 91

Operating and Maintenance Problems..... 99

Description and Estimated Costs of an Improved Precipitator..... 103

References..... 107

Appendices

1 Description of Methods..... 110

2 Impactor Substrate Weight Changes for Blank Runs.... 147

3 Voltage-Current Data..... 150

4 Size-Dependent Elemental Concentration Data..... 180

FIGURES

Number		Page
1	Ductwork and precipitator arrangement for Navajo Station, Unit 3	10
2	Precipitator chamber arrangement	11
3	Rapper control arrangement	13
4a	Chronological display of impactor and ultrafine measurements	16
4b	Chronological display of mass train measurements	17
5	Differential size distributions, Chamber 8 inlet	28
6	Average inlet differential size distribution	29
7	Average inlet cumulative size distribution	30
8	Outlet differential size distribution	31
9	Fractional efficiency for Chamber 8 and total ESP	32
10	Average outlet cumulative size distribution, Total ESP	34
11	Relative concentration of particles with and without soot blowing, Chamber 8 Outlet	35
12	Relative concentration of particles with and without soot blowing, stack location	36
13	Relative concentration of 0.092 μm particles with and without soot blowing, Chamber 8 Inlet	37
14	Differential number size distributions, Chamber 8 Inlet	38
15	Differential number size distributions, outlet sampling locations	39
16	Resistivity vs temperature, 7/15-16/77	42
17	Resistivity vs temperature, 7/18-19/77	43

Figures
(Continued)

18 Resistivity vs temperature, 7/21-22/77..... 44

19 Resistivity vs temperature, 8/2-3/77..... 45

20 Resistivity vs temperature, Utah Coal..... 46

21 Voltage-current curves for chambers 7 and 8, July 12-13, 1977..... 63

22 dM/dlogD vs particle diameter for all impactors operated at the main inlet of the #3 precipitator and cyclone run #7..... 65

23 dM/dlogD vs particle diameter for all impactors operated at the inlet of chamber #8 and cyclone run #3..... 66

24 dM/dlogD vs particle diameter for all impactors operated at the outlet of chamber #8 and cyclone run #5..... 67

25 Apparent elemental collection efficiency (chamber 8) 72

26 Particles/minute vs time for 6-12 μm particles, February 1, 1977..... 74

27 Ultrafine and impactor fractional efficiencies for rap-no rap test..... 75

28 Theoretical voltage current relationships for wire diameter of 0.268 cm (0.1055 in), wire to plate spacing of 11.45 cm (4.5 in), and wire to wire spacing of 22.9 cm..... 78

29 Comparison of theoretical (b_e = 15 cm^2/volt-sec) and experimental (C field, ch. 7 & 8, July 15, 1977) voltage-current curve..... 80

30 Theoretical and experimental voltage-current relationships for various wire diameters..... 82

31 Voltage waveforms for C field, ch. 7 & 8..... 83

32 Voltage-current relationship for C fields, ch. 7 & 8 and ch. 5 & 6..... 84

33 Outlet field voltage-current curves for ch. 7 & 8 (Navajo) and another hot-side precipitator installation..... 86

Figures
(Continued)

34 Measurements and model projections of collection efficiency for hot-side operating parameters..... 87

35 Model projection for cold-side operating parameters..... 90

TABLES

Number		Page
1	Partial list of hot-side electrostatic precipitator installations	5
2	Predicted performance of units 1, 2, and 3 of the Navajo Generating Station	9
3	Mass concentrations obtained during Phase I with mass trains and impactors	21
4	Average inlet and outlet parameters, chamber 8	22
5	Statistical analysis of effect of soot blowing on mass emissions	22
6	Comparison of inlet mass train and impactor loadings.	24
7	Phase II, main inlet and stack impactor mass loadings	24
8	Phase II, main inlet and stack parameters	26
9	Average blank corrections for impactor components	26
10	In situ resistivity data	41
11	Chemical analysis of Utah coal ash used for Figure 20	48
12	Coal analyses, Phase I	49
13	Coal analyses, Phase II	50
14	Ash analyses, Phase I and Phase II	51
15	Phase I gas analyses	53
16	Phase II gas analyses	55
17	Average electrical operating parameters, chambers 7 and 8, Phase I	59
18	Voltage-current curve data, chambers 7 and 8	61
19	Cyclone assembly operating parameters	64
20	Mass concentration and efficiency from cyclone assembly (Phase I)	69

Tables
(Continued)

21	Concentration of elements listed in parts per million by weight	70
22	Elemental penetration across chamber #8	71
23	Unit #3 precipitator cost	92
24	Operating and maintenance costs for Unit #3, ash handling system	93
25	Operating and maintenance costs for Unit #3, normal maintenance, repair, and operations	95
26	Operating and maintenance costs for Unit #3 ESP, charges for testing, adjusting and/or modifications.	96
27	Estimated power cost of precipitator	97
28	Summary of operating costs	98
29	ESP chamber availability	102
30	Recommended design parameters for improved performance	105

ACKNOWLEDGMENTS

The assistance of Dr. Leslie E. Sparks, Project Officer, Environmental Protection Agency, is greatly appreciated. The assistance and cooperation of Salt River Project personnel during the test program and in compiling the required information for the engineering analysis are also gratefully acknowledged. The cooperation of the Electric Power Research Institute is also greatly appreciated.

SECTION 1

INTRODUCTION

OBJECTIVE

This report describes the methods employed for and the results obtained from an evaluation of the performance and economics of a hot-side electrostatic precipitator installed on a 750 MW coal-fired utility boiler firing low-sulfur Western coal.

SCOPE OF WORK

The major tasks performed in accomplishing this evaluation were as follows:

- A limited survey of utilities using hot-side electrostatic precipitators, followed by the selection of a site for the evaluation program. The Navajo Generating Station of the Salt River Project in Page, Arizona, was selected.

- The preparation of a detailed test plan which described a field test designed to determine the performance of the precipitator.

- The performance of a two-phase test program which included characterization of the performance of an individual chamber of the dust collector (Phase I) and the performance of the entire precipitator (Phase II). The data obtained included overall mass collection efficiency, efficiency as a function of particle diameter, flue gas flow rates and composition, coal and fly ash compositions, precipitator electrical operating parameters, and dust resistivity. A separate and earlier test program, sponsored by EPRI and the Salt River Project, was conducted to determine the collection efficiency losses due to electrode rapping. Results from this program are included for completeness.

- An engineering analysis of the electrostatic precipitator system. This portion of the program was conducted with the assistance of Salt River Project and Bechtel Corporation personnel. The analysis included a projected design for a cold-side precipitator installed on the same boiler. The SoRI electrostatic precipitator mathematical model was used in the analysis.

SECTION 2

CONCLUSIONS

The following conclusions have been obtained from this study:

(1) The overall mass collection efficiency of an isolated chamber (Chamber 8) of the electrostatic precipitator system was 99.22%. A minimum value of 92% was determined at 0.50 μm particle diameter in the efficiency as a function of particle diameter relationship. These results were obtained with an average secondary voltage of 22 kV, an average secondary current density of 40 nA/cm^2, a specific collection area of 52.6 $m^2/(m^3/sec)$, and a dust resistivity (*in situ* determination) of approximately $5x10^9$ ohm-cm at 350°C.

(2) The apparent collection efficiency of the entire precipitator, based on a limited Brink impactor traverse of the main inlet and an Andersen impactor traverse of the stack sampling location, was 98.56%. The stack location measurements indicated a total particulate mass emission rate of 30.8 ng/J (0.0716 $lb/10^6$ Btu) of which 9.03 ng/J (0.021 $lb/10^6$ Btu) consisted of particles with diameters less than 2.0 μm.

(3) Measured values of dust resistivity at 350°C (both *in situ* and laboratory) are in reasonable agreement with those obtained from predictions based on ash composition.

(4) Voltage waveforms and secondary voltage-current relationships obtained during the test period exhibited certain characteristics similar to back corona from highly resistive dust layers at 150°C. However, overall and fractional efficiency data from the test measurements are significantly larger than those obtained from a theoretical model when the observed operating parameters are used as input data. Thus, if a bipolar charging environment from back corona does exist, the deleterious effects are partially compensated for by a phenomena not represented in the model. It is hypothesized that a significant portion of the corona current is carried by free electrons, which results in higher values of charge on the particles than those predicted by the present charging model based on ionic values of charge carrier mobility.

(5) Attainable values of secondary voltage are significantly lower than those observed with hot-side precipitators collecting ash from Eastern coals at approximately the same temperature. The low voltages are hypothesized to result from a combination of high effective mobilities for the charge carrying species of the gas stream and an electrical discharge process which occurs in the deposited dust layer and which persists at voltages below the normal corona onset voltage. The operating voltages and the V-I relationships were found to be strongly dependent upon electrode cleanliness, even though the measured values of dust resistivity were relatively low.

(6) The sensitivity of hot-side precipitator operation to resistivity variation in a resistivity region (2×10^{10} to 8×10^{8} ohm-cm) where no sensitivity was expected was observed when load dropped from 800 to 400 MW and the precipitator operating temperature dropped from 360°C to 233°C. The TR set panel meters indicated heavy sparking, and collection efficiency decreased even though the specific collection area was approximately doubled. The drop in collection efficiency could undoubtedly have been avoided if the TR set controllers had maintained the operating points at low sparking rates. The test results are important, however, in that they indicate the factors which must be considered if a hot-side precipitator is to be used in a variable temperature operation. (These results were obtained prior to the EPA-sponsored test series.)

(7) The two principal causes of the lower than desired performance of the unit are the relatively low operating voltages and the relatively low values of specific collecting area. The recommended value of specific collecting area to achieve the design collection efficiency of 99.5% is 93.9 $m^2/(m^3/sec)$, based on the results during the test period. An alternative approach to the large increase in plate area, which could not be quantified by the measurements performed during this test series, is to determine the relationship between dust deposits, voltage-current curves, and collection efficiency. Pilot-scale experiments at the plant site are recommended to determine if it is practical to consistently achieve the "clean plate" values of performance which have been observed.

(8) The turnkey cost of the electrostatic precipitator system, including the ash handling system, duct work, and auxiliaries was estimated as $34,940,000, or $44/kW in 1977 dollars.

(9) The annual operating costs for the electrostatic precipitator system from June 1976 to June 1977 were $1,271,000, or 0.23 mills/kWh. If the amortized capital costs are included (from 8 above), the operating costs are 1.16 mills/kWh, based on 7000 hr/year.

(10) Although the precipitator has not operated reliably with respect to design efficiency, it has been reliable from a mechanical standpoint. The most significant maintenance problems were air infiltration and ash buildup in hoppers.

(11) The estimated cost of an improved precipitator system, based on the plate area requirements indicated by performance during the test period, is $60,440,000, or $75.5/kW (1977 dollars). The estimated costs of cold-side designs for 99.5% minimum collection efficiency were 52.4 and 65.1 $/kW, based on fly ash resistivities of 9×10^{10} and 7×10^{11} ohm-cm, respectively.

SECTION 3

PRECIPITATOR EVALUATION

HOT-SIDE PRECIPITATOR SURVEY AND SITE SELECTION

Table 1 gives the results obtained from a limited survey of utilities concerning the usage of hot-side precipitators for collecting ash from low-sulfur coals. The Navajo Generating Station is the largest existing hot-side precipitator installation and collects ash from a representative low sulfur, but not necessarily low sodium, Western coal. The Navajo Station has also experienced precipitator operating problems which are generally typical of those encountered at other similar installations. It was selected as the test site for the following reasons:

1. The management of the Project agreed to participate in the evaluation program and to provide valuable assistance in the performance of the field test and the engineering analysis.

2. The management of the Project maintains an active task force for the purpose of studying and solving the problems associated with the hot-side precipitator. Therefore, the site offered the potential of providing useful information concerning practical operating problems associated with hot-side precipitator systems.

3. The existing sampling ports offered considerable flexibility for the test program.

4. The design parameters of the precipitator system were representative of the "state of the art" for hot-side precipitators.

5. Southern Research Institute had performed additional tests under EPRI and Salt River Project sponsorship which would be useful in conducting the evaluation.

DESCRIPTION OF FACILITY

The Navajo Generating Station is located approximately four miles east of Page, Arizona, on the Navajo Indian Reservation at an elevation of 1330.45 m (4365 ft) and consists of three 750 MW generating units. The test program was conducted on the precipitator installed on Unit Three.

TABLE 1

SURVEY OF UTILITIES OPERATING HOT-SIDE ELECTROSTATIC PRECIPITATORS AND BURNING LOW-SULFUR WESTERN COALS

MW's	Volume Flow KACFM	Volume Flow Am^3/min	Design Temperature °F	Design Temperature °C	SCA $ft^2/KACFM$	SCA $m^2/(m^3/sec)$	Efficiency %	Test Efficiency %	Operating and/or Maintenance Problems
Public Service Co. of Colorado - Comanche # 1 - Research-Cottrell									
350	2514	1187	828	442	296	58.3	99.59		Low secondary voltages and currents; expansion problems
Public Service Co. of Colorado - Comanche # 2 - Research-Cottrell									
350	2644	1248	690	366	307	60.4	99.5		Low secondary voltages and currents
Wisconsin Power and Light Co., Columbia #1 - Research-Cottrell									
520	2770	1307	810	432	269	53	99.5	91	Bearing side plate failure; ash buildup on plates
Iowa Public Service Co. - George Neal #1 - Research-Cottrell									
138	691	326	680	360	220	43.3	99.0	91	Wire failure
Southwestern Electric Power Co. - Cason #1 - Research-Cottrell									
528	3025	714	750	399	323	65.6	99.6		
City of Cedar Falls, Iowa - Streeter - Research-Cottrell									
40	248	117	802	427	267	52.6	99.6		Wire failure
Salt River Project - Navajo #1 - Joy-Western									
750	3940	1860	662	350	307	60.4	99.5		High ash levels in hoppers; expansion problems; velocity distribution; low secondary voltages and currents
Salt River Project - Navajo #2 - Joy-Western									
750	3940	1860	662	350	307	60.4	99.5		
Salt River Project - Navajo #3 - Joy-Western									
750	3940	1860	662	350	307	60.4	99.5		
Public Service Co. of New Mexico - San Juan #1 - Joy-Western									
330	2800	1322	700	371	398	78.3	99.5		
Public Service Co. of New Mexico - San Juan #2 - Joy-Western									
330	2800	1322	700	371	398	78.3	99.5		
Iowa Power and Light Co. - Des Moines #10 - UOP									
71	410	194	645	341	246	48.4	99.3	99.3	Swinging plates; wire failure; rapper control failure; high voltage insulator failure
Iowa Power and Light Co. - Des Moines #11 - UOP									
116	620	293	635	335	244	48.0	99.3	99.5	
Iowa Power and Light Co. - Council Bluffs #1 - UOP									
47	284	134	692	367	355	69.9	99.3	98.0	
Iowa Power and Light Co. - Council Bluffs #2 - UOP									
90	421	199	624	329	331	65.2	99.3	98.3	
Colorado UTE Electric Assn. Inc. - Hayden #1 - Buell									
168	1155	545	775	413	360	70.9	99.6	99.19	Ash handling; low secondary voltages and currents
San Antonio Public Service Bd. - J.T. Deely #3 - Buell									
430	1362	643	850	454	313	61.6	99.4		Wire failure; structure failure
Salt River Project - Hayden #2 - Wheelabrator-Frye									
250	1684	795	695	368	335	65.9	99.6	99	Low secondary voltages and currents
Omaha Public Power District - Wright #8 - Belco									
90	510	241	707	378	320	63	99.6	99	
Nebraska Public Power District - Sheldon #1 - Belco									
105	541	255	680	360	252	49.6	97.9		
Nebraska Public Power District - Sheldon #2 - Belco									
120	670	316	710	377	261	51.4	97.9		
Colorado Springs Dept. of Pub. Utilities - Martin Drake #7 - American Standard									
137	850	401	710	377	292	57.5	99.35	99.2	Wire failure

(continued)

TABLE 1 (continued)

UTILITIES WHICH BURN LOW-SULFUR COAL AND HAVE HOT-SIDE ELECTROSTATIC PRECIPITATORS UNDER CONSTRUCTION

MW's	Volume Flow KACFM	Volume Flow Am^3/min	Design Temperature °F	Design Temperature °C	$ft^2/KACFM$	$m^2/(m^3/sec)$	Efficiency %	Test Efficiency %	
Houston Lighting and Power Co. - W.A. Parish #5 - Joy-Western									
660	3357	1585	719	382			99.89	solved problems – changed operating procedures	Under construction
Houston Lighting and Power Co. - W.A. Parish #6 - Joy-Western									
660	3357	1585	719	382			99.89		Under construction
Upper Peninsula Power Co. - Presque Isle #7 - Joy-Western									
80	530	250	730	388	159	31.3	99.2		Under construction
Upper Peninsula Power Co. - Presque Isle #8 - Joy-Western									
80	530	250	730	388	159	31.3	99.2		Under construction
Upper Peninsula Power Co. - Presque Isle #9 - Joy-Western									
80	530	250	730	388	159	31.3	99.2		Under construction
Gulf States Utilities Co. - Roy S. Nelson #5 - Joy-Western									
540	3090	1458	800	427			99.5		Under construction
Salt River Project - Coronado #1 - Joy-Western									
350	2800	1322	760	404	307	60.4	99.875		Under construction
Salt River Project - Coronado #2 - Joy-Western									
350	2800	1322	760	404	307	60.4	99.875		Under construction
Central Power and Light Co. - Coletocreek #1 - Joy-Western									
550	3738	1764	677	358			99.6		Under construction
Iowa Public Service Co. - George Neal #4 - UOP									
575	4200	1982	780	416	420	82.7			Under construction
Omaha Public Power District - Nebraska City Station - Wheelabrator-Frye								in operation	
575	3540	1671	755	402	∿350	68.9	99.3		Under construction
Northern Indiana Public Service Co. - Schahfer #14 - PCW									
487	2474	1168	660	349	326	64.2	99.6		Under construction
Arkansas Power & Light Co. - White Bluff St. #1 - PCW									
800	5141	2427	815	435	370	72.8	99.5		Under construction
Arkansas Power & Light Co. - White Bluff St. #2 - PCW									
800	5141	2427	815	435	370	72.8	99.5		Under construction
Arkansas Power & Light Co. - White Bluff St. #2 - PCW									
800	5141	2427	815	435	370	72.8	99.5		Under construction
Arkansas Power & Light Co. - White Bluff St. #2 - PCW									
800	5141	2427	815	435	370	72.8	99.5		Under construction

Unit Description

Units 1, 2, and 3 at the Navajo Generating Station are C-E supercritical, combined circulation, radiant, reheat steam generators with a center water wall dividing the furnace into two halves. The units are designed to deliver superheated steam at a rate of 40822.5 Kg/min (5,400,000 pounds per hour) (maximum continuous) at 576.1°C (1005°F) and 252.4 kg/cm^2 (3590 psig) (superheat outlet) to a 750 MW turbogenerator. The reheater is designed to handle 36664.7 kg/min (4,850,000 pounds per hour), reheated from 306.1°C (583°F) to 538.9°C (1002°F).

The unit, which is a divided furnace design, has each furnace half fired through four tilting tangential windbox assemblies. The main fuel (coal) can be admitted to the furnace through seven elevations of pulverized coal nozzles. Six elevations of Oil Eddy Plate ignitors and one elevation of retractable warm-up oil guns are provided for lighting off and warming up the unit and for ignition of the pulverized coal admitted through adjacent nozzles. Table 2 provides predicted performance data for the boiler system.

Precipitator Description

The electrostatic precipitators installed on units 1, 2, and 3 at the Navajo Generating Station were designed by the Western Precipitation Division of Joy Manufacturing Company. Each precipitator consists of two levels (Figure 1) with eight chambers per level (Figure 2). The total unit was designed to operate with a volume flow rate of 1859.68 m^3/sec (3,940,000 acfm) at 350°C (662°F) with 99.5 percent collection efficiency.

Each of the sixteen isolatable chambers consists of six electrical fields in the direction of gas flow and thirty-five gas passages spaced 22.86 cm (9 in) apart. The collection electrodes in each of the six fields are 1.8288 m (6 feet) in depth and 9.144 m (30 feet) high. The discharge electrodes have a diameter of 2.68 mm (0.1055 inches) and the average spacing between each wire per field is 22.86 cm (9 inches) [8 wires per gas passage per 1.83 m (6 ft) field]. Each precipitator is powered by 48 transformer rectifiers, and each transformer rectifier powers parallel fields in parallel chambers (Figure 2). Each precipitator has a total collecting area of 112371.84 m^2 (1,209,600 ft^2) which results in a design specific collection area (SCA) of 60.43 m^2/(m^3/sec) (307 ft^2/1000 acfm).

Transformer-Rectifiers--

The high voltage direct current power for the precipitator discharge electrodes is provided by General Electric Full Wave Transformer Rectifier Sets. These sets are located on the roof of each precipitator and are connected to the high voltage discharge electrodes through a ventilated, ducted system of high voltage lines.

TABLE 2

PREDICTED PERFORMANCE OF UNITS 1, 2, and 3 OF THE NAVAJO GENERATING STATION, PREPARED BY COMBUSTION ENGINEERING, INC.

Predicted Performance*		Control Load	M.C.R.	M.C.C.
Fuel		Pulverized Coal		
Evaporation	lb/hr	2,700,000	5,400,000	5,535,000
	Kg/hr	1,224,693	2,449,386	2,510,621
Feedwater Temperature	°F	440	507	508
	°C	227	264	264
Superheater Outlet Temperature	°F	1005	1005	1005
	°C	541	541	541
Superheater Outlet Pressure	psig	3525	3590	3600
	Kg/cm^2	248	252	253
Superheater Pressure Drop	psi	53	207	217
	Kg/cm^2	3.73	14.55	15.26
Reheater Flow	lb/hr	2,490,000	4,850,000	4,972,000
	Kg/hr	1,129,439	2,199,912	2,255,249
Reheater Inlet Temperature	°F	495	583	587
	°C	257	306	308
Reheater Inlet Pressure	psig	345	676	684
	Kg/cm^2	24	48	48
Reheater Outlet Temperature	°F	1002	1002	1002
	°C	539	539	539
Reheater Pressure Drop	psi	15	30	31
	Kg/cm^2	1.05	2.11	2.18
Economizer Pressure Drop	psi	25	39	40
	Kg/cm^2	1.05	2.74	2.81
Gas Drop, Furnace to Econ. Outlet	"wg	2.90	7.45	7.67
	mmHg	5.42	13.92	14.33
Gas Drop, Econ. Outlet to A.H. Outlet	"wg	2.95	7.55	7.78
	mmHg	5.51	14.10	14.53
Gas Temp., Entering Air Heater	°F	560	658	662
	°C	293	348	350
Gas Temp., Leaving Air Heater, Uncorr.	°F	211	260	261
	°C	99	127	127
Gas Temp., Leaving Air Heater, Corr.	°F	201	250	251
	°C	94	121	122
Air Temp., Entering Air Heater	°F	70	70	70
	°C	21	21	21
Air Temp., Leaving Air Heater	°F	508/522	582/609	584/610
	°C	264/272	306/321	307/321
Air Press. Entering Air Heater	"wg	5.80	10.90	11.15
	mmHg	10.84	20.36	20.83
Ambient Air Temperature	°F	70	70	70
	°C	21	21	21
Excess Air Leaving Economizer	%	30	18	18
Fuel Fired	lb/hr	355,000	652,000	667,000
	Kg/hr	161,024	295,741	302,545
Efficiency	%	89.52	88.77	88.75

*Notes: These performance figures are predicted only and are not to be construed as being guaranteed except where the points coincide with the guarantees.

Operation of this unit in excess of the above specified maximum continuous capacity (M.C.C.) may result in damage to the equipment and/or increased maintenance.

Superheat steam temperature control range is from 1,224,693 to 2,449,386 Kg/hr (2,700,000 to 5,400,000 lb/hr)
Reheat steam temperature control range is from 1,129,439 to 2,199,912 Kg/hr (2,490,000 to 4,850,000 lb/hr)

Control Load - half load control point

M.C.R. - Maximum Continuous Rating

The fuel specifications on which the guarantees are based are as follows:

Black Mesa Sub-Bituminous Coal H.H.V. 5958.3 Cal/g (10,725 BTU/lb)

C	61.29%
H	4.37
O	12.13
N	1.00
S	0.50
Ash	10.43
Moist.	10.27
Cl	0.01
Total	100.00%

Fixed Carbon	41.36%
Volatile	37.94
Moisture	10.27
Ash	10.43
Total	100.00%

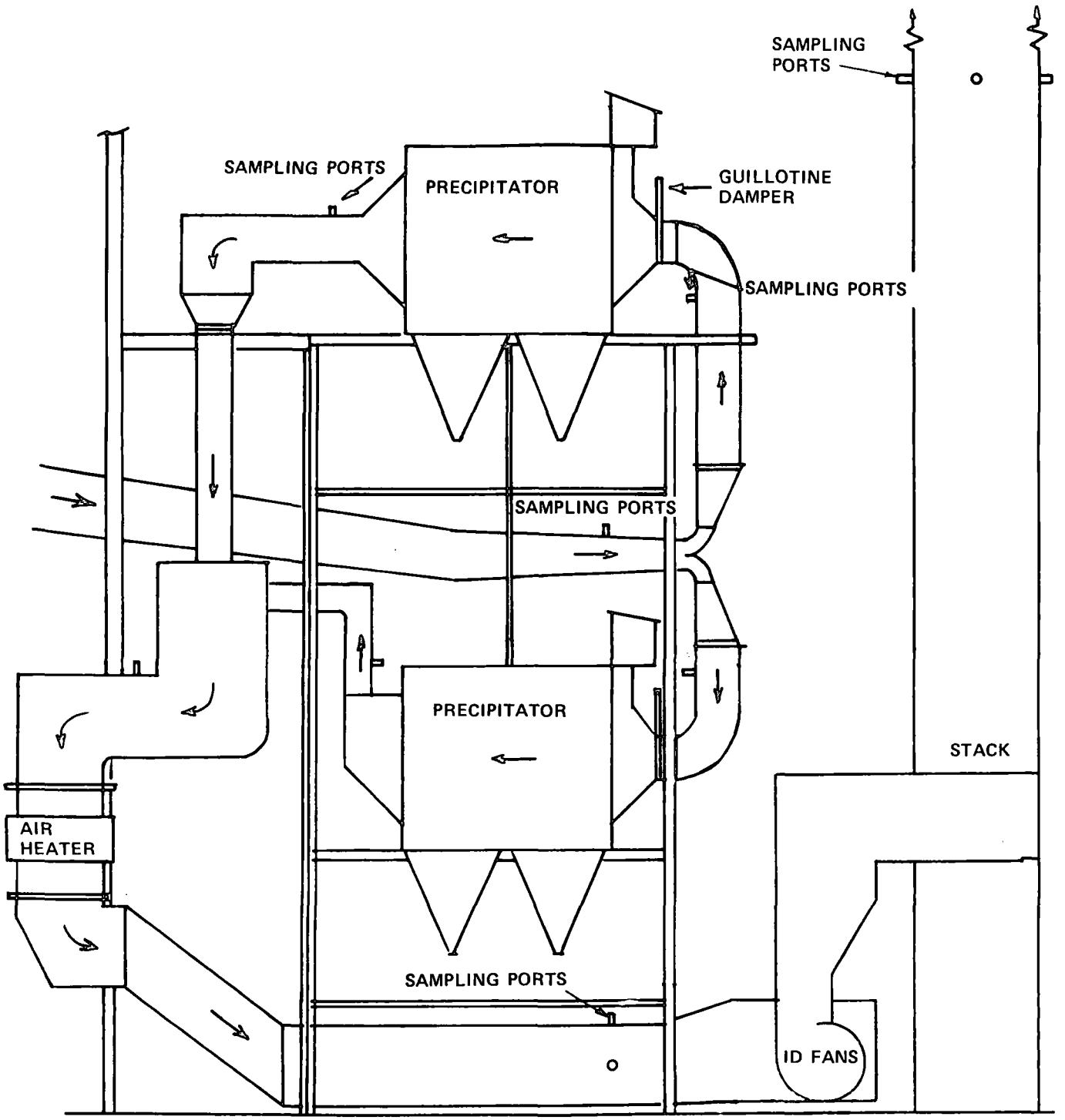

Figure 1. Ductwork and precipitator arrangement for Navajo Station, Unit 3.

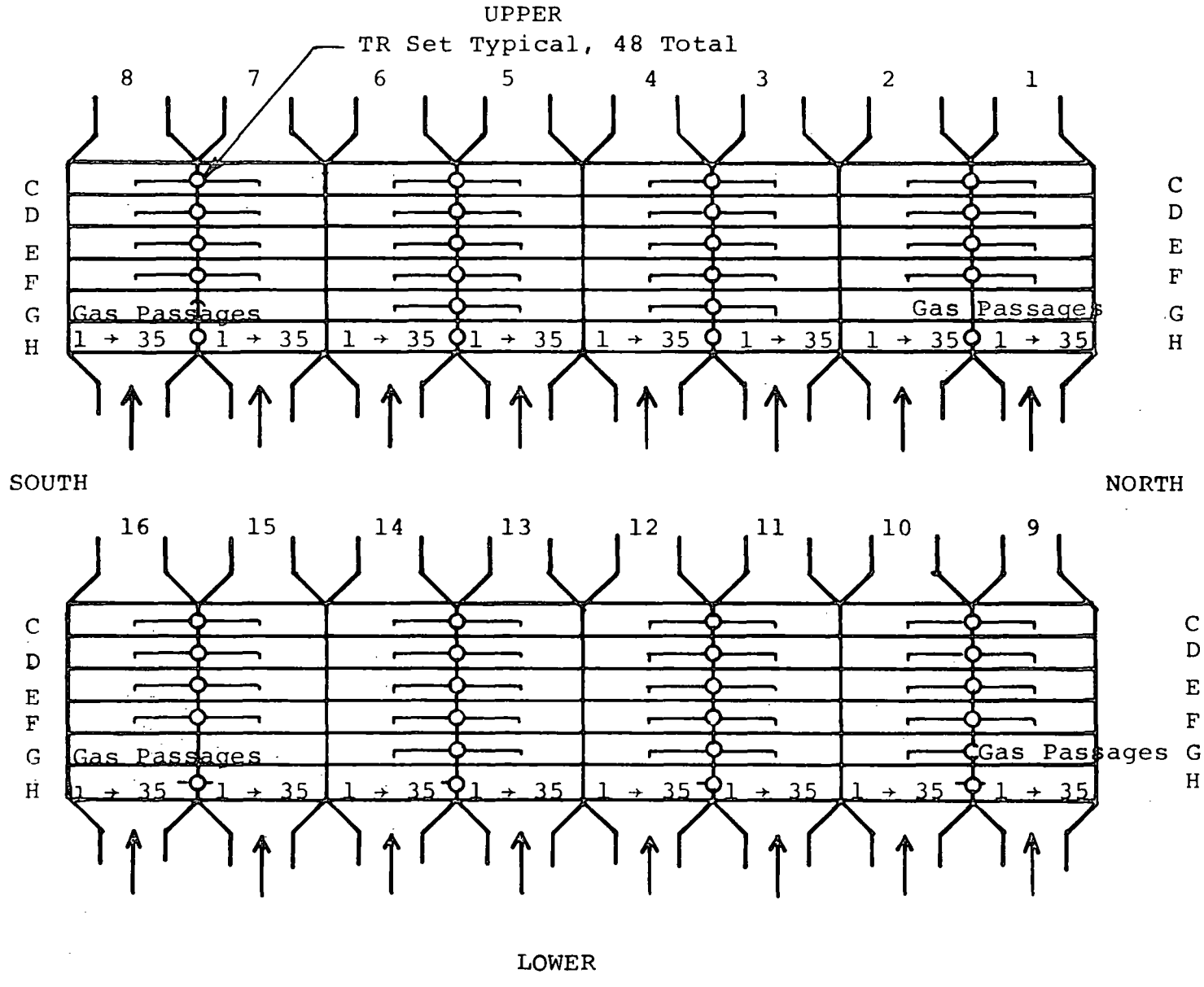

Figure 2. Precipitator chamber arrangement.

The transformer rectifier unit consists essentially of a high-voltage transformer core and coil, silicon rectifier and a high-voltage switch all contained in a common oil filled tank. The primary (low-voltage) winding of the transformer consists of a single coil. The secondary (high-voltage) winding of the transformer consists of a single coil in a continuous layer-wound arrangement. The function of the transformer is to step up the AC supply voltage to the desired value before rectifying it by means of the silicon rectifier unit. The silicon rectifier unit is a full-wave bridge circuit with its output connected to the high voltage bushings.

There are a total of 48 transformer rectifier sets (24 on the upper precipitator and 24 on the lower precipitator), each of which, as stated previously, powers parallel fields in parallel chambers. The transformer rectifiers which power fields "H" and "G" are rated at 45 kV and 1000 ma with a reactor rating of 75 kVA. The transformer rectifiers which power fields "F" and "E" are rated at 45 kV and 1200 ma with a reactor rating of 87.5 kVA. The transformer rectifiers which power fields "D" and "C" are rated at 45 kV and 1600 ma with a reactor rating of 112.5 kVA.

Rapping System--

The rappers which are used to remove the collected particulate from the collecting and discharge electrodes, are electromagnets which are operated by pulsating direct current. The rappers are operated automatically by a matrix type rapper control system which is capable of varying the "ON" and "OFF" time between the operation of each rapper and the intensity of each rapping pulse.

Figure 3 represents the rapping control program boards for a typical chamber of the precipitator as originally installed. The original rapper program had approximately five minute relays which controlled all the wire and plate rappers in two adjoining fields of one chamber. The first row of the program board controlled all the rappers on fields H and G, the second row controlled the rappers in fields F and E, and the third row controlled the rappers in fields D and C.

The rapping program steps through each relay until it reaches the end of the second program board or a homing pin and then returns to the first relay in the first programming board. The total time for each cycle of the original rapping program was 100 minutes; and during that 100 minutes the first two fields were rapped nine times, the third and fourth fields five times, and the last two fields four times. Prior to Phase I of the test program, the Salt River Project changed the rapping control program boards to separate the wire and plate rappers so all rappers in one field would not operate sequentially.

ORIGINAL RAPPER SETTING CHAMBERS 7 & 8

FIELDS	PROGRAM CARD NO. 1										PROGRAM CARD NO. 2									
H&G		5:00		5:00		5:00		5:00		5:00		5:00		5:00		5:03		5:00		
F&E	5:00				5:00				5:00				5:00				5:00			
D&C			5:00				5:00				5:00				5:07					
																			0	0

HOMING PINS

MODIFIED RAPPER SETTING, UPPER PRECIPITATOR

CHAMBERS	FIELDS C&D																			
1&5	7:40				6:40				7:45				7:00							
2&6		6:45				9:45				7:46				7:40						
3&7			6:35				6:45				7:50				8:40					
4&8				8:45				8:45				7:30				7:50				
																	0	0	0	0

CHAMBERS	FIELDS E&F																			
1&5	2:30				3:05				3:20				3:20							
2&6		3:15				3:40				3:20				3:20						
3&7			3:15				3:20				6:50				3:30					
4&8				3:30				3:20								4:10				
																	0	0	0	0

CHAMBERS	FIELDS G&H																			
1&5	2:50				2:50				2:45				2:40							
2&6		2:50				2:50				2:50				2:50						
3&7			2:50				2:55				2:30				3:10					
4&8				2:50				2:50				3:00				2:40				
																	0	0	0	0

FIELDS	WIRES																			
G&H	3:20			3:30			3:35			3:35			3:35							
E&F		3:30			3:30			3:35			3:25			3:25						
C&D			3:40			3:30			3:30			3:30			3:40					
																2:00				
																	0	0	0	0

NOTE

TIMES FOR RELAYS ARE APPROXIMATE

Figure 3. Rapper control settings (times in minutes)

Figure 3 presents the rapping program cards and the changed rapping program for the upper half of the precipitator. Although this change separated the wire and plate rappers from one relay of a control card, it is possible for all rappers of one chamber (wires and plates) to be activated during the time span of one relay since each rapper control program operated independently of the others.

Ash Handling System--

After collection in the precipitator hoppers, the fly ash passes through pressurized type Nuva feeders into a pressurized pipe and is transported under pressure to the fly ash storage bin. The storage bin is equipped with a fabric filter dust collector on the low pressure or vented side of the bin. From the storage bin the ash is conveyed to the fly ash loading area where it is loaded into trucks for transport to the ash fill area. As the ash is loaded into the ash trucks a water spray is used to minimize the loss of ash during loading and transport to the fill area.

The precipitator ash conveying system is a nearly continuous operation. The control system for the Nuva feeders steps through its program from one feeder to another whenever the pressure drop across a Nuva feeder reaches a predetermined minimum.

TEST PROGRAM

The test program for the Unit 3 precipitator was designed to evaluate the precipitator as a whole and one of the sixteen isolatible chambers. The test program was conducted during July and August of 1977, and all testing was performed at night due to the extreme temperatures at the sampling locations during daylight hours.

Phase I

Phase I of the test program was conducted from July 10 through July 23, 1977, and consisted of an evaluation of Chamber No. 8. Particle size measurements were obtained with impactors at the inlet and outlet sampling locations for fractional efficiency determinations, and total mass loadings were obtained with mass trains to enable calculation of overall mass efficiency. Gas composition data, including SO_2 and SO_3 analyses, were obtained at the outlet of Chamber No. 8. Ultrafine particle size data with an Electrical Aerosol Analyzer were obtained sequentially at the outlet and inlet sampling locations of Chamber No. 8 for fractional efficiency determinations for particle diameters less than 0.5 μm. Five-stage series cyclones were operated sequentially at the inlet and outlet sampling locations to obtain samples for ion-excited x-ray analysis in order that elemental composition as a function of particle diameter could be determined. Boiler

operating data, hourly secondary voltages and current readings, coal samples and ash samples from Chamber No. 8 and the Unit 3 ash silo were obtained during each test day. Secondary voltage-current curves were obtained on each of the six transformer rectifiers which powered Chambers 7 and 8. Figure 4A illustrates the time of operation and location of the ultrafine sizing systems and each impactor run during Phase I and Phase II of the test program. Figure 4B illustrates the time of operation and location of each mass traverse during the test program. Also illustrated in Figures 4A and 4B are the times for soot blowing and valve testing. The valve tests were required of the unit operators and resulted in the decrease of unit load to approximately 750 MW.

Phase II

Phase II of the test program was scheduled to be conducted from July 31 to August 14, 1977. Tests scheduled for August 5 and 6 were cancelled due to operational problems with Unit No. 3 and on August 8, after conferring with the project officer, the remainder of the test program was cancelled. Tests which were scheduled during Phase II included particle size measurements, with impactors and ultrafine equipment, at the main inlets and stack, mass train measurements at the main inlets and stack, resistivity measurements ahead of and downstream from the air preheaters, voltage current readings, gas analyses, and cyclone samples obtained with the five-stage series cyclones for ion-excited x-ray analysis.

During the first week of Phase II, cyclone samples were obtained at the main inlet and impactors were operated at the main inlet and stack sampling locations. Voltage-current readings and gas analysis data were also obtained during the first week of Phase II. Resistivity measurements scheduled for the first week of Phase II were not obtained due to material failure problems in the "Hot" Probe. The resistivity data scheduled to be obtained downstream from the air preheaters during the second week of testing was later obtained on August 21-23, 1977. Due to the plant outage, no overall efficiency measurements with mass trains were obtained. Opacity data, which were scheduled to be measured at the stack coincident with mass train traverses, were also not obtained.

MEASUREMENT TECHNIQUES

Brief descriptions of the measurement techniques are given in the following sections. More detailed discussions and example calculations are given in the Appendix.

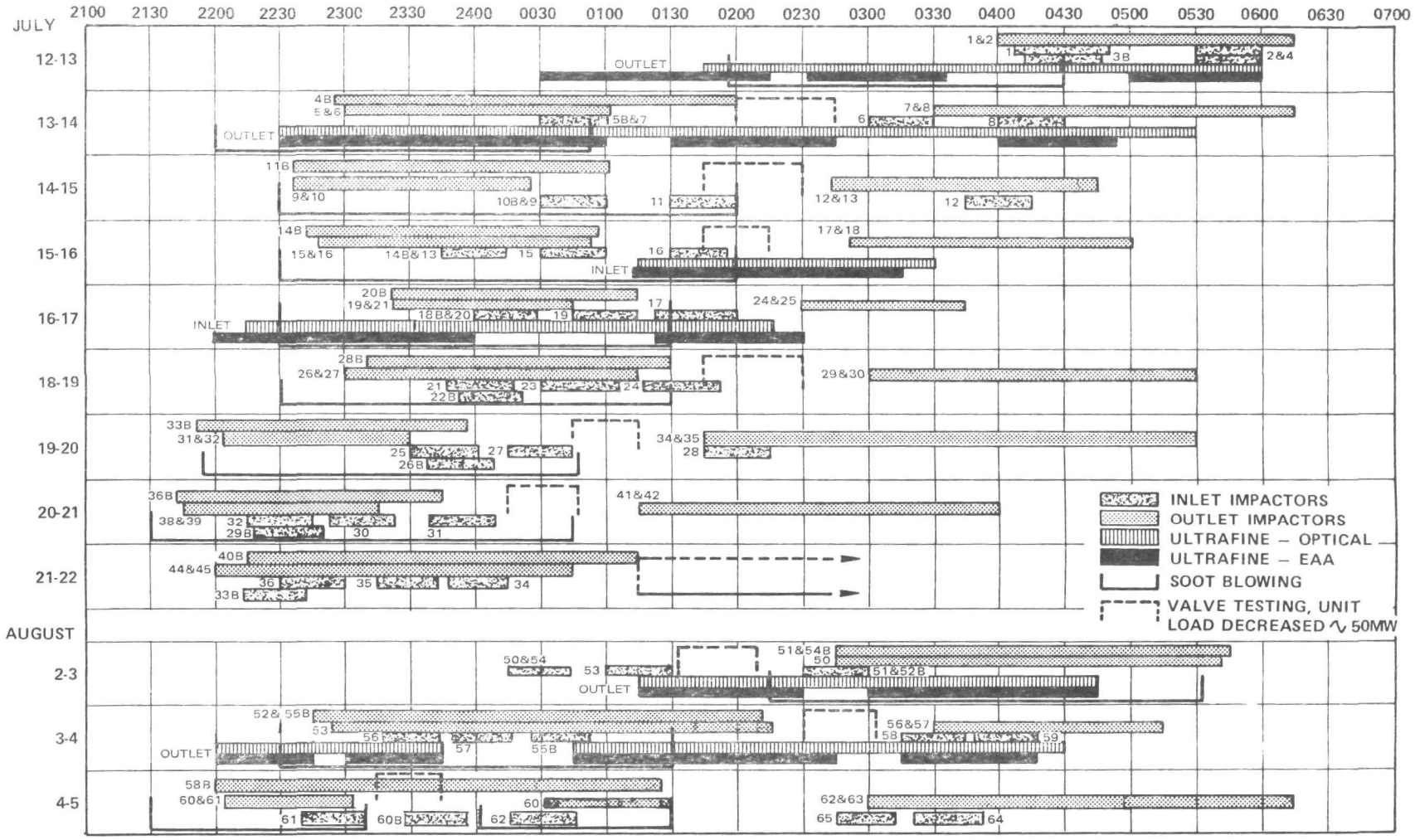

Figure 4a. Chronological display of impactor and ultrafine measurements.

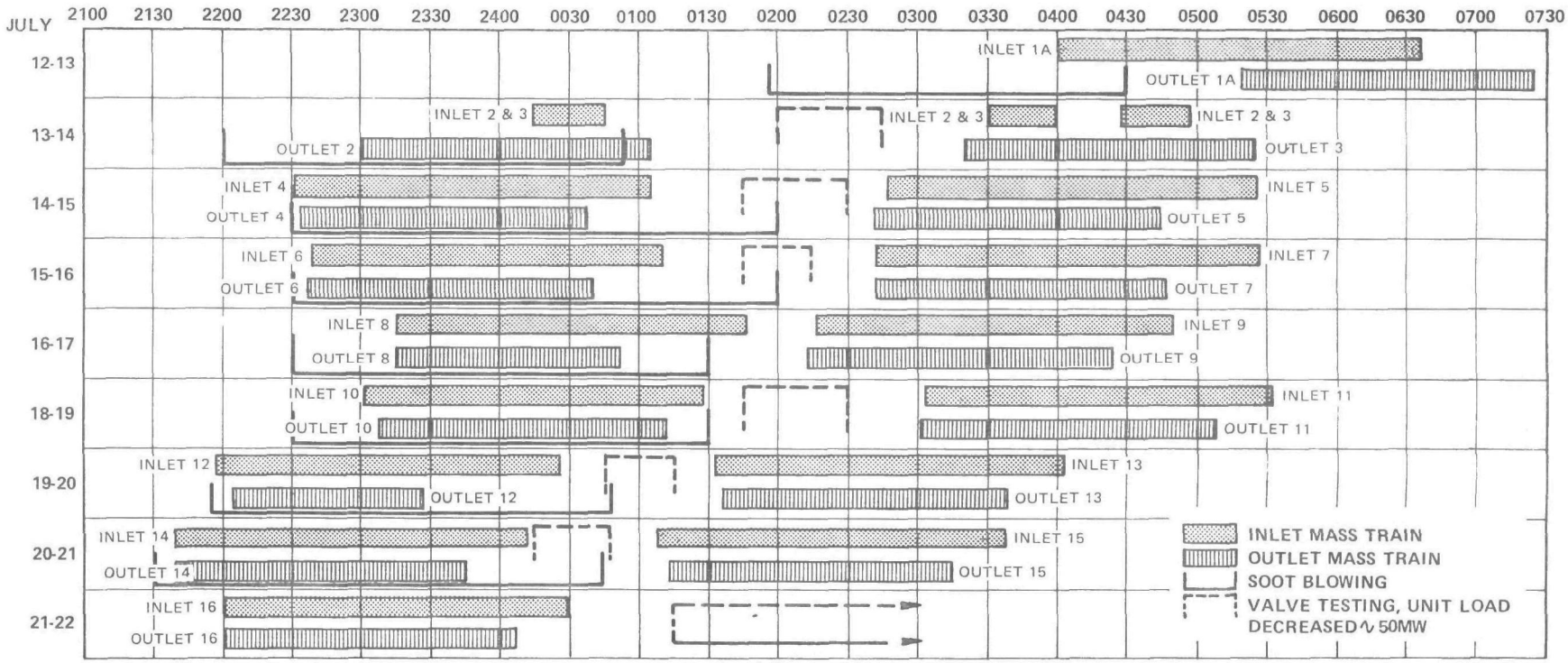

Figure 4b. Chronological display of mass train measurements.

Mass Measurement

Mass loading determinations were conducted at the inlet and outlet sampling locations of Chamber No. 8. Alundum in-stack filters were used at the inlet while Gelman 47 mm filters were used in-stack at the outlet to collect the particulate mass. Thirty-six and forty-two point isokinetic traverses were conducted across the inlet and outlet sampling locations, respectively.

Impactor Measurements

Calibrated cascade impactors were used at the inlet and outlet sampling locations to obtain particle size and particle mass distributions for particles between approximately 0.50 μm to 10 μm. Modified Brink Cascade Impactors were used at the main precipitator inlet and the inlet to Chamber No. 8 while Andersen Mark III Cascade Impactors were used at the outlet of Chamber No. 8 and the stack sampling location. Glass fiber substrates which were conditioned in the laboratory, by acid washing, and *in situ*, by passing filtered flue gas through them, were used in all impactors. Blank impactor runs were conducted each test day for each type of impactor with the exception of an Andersen Blank on the first test day. The blank impactor runs were conducted at approximately the same flow rate (1.4×10^{-5} m^3/sec (0.03 cfm) for the Brink and 1.9×10^{-4} m^3/sec (0.4 cfm) for the Andersen) and for approximately the same sample time ($\sim$30 minutes for the Brink and $\sim$ 150 minutes for the Andersen) as the "real" sampling runs. Data reduction was performed with a computer program described in Reference 1.

Ultrafine Size Measurements

A Thermo-Systems, Inc. Model 3030 Electrical Aerosol Analyzer (EAA) was used sequentially at the outlet and inlet sampling locations of Chamber No. 8 and at the stack sampling location to determine concentration vs. size information in the diameter range of 0.015 μm to approximately 0.30 μm. The operating principle of the EAA[2] is based on placing a known charge on the particles and then precipitating the particles under closely controlled conditions. Size selectivity is obtained by varying the electric field in the precipitator section of the mobility analyzer. The mobility of charged particles is monotonically related to particle diameter in the operating regime of the instrument. An optical single particle counter (Royco 225) was used in parallel with the mobility analyzer to provide particle size distribution data over the approximate particle diameter range from 0.3 to 2 μm.

A dilution system is required for the EAA and Royco because the sizing instrumentation cannot tolerate raw flue gases as sampling streams nor cope with particle concentrations encountered in flue gases. The required dilution typically ranges from 10:1 to 1000:1 depending upon the particulate source and the location of the sampling point with respect to the control device.

Resistivity Measurements

In situ resistivity measurements were conducted with a point-to-plane electrostatic collection instrument[3] at the main inlet of Unit #3 and downstream from the air preheater. The device is inserted into the flue gas environment and allowed to reach near thermal equilibrium with the gas stream. The dust thickness gage is set at zero and the measurement cell positioned for collection. A clean electrode voltage vs. current characteristic is recorded. The current density for collection is selected and a dust layer is precipitated electrostatically. After collection of the dust layer has occurred, a second voltage vs. current characteristic is recorded. A comparison of the two voltage-current curves provides one method for determining resistivity in the absence of electrical breakdown in the dust layer. The measurement electrode is then lowered to contact the dust layer and the layer thickness is determined. The resistance of this known geometrical configuration (right cylinder) is measured, and the resistivity is then determined from the measured resistance.

Laboratory resistivity measurements were conducted on ash samples collected from the 'A' hopper of Chamber No. 8 and the Unit No. 3 ash silo. The laboratory resistivity measurements were conducted in an ASME Power Test Code 28 type apparatus[3] and a controlled laboratory environment.[4]

Gas Composition Determination

Gas analysis measurements were conducted at the inlet and outlet sampling location of Chamber No. 8, at the main inlet, and at the stack. Commercial Orsat-type analyzers were used for oxygen and carbon dioxide determinations. The moisture content of the flue gas was determined at the outlet sampling locations by pulling a known volume of gas through a preweighed packed drierite column. The drierite column was then weighed and the moisture content calculated from the weight change. The concentrations of sulfur trioxide and sulfur dioxide were also determined at the outlet sampling locations. The sulfur trioxide samples were collected by a condensation method[5] while the sulfur dioxide was collected in a hydrogen peroxide solution, which oxidized the sulfur dioxide to sulfur trioxide. Each of the sampling techniques for the oxides of sulfur produced a sample for analysis that consisted of a dilute sulfuric acid solution. The concentrations of acid (from which the SO_x concentrations may be calculated) were determined by barium perchlorate titration using thorin indicator.

Cyclones Used for Obtaining Samples for Ion-Excited X-Ray Analysis

Five-stage series cyclones were used to obtain size fractionated samples for ion-excited x-ray analysis.[6] The cyclones were operated at one point in the flue and at an average isokinetic

flow rate. The particulate catch from the cyclones was analyzed by the University of California's Crocker Nuclear Laboratory in Davis, California. The elemental analysis system[7] is based on ion-excited x-ray emissions (IXA) and provides a sensitivity over a wide range of elements.

Voltage-Current Measurements

During Phase I, primary and secondary voltages and currents were recorded from the transformer control cabinets which powered chambers 7 and 8. Voltage divider resistor assemblies were attached to the high voltage side of each of the transformers of chambers 7 and 8 and secondary voltage vs. current curves were obtained during Phase I. Photographs of voltage waveforms were also obtained.

During Phase II of the test program, primary and secondary voltages and currents were recorded for each of the forty-eight transformer control cabinets.

TEST RESULTS

Mass Train Measurements

Since the test program was conducted on a hot-side precipitator upstream from the air heater, there was concern that boiler soot blowing operations could significantly influence the particulate concentration. Therefore, mass train and impactor runs were scheduled to occur in soot blowing and non-soot blowing periods, as indicated in the chronological displays of Figures 4A and 4B. Table 3 contains the mass concentration data obtained with the mass trains and impactors during Phase I. Also included are gas flows, temperature, and O_2 and CO_2 concentrations obtained with the mass train and gas analysis systems. The calculated values of precipitator collection efficiency are included when appropriate, along with the specific collecting area, which is based on an average of the inlet and outlet actual gas flow rates.

The inlet and outlet gas flows indicate that a significant in-leakage of air occurs across the chamber, accompanied by a temperature drop. Since this apparent leakage had been noted in a previous test series on Chamber 8 and indicated approximately 8% in-leakage accompanied by a 29°C temperature drop, the inlet and outlet temperature and pitot systems were checked against one another at the outlet sampling location prior to starting the test series. The pitot systems were found to be in agreement when checked at the same point, and the temperature measuring systems were within 2°C of one another. A comparison of average inlet and outlet temperatures, oxygen contents, mass loadings, and gas flows for the Phase I test series is given in Table 4. The data in Table 4 indicate that the average outlet volume flow is 16% greater than the inlet.

TABLE 3

MASS CONCENTRATIONS OBTAINED DURING PHASE I
WITH MASS TRAINS AND IMPACTORS

Date	7/12-13/77		7/13-14/77		7/14-15/77		7/15-16/77		7/16-17/77		7/18-19/77		7/19-20/77		7/20-21/77		7/21-22/77
Run #	1	1A	2[2]	3[4]	4	5	6	7	8	9	10	11	12	13	14	15	16
INLET	S[1]	NS	S	NS	S	NS	S	NS	S	NS	S	NS	S	NS	S	NS	NS
Temp. °C	350.0		362.2		366.1	362.8	360.0	360.6	366.1	363.3	353.3	352.8	367.2	367.8	364.4	363.9	366.1
O_2	4.2		3.5	5.6	5.0	5.4	3.8	4.0	3.8	4.2	3.7	4.2	3.9	4.2	4.2	4.2	4.2
CO_2	13.7		15.0	14.0	13.7	13.6	14.9	15.2	15.0	14.7	14.8	15.0	15.0	14.7	14.9	14.5	14.7
Vol. Flow, dsm^3/sec	44.31		45.54		43.28	45.03	44.75	44.62	44.62	44.56	44.35	44.89	44.40	44.83	44.21	43.60	43.17
Grain Loadings;																	
Mass Train, g/dsm^3	--	5.4849	6.0852	5.1754	8.1375	5.9126	8.3778	6.8727	6.8061	6.0845	7.3962	6.6988	7.3296	5.5977	6.7874	7.5626	8.0262
Impactors, g/dsm^3	1.5355	2.5188	4.4721	4.0658	5.3302	3.3374	7.3689	--	5.8501	--	4.2335	--	6.4838	4.9456	5.9307	--	5.6458
OUTLET																	
Temp. °C	324.4		331.1	335.0	333.9	330.0	331.1	330.6	337.2	331.7	325.0	326.1	333.3	331.1	331.7	329.4	328.9
O_2	4.3		5.4	4.8	6.2	5.4	4.3	5.3	4.5	5.3	4.6	4.8	4.4	4.8	5.3	4.7	4.1
CO_2	15.1		14.6	14.7	14.2	14.2	15.1	14.1	15.2	14.0	15.1	14.6	14.8	14.7	14.3	14.5	15.3
Vol. Flow, dsm^3/sec	50.96		51.68	51.59	51.41	50.08	50.20	51.56	51.46	52.24	52.62	52.30	52.21	51.99	51.17	51.33	51.51
Grain Loadings;																	
Mass Train, g/dsm^3	--	0.0522	0.0531	0.0693	0.0401	0.0412	0.0336	0.0403	0.0680	0.0732	0.0838	0.0423	0.0391	0.0414	0.0515	0.0744	0.0423
Impactors, g/dsm^3	--	0.0496	0.0320	0.0291	0.0327	0.0190	0.0333	0.0194	0.0532	0.0270	0.0477	0.0256	0.0437	0.0383	0.0299	0.0770	0.0439
SCA[3], $m^2/(m^3/sec)$	53.32		52.23	52.59	53.44	52.90	53.24	53.11	51.57	51.84	52.60	52.19	51.96	52.13	53.05	52.92	53.15
Efficiency, %																	
Mass Trains	--	99.05	99.13	98.66	99.51	99.30	99.60	99.41	99.00	98.80	98.87	99.37	99.47	99.26	99.24	99.02	99.47
Impactors	--	98.03	99.28	99.28	99.39	99.43	99.55	--	99.09	--	98.87	--	99.32	99.23	99.50	--	99.22

1. S denotes tests which were conducted while soot blowers were operational, whereas, NS denotes non-soot blowing test periods.
2. Inlet mass train and impactor data obtained from a two point, one port traverse.
3. Calculated by averaging the inlet and outlet volume flow and using a collection area of $7023.24 m^2$
4. Inlet mass train and impactor data obtained from a two port, two points per port, traverse.

TABLE 4. AVERAGE INLET AND OUTLET PARAMETERS
CHAMBER 8

	Inlet	Outlet	
Temperature, °C	361	330	
Vol. Flow, dsm^3/sec	44.4	51.5	
O_2, % (dry basis)	4.26	4.88	
Mass Concentrations, g/dsm^3			Average Collection Efficiency, %
Impactor	5.19	0.0384	99.26
Mass Train	6.77	0.0529	99.22
Number of Runs			
Impactor	27	32	
Mass Train	16	16	

TABLE 5. STATISTICAL ANALYSIS OF EFFECT OF SOOT BLOWING ON MASS EMISSION - PHASE I SERIES
CHAMBER 8

	Inlet				Outlet			
	Mass Trains		Impactors		Mass Trains		Impactors	
	NS	S	NS	S	NS	S	NS	S
$\bar{x}$, g/dsm^3	6.38	7.28	4.32	5.62	0.0530	0.0527	0.0377	0.0393
σ, g/dsm^3	0.98	0.80	1.81	2.00	0.0150	0.0178	0.0189	0.0102
γ	16		20		14		28	
t	2.02		1.70		0.036		0.306	
t_{99}	2.92		2.84	t_{50}	0.692		0.683	
t_{98}	2.58		2.53					
t_{95}	2.12		2.09					
t_{90}	1.75		1.72					
t_{80}	-		1.32					

$\bar{x}$ = average of sample
σ = standard deviation
γ = degrees of freedom
t = Student's "t" value
t_n = Critical t value for γ at indicated confidence level

Since the difference in inlet and outlet flows was unexpectedly large, in-leakage was further examined by performing an adiabatic mixing calculation to determine the air in-leakage necessary to cause the observed temperature drop. The calculation demonstrates that 11% in-leakage would be required to produce the observed 31°C temperature drop in the absence of other heat losses using the measured inlet flow. Since other losses to ambient air would occur, the temperature profile averages indicate that in-leakage must be less than 11%. The oxygen concentrations determined by single point analyses during the mass train tests indicated in-leakage of about 7%. We conclude that, since the mass train systems were checked against one another, a part of the difference in indicated flow results from integration errors in obtaining the true flow from a limited number of traverse points. The actual in-leakage is estimated to range between 7 and 11%.

The mass concentration data were analyzed to determine whether soot blowing operations in the boiler significantly increased total particulate loadings. Average particulate concentrations and sample standard deviations were computed for the with and without soot blowing data sets for both the mass train and impactor sampling systems. A procedure given by Hoel[8] was used to estimate the "t" variable and the number of degrees of freedom required for using the Student's "t" distribution to examine the difference of two means. The results of these calculations are given in Table 5, and the following conclusions are apparent:

- The mass train data indicate significant mass loading increases during the soot blowing periods at the 90% confidence level.
- Similarly, the impactor-derived mass concentrations show an increase during soot blowing at the 80% confidence interval.
- No significant differences were observed as a result of soot-blowing by either sampling system at the precipitator outlet.

Previous test results had indicated unusually large disagreement between impactor and mass train determinations of inlet mass loadings for Chamber 8 which were thought to result from stratification in the duct. Therefore, an experiment was conducted in which the modified Brink impactors were operated at an average isokinetic flow rate for two points in a single port for a total sampling time of 30 minutes. Mass train sampling, also for a total of 30 minutes, immediately followed the impactor sampling, but the mass train was operated isokinetically at the two points. The experiments were repeated for ports 1, 2, and 3; and the results are presented in Table 6. The results indicated that the ratio of impactor to mass train total concentrations were within the expected range for coal-fired power boilers. All other runs with impactors

Table 6

Comparison of Inlet Mass Train and Impactor Loadings

Date	7/13-14/77			
Port #	1*	2	3	Phase I Average, All Other Runs
Impactor mg/dsm^3	4472	4809	3322	5232
Mass Train mg/dsm^3	6085	5628	4723	6934
Ratio of Impactor/Mass Train	.735	.854	.703	.755

* Loadings from Ports 1, 2 and 3 were obtained from a two point traverse, the impactors were operated at an average isokinetic flow rate and the mass trains were operated isokinetically. Each system was operated for 30 minutes per port. The mass train immediately followed the impactor at each port.

Table 7

Phase II, Main Inlet and Stack Impactor Mass Loadings

Date	8/2-3/77		8/3-4/77		8/4-5/77	
Condition[1]	S	NS	S	NS	S	NS
Main, g/dsm^3	2.2958	4.5175	6.0185	4.4645	5.0123	8.5836
Stack, g/dsm^3	0.0546	--	0.0525	0.0678	0.0851	0.1244

[1]S = Soot Blowing, NS = Non Soot Blowing

at the inlet were conducted with either a five- or six-point traverse per port; whereas, the mass trains always conducted a six-point traverse for each port.

Outlet sampling with the Andersen impactors was conducted by obtaining a six point traverse per port, which was the same procedure used with the mass trains. The Andersen impactors traversed the entire duct, and therefore were operated at a flow rate isokinetic to the average velocity in the duct. The mass train followed the usual procedure of isokinetic sampling at each point. The data in Table 4 indicate that the impactors obtained 77 and 73% of the total mass sampled by the mass trains at the inlet and outlet, respectively.

Overall mass efficiency data for the entire precipitator were not obtained during Phase II as a result of a plant outage, as was discussed previously. However, impactors were operated at the stack and at the main inlet sampling locations. The results obtained are given in Tables 7 and 8. Due to the small fraction of the total inlet duct that can be traversed with the Brink impactors during the with and without soot blowing periods, no conclusions could be drawn concerning the effect of soot blowing on total inlet mass concentrations from the impactor data. A comparison of the data in Tables 4 and 8, however, indicate that the precipitator as a whole was not performing as well as Chamber 8. The volume flow at the stack is consistent with the outlet flow from Chamber 8 (860/16 = 53.8 dsm^3/sec vs. 51.5 dsm^3/sec for Chamber 8), and the simultaneous oxygen determination at the inlet and the stack indicate that total in-leakage across the entire precipitator and the air preheater is approximately 10.7%.

Impactor Measurements

Inlet and outlet impactor sampling was conducted as previously discussed and as illustrated in Figure 4a to determine precipitator collection efficiency and particulate concentrations as a function of particle size. In accordance with Particulate Technology Branch Directives, blank substrate weight changes were determined to obtain appropriate blank correction factors for the flue gas - substrate reactions. The results of the blank runs, which were conducted *in situ* simultaneously with the real runs, are summarized in Table 9. The data from all blank determinations are given in Appendix 2. The "nozzle wash" weight gains shown in Table 9 result from the evaporation of an amount of distilled water equal to that used for nozzle washes in the real runs. The distilled water source used during Phase II apparently contained a significant dissolved solids content. The appropriate correction factors from Table 9 were used prior to the calculation of the size distributions from the "real" data sets.

Table 8

Phase II, Average Inlet and Stack Parameters
(From Impactor Sampling Systems)

	Inlet	Stack
Temperature, °C	368	161
Vol. flow, dsm^3/sec	-	860
O_2, % (dry basis)[1]	3.90	5.55
Mass concentration, g/dsm^3	5.40	0.0776
Number of runs	12	10
Apparent collection efficiency, %	98.56	

[1]Orsat data from Table 16

Table 9

Average Blank Corrections for Impactor Components

Components	Phase I	Phase II
	Mass change, mg	Mass change, mg
Brink filter	0.12 gain	0.12 gain
Brink stage	0.07 gain	0.00
Andersen filter	0.14 gain	0.13 gain
Andersen stage	0.13 loss	0.32 gain
Andersen nozzle wash	1.60 gain	10.48 gain

Figure 5 illustrates the particle size distribution obtained by the modified Brink impactors at the inlet to Chamber 8 with and without soot blowing. The data are presented on a differential basis to illustrate the particulate mass as a function of particle diameter. Since the area under the DM/DLOGD vs. diameter curve is directly proportional to particulate concentration, the relative mass in various size bands can be qualitatively determined by examination of the curve. The error bars represent fifty percent confidence intervals. It is apparent that the bars for the with and without soot blowing periods intersect for most size intervals smaller than 8.0 μm diameter. The majority of the difference in mass concentration between the with and without soot blowing data sets occurs for sizes greater than 8.0 μm diameter.

The size distribution shown in Figure 5 is typical of the bimodal distributions produced by pulverized coal-fired boilers, with one mode occurring at about 2.0 μm particle diameter, and the other occurring at a diameter greater than 10.0 μm. The mass median diameter of the entire distribution, based on the impactor determinations of cumulative and total mass loading, is approximately 13 μm. If it is assumed that the difference in mass loadings between the impactor and mass train sampling systems results from under sampling of >20 μm diameter particles by the impactors, the mass median diameter of the distribution increases to 16 μm. This value is based on the extrapolated cumulative mass loadings obtained from the impactor data reduction program and the total particulate concentration obtained with the mass train.

In view of the relatively small differences indicated in Figure 5 between the with and without soot blowing data sets in the size ranges of interest, the results from the two sampling periods were combined. Figure 6 provides the grand average differential size distributions obtained during Phase I and II at the Chamber 8 and at the main inlets, respectively. These distributions are also given on a cumulative mass concentration basis in Figure 7. The data sets obtained at the two locations indicate some departure from each other in the differential mass loadings in the 1 to 2 μm diameter region, but the cumulative distributions are nearly identical.

In contrast to the similarity observed between size distribution data obtained at the main inlet and the Chamber 8 inlet, significantly different results were obtained at the stack location compared to those of the previous test series at the Chamber 8 outlet. The outlet differential size distributions are illustrated in Figure 8. Although the distributions tend to merge at approximately 0.8 μm diameter, the stack outlet data exhibit substantially higher loadings from 0.8 to >10.0 μm particle diameter. These differences are also reflected in the fractional efficiency results given in Figure 9. The apparent fractional efficiency data representing the entire precipitator necessarily includes the influence of any size distribution changes which result from cooling the flue gas and passing it through the preheater. The data obtained with the ultrafine system is discussed in the next section.

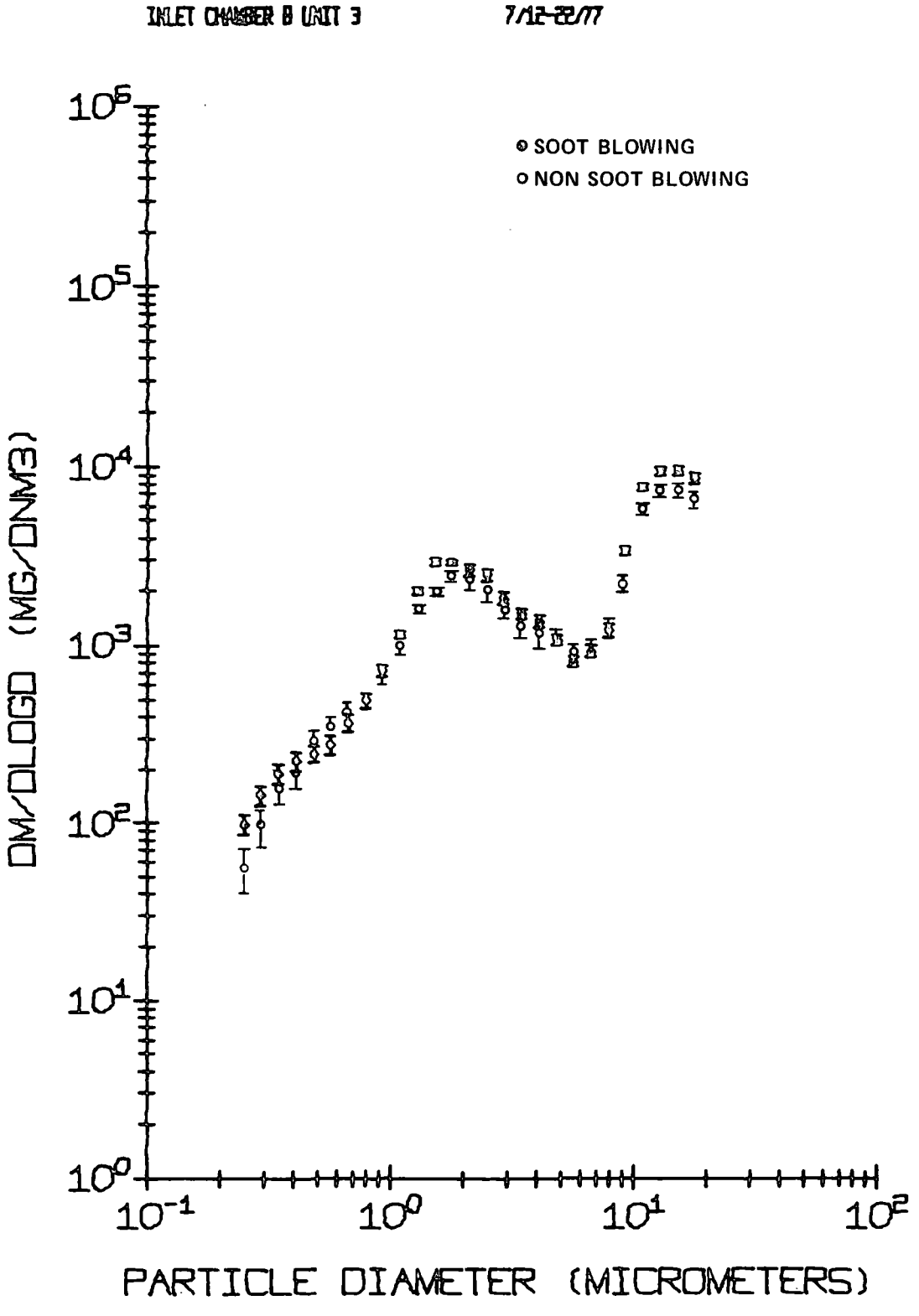

Figure 5. Differential size distributions, Chamber 8 inlet.

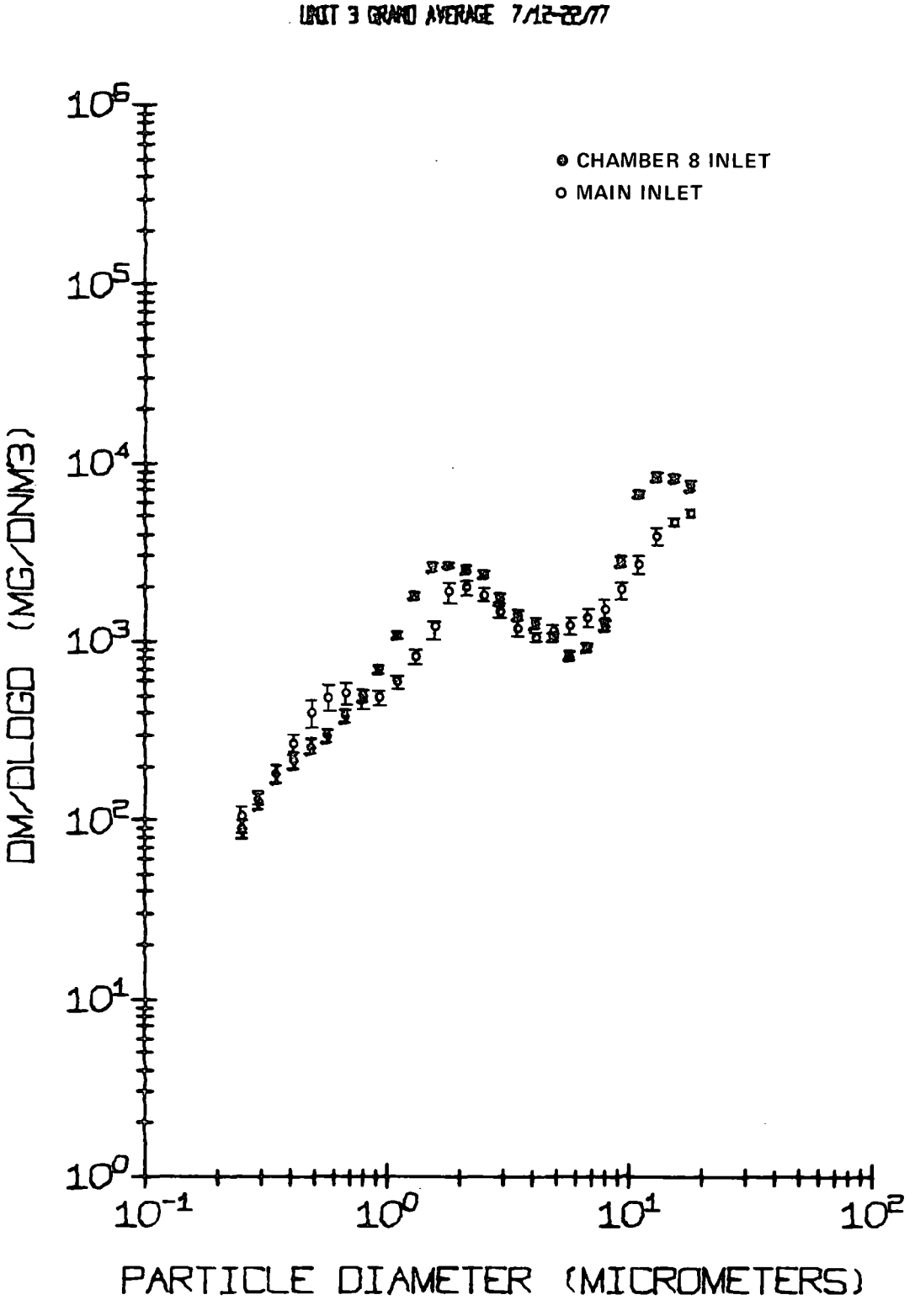

Figure 6. Average inlet differential size distribution.

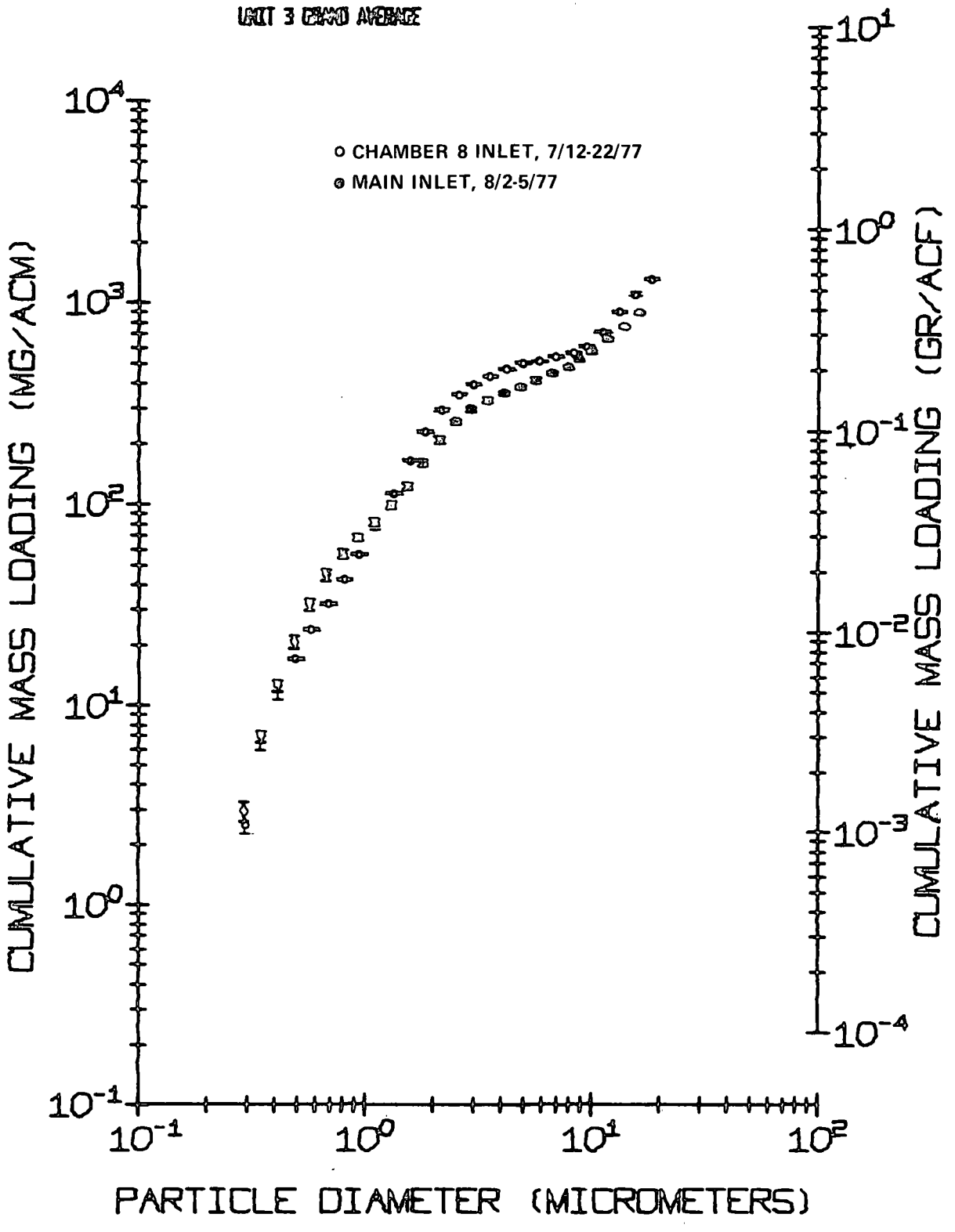

Figure 7. Average inlet cumulative size distribution.

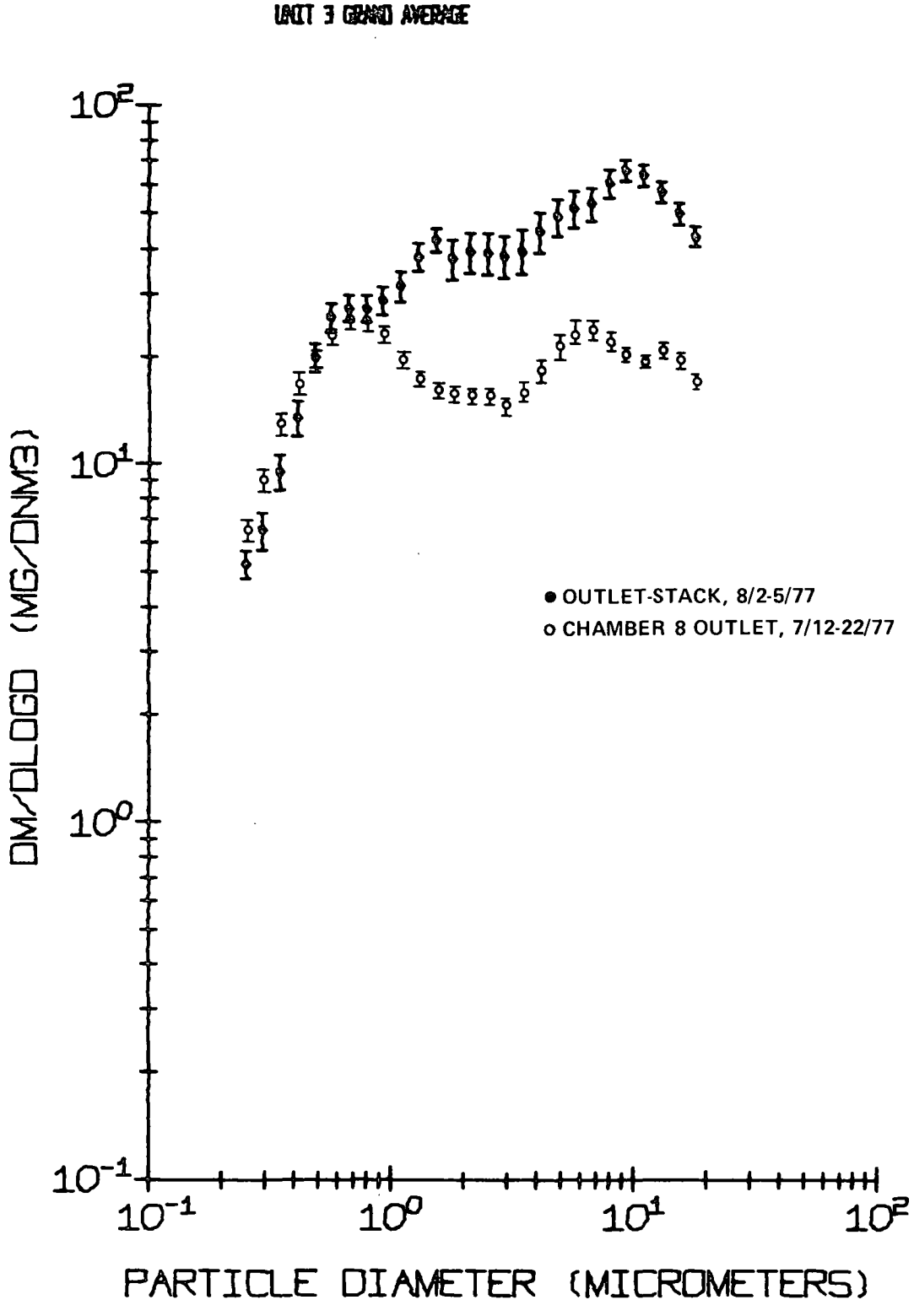

Figure 8. Outlet differential size distribution.

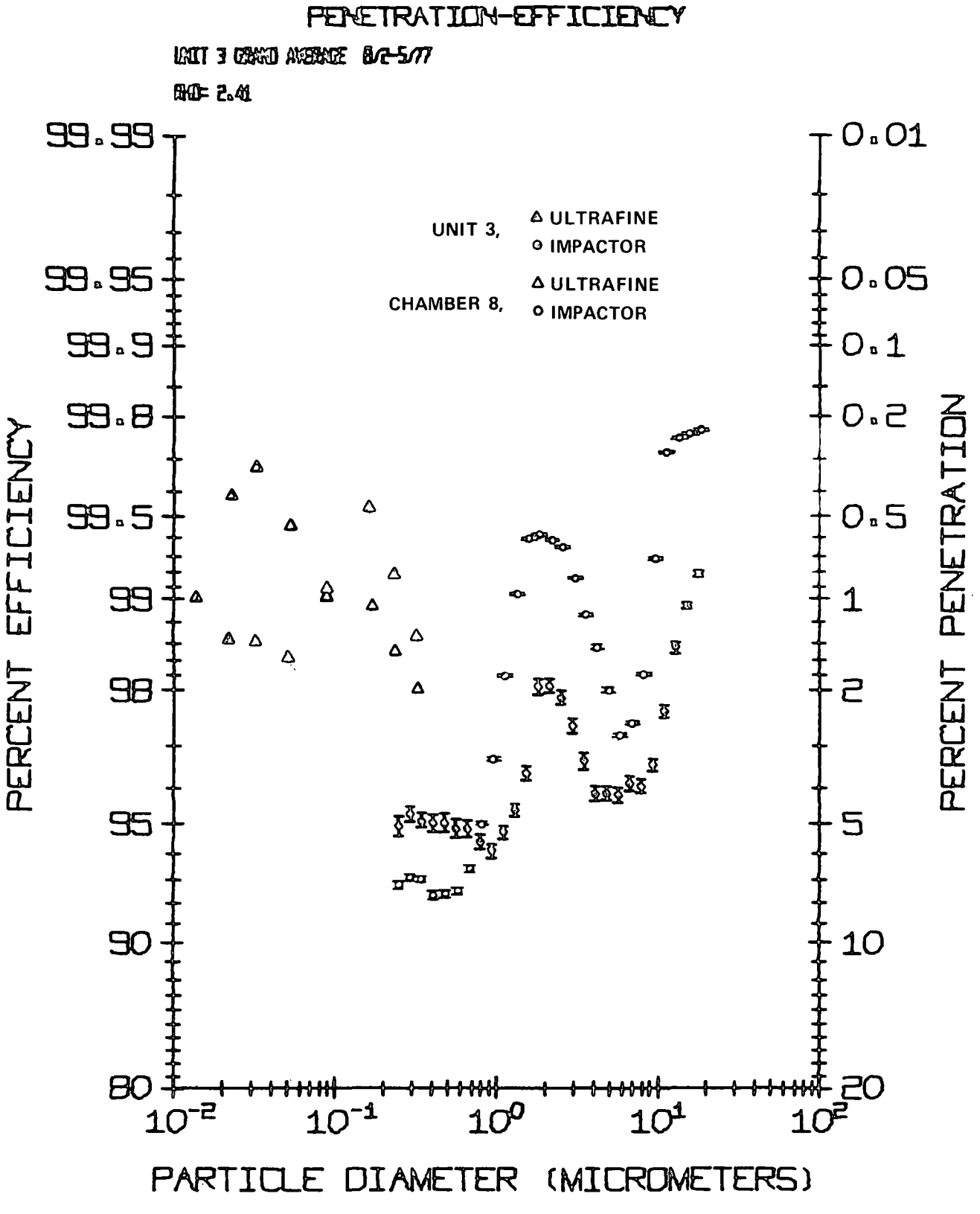

Figure 9. Fractional efficiency for Chamber 8 and total ESP.

Figure 10 gives the cumulative mass concentration as a function of particle diameter obtained during Phase II at the stack sampling location. The outlet size distribution represents cumulative mass emissions of approximately 4.73 ng/J (0.011 lb/10^6 Btu), 9.03 ng/J (0.021 lb/10^6 Btu), 22.36 ng/J (0.052 lb/10^6 Btu), and 30.79 ng/J (0.0716 lb/10^6 Btu) at particle diameters of 1.0, 2.0, 10.0, and 100.0 μm respectively. The largest particle diameter is an arbitrarily chosen upper limit at which the total particulate mass concentration is plotted.

Ultrafine Measurements

The sample extraction and dilution system with the Electrical Aerosol Analyzer and optical particle counter was employed sequentially at the outlet and inlet of Chamber 8 during the first week of Phase I and at the stack sampling location during Phase II. Figure 11 illustrates the relative variations with time observed at the outlet of Chamber 8 for 0.092 diameter particles with the EAA and for the particle concentrations obtained by the optical particle counter (operating in a parallel arrangement with the EAA) over the diameter range 0.36 to 0.59 μm. Similar data obtained at the stack sampling location are shown in Figure 12, and Figure 13 shows relative concentrations as a function of time for 0.092 μm particles at the Chamber 8 inlet. These data indicate that small particle emission rates exhibit significant short term temporal variations that are not directly related to soot blowing operations in the boiler.

Figure 14 contains the differential number size distribution ($\Delta N/\Delta LOGD$) calculated for the Chamber 8 inlet sampling location from the EAA, optical particle counter, and impactor data sets. The comparison indicates considerable disagreement in the overlap region, although the data would form a nearly continuous curve if the ultrafine system points above 0.1 μm diameter are disregarded. Figure 15 contains $\Delta N/\Delta LOGD$ data from the ultrafine system at the stack and the Chamber 8 outlet sampling location. These data indicate that the ultrafine particle emissions at the stack outlet are not significantly different from those measured at the chamber outlet. This is consistent with Figure 8 in which the impactor-derived dM/dLOGD values coincide for the sub-micron range at the two sampling locations. However, the ultrafine and impactor systems show disagreement in the overlap region at the stack sampling location in the same direction as indicated at the inlet in Figure 14. Possible causes of the disagreement are: (1) non-ideal impactor performance not sufficiently accounted for by existing calibration procedures at ambient temperature, (2) the effect of SO_2 on the results obtained with the EAA (see Marlow[9]), (3) spatial concentration variations which influence single point results compared with those obtained by a traverse.

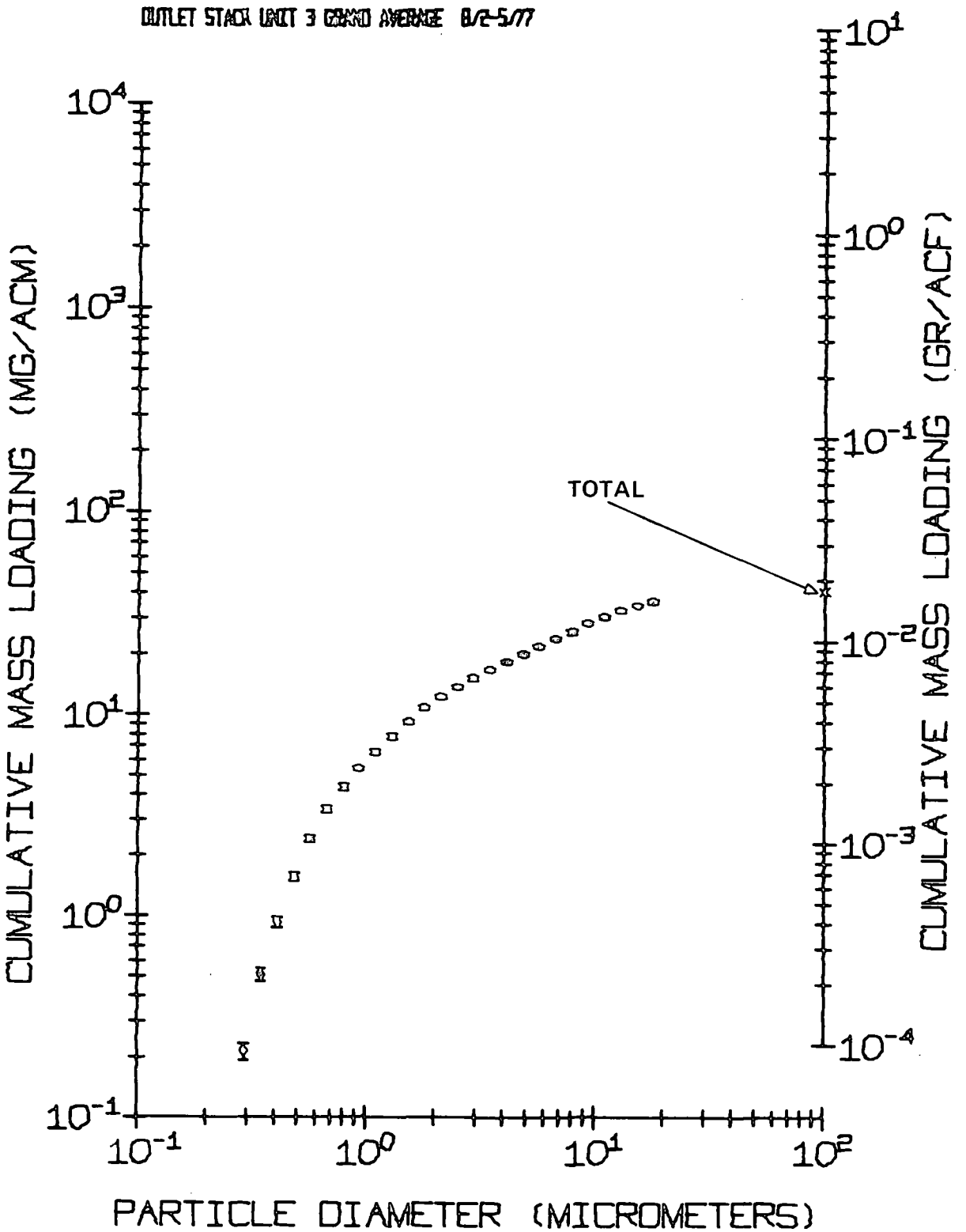

Figure 10. Average outlet cumulative size distribution, total ESP.

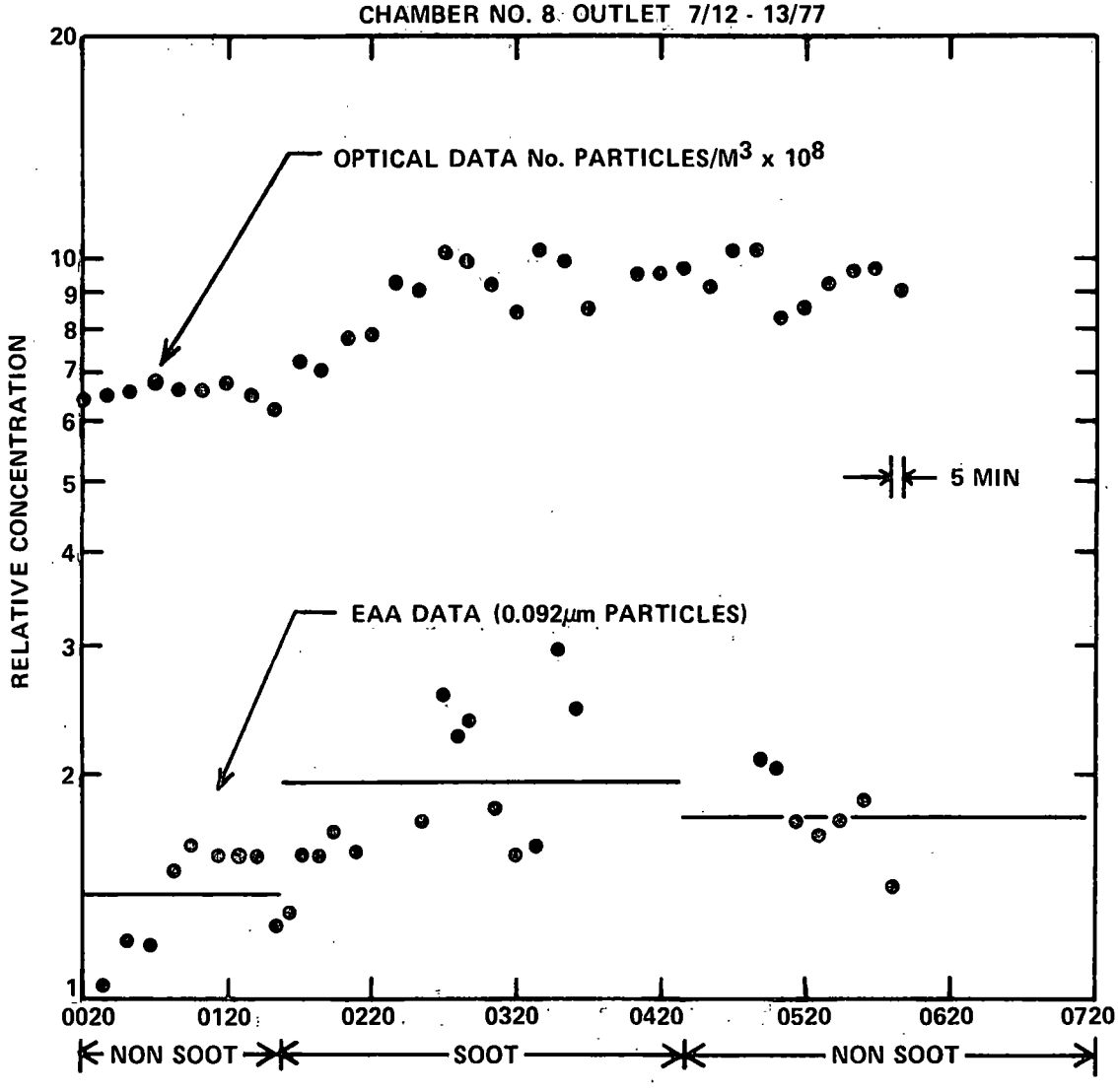

Figure 11. Relative concentration of particles with and without soot blowing, Chamber 8 outlet, 7/12-13/77.

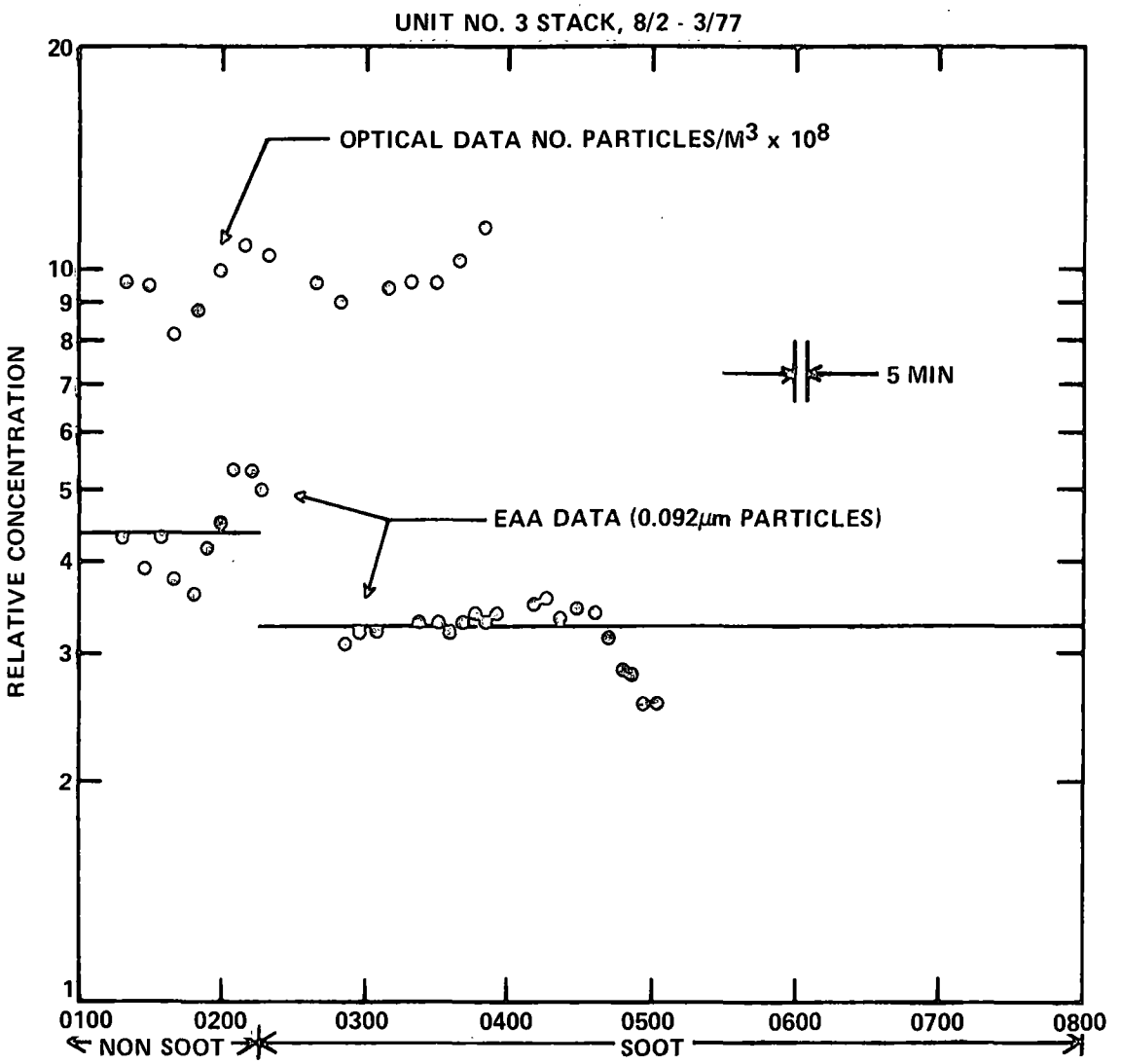

Figure 12. Relative concentration of particles with and without soot blowing, stack location (8/2-3/77).

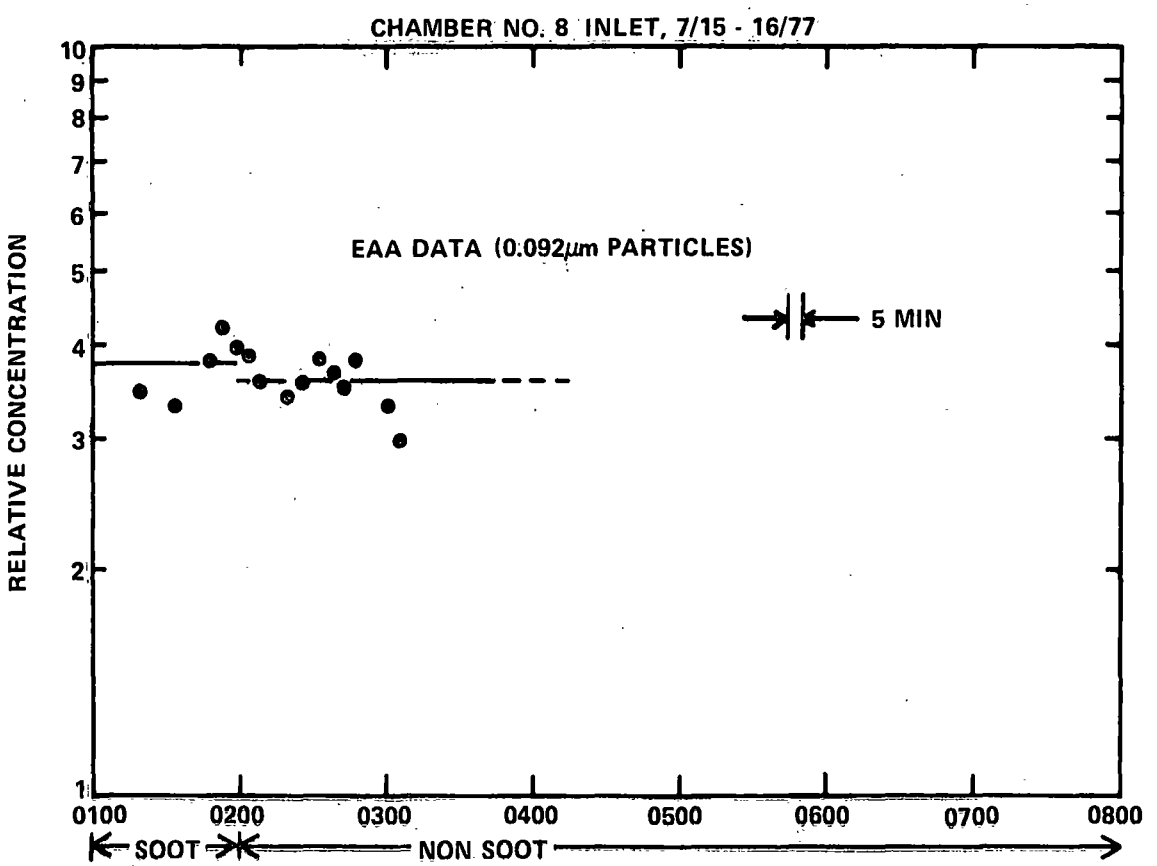

Figure 13. Relative concentration of 0.092 μm particles with and without soot blowing, Chamber 8 inlet, 7/15-16/77.

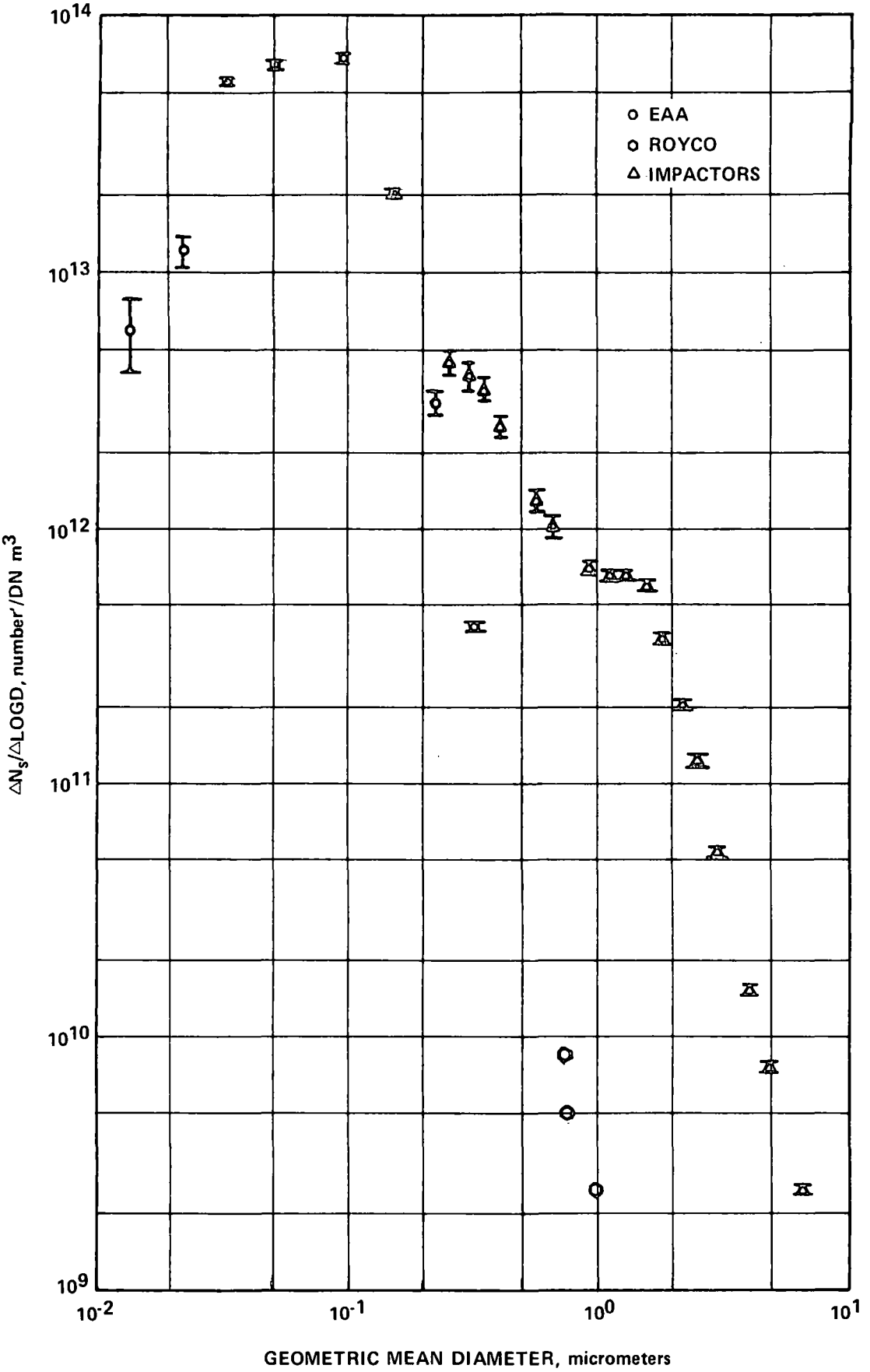

Figure 14. Differential number size distributions, Chamber 8 inlet.

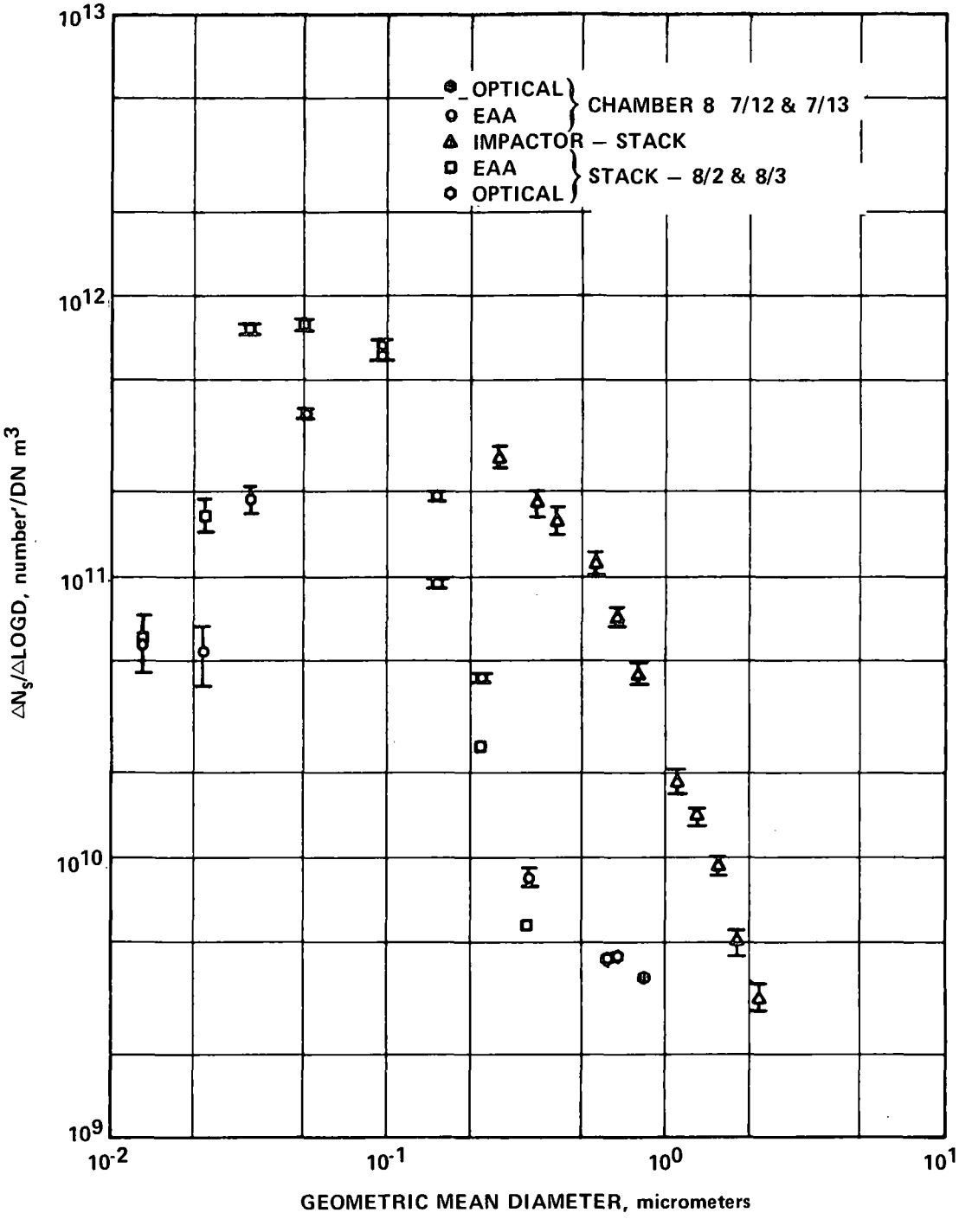

Figure 15. Differential number size distribution, outlet sampling locations.

The fractional efficiencies derived from the ultrafine system data are plotted in Figure 9 along with the inertially-obtained fractional efficiencies from the impactors. Although the two measurement methods produce results displaced from each other, the existence of a minimum collection efficiency as predicted by theory in the region between 0.1 and 0.8 μm diameter is indicated by the trend shown by each system in this size range.

Resistivity Measurements

In situ resistivity measurements were obtained at the main inlet of Unit 3 and downstream from the air preheater. The results from these measurements are presented in Table 10. Resistivity data were scheduled to be taken during the second week of Phase II downstream from the air preheater. However, these data were not taken until August 21-23 due to the plant outage. The data obtained at this location with the in situ probe are of questionable value because of the limited amount of dust which could be collected by the probe from the relatively low dust loadings which existed downstream from the precipitator and air heater. After operating for several hours, dust layers of only 0.015 and 0.02 cm thickness were collected.

Laboratory resistivity measurements were conducted on four ash samples obtained during the test program. These data are presented in Figures 16, 17, 18, and 19, along with predicted resistivities. Figure 18 also contains the high temperature in situ data obtained during approximately the same time period. The 355°C data were taken with an environment of dry nitrogen only while the data taken at 154°C and 112°C were taken in the environment indicated in each figure. Each of the laboratory measurement resistivity data points were extrapolated to an electric field stress of 10 kV/cm to agree with the electric field used in the resistivity predictions.

The predicted resistivity, using the method in EPA Report EPA 650/2-74-074 is referred to as Method 1, whereas the predicted resistivity referred to as Method 2 is a result of ongoing research at Southern Research Institute sponsored by the Environmental Protection Agency. The predicted data from Method 1 is for a porosity of 50% and differs slightly from Method 2 due to the additional research and sophistication of the prediction methods. The predicted data (Method 2) and laboratory measured data at 112°C differ since the data used to develop the predictive technique were obtained at 112°C after a long time exposure to the environment (∿5 hrs) and the laboratory data were taken as soon as the ash and environment equilibrated (20 minutes).

Figure 20 contains predicted resistivity (Method 2) using an analysis of coal ash from another coal source which has been used at Navajo (Utah coal), but which was not in use during the EPA-sponsored test series. These data are included to indicate the

TABLE 10. IN SITU RESISTIVITY DATA, NAVAJO GENERATING STATION

Date	Temperature°C	Resistivity, ohm-cm	Location
7/21/77	346.7	1.7×10^{9}	Main Inlet
7/22/77	352.2	3.9×10^{9}	Main Inlet
7/22/77	348.9	9.5×10^{9}	Main Inlet
7/22/77	353.3	3.6×10^{9}	Main Inlet
8/21/77*	152.2	3.8×10^{12}	Stack Inlet
8/22-23/77*	134.4	9.0×10^{12}	Stack Inlet

*Questionable because of small layer (0.2 mm) in probe.

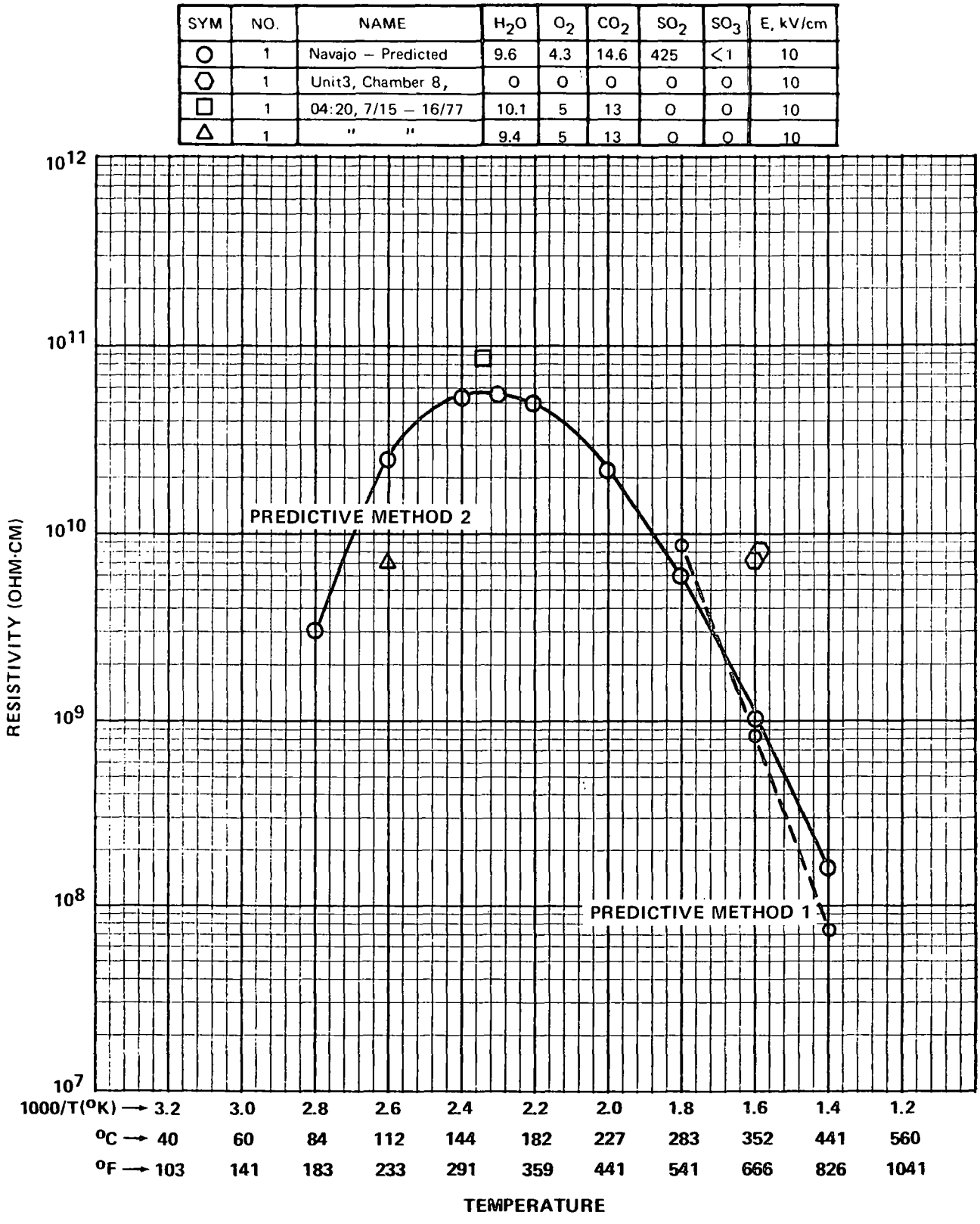

Figure 16. Resistivity vs. temperature, 7/15-16/77.

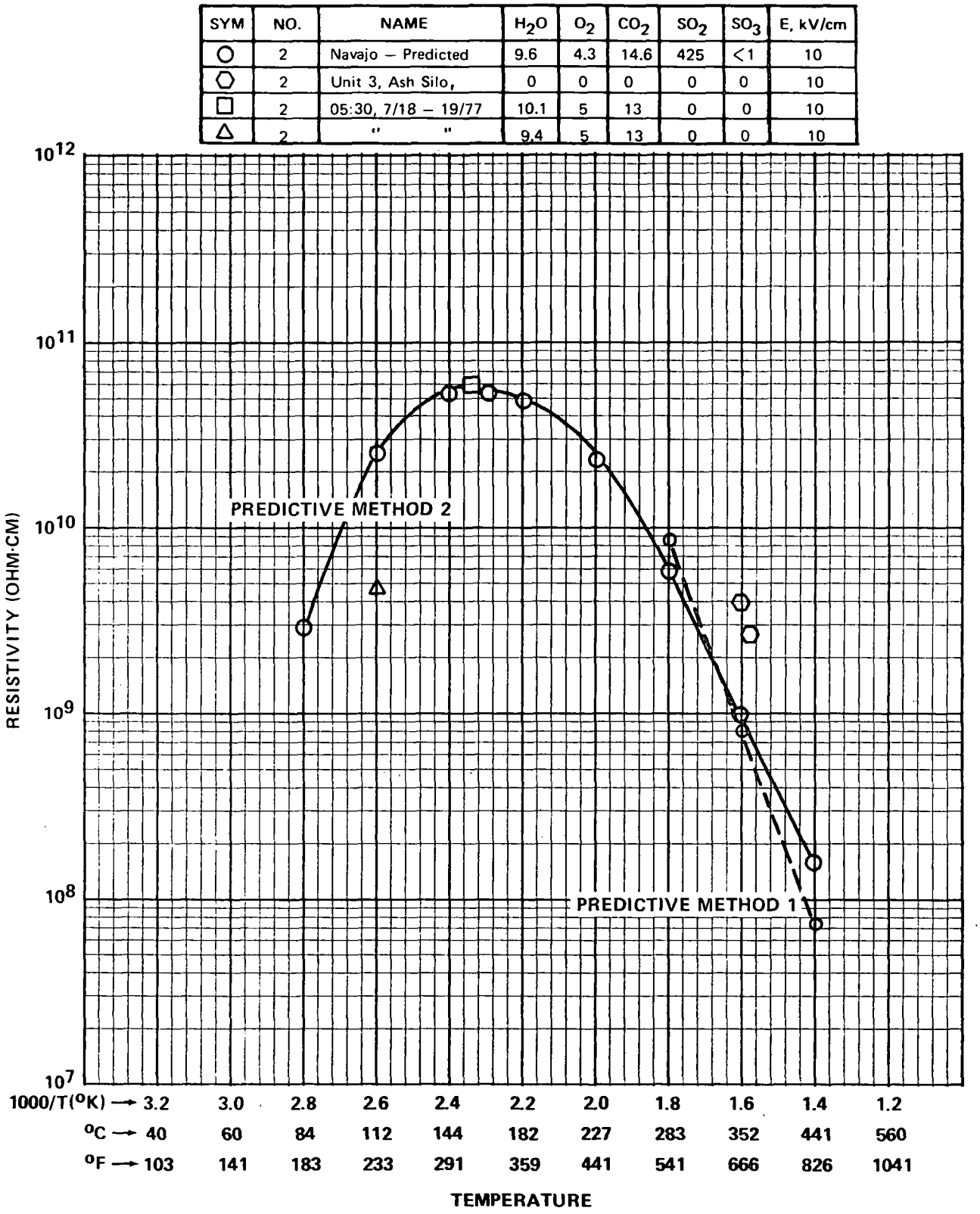

Figure 17. Resistivity vs. temperature, 7/18-19/77.

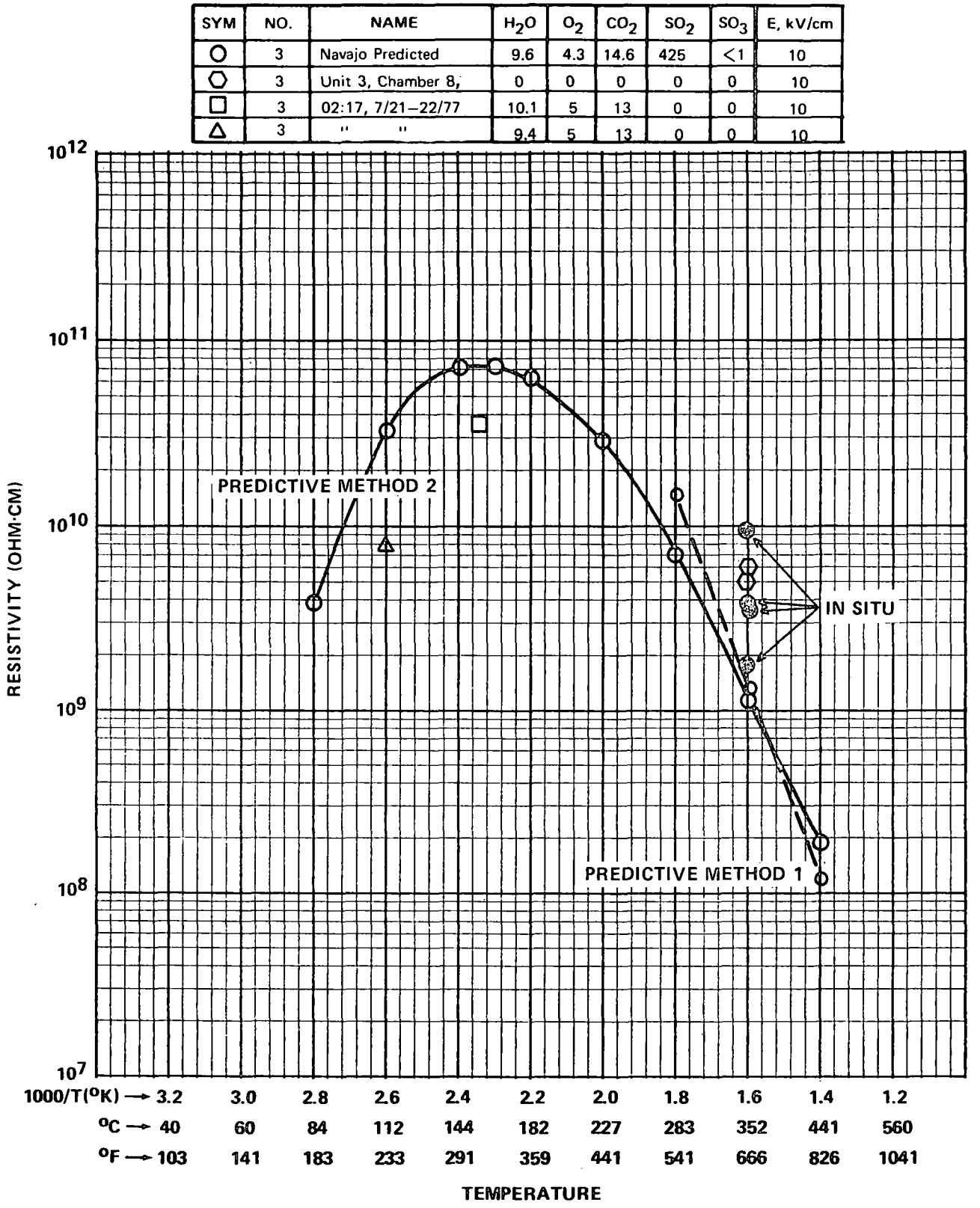

Figure 18. Resistivity vs. temperature, 7/21/77-7/22-77.

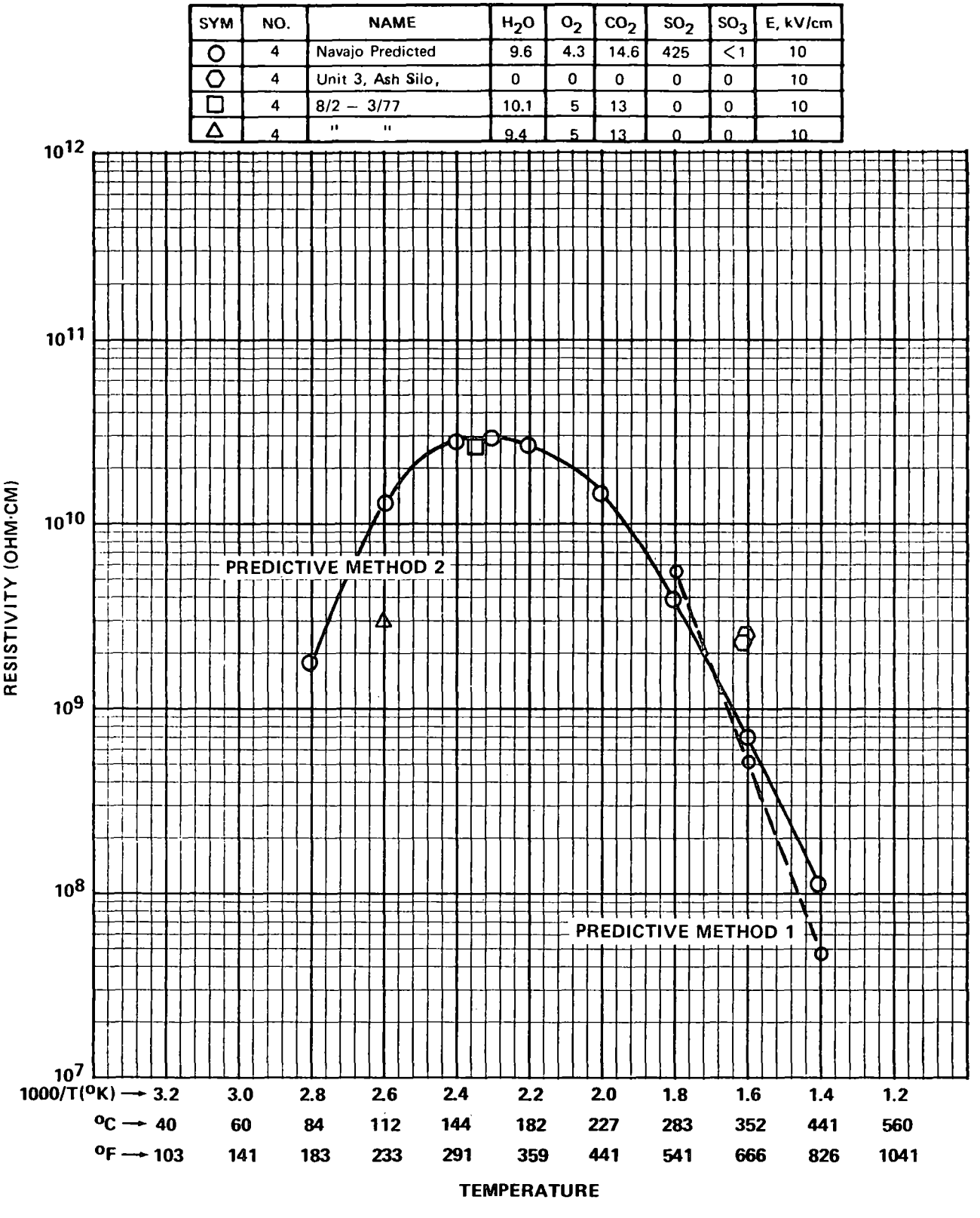

Figure 19. Resistivity vs. temperature, 8/2-3/77.

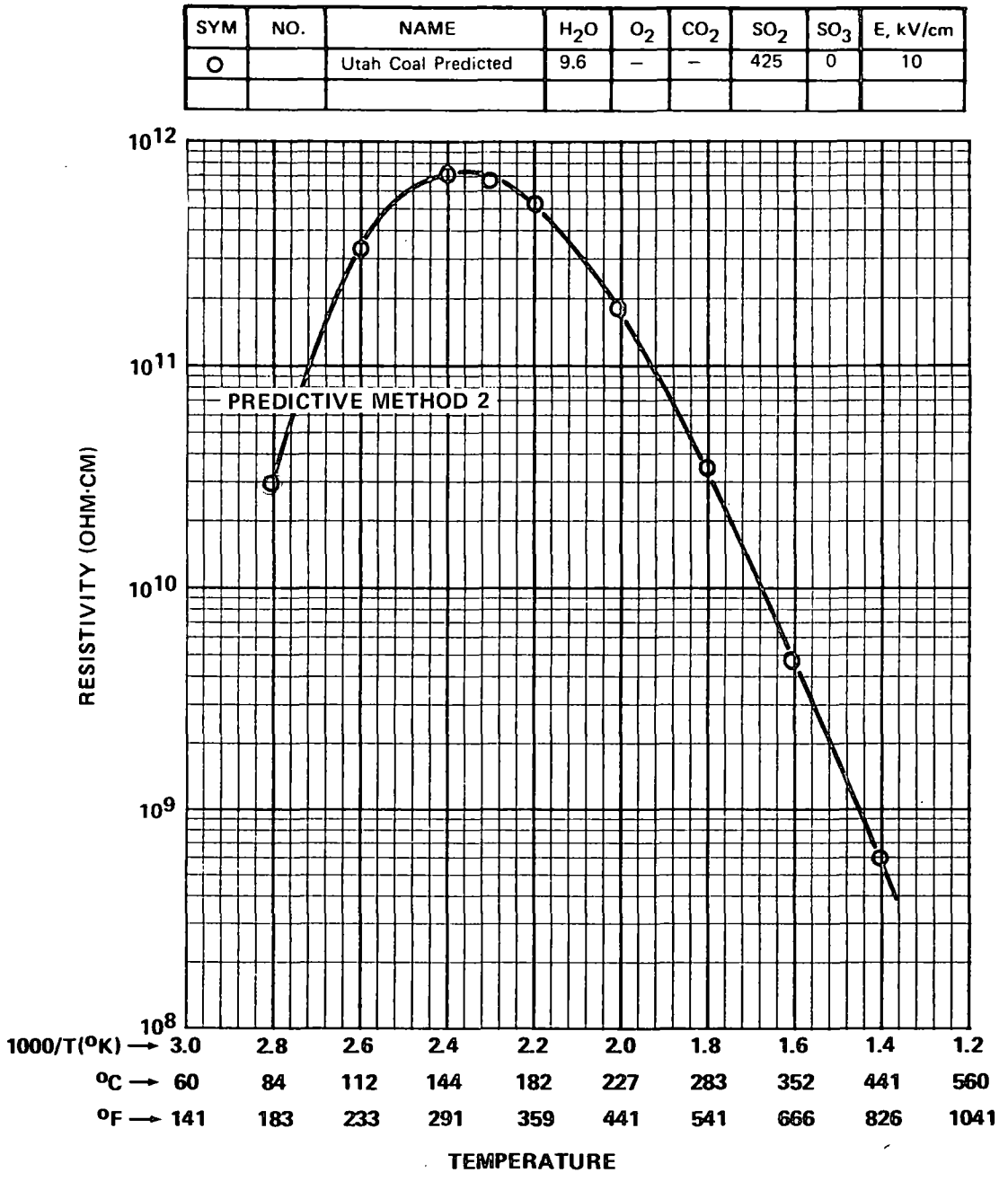

Figure 20. Resistivity vs. temperature, Utah Coal.

range of dust resistivities which may be encountered at the Navajo Generating Station; the ash analysis upon which Figure 20 is based is provided in Table 11. Compositions for the other graphs are given in Table 14.

The following conclusions have been derived from the resistivity data:

- The measured and predicted laboratory and in situ data at 350°C show reasonable agreement.
- The resistivity was relatively constant during the test series.
- The in situ and laboratory data at 130-150°C are in disagreement by about two orders of magnitude. Because of the difficulty in collecting a sample for in situ measurements, the laboratory data are considered more reliable.

The effects of these data on precipitator performance and projected design are discussed in a subsequent section.

Coal and Ash Analyses

Tables 12 and 13 present the proximate and ultimate analyses obtained from coal samples collected during each day of testing for Phase I and Phase II, respectively. Chemical analyses were obtained for selected ash samples obtained during Phase I and Phase II from the inlet hopper of Chamber #8 and Unit Three ash silo. These analyses are presented in Table 14 and are the data used for the indicated samples in Figures 16, 17, 18, and 19 in the resistivity prediction methods. Note that no samples indicate a sodium oxide content in the low range.

Gas Composition Measurements

Gas composition determinations were made at the outlet of Chamber 8 during Phase I using methods previously described. During Phase II of the test program, data were obtained at the main inlet and at the stack sampling locations. Simultaneous Orsat determinations were conducted at these two locations during Phase II for the purpose of determining in-leakage, as was discussed in the section on mass train measurements. Gas composition data from the Phase I and Phase II analyses are presented in Tables 15 and 16, respectively. The SO_x determinations indicate that SO_3 concentrations were never above the detection limit of $\sim$0.5 ppm at either the inlet or outlet to the precipitator or at the stack sampling location.

TABLE 11. CHEMICAL ANALYSIS OF UTAH COAL ASH USED FOR FIGURE 20[1]

Compound	%
Li_2O	0.01
Na_2O	0.47
K_2O	1.84
MgO	3.15
CaO	13.35
Fe_2O_3	4.30
Al_2O_3	16.46
SiO_2	52.64
TiO_2	0.81
P_2O_5	0.11
SO_3	0.67

1. Analysis provided by Salt River Project from Commercial Testing and Engineering Company data.

TABLE 12. COAL ANALYSES, PHASE I

DATE	7/13-14/77	7/14-15/77	7/15-16/77	7/16-17/77	7/18-19/77	7/19-20/77	7/20-21/77	7/21-22/77
PROXIMATE ANALYSIS								
As Received								
% Moisture	10.38	12.85	12.21	11.77	11.95	11.93	11.80	12.34
% Ash	9.01	6.75	7.44	6.84	6.45	6.31	6.05	9.27
% Volatile	35.27	38.11	38.36	38.41	39.53	39.13	39.19	37.81
% Fixed Carbon	45.34	42.29	41.99	42.99	42.07	42.63	42.96	40.59
BTU	11392	10866	10903	11091	11106	11176	11199	10630
% Sulfur	.73	.47	.46	.39	.46	.41	.41	.48
Dry Basis								
% Ash	10.05	7.74	8.47	7.75	7.33	7.16	6.86	10.57
% Volatile	39.36	43.73	43.70	43.53	44.89	44.43	44.43	43.13
% Fixed Carbon	50.59	48.53	47.83	48.72	47.78	48.41	48.71	46.30
BTU	12712	12468	12420	12570	12614	12689	12698	12126
% Sulfur	.82	.54	.52	.44	.52	.47	.46	.55
ULTIMATE ANALYSIS								
As Received								
% Carbon	64.03	61.87	62.08	62.99	63.02	63.15	63.78	60.58
% Hydrogen	4.30	4.35	4.62	4.49	4.51	4.48	4.37	4.16
% Nitrogen	0.27	0.83	1.02	0.71	1.12	1.11	1.08	1.39
% Chlorine	0.13	0.02	.02	0.04	0.04	.08	0.07	.05
% Oxygen (diff.)	11.15	12.86	12.15	12.77	12.45	12.53	12.44	11.73
Dry								
% Carbon	71.45	70.99	70.71	71.40	71.57	71.70	72.31	69.11
% Hydrogen	4.80	4.99	5.26	5.09	5.12	5.09	4.96	4.74
% Nitrogen	0.30	0.95	1.16	0.80	1.27	1.26	1.22	1.58
% Chlorine	0.14	0.02	.03	0.04	0.04	.09	0.08	.06
% Oxygen (diff.)	12.44	14.77	13.85	14.48	14.15	14.23	14.11	13.39

TABLE 13. COAL ANALYSES, PHASE II

DATE	8/2-3/77	8/3-4/77	8/4-5/77
PROXIMATE ANALYSIS			
As Received			
% Moisture	11.41	11.95	7.85
% Ash	9.67	11.38	12.50
% Volatile	38.11	37.64	35.02
% Fixed Carbon	40.80	39.02	44.63
BTU	10750	10383	11162
% Sulfur	.50	.62	.75
Dry Basis			
% Ash	10.92	12.93	13.57
% Volatile	43.02	42.75	38.00
% Fixed Carbon	46.06	44.32	48.43
BTU	12134	11792	12113
% Sulfur	.56	.70	.81
ULTIMATE ANALYSIS			
As Received			
% Carbon	60.63	59.14	65.55
% Hydrogen	4.39	4.15	4.26
% Nitrogen	1.08	1.01	1.21
% Chlorine	0.04	0.04	.18
% Oxygen (diff.)	12.28	11.71	7.70
Dry			
% Carbon	68.43	67.16	71.13
% Hydrogen	4.95	4.71	4.62
% Nitrogen	1.22	1.15	1.31
% Chlorine	0.05	0.05	.20
% Oxygen (diff.)	13.87	13.30	8.36

TABLE 14. ASH ANALYSES, PHASE I AND PHASE II

Navajo Unit #3 Ash Analyses[1]

Date	7/13-14/77	7/13-14/77	7/15-16/77	7/15-16/77	7/18-19/77
Sample obtained From	Chamber 8[2]	Ash Silo	Chamber 8	Chamber 8	Chamber 8
Time	04:40	05:20	04:20	04:58	05:00
Li_2O	0.01	0.01	0.01	0.01	0.01
Na_2O	1.96	1.80	1.68	1.77	1.90
K_2O	1.18	1.25	1.37	1.34	1.36
MgO	2.00	1.75	2.00	1.95	2.00
CaO	9.85	7.36	7.85	8.24	8.09
Fe_2O_3	5.61	5.46	5.91	6.03	5.73
Al_2O_3	20.2	24.2	23.8	22.3	22.1
SiO_2	54.4	57.6	58.2	57.0	57.4
TiO_2	0.90	0.95	1.00	0.95	1.00
P_2O_5	0.51	0.47	0.43	0.57	0.39
SO_3	0.79	0.68	0.51	0.60	0.66
LOI	0.66	0.84	0.41	0.43	0.58
Soluble $SO_4^=$	0.59	0.50	0.56	0.49	0.54

[1]Analyses obtained from ignited samples except Soluble $SO_4^=$.

[2]Ash samples from Chamber #8 were obtained from the inlet hopper, which received ash from half of Chamber #8.

TABLE 14
(Continued)

Navajo Unit #3 Ash Analyses[1]

Date	7/18-19/77	7/21-22/77	7/21-22/77	8/2-3/77	8/3-4/77	8/4-5/77
Sample obtained From	Ash Silo	Chamber 8[2]	Ash Silo	Ash Silo	Ash Silo	Ash Silo
Time	05:30	02:17	02:40	AM	AM	04:40
Li_2O	0.01	0.01	0.01	0.01	0.01	0.01
Na_2O	1.65	1.42	1.61	2.20	1.80	1.84
K_2O	1.34	1.05	1.20	1.27	1.38	1.83
MgO	1.90	1.85	1.90	1.70	1.65	1.65
CaO	7.55	6.73	7.93	7.12	6.25	5.51
Fe_2O_3	5.78	5.05	5.57	5.25	5.34	5.68
Al_2O_3	22.2	25.5	22.0	20.1	20.8	20.8
SiO_2	57.3	56.3	58.0	56.9	60.2	61.5
TiO_2	0.95	1.00	0.95	0.95	1.00	1.00
P_2O_5	0.41	0.31	0.33	0.50	0.34	0.32
SO_3	0.62	0.71	0.69	0.68	0.58	0.56
LOI	0.70	2.62	1.14	1.14	1.62	0.78
Soluble $SO_4^=$	0.53	0.53	0.53	0.53	0.44	0.45

[1]Analyses obtained from ignited samples except Soluble $SO_4^=$.

[2]Ash samples from Chamber #8 were obtained from the inlet hopper which received ash from half of Chamber #8.

Table 15

Navajo Generating Station
Unit #3 Outlet of Chamber #8
Gas Analyses

Phase I

Date	Time	Volume, %			ppm, v/v	
		CO_2	O_2	H_2O	SO_2	SO_3
7/11-12/77	03:30			9.4		
7/12-13/77	23:00-23:30	14.8	4.4	9.7		
	00:00-01:00				405	<0.5
	01:00-02:00				415	<0.5
	02:00-03:00				405	<0.5
	03:00-04:00				400	<0.5
	04:00-04:30	15.2	5.0			
	05:00			9.7		
7/13-14/77	22:30-23:00	15.2	4.6			
	23:00-00:30			8.7		
	00:30-01:30				405	<0.5
	01:30-03:00				430	<0.5
	03:00-04:00			8.8	415	<0.5
	04:30-05:00	15.0	5.2			
7/14-15/77	22:30-23:00	14.8	4.2	9.4		
	23:00-00:30				435	<0.5
	01:00-02:00	14.8	4.6		460	<0.5
	02:00-03:00				450	<0.5
	03:00-04:30				460	<0.5
	05:00-05:30	14.6	4.5	9.3		
7/15-16/77	22:30-23:00	15.1	4.3	9.9		
	23:30-01:00				455	<0.5
	01:00-02:00				465	<0.5
	02:00-03:30				465	<0.5
	03:30-05:00	15.0	4.2		460	<0.5
	05:00			9.9		
7/16-17/77	22:30-23:00	15.2	4.5			
	23:30-00:00			9.6		
	00:00-01:00				400	<0.5
	01:00-02:00				380	<0.5
	02:00-03:30				390	<0.5
	03:30-04:30				390	<0.5
	04:30-05:00	14.4	5.2	9.9		
7/18-19/77	22:00-23:00	15.1	4.5	9.6		
	23:00-01:00				410	<0.5
	01:00-02:00				425	<0.5
	02:00-03:00				430	<0.5
	03:00-04:30				425	<0.5
	05:00-05:30	14.6	4.8	10.2		
	05:30-06:15				415	<0.5

Table 15(Con't)

Date	Time	Volume, %			ppm, v/v	
		CO_2	O_2	H_2O	SO_2	SO_3
7/19-20/77	22:00-23:00	14.8	4.4			
	23:00-00:00			9.7		
	00:00-01:00				420	<0.5
	01:00-02:00				400	<0.5
	02:00-03:30				400	<0.5
	03:30-04:00	15.0	4.2	9.4	420	<0.5
7/20-21/77	22:00-23:00	14.3	5.3	9.8		
	23:00-01:00				420	<0.5
	01:00-02:00				430	<0.5
	02:00-03:00				420	<0.5
	03:00-04:00				430	<0.5
	04:00-04:30			9.6		
7/21-22/77	22:00-22:30	15.3	4.1	10.2		
	22:30-00:00				430	<0.5
	00:00-01:00				490	<0.5

Table 16

Navajo Generating Station
Unit #3
Gas Analyses
Phase II

8/1-2/77 Stack Gas Analyses

Time	Volume, % CO_2	O_2	H_2O
01:00-01:30	12.8	5.8	
03:30			8.7

8/2-3/77 Main Inlet Orsat Traverse
Main Inlet A Side

Port #	Time	Volume, % CO_2	O_2
1	22:45	15.9	4.7
2	21:30	14.9	4.2
3	22:00	15.3	4.5
4	23:15	15.5	4.1
5	03:35	14.4	4.4
6	03:45	14.8	4.4
7	04:00	14.7	4.9
8	23:30	15.1	4.3
9	23:45	14.9	4.2
10	00:15	14.7	4.1
11	00:30	14.2	4.1
12	02:00	14.7	5.0
13	02:15	14.9	5.0
14	02:30	15.4	4.3
15	02:40	15.4	4.6
16	02:55	15.6	4.2
Main Inlet B Side			
17	03:00	15.0	4.8
18	02:45	14.7	5.1
19	02:40	14.9	4.9
20	02:30	14.4	4.8
21	02:20	15.0	4.7
22	02:05	14.9	4.7
23	00:50	14.3	4.1
24	00:35	14.2	4.2
25	00:25	14.4	4.4
26			
27	23:50	14.9	4.3
28	23:35	15.0	4.4
29	23:20	15.0	4.0
30	22:55	14.6	4.7
31	22:30	14.6	4.8
32	22:10	15.2	4.2

Table 16 (Cont'd)

Stack Gas Analyses

Time	Volume, % CO_2	O_2	H_2O	ppm, v/v SO_2	SO_3
03:15-03:30	14.1	5.7	8.6		
03:30-04:15				400	<0.5

8/3-4/77 Simultaneous Main Inlet and Stack Orsats

Inlet Port #	Time	Inlet CO_2	O_2	Stack CO_2	O_2
1	22:20	15.0	3.6	14.7	5.6
3	23:40	16.0	3.6	15.4	5.2
9	22:50	15.3	3.5	14.8	5.6
13	23:05	15.4	3.2	15.1	5.7
16	23:20	15.5	4.1	15.1	5.6
17	00:55	16.0	3.0	14.2	5.4
21	01:00	15.8	3.5	14.5	5.3
25	01:10	15.8	3.6	14.2	5.4
29	01:20	16.0	4.7	14.5	5.0
32	01:35	15.9	3.0	14.1	5.4
	avg.	15.7	3.6	14.7	5.4

Stack Gas Analyses

Time	Volume, % H_2O	ppm,v/v SO_2	SO_3
02:45	9.5		
03:00-03:30		415	<0.5
03:30-04:00		445	<0.5

8/4-5/77 Simultaneous Main Inlet and Stack Orsats

Port #	Time	Inlet CO_2	O_2	Stack CO_2	O_2
1	21:50	14.0	4.6	13.8	5.7
5	22:13	15.1	3.9	14.1	5.6
8	22:20	15.4	4.6	13.8	5.7
13	22:35	15.6	4.2	14.0	5.8
16	22:45	14.8	4.6	14.2	5.7
17	01:25	15.4	3.8	13.7	5.5
20	01:15	15.2	4.3	13.8	6.0
24	01:00	14.8	4.2	14.0	5.9
28	00:53	14.9	3.6	14.2	5.4
32	00:45	15.8	4.1	14.1	5.7
	avg.	15.1	4.2	14.0	5.7

Table 16 (Cont'd)

Stack Gas Analyses

Time	Volume, % H_2O	ppm,v/v SO_2	ppm,v/v SO_3
03:00	8.9		
03:30-04:00		500	<0.5
04:00-04:30		490	<0.5

Voltage Current Measurements

The voltage-current characteristics of the precipitator were monitored during the test program as follows:

- Voltage divider resistor assemblies were attached to the high voltage bus-bars feeding Chambers 7 and 8 during Phase I. Corrected secondary voltages and voltage waveform photos from an oscilloscope were obtained.

- Voltage-current curves were obtained for each electrical field of Chamber 7 and 8 during Phase I.

- Secondary and primary voltages and currents were obtained from panel meter readings for Chambers 7 and 8 during Phase I, and from all power supplies on the Unit 3 precipitator during Phase II.

Table 17 contains the average electrical operating parameters for Chambers 7 and 8 during each test period of Phase I. Table 18 contains panel meter readings and corrected secondary voltages for the voltage-current curves obtained on July 13, 1977. These data are plotted in Figure 21. The remainder of the voltage-current curves and the meter readings obtained during Phase I for each transformer rectifier set are presented in Appendix 3. The data recorded from all transformer-rectifier control panels during Phase II are also given in the Appendix. These data are discussed further in the theoretical analysis section.

Elemental Composition as a Function of Particle Diameter

Due to the elevated sampling temperatures, it was not possible to use the substrates developed by Ensor[10] for obtaining size-classified samples from impactor stages for subsequent analysis by an ion-excited x-ray technique (IXA). Greased impactor substrates exhibit unacceptable weight losses at 350°C, and therefore only conditioned glass fiber material was suitable as a substrate. Unfortunately, these materials provide an unacceptable background for the IXA method, and it was therefore necessary to use a five-stage series cyclone assembly for obtaining size fractionated samples.

The cyclone assembly was operated at single points at the inlet and outlet of Chamber 8 (Phase I) and at the main inlet location (Phase II). Calculated cut points and pertinent operating data for the cyclones are presented in Table 19. Note that it was necessary to operate at the precipitator outlet for almost 47 hours to obtain approximately 40 mg of sample in cyclone V. Comparisons between differential mass distributions obtained with the cyclone assembly and the impactor traverses are given in Figures 22-24. The lack of agreement may be due in part to

Table 17

Navajo Generating Station
Unit #3
Average Voltage and Current Meter Readings

Chambers 7 & 8

TR#	Primary Volts	Primary Amps	Secondary KV	Secondary MA	Corrected KV[1]	Spark Rate, sparks/min.
7/12-13/77						
H	194.0	103.5	28.9	437.0	26.7	112
G	198.5	123.2	27.1	558.5	25.8	92
F	200.0	179.5	23.2	1030.5	21.8	60
E	182.5	179.0	24.3	1022.5	20.8	38
D	175.4	250.0	21.5	1139.5	19.5	16
C	170.0	253.2	20.0	1420.0	17.3	15
7/13-14/77						
H	178.2	69.7	28.8	281.2	26.8	69
G	178.7	76.8	25.7	384.3	25.2	88
F	195.0	156.6	23.1	804.3	22.2	61
E	180.6	180.0	23.9	987.5	21.2	51
D	176.2	245.0	21.5	1156.2	19.8	75
C	170.0	249.2	20.3	1386.8	17.4	12
7/12-15/77						
H	185.8	71.6	30.2	305.0	27.5	93
G	195.0	92.5	27.6	448.3	26.1	33
F	201.6	169.5	23.7	943.3	22.3	42
E	192.5	193.9	24.2	1066.7	20.9	66
D	177.1	252.1	21.4	1179.1	19.0	--
C	175.0	251.6	21.3	1640.0	18.0	--
7/15-16/77						
H	192.5	85.6	30.8	353.1	27.9	81
G	198.1	105.6	27.8	521.2	25.9	63
F	202.5	181.8	23.8	978.7	22.5	63
E	188.1	195.6	24.1	1081.2	21.1	28
D	180.0	246.0	22.3	1125.6	19.9	53
C	176.6	255.6	21.2	1430.6	17.8	28

1. Obtained with voltage divider assembly.

Table 17 (Con't)

TR#	Primary Volts	Primary Amps	Secondary KV	Secondary MA	Secondary Corrected KV	Spark Rate, sparks/min.
7/16-17/77						
H	190.0	80.7	30.0	337.1	27.6	109
G	182.8	77.8	26.8	365.7	24.7	39
F	200.0	172.5	23.5	948.5	22.5	50
E	185.0	197.8	24.0	1102.8	21.0	35
D	180.7	252.5	22.1	1153.5	16.3	61
C	175.0	254.2	20.8	1417.0	17.0	20
7/18-19/77						
H	194.7	101.5	29.9	417.0	27.5	78
G	183.0	75.0	26.1	391.0	24.2	82
F	196.5	169.0	22.9	892.0	21.5	43
E	180.0	168.5	23.5	1079.0	20.3	33
D	171.0	219.5	21.7	948.0	19.9	40
C	172.9	251.8	20.5	1433.0	17.5	25
7/19-20/77						
H	195.8	100.0	30.0	411.6	27.0	75
G	189.1	147.5	26.8	636.6	25.3	125
F	200.0	177.5	23.1	1025.8	22.6	70
E	189.5	200.0	23.0	1100.0	20.6	--
D	180.0	253.6	21.5	1206.6	18.9	25
C	170.0	250.0	20.3	1417.5	16.9	--
7/20-21/77[a]						
H	195.0	88.3	30.2	353.0	27.2	45
G	209.0	147.0	27.4	727.0	25.8	125
F	202.0	185.0	23.4	1043.0	22.8	60
E	186.7	196.7	23.9	1116.0	21.4	33
D	176.0	228.0	21.2	1083.0	18.6	160
C	177.3	250.0	20.5	1400.0	17.1	40
7/21-22/77[a]						
H	192.5	65.0	31.1	260.0	28.0	40
G	203.0	123.0	27.8	620.0	26.2	320
F	205.0	185.0	23.8	1050.0	23.2	80
E	182.5	177.5	24.5	930.0	21.9	160
D	175.0	245.0	22.0	1060.0	19.3	60
C	180.0	250.0	21.2	1430.0	17.7	30

a) Corrected KV calculated from ratio of meter to corrected KV data of 7/19-20/77 because voltage divider data not available for 7/20-22/77.

TABLE 18

Panel meter readings obtained for voltage-current curves and corrected secondary voltages as measured with voltage dividers

Chambers 7 & 8, 7/13/77, 'H' Field

Primary Voltage	Primary Current	Spark Rate	Secondary Voltage	Secondary Current	Corrected Secondary Voltage	Current Density
V	A	Sparks/ min	KV	MA	KV	nA/ cm^2
85	--	--	19	--	18.3	--
160	20	--	28.4	100	26.8	4.3
170	50	100	29.5	200	27.1	8.5
180	65	120	28.5	260	27.4	11.1
185	75	150	29	320	27.2	13.7
190	100	300	29	400	27.4	17.1
195	110	500	28.8	450	26.8	19.2

Chambers 7 & 8, 7/13/77, 'G' Field

75	--	--	18.7	--	16.8	--
150	20	--	25	100	24.2	4.3
160	40	20	25.5	200	25.2	8.5
170	70	50	26.5	300	25.5	12.8
180	80	100	27	400	25.7	17.1
190	100	150	26.5	500	25.3	21.4
195	120	350	26	600	25.0	25.6

Chambers 7 & 8, 7/13/77, 'F' Field

105	--	--	19	20	17.9	.9
135	20	--	21.4	100	20.4	4.3
150	50	--	22.1	200	21.1	8.5
154	68	--	22.2	300	21.3	12.8
165	85	--	22.3	400	21.4	17.1
170	110	--	22.4	500	21.7	21.4
180	125	--	22.6	600	21.5	25.6
185	145	--	22.4	700	21.5	29.9
190	157	--	22.5	800	21.8	34.2
195	170	50	23	900	22.1	38.4
200	180	450	23	1000	20.3	42.7

TABLE 18 (Con't)

Primary Voltage V	Primary Current A	Spark Rate Sparks/min	Secondary Voltage KV	Secondary Current MA	Corrected Secondary Voltage KV	Current Density nA/cm^2
Chambers 7 & 8, 7/13/77, 'E' Field						
100	--	--	20	--	17.5	--
130	20	--	23	100	20.1	4.3
140	50	--	23	200	20.5	8.5
150	67	--	23.5	300	20.6	12.8
155	80	--	23.5	400	20.7	17.1
157	105	--	24	500	20.8	21.4
165	120	--	24	600	20.8	25.6
170	140	--	23.8	700	20.9	29.9
175	155	20	23.8	800	20.8	34.2
180	170	30	24	900	21.1	38.4
185	185	125	23.5	1000	21.0	42.7
Chambers 7 & 8, 7/13/77, 'D' Field						
105	--	--	19.5	--	17.7	--
134	50	--	20.5	100	18.7	4.3
140	102	--	20.8	250	18.9	10.7
148	132	--	20.9	400	19.1	17.1
150	150	--	21	500	19.1	21.4
160	180	20	21.3	650	19.2	27.8
164	200	40	21.4	800	19.1	34.2
168	215	50	21.5	900	19.3	38.4
172	233	100	21.5	1000	19.5	42.7
175	245	120	22	1100	19.7	47.0
180	257	200	22.4	1200	19.8	51.3
Chambers 7 & 8, 7/13/77, 'C' Field						
110	--	--	19	100	17.2	4.3
115	55	--	19.8	250	17.4	10.7
138	90	--	20	400	17.3	17.1
140	110	--	20	500	17.2	21.4
148	138	--	20	650	17.1	27.8
150	155	--	20	750	16.9	32.0
155	180	--	20	900	16.9	38.4
160	200	--	20	1000	16.9	42.7
164	220	--	20	1150	17.1	49.1
164	234	--	20	1250	17.2	53.4
170	252	--	20.4	1400	17.4	59.8
175	262	--	20.8	1500	18.0	64.1

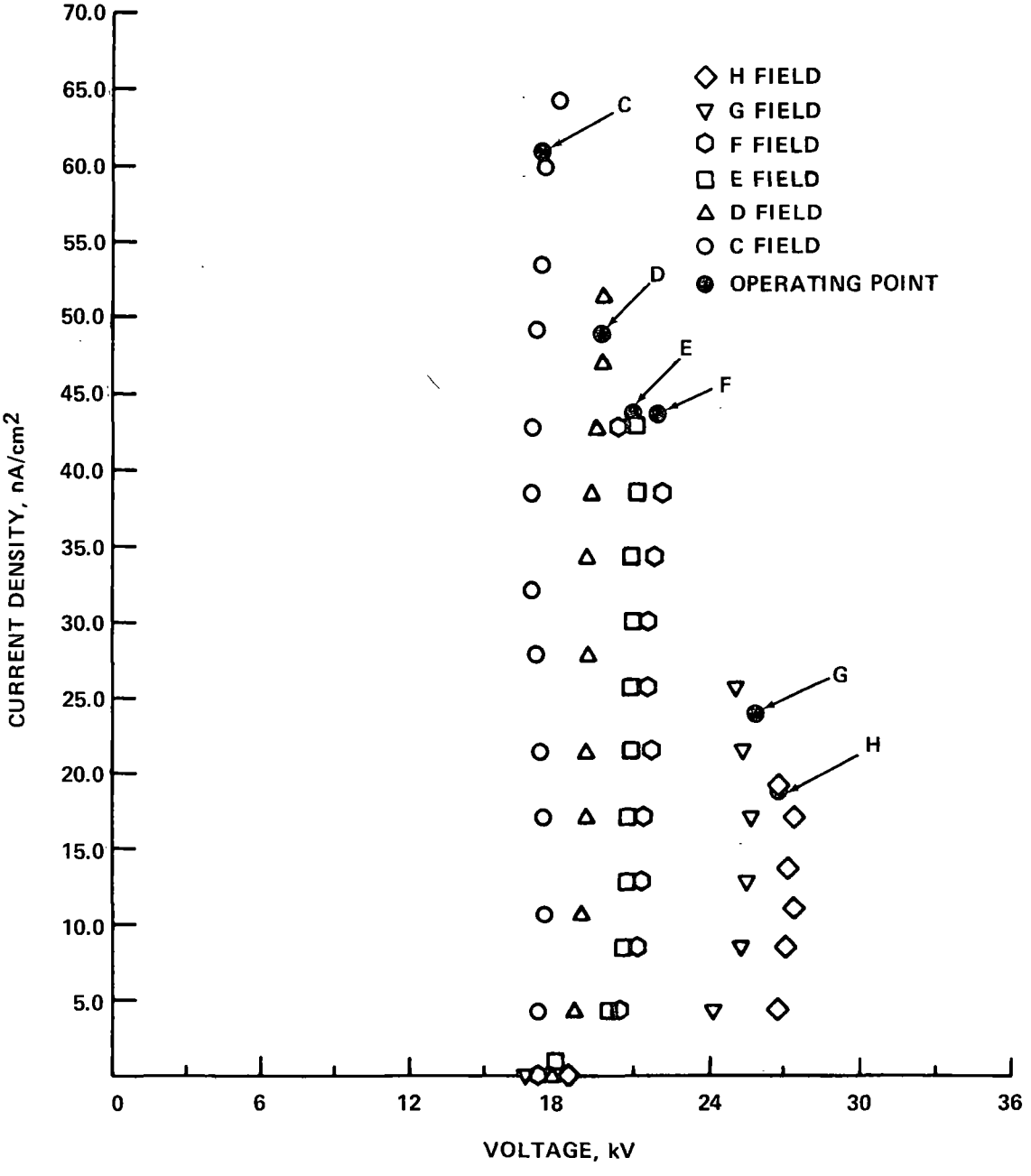

Figure 21. Voltage-current curves for Chamber 7 and 8, July 12-13, 1977.

TABLE 19. CYCLONE ASSEMBLY OPERATING PARAMETERS

Run #	CYC 3		CYC 5		CYC 7	
Location	Chamber #8, Inlet		Chamber #8, Outlet		Main Inlet	
Date	7/14-15/77		7/18-19/77		8/3-4/77	
Cyclone	Wt.,g	D_{50},μm	Wt.,g	D_{50},μm	Wt.,g	D_{50},μm
I	12.6246	7.2	0.3762	6.8	5.7684	6.8
II	3.4288	3.5	0.2016	3.2	9.1620	3.2
III	1.2157	2.3	0.2046	2.1	3.2084	2.1
IV	0.7791	1.2	0.2293	0.96	1.4835	0.96
V	0.1002	0.5	0.0421	0.46	0.5308	0.45
F	0.1179		0.0336		0.1232	

Ambient Pressure, "Hg	25.57	25.44	25.75
Stack Pressure, "Hg	24.76	24.76	24.76
Ambient Temperature,°F	85	85	100
Ambient Temperature,°C	29.4	29.4	37.8
Stack Temperature,°F	685	630	700
Stack Temperature,°C	362.8	323.2	371.1
Flowrate, ACFM	1.068	1.107	1.201
Flowrate, Am^3/min	0.0302	0.0314	0.0340
Sample duration, minutes	270	2795	258
Maximum Particle Diameter, μm	32	32	107
Moisture,%	9.2	9.5	9.5

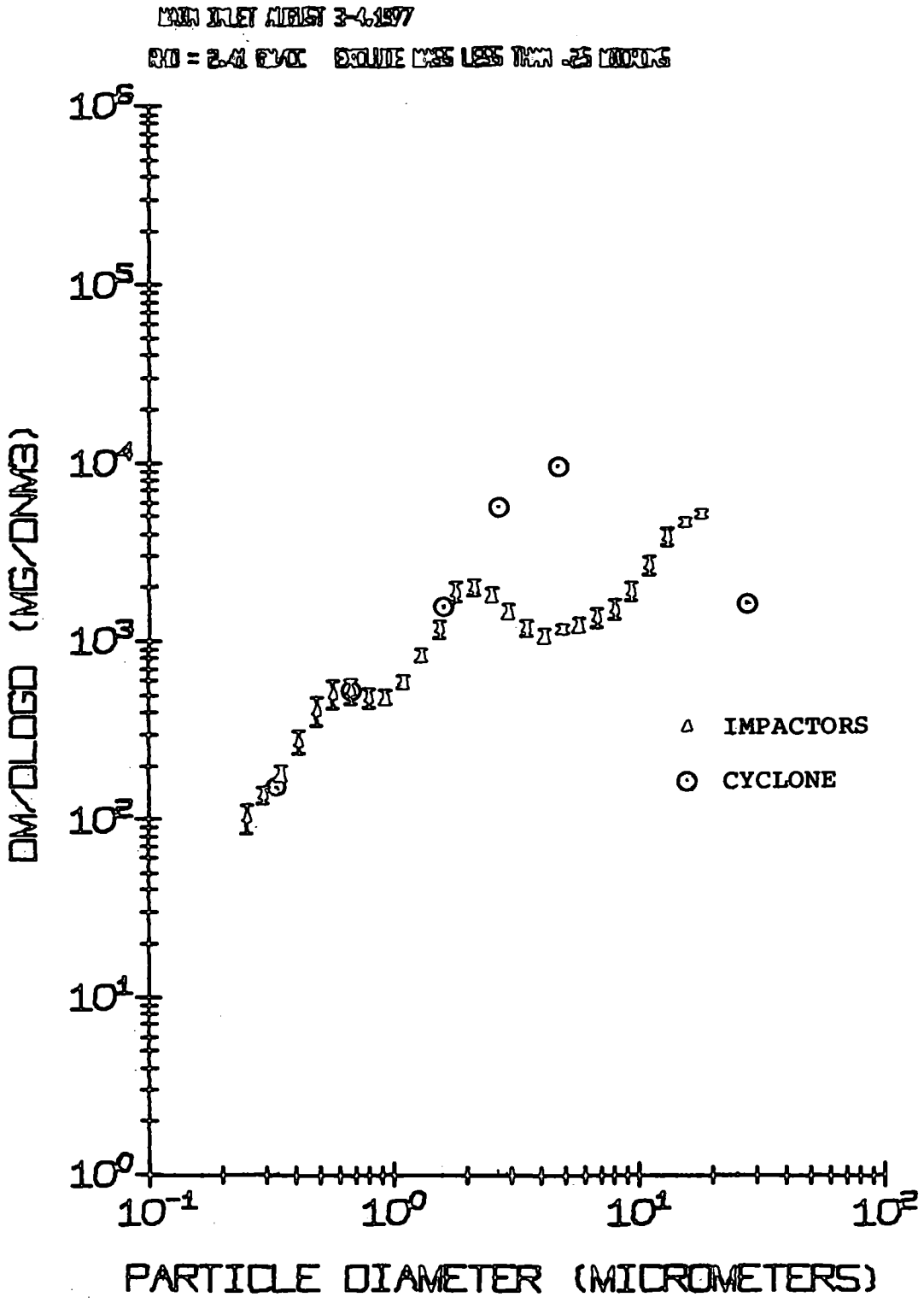

Figure 22. dM/dlogD vs. particle diameter for all impactors operated at the main inlet of the #3 precipitator and cyclone run #7.

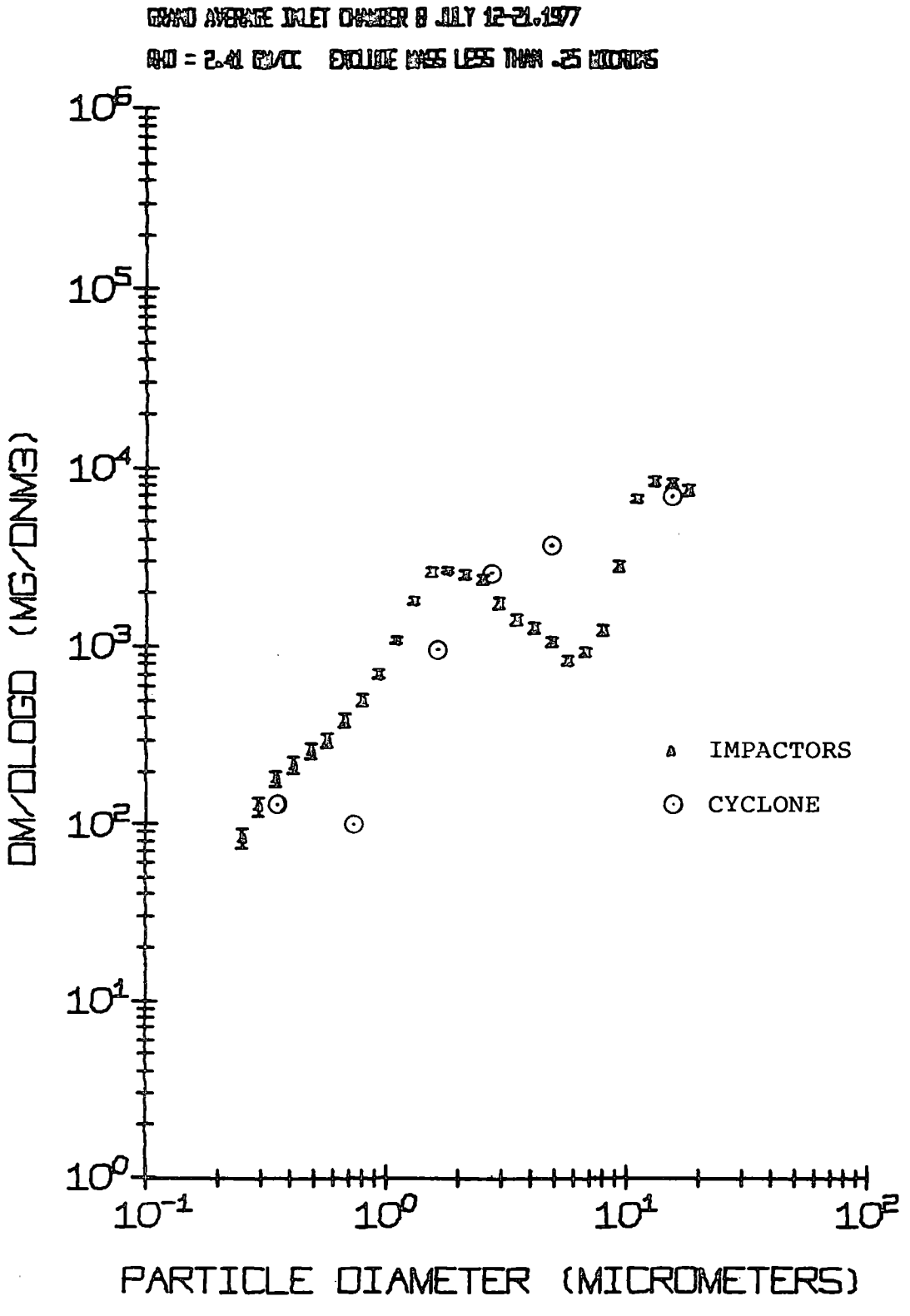

Figure 23. dM/dlogD vs. particle diameter for all impactors operated at the inlet of chamber #8 and cyclone run #3.

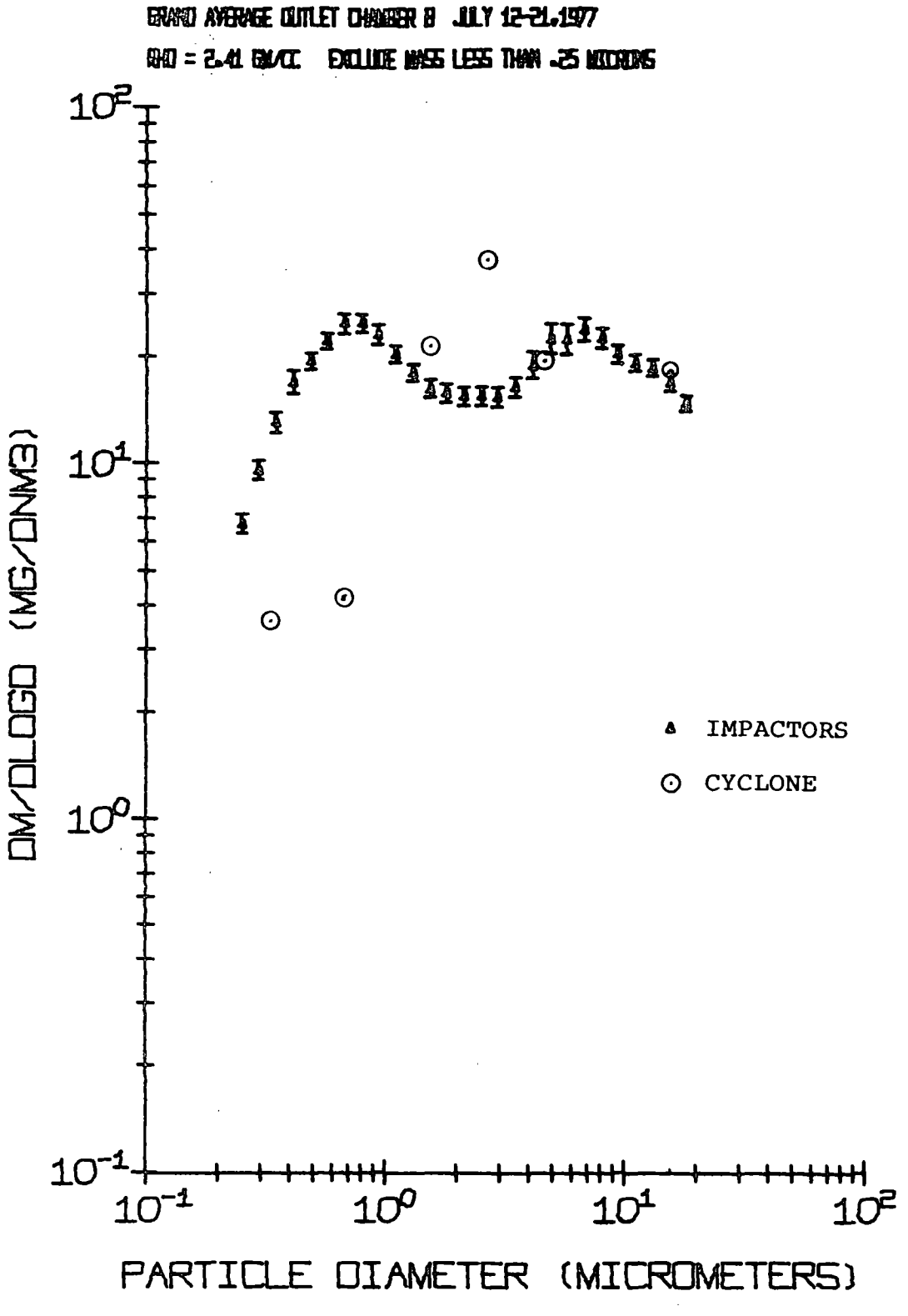

Figure 24. dM/dlogD vs. particle diameter for all impactors operated at the outlet of chamber #8 and cyclone run #5.

differences in integration time and mass concentration gradients, but it is also possible that the theoretical extrapolation of ambient temperature calibration data for both systems introduce significant sizing errors at 350°C. It appears that better agreement was obtained at the inlet (Brink vs. cyclone) than at the outlet (Andersen vs. cyclone).

Table 20 contains the mass concentrations per cyclone which were used in the calculation of elemental concentrations and elemental penetrations. Table 21 presents the data obtained by Crocker Nuclear Laboratories as parts per million by weight from samples of the collected material in each cyclone. The back-up filter, since it consisted of glass fiber, was again unsuitable for this type of analysis. Table 22 gives elemental penetration as a function of particle diameter across Chamber 8, and Figure 25 gives penetration as a function of particle diameter for selected elements and for the total mass collected with the cyclones. These data indicate the trace elements generally follow the mass collection curve. It should be noted that the penetrations are calculated from sequential single point samples, and are therefore qualified as "apparent" penetrations.

Enrichment ratios were computed as suggested by Ensor,[11] except that all concentrations were normalized to iron. These data are presented in Appendix 4, along with elemental concentrations in units of mass per volume of dry standard flue gas as a function of particle diameter.

Summary of Results from Previous Tests

As stated previously, Southern Research Institute conducted field tests on Chamber 8 of Unit 3 under the sponsorship of EPRI and the Salt River Project prior to the performance of the EPA test series. This section will summarize the results from this work as it relates to the objectives of the EPA project. The objectives of the EPRI-SRP series were:

(1) Examine the effect of gas velocity distribution on precipitator performance.

(2) Conduct a rapper optimization study by changing rapping system activation time intervals.

(3) Determine whether emissions are increased as a result of hopper in-leakage.

(4) Determine the contribution of electrode rapping to particulate emission from the precipitator.

TABLE 20. MASS CONCENTRATION AND EFFICIENCY FROM CYCLONE ASSEMBLY (PHASE I)

Cyclone	Average D_{50}	Mass Concentration, mg/DSCM Inlet(Run 3)	Outlet(Run 5)	Efficiency
1	7.0	4.45×10^{3}	11.8	99.73
2	3.35	1.21×10^{3}	6.31	99.48
3	2.2	4.29×10^{2}	6.40	98.51
4	1.08	2.75×10^{2}	7.17	97.39
5	0.48	3.53×10^{1}	1.32	96.26
	Filter	4.16×10^{1}	1.05	97.48
TOTAL		6.44×10^{3}	34.05	99.47

TABLE 21

CYCLONE RUN #3 CHAMBER #8, INLET 7/14-15/77
CONCENTRATION OF ELEMENTS LISTED IN PARTS PER MILLION BY WEIGHT

Cyclone #	K	Ca	Ti	Ba	V	Cr	Mn	Fe	Cu
1	4728.4	34145.6	5561.5	212.0*	613.8	40.0*	77.8	28767.0	49.3
2	8193.7	50201.5	7494.2	486.0*	1142.4	88.0*	76.0*	39505.5	83.1
3	7940.3	50712.3	7350.4	650.0*	1461.3	114.0*	100.0*	40076.4	84.6
4	7810.0	45960.6	6928.7	864.0*	1512.4	691.2	134.0*	38931.5	95.3
5	9598.3	58729.0	10722.9	1821.0*	3151.5	307.0*	427.1	47743.1	207.8

	Zn	As	Pb	Br	Rb	Sr	Zr	Mo
1	66.8	12.5	18.7	5.0*	48.1	1429.9	157.3	25.0*
2	177.3	20.8	61.3	14.0*	66.6	1775.4	152.3	43.6
3	267.9	77.6	111.2	20.0*	70.8	1704.1	128.8	92.0*
4	364.0	37.0	114.4	27.0*	52.8	1443.9	142.6	334.6
5	385.3	45.5	188.4	57.0*	68.8	2211.7	145.0*	261.0*

CYCLONE RUN #5 CHAMBER #8, OUTLET 7/18-19/77

	K	Ca	Ti	Ba	V	Cr	Mn	Fe	Cu
1	5952.3	49867.9	6761.8	504.0*	1443.1	88.0*	76.0*	33208.5	79.5
2	6157.0	50105.6	6770.0	539.0*	1468.3	93.0*	81.0*	32578.9	59.9
3	6786.6	47390.7	6726.7	697.0*	1586.9	115.0*	101.0*	32709.6	113.5
4	7116.0	48112.2	7525.1	892.0*	1971.4	203.6	129.0*	35511.3	102.6
5	6039.3	47250.7	7377.8	1084.0*	2566.9	176.0*	158.0*	31582.0	116.5

	Zn	As	Pb	Br	Rb	Sr	Zr	Mo
1	194.0	9.0*	114.5	14.0*	43.8	1732.8	110.6	66.0*
2	202.5	10.0*	117.3	16.0*	42.8	1712.6	98.7	75.0*
3	232.4	30.3	99.7	22.0*	51.8	1558.6	97.6	100.0*
4	351.8	32.0	117.3	28.0*	56.3	1619.0	112.0	131.0*
5	372.3	51.6	113.3	36.0*	32.1	1642.5	91.0*	164.0*

CYCLONE RUN #7 MAIN INLET 8/3-4/77

	K	Ca	Ti	Ba	V	Cr	Mn	Fe	Cu
1	6073.9	25109.3	5463.5	206.0*	633.3	39.0*	106.2	30249.1	41.8
2	8209.9	29333.3	6210.3	325.0*	772.3	59.0*	134.6	33791.8	53.2
3	9474.1	32191.6	7180.4	424.0*	827.5	77.0*	129.1	36951.3	69.7
4	10166.6	33178.7	7043.5	628.0*	1229.5	111.0*	183.7	37301.9	78.9
5	10064.2	30901.4	7542.7	670.0*	1278.1	120.0*	190.5	40185.6	76.6

	Zn	As	Pb	Br	Rb	Sr	Zr	Mo
1	53.0	11.5	25.2	5.0*	65.2	1305.6	204.7	24.0*
2	83.9	26.5	23.3	9.0*	87.0	1432.6	182.3	40.0*
3	150.7	22.4	61.3	12.0*	90.2	1515.3	147.6	53.0*
4	220.2	24.7	88.5	19.0*	87.1	1420.1	129.5	85.0*
5	240.6	48.0	92.4	20.0*	104.8	1534.1	119.7	90.0*

*Denotes upper limit of element not found.

TABLE 22

ELEMENTAL PENETRATION ACROSS CHAMBER #8

Avg. D_{50}	Cyclone #	K	Ca	Ti	Ba	V	Cr	Mn	Fe	Cu
7.00	1	0.0033	0.0039	0.0032	0.0063*	0.0062	0.0058*	0.0026*	0.0031	0.0043
3.35	2	0.0039	0.0052	0.0047	0.0058*	0.0067	0.0055*	0.0056*	0.0043	0.0038
2.20	3	0.0128	0.0140	0.0137	0.0160*	0.0162	0.0151*	0.0151*	0.0122	0.0200
1.08	4	0.0238	0.0273	0.0284	0.0270*	0.0340	0.0077	0.0251*	0.0238	0.0281
0.48	5	0.0235	0.0300	0.0257	0.0222*	0.0304	0.0214*	0.0138*	0.0247	0.0209

		Zn	As	Pb	Br	Rb	Sr	Zr	Mo
7.00	1	0.0077	0.0019*	0.0162	0.0074*	0.0024	0.0032	0.0019	0.0070*
3.35	2	0.0060	0.0025*	0.0100	0.0060*	0.0034	0.0050	0.0034	0.0090*
2.20	3	0.0130	0.0058	0.0134	0.0164*	0.0109	0.0137	0.0113	0.0162*
1.08	4	0.0252	0.0226	0.0268	0.0271*	0.0278	0.0293	0.0205	0.0102*
0.48	5	0.0360	0.0423	0.0224	0.0235*	0.0174	0.0277	0.0234*	0.0234*

*Denotes upper limit of element not found.

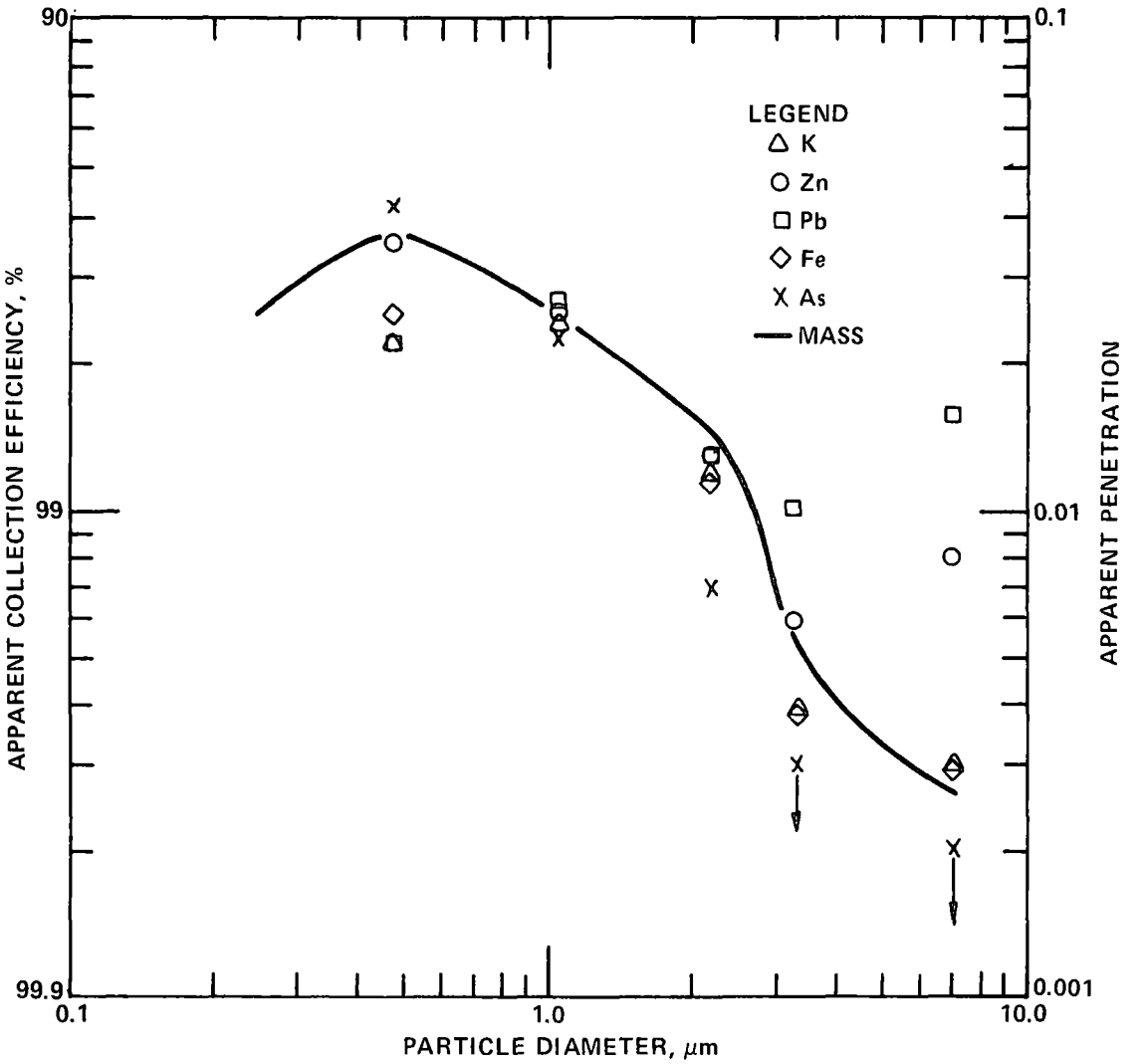

Figure 25. Apparent elemental collection efficiency. (Chamber 8)

The principal conclusions derived from the test results were:

(1) The fraction of emissions attributable to rapping was decreased by an increase in the outlet field rapping intervals.

(2) A reduction in the normalized standard deviation of the gas velocity distribution from 44% to 17% (at the inlet) did not appear to significantly improve collection efficiency under the conditions of the test.

(3) The two principal causes of the lower than desired performance of the unit are the relatively low operating voltages and the relatively low values of specific collecting area.

(4) The pressurization and depressurization of the ash removal system did not cause a measurable change in emissions from chamber 8.

(5) Half-load operation can have serious detrimental effects on the performance of the precipitator.

These conclusions will be discussed in more detail in the subsequent section concerning theoretical analysis.

The measurement of particulate emissions resulting from electrode rapping were conducted by (1) using an extractive sampling system with a size selective diluter and an optical particle counter, (2) traversing the duct with impactor and mass train sampling systems using an alternating sampling plan in which rappers were energized and subsequently de-energized.

Figure 26 contains data for concentration of 6-12 μm diameter particles vs time obtained at the outlet of chamber 8 with the extractive sampling system. Each data point on the graph represents a 10-minute integration time. Points A and C correspond with the inlet and outlet field raps, respectively. The data points labeled C will necessarily include inlet and outlet field raps due to the 10-minute integration time. The center fields and wire rappers are not distinguishable on this graph from the background data, but were noticeable when they occurred. Note that the outlet fields (C and D) exhibit two large rapping puffs, suggesting layer buildup until rapping forces were sufficient to dislodge the layer.

Figure 27 contains the fractional efficiency data obtained with the EAA and impactor systems with and without electrode rapping. It is apparent that the most pronounced effect of rapping occurs for particle diameters of 2.0 μm and larger. The total mass attributed to rapping, expressed as a fraction of

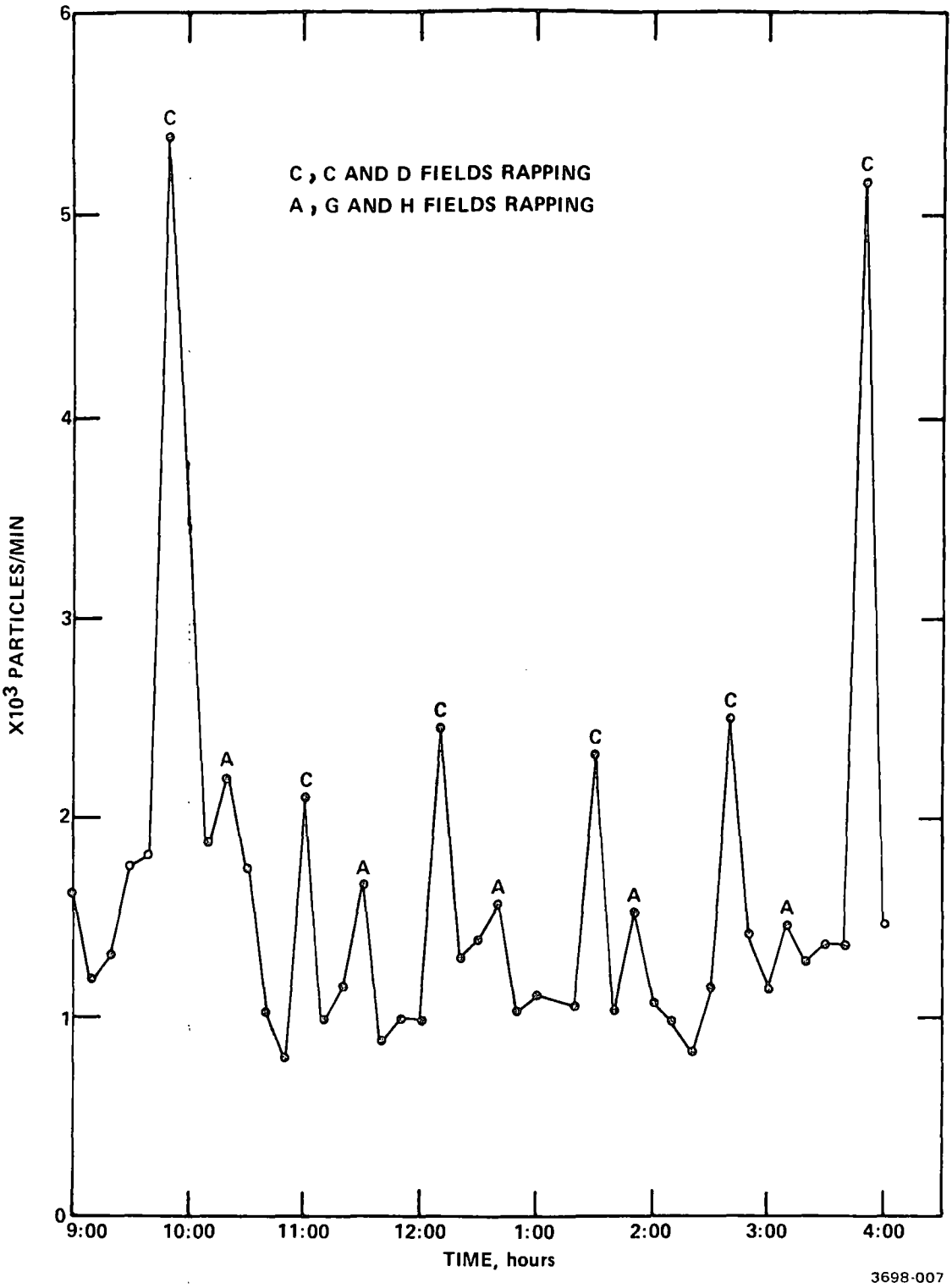

Figure 26. Particles/Minute vs. time for 6-12 micron particles, February 1, 1977.

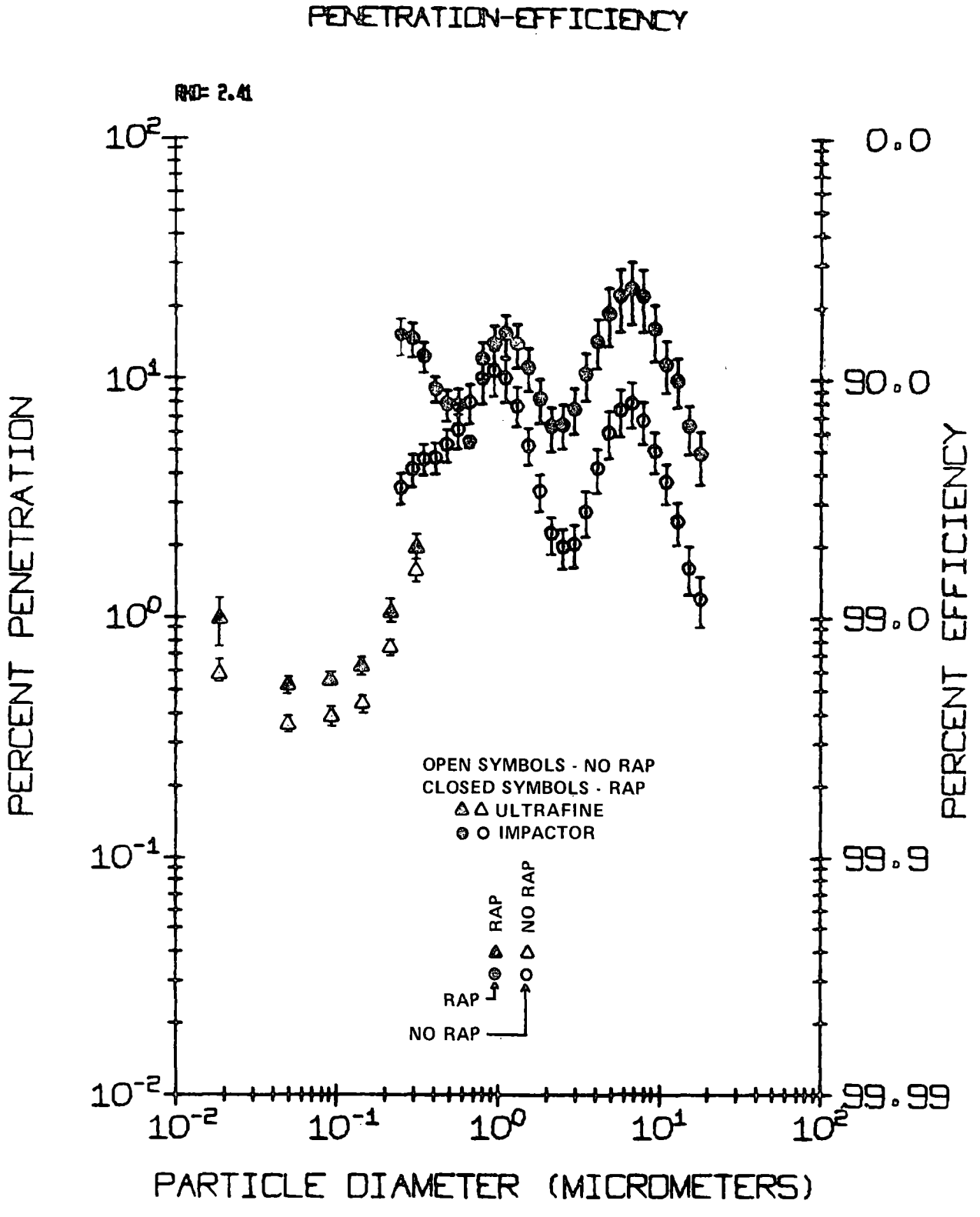

Figure 27. Ultrafine and impactor fractional efficiencies for Rap-No Rap test.

Navajo

outlet emissions, was estimated to range between 44 and 63% based on the impactor and mass train traverses. The performance of chamber 8 was somewhat higher during the EPA-sponsored series (99.2 vs 98.98%), and this is reflected in the fractional efficiency data of Figures 9 and 27.

THEORETICAL ANALYSIS

Voltage-Current Relationships

The collection rate of particulate matter in an electrostatic precipitator is a function of the applied voltage and the resulting corona current. Therefore, an understanding of the factors which limit particle collection rates under a given set of conditions requires an analysis of the relationship between the applied voltage and corona current.

For wire plate geometry, the relationship between applied voltage and the electric field distribution in the space between wire and plate for a given value of current may be obtained by a numerical solution of Poisson's equation and the continuity equation at steady state conditions. The method employed for this calculation is a numerical technique introduced by Leutert and Böhlen[12] in which the applicable partial differential equations are solved simultaneously under boundary conditions for wire-plate geometry. The equations which must be solved are written in discrete form in two dimensions as

$$\frac{\Delta^2 V}{\Delta x^2} + \frac{\Delta^2 V}{\Delta y^2} = \frac{-\rho}{\varepsilon_0} \qquad (1)$$

and

$$\rho^2 = \varepsilon_0 \frac{\Delta V}{\Delta x}\frac{\Delta \rho}{\Delta x} + \frac{\Delta V}{\Delta y}\frac{\Delta \rho}{\Delta y} \qquad (2)$$

where

ρ = space charge, coul/m^3;
y = distance parallel to gas flow from wire to wire, m;
x = distance perpendicular to gas flow from wire to plate, m;
ε_0 = permittivity of free space, coul^2/(N-m^2); and
V = potential, volts.

The numerical procedure consists of an iteration technique in which the space charge density at the wire is adjusted until all the boundary conditions, which include the applied voltage and the corona current, are satisfied. For each choice of space charge density at the wire, the procedure iterates on a grid of electric potential and space charge density until convergence is obtained. The program then checks to determine whether the boundary condition on the average current density at the plate is met by using the expression

$$\bar{j} = (b_e \sum_{i=1}^{N} \rho_{pi} E_{pi})/N \qquad (3)$$

where

$\bar{j}$ = average current density at the plate (A/m^2);
b_e = effective charge carrier mobility ($m^2/V\text{-sec}$);
ρ_{pi} = space charge densities for points on the plate ($coul/m^3$);
E_{pi} = electric field strengths for points on the plate, V; and
N = number of grid points in the direction of gas flow.

If the boundary condition on the average current density at the plate is not met, then the space charge density at the wire is adjusted and the iteration procedure is repeated.

The foregoing procedure provides a method of obtaining electric field distribution for instances in which voltage and current are known parameters, and is used in the calculation of theoretically predicted collection efficiencies.[13] McDonald et al[14] have described a technique, based on the same mathematical relationships, which may be used to generate a voltage-current characteristic for wire plate geometry. The results obtained from this technique are a function of the electrode geometry and the value used for effective charge carrier mobility. Poisson's equation and the continuity equation are solved as previously described for a series of points on the voltage-current curve, but with a different set of boundary conditions imposed. The space charge density in the region of ionization near the discharge electrode is calculated from an arbitrarily chosen value of average current density at the plate. The space charge density near the wire and the average current density at the plate provide boundary conditions which are held fixed, while the voltage at the wire is adjusted until solutions are found to equations 1 and 2 which satisfy all the boundary conditions.

McDonald's procedure has been used to analyze the voltage-current relationships obtained during the test series at the Navajo Generating Station. Figure 28 contains voltage-current curves from a computer program used to implement the method. These results are based on the existing wire diameter of 0.268 cm (0.1055 in), although, as will be shown later, the results are quite sensitive to wire diameter variations which could result from dust deposits. The curves indicate the importance of charge carrier mobility in the prediction of electrical operating parameters. The mobility values shown in Figure 28 are representative of a range which would be expected if voltage-current curves were obtained at temperatures ranging from ambient to ∿350°C and with gases consisting of atmospheric air at ambient temperature and typical flue gas components at 350°C.

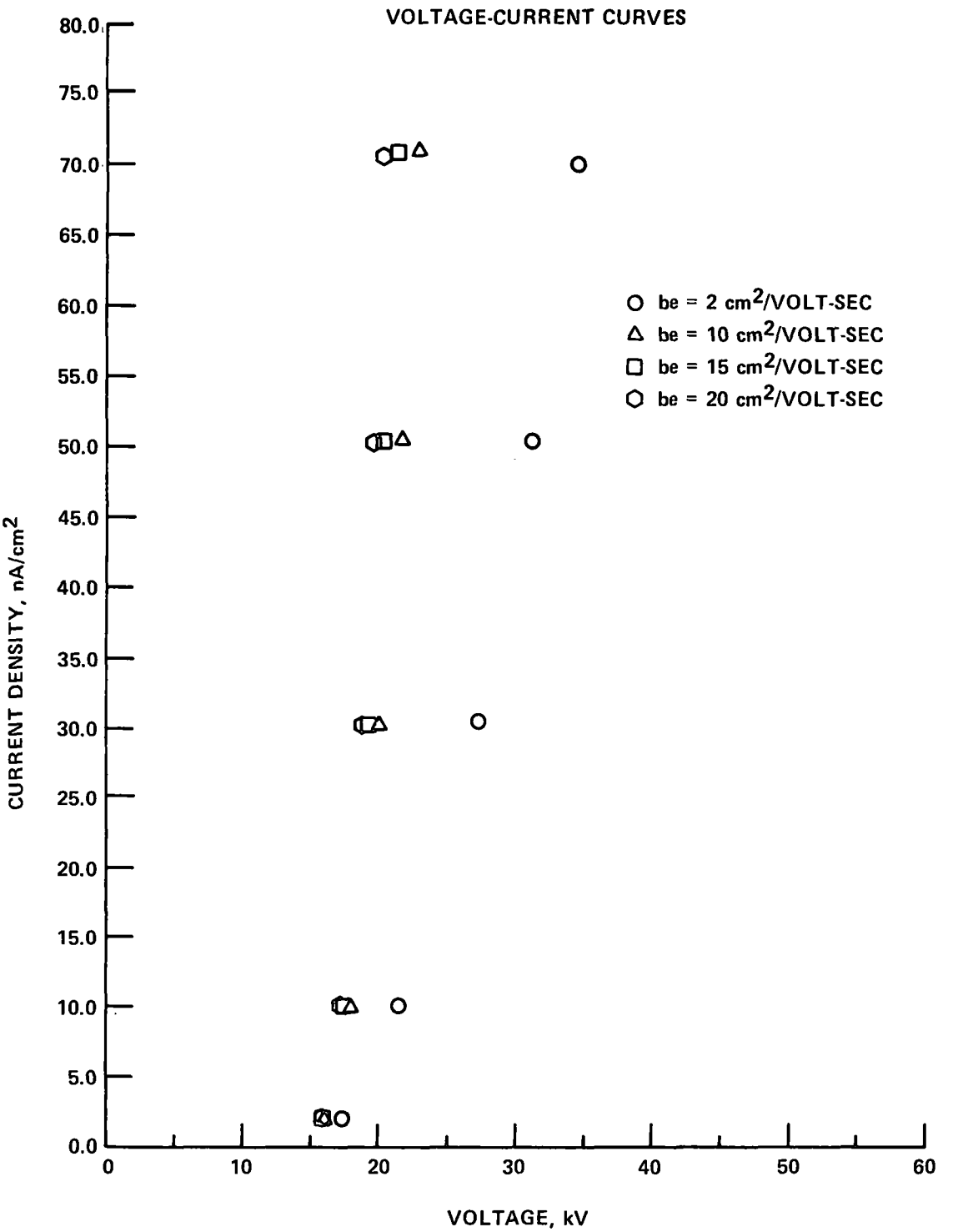

Figure 28. Theoretical voltage-current relationships for wire diameter of 0.268 cm (0.1055 in), wire to plate spacing of 11.45 cm (4.5 in), and wire to wire spacing of 22.9 cm (9.0 in).

Recent measurements with an apparatus designed to determine charge carrier mobility indicate b_e values of 15-20 cm^2/volt-sec may be encountered at the operating conditions of the Navajo Station precipitator.[15] These data also indicate that (1) the gas charge carrier mobilities may be sensitive to small composition changes, and (2) extrapolation of reduced mobility values for flue gas using ideal gas law temperature and pressure ratios to operating conditions does not give a result in agreement with the measured values under these conditions. For example, available data indicate that 3.0 cm^2/volt-sec is an appropriate value for reduced effective mobility (0°C, 1 atm) in a typical flue gas. An ideal gas law type of extrapolation to the precipitator environment at Navajo results in a b_e value of about 8.2 cm^2/volt-sec, or approximately one-half the value indicated by the in situ measurement.

Since the last field of the precipitator will experience the lowest dust concentration and associated particulate space charge, an evaluation of the theoretical voltage-current characteristics can best be performed through a comparison of the theoretical curves with actual data from a typical outlet field. Procedures have been devised for estimating the effects of particulate space charge on voltage-current characteristics, but this issue constitutes an additional complication which need not be considered in this discussion. Figure 29 indicates that the theoretically derived voltage-current curve closely simulates a typical "C" field curve from chamber 8, which was obtained after testing on July 15, 1977. The theoretical calculations were based on the actual electrode geometry, an assumed "roughness factor" for the discharge electrode of 0.9, and an effective carrier ion mobility of 15 cm^2/volt-sec.

The procedure for generating the V-I curve contains no expressions which represent the influence that dust deposits on the electrodes might have on voltage-current characteristics, other than the "roughness factor" for the discharge electrode which is related to dust deposits on the wire. Therefore, the agreement between the theoretical and actual voltage-current relationships shown in Figure 29 contains an inference that the voltage-current relationships at Navajo are not influenced by dust layer phenomena. However, the following observations strongly indicate that dust deposits are influencing the functional relationship between applied voltage and corona current in a manner which is not adequately represented by equations 1 and 2.

- The voltage-current relationships do not respond to changes in electrode diameter in accordance with theoretical predictions.

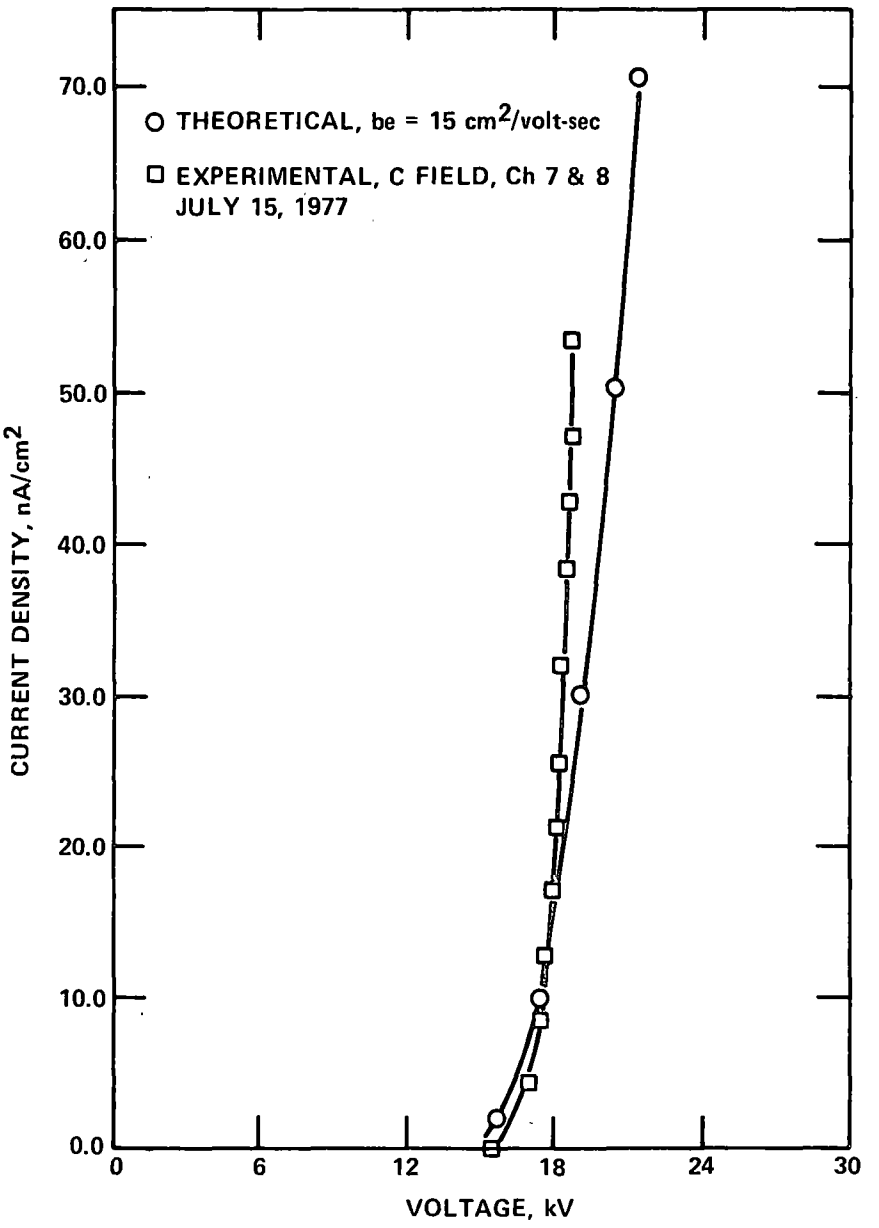

Figure 29. Comparison of theoretical (b_e = 15 cm^2/volt-sec) and experimental (C Field, Ch. 7 & 8, July 15, 1977) voltage-current curve.

- Photographs of voltage-current waveforms suggest a back corona type of discharge at high current levels.

- There is some evidence of hysteresis in the V-I curves from the outlet field.

- The V-I curves are influenced by electrode cleanliness.

- Precipitator performance is influenced by dust resistivity changes in a range of resistivity values below that which would be expected to limit performance.

Figure 30 compares theoretical and actual V-I curves for various wire sizes. The data for C field of Chambers 1 and 2 were obtained after 0.457 cm (0.18 in) diameter wires had been installed in an effort to improve operating voltages. Although the voltage required for a given current does appear to have been increased by the larger wires, the degree of increase is much less than theoretically predicted. These data suggest that factors other than discharge electrode geometry are limiting the attainable voltages for given current levels.

Figure 31 illustrates voltage waveforms obtained from C field of Chambers 7 and 8, at corona start, the "knee" of the V-I curve, and at the maximum operating point under automatic control. These waveforms illustrate that the voltage between the discharge and collecting electrodes drops below the corona onset voltage at high current densities, indicating that the energy stored in the capacitance of the precipitator is being drained by a discharge process which continues down to voltages as low as approximately 10 kV. Normally, the discharge process stops when the applied voltage drops to the corona onset value. Electrical breakdown in the dust layers on the collecting electrodes is a possible explanation.

Further evidence of dust layer effects is observed by a comparison of V-I curves obtained from C field, Chambers 7 and 8. Immediately following start-up from an outage during which the chambers were washed and new wires were installed in the C field, comparisons were made between the clean electrode curves and those obtained after considerable operating time had elapsed. Figure 32 illustrates the change in the voltage-current curves from May to August of 1977. Although some of this change may be due to changes in ash characteristics, a comparison with the data from C field of Chambers 5 and 6, which were taken at the same time, clearly shows the effect of electrode cleaning on the shape of the voltage-current relationship.

The influence of dust resistivity changes on precipitator performance was observed during a half-load test on Chamber 8 of unit 3. This test was conducted during the test series of January 1977. As the precipitator operating temperature dropped

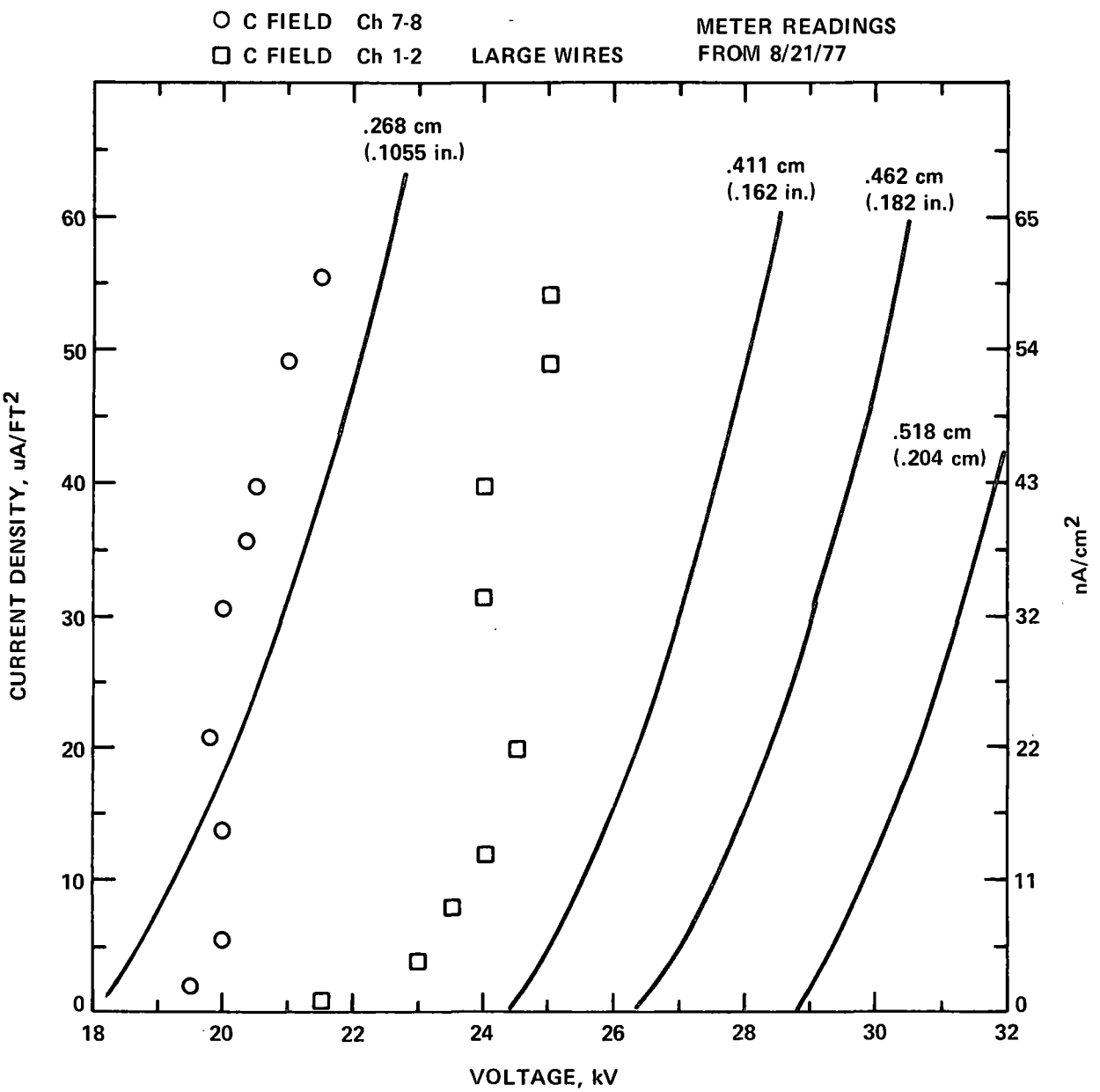

Figure 30. Theoretical and experimental voltage-current relationships for various wire diameters.

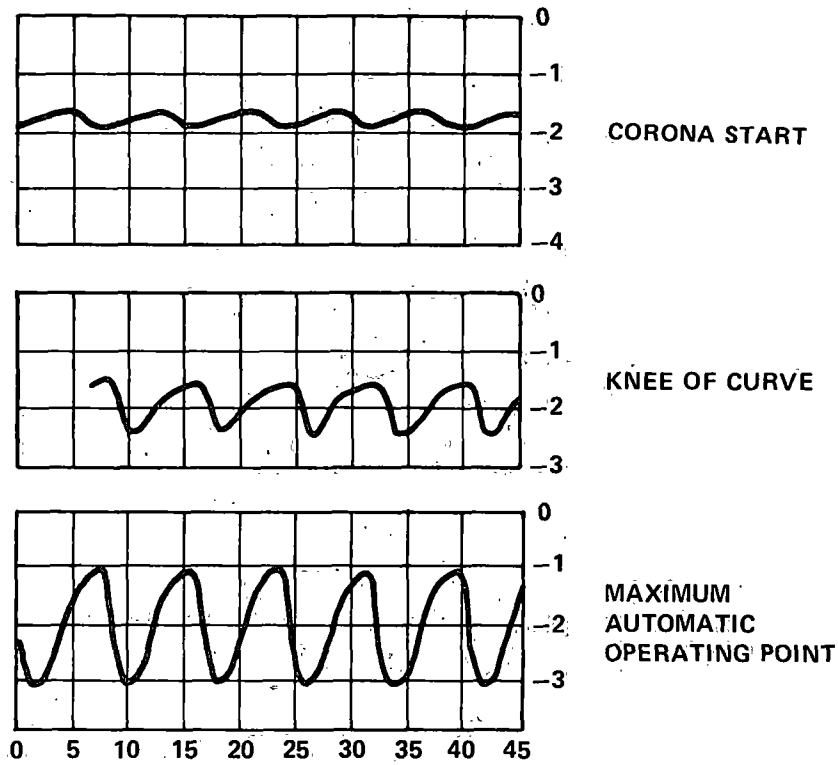

Figure 31. Voltage waveforms for C Field, Chambers 7 and 8.

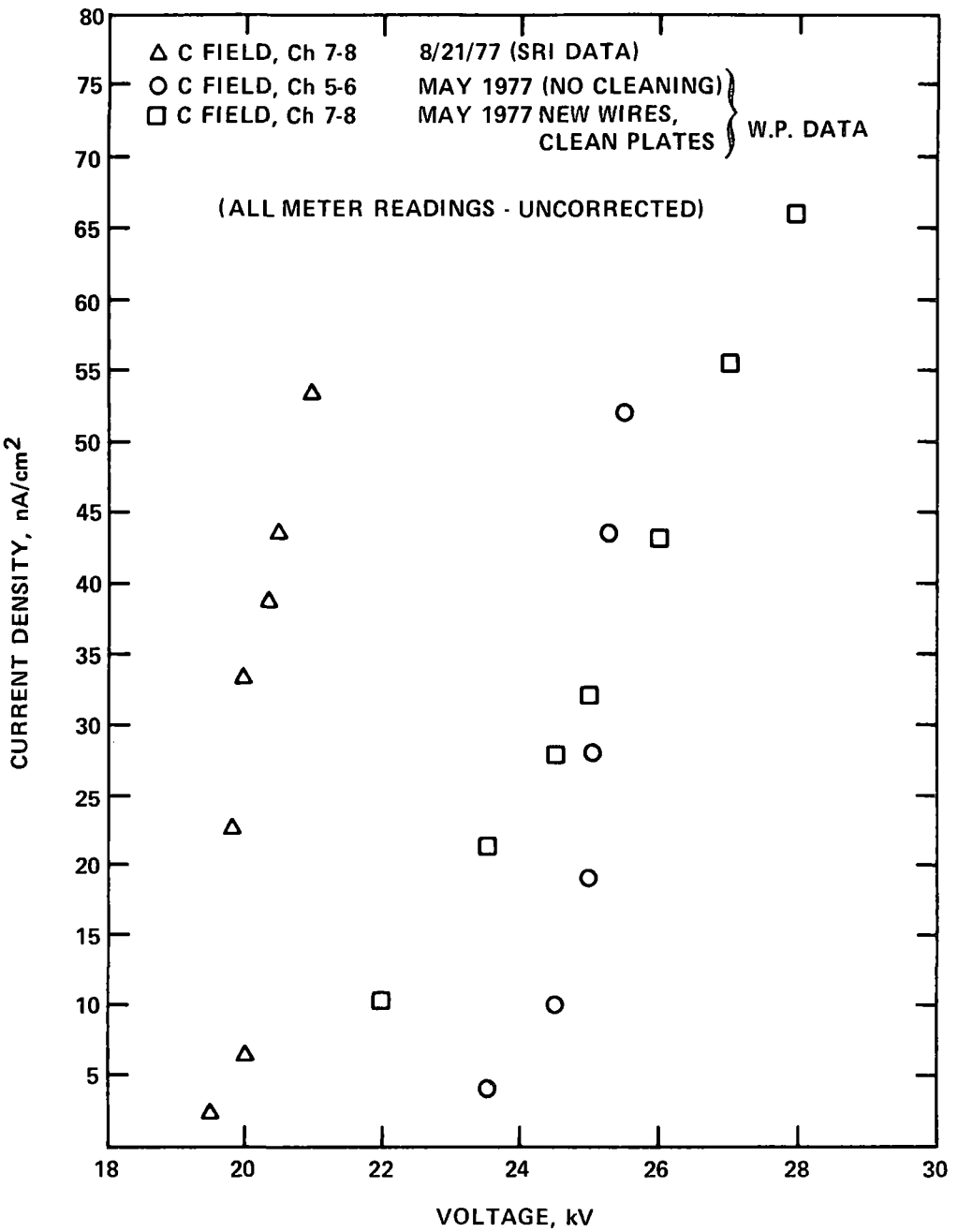

Figure 32. Voltage-current relationships for C Fields, Chambers 7 and 8 and Chambers 5 and 6.

from 360 to 233°C, the TR sets exhibited heavy sparking, and the operating points were much lower under automatic control at half-load conditions than they were at 800 MW. The collection efficiency dropped from 99.26 to 92.17%, even though the specific collecting area of the precipitator was doubled as gas flow decreased. The electrical operating characteristics suggest that dust resistivity increased to the point that breakdown was occurring in the deposited dust layer and that the resulting sparking severely limited the performance of the unit. Laboratory resistivity data indicated that dust resistivity would increase from 8×10^{8} to 2×10^{10} ohm-cm due to the temperature drop associated with half-load operation.

Figure 33 illustrates the effect of half-load operation on the voltage-current curves and the operating points at Navajo for the outlet fields. Also shown is a voltage-current curve from another hot-side precipitator outlet field. "Plant 4" was tested under another program sponsored by EPRI, and illustrates that the steep V-I curves observed at Navajo are not always experienced with hot-side operation. The collection efficiency degradation observed with half-load operation at Navajo probably could have been avoided with properly operating TR set controls, but the test results are important in that they indicate a sensitivity of precipitator operation to resistivity variations in a region where no sensitivity was expected.

Model Projections

The preceding discussion indicates that the low operating voltages observed at Navajo may result from a combination of high effective mobilities for the charge carrying species of the gas stream and an electrical discharge process which occurs in the deposited dust layer and which persists at voltages below the normal corona onset voltage. Comparison of actual precipitator performance with projections of a mathematical model[16] under cold-side conditions where sparking and back corona were occurring indicated, as would be expected, that the actual performance was lower than the theoretical projection. This results from the deleterious effects of a bipolar charging environment on particle collection in a negative corona field.

Figure 34 contains comparisons between projections of the mathematical model and field measurements of overall mass collection efficiency for Chamber 8 and for the entire precipitator. The input data for the model included measured values of operating voltage and current levels, particle size distribution, gas flow, and precipitator geometry. The comparison shows that the model significantly underpredicts the measured overall mass collection efficiency of Chamber 8, which was obtained with both mass train and impactor sampling systems. The underprediction suggests a fundamental difference between the apparent back corona characteristics observed for Chamber 8 and those observed

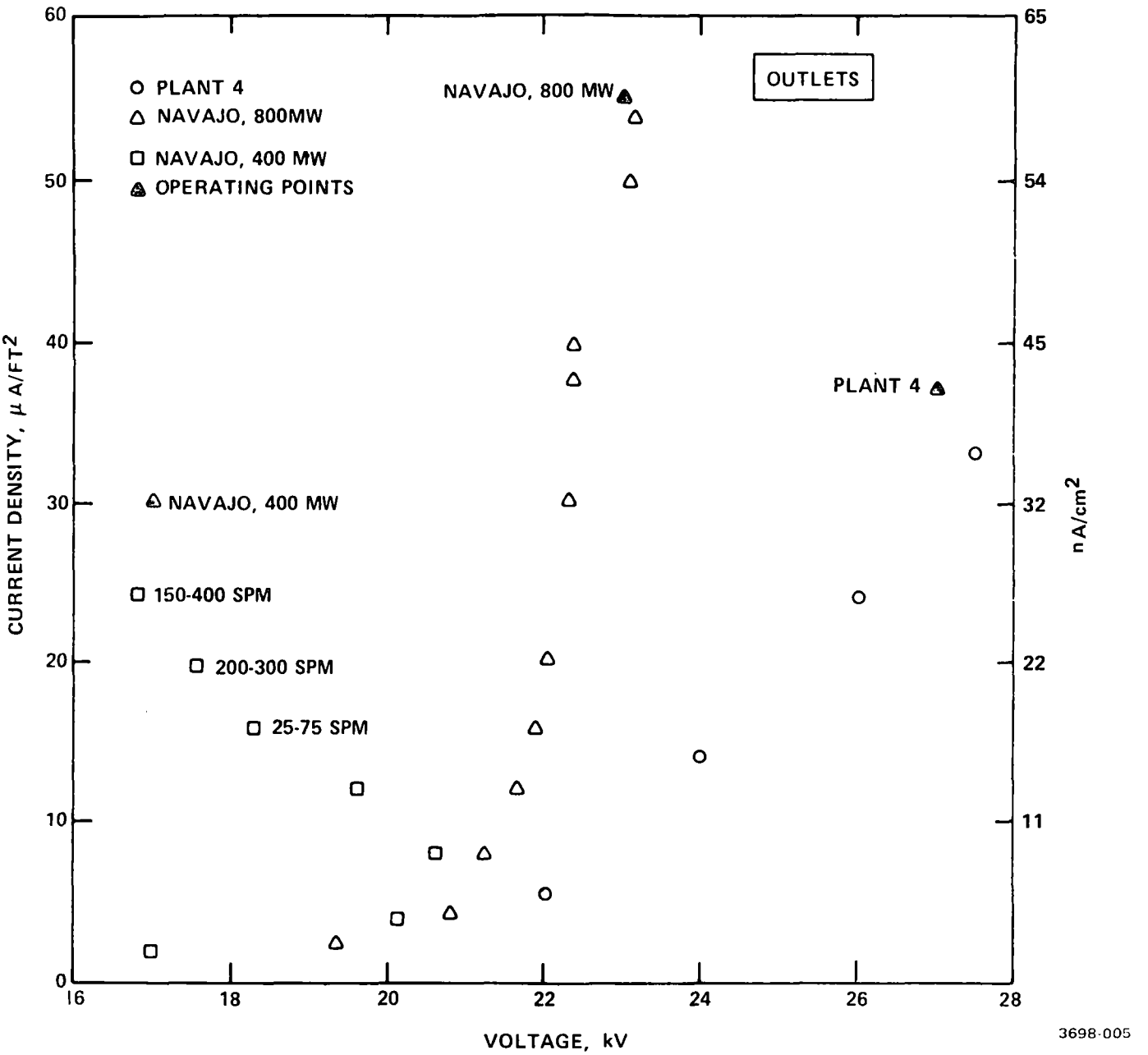

Figure 33. Outlet field voltage-current curves for Chambers 7 & 8 (Navajo) and another hot side precipitator installation.

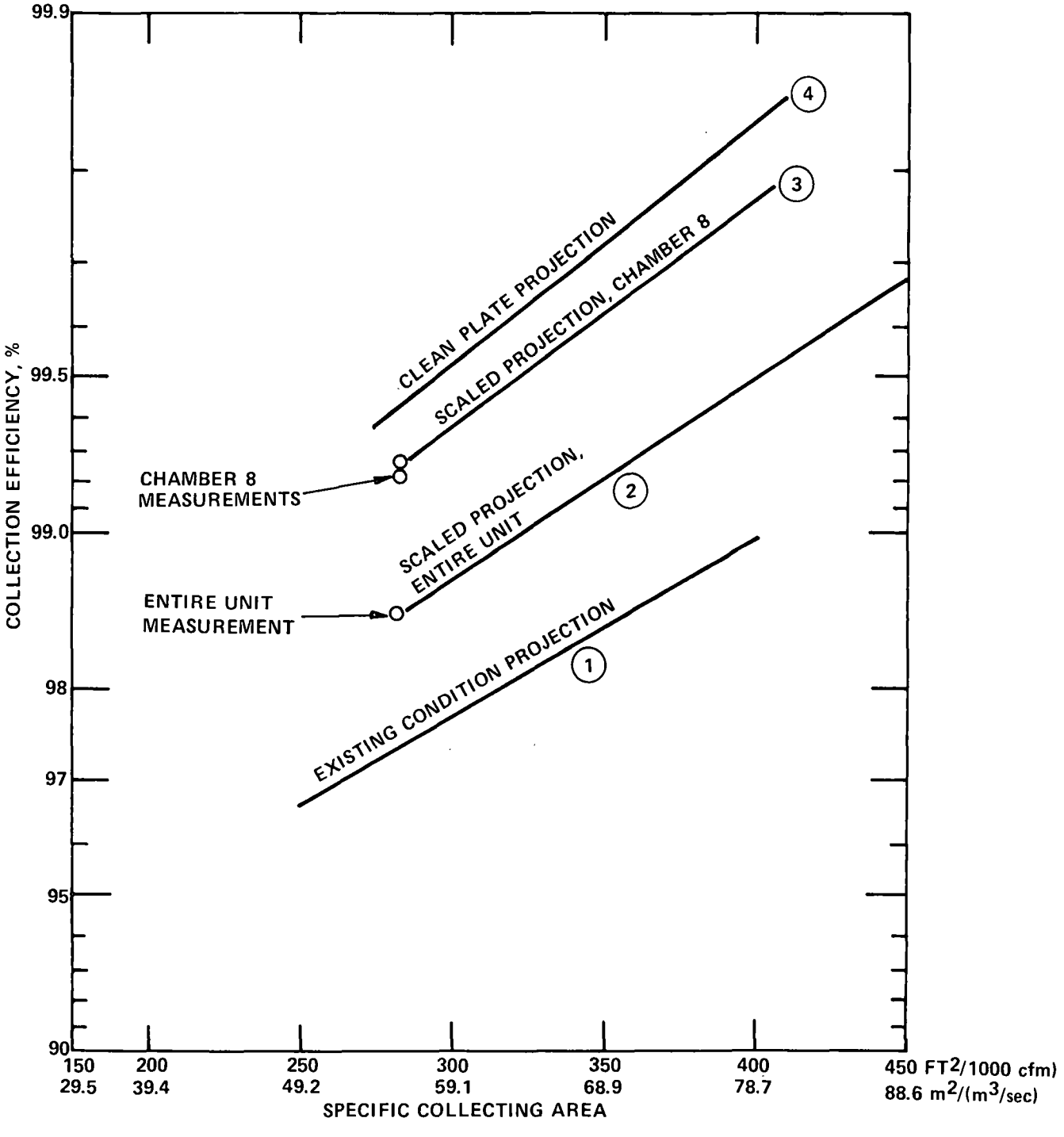

Figure 34. Measurements and model projections of collection efficiency for hot-side operating parameters.

for cold-side (150°C) operating conditions with high resistivity dusts ($\sim 1 \times 10^{12}$ ohm-cm). Particle charging by free electrons is a possible cause for the underprediction, and current transport by free electrons may be a factor in the high values of effective mobility which are indicated by the in situ measurements. Electron mobilities are of the order of 100 to 1000 times the value of typical electronegative gas ion mobilities, and the mathematical relationships for projecting particle charging rates are no longer valid.

Given the large underprediction that results when the model is applied with the measured operating parameters at Navajo, it is necessary to adjust the input voltages (which, in effect, scales the results to agree with the overall mass efficiency) in order to use the particle size dependent relationships in the model for estimating overall efficiency as a function of specific collecting area. Line 3 in Figure 34 gives the model results when the input voltages are increased 33%. Line 2 was obtained with the same input data but with larger values of the parameters used to represent nonideal effects due to the reduced performance of the entire unit compared to that of Chamber 8. The indicated requirement of specific collecting area for the design efficiency of 99.5% is 78.7 $m^2/(m^3/sec)$ or 400 $ft^2/1000$ acfm. The recommended value of specific collecting area is 93.9 $m^2/(m^3/sec)$ or 477 $ft^2/1000$ acfm, which contains a safety margin of 19%. Line 4 was obtained using voltage and current values measured with a hot-side precipitator collecting ash from an Eastern coal. All other input parameters were obtained from the Navajo test series on Chamber 8.

The collection efficiency relationship indicated by line 4 is what the model would predict in the absence of significant dust layer effects or unusually high values of effective charge carrier mobilities. This projection indicates that the design efficiency (99.5%) is theoretically attainable at the design value of SCA if the expected electrical operating conditions could be achieved. Obviously, the presence of the anomalous electrical operating conditions observed during the test period causes a significant degree of uncertainty in performance projections at other values of specific collecting area. Studies with a hot-side pilot precipitator at the Navajo Station are recommended to determine the relationship between dust layer thickness, dust composition, and electrical operating parameters. Particle charge measurements at the precipitator outlet are also recommended to determine whether the existing model for calculating particle charging rates is valid for the conditions observed at Navajo.

In view of the problems encountered in meeting the design efficiency with the hot-side precipitator at Navajo, it is of interest to examine possible design parameters for a cold-side

unit collecting the same ash. The dust resistivities which must be considered at 155°C are given below.

Source	Resistivity, ohm-cm (155°C) Predicted	Measured (Laboratory Method)
Figure 16 - Peabody Coal	6×10^{10}	8.5×10^{10}
Figure 17 - Peabody Coal	6×10^{10}	6×10^{10}
Figure 18 - Peabody Coal	7×10^{10}	2.5×10^{10}
Figure 19 - Peabody Coal	2×10^{10}	1.8×10^{10}
Figure 20 - Utah Coal	7×10^{11}	Not Available

These data illustrate that "worst case" values of resistivity for the Peabody and Utah coals, respectively are 8.5×10^{10} ohm-cm and 7×10^{11} ohm-cm. Estimated electrical operating parameters for the cold-side model projections are 23.8 kV and 2.0 nA/cm^2 for the Utah coal, and 25.8 kV, 9.9 nA/cm^2 for the Peabody coal.

Figure 35 contains the model projections for cold-side operating conditions at Navajo. These projections were obtained using the geometrical configuration of the existing hot-side precipitator and the particle size distribution measured at the inlet to the hot-side unit. The estimated specific collecting areas requirement for the Peabody and Utah coals at the design efficiency of 99.5% are 106.3 m^2/(m^3/sec) (540 ft^2/1000 acfm) and 139.8 m^2/(m^3/sec) (710 ft^2/1000 acfm), respectively. The recommended specific collecting areas are increased over these values by about 20% to allow a reasonable safety margin for dust composition changes and mechanical problems with the precipitator. The design configuration for the hot- and cold-side units are given in the next section.

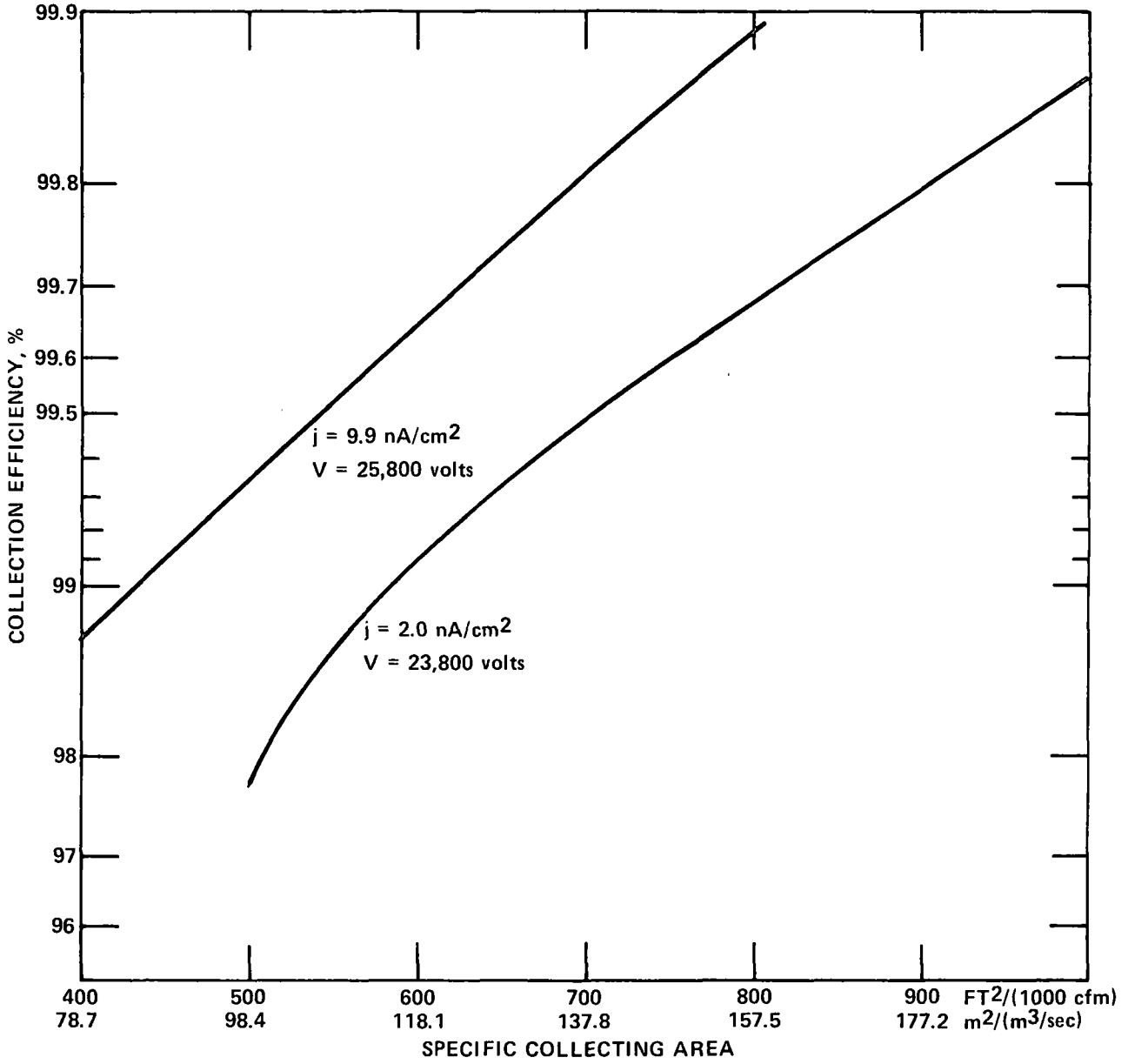

Figure 35. Model projection for cold side operating parameters.

SECTION 4

ENGINEERING ANALYSIS

CAPITAL AND OPERATING COSTS OF EXISTING UNIT

Table 23 presents the cost of Unit 3 precipitator in 1977 dollars. The 1977 costs were arrived at by taking the actual contracted dollars assigned to Unit 3 precipitator for most of the items in Table 23, adding a twenty percent distributable cost to each, then adding nine percent of the contracted and distributable costs for engineering costs and finally escalating each cost element to 1977 at seven and one-half percent per year.

The precipitator and ductwork were purchased from Joy-Western in 1973 and erection labor and subcontracts and equipment insulation were assumed to be 1975 charges. The ash collection and storage system was purchased in 1971 for all three units at Navajo and the cost in Table 23 reflects one-third of that total purchase. The installation of the ash collection and storage system was assumed to have been completed in 1973. One-third of the total was charged to the Unit 3 precipitator.

The charges associated with incremental costs of ESP to ID fans, accessory electrical equipment, instrumentation, miscellaneous foundations, major auxiliary building foundations, earthwork and architectural features were reported by the Bechtel Corporation and were assumed to have been 1975 charges. The majority of the ash handling machinery was purchased in 1974 and the cost in Table 23 reflects one-third of the total equipment cost in 1977 dollars.

The cost of the precipitator for Unit 3 in 1977 dollars is $46.58/kW, based on the total of Table 23 and the design generating capacity of Unit 3 of 750 MW ($43.67/kW for the 800 MW operating point). The unit area costs of the entire precipitator installation is $312/m^2 ($29/ft^2).

Table 24 presents the operating and maintenance costs associated with the ash handling system which were charged to Unit 3 from July 1, 1976 to July 1, 1977. The charges from the electrical department and maintenance department are combined since the majority of the work on the precipitator and associated equipment requires that both departments be involved. The hourly

TABLE 23

Unit #3 Precipitator Cost

Item	1977 Cost (7.5%/yr esca.)
#3 ESP	4,877,844.37
#3 ESP Labor & Subcontracts	3,852,960.07
#3 ESP Ductwork	3,304,863.69
Change in Materials	283,845.23
Accelerated Delivery of Materials	849,022.95
Equipment Insulation	2,155,481.00
Other Materials	227,755.50
Ash Collection & Storage System	4,275,476.12
Ash Collection & Storage System Installation	3,575,686.57
Ash Handling Piping	483,861.84
Incremental Costs of ESP to ID Fans	454,978.81
Accessory Electrical Equipment	7,637,144.27
Instrumentation	751,527.49
Misc. Foundations	721,737.22
Major Aux. Building Foundations	4,062.31
Earthwork	54,164.14
Architectural Features	844,960.64
Ash Handling Machinery	580,666.96
	$34,940,000.00

TABLE 24

Operating and Maintenance Costs for Unit #3, Ash Handling System, July 1, 1976 to July 1, 1977

Description	Man Hours	Labor	Materials	Contract Services	Other	Labor* OVH	Total
Gallion Blade	67	565.79	3365.22	0	0	78.96	4009.97
Cat Loader	172	1700.27	3424.69	914.33	0	238.42	6277.71
D4 Dozer	88	848.69	431.54	0	0	118.87	1399.10
Ash Truck #138	251	2591.24	5920.05	3680.80	77.95	364.70	12634.74
Grad All	100	1017.46	1391.98	0	0	143.27	2552.71
380 Dozer	848	8451.24	22342.49	0	0	1196.63	31990.36
Ash Truck #156	208	1946.37	12181.18	890.73	77.95	271.91	15368.14
Ash Truck #161	265	2643.41	4749.67	299.67	0	385.48	8078.23
Ash Truck #162	231	2227.22	4348.14	0	0	313.66	6889.02
Ash Truck #179	148	1431.55	3848.83	50.00	0	201.30	5531.68
Loader	77	739.41	642.64	530.33	0	102.41	2014.79
Rental Scraper	0	0	0	0	21302.00	0	21302.00
							$118,048.45
Cost Adjustments	80	96.26	90714.92	0	128.85	38.50	90978.53
Electrical and/or Maintenance Dept.	12477	105038.35	27206.23	0	0	14651.84	147842.42
Misc.	37	422.18	98100.00	4944.00	524.00	59.74	104049.92
							$342,870.87
						TOTAL	$460,919.32

*Employee benefits: e.g., Workmans Comp., Insurance, Payroll Taxes, etc.

charges for maintenance or repair of equipment charged to the separate areas (e.g., ash handling system, precipitator, etc.) are recorded in total without a breakdown by department.

Table 25 presents the normal maintenance, repair and operation charges for the Unit 3 precipitator from July 1, 1976 to July 1, 1977. These costs reflect maintenance items such as: wire replacement, hopper service (high ash buildup in hoppers), wire clinker removal, repair of electrical bus duct failures, straightening of bowed collection plates, etc.

Table 25 does not include costs which would be associated with routine checking or monitoring of the precipitator. The estimated manhours for the separate departments, based on maintenance starting with no deficiencies, required for normal checking, monitoring or tuning of the precipitator are: 1) operations - 1 man, 30 minutes/shift; 2) electricians - 2 men, 8 hours/day; 3) mechanics - 1 man, 3 hours/day; 4) engineering technicians - 2 men, 8 hours/day, 2 days/month; 5) engineering - 2 hours/week. These routine checks and monitoring duties total an estimated 7,970 manhours/year/unit, which represent a cost of $100,277 at $12.58/manhour.

Table 26 presents charges assigned to the Unit 3 precipitator from July 1, 1976 to July 1, 1977 for testing, adjusting and/or modifications of the precipitator. These charges include the rewiring of the rapper control panels in order to separate the wire rappers from the same programming card as the plate rappers. The costs incurred during overhaul for the precipitator included: installation of ladders at the inlet of each chamber to provide access for the adjustment of the "zigzag" (gas distribution) plates, installation of "egg-crate" gas distribution devices in each chamber, installation of platforms in the hoppers to provide access to the discharge and collection electrodes, straightening of bowed collection plates, etc.

The estimated cost of electrical power to operate the Unit 3 precipitator is given in Table 27. The estimate of 2.5¢ per kilowatt hour was used since SRP sells power for approximately 2.5¢ per kilowatt hour. The voltage current meter readings of 8/1-2/77 were used to calculate the power consumption of the transformer rectifiers. The purge air system for the high-voltage bus ducts and the ash system blowers were assumed to operate at their maximum ratings. The incremental power consumption of the ID fans was calculated using 12.7 mm (1/2 inch) pressure drop across the precipitator. Table 28 summarizes the operating costs for the precipitator installation.

TABLE 25

Operating and Maintenance Costs for Unit #3 ESP, Normal Maintenance, Repair, and Operations, July 1, 1976 to July 1, 1977

Description	Man Hours	Labor	Materials	Contract Services	Other	Labor* OVH	Total
Cost Adjustments	442.0	5103.31	26220.77	0	0	2092.34	33416.42
Administration	0	0	1459.32	0	0	0	1459.32
Operations	0	0	15.79	0	0	0	15.79
Electrical and/or Maintenance Dept.	13993.5	114009.04	29.84	0	0	15801.77	129841.65
Engineering	1009.5	8777.59	84.99	0	697.30	1226.69	10786.57
Misc.	2.0	15.20	5.00	0	0	2.06	22.26
							$175,542.01

*Employee benefits: e.g., Workmans Comp., Insurance, Payroll Taxes, etc.

TABLE 26

Operating and Maintenance Costs for Unit #3 ESP, Charges for Testing, Adjusting and/or Modifications, July 1, 1976 to July 1, 1977

Description	Man Hours	Labor	Material	Contract Services	Other	Labor* OVH	Total
Cost Adjustments	49.5	505.35	19991.43	187206.00	8434.99	202.14	216,339.91
Administration	0	0	35.66	0	0	0	35.66
Operations	10.0	109.38	5.00	0	0	14.84	129.22
Electrical and/or Maintenance Dept.	5711.0	53115.26	2936.87	0	94.28	7400.39	63,546.80
Engineering	0	0	312.16	0	204.84	0	517.00
Misc.	161.0	1724.47	3.82	0	44.00	427.95	2,201.24
							$282,769.83
Overhaul Costs for Unit #3 ESP,3/25/77-5/3/77	2181.5	23022.90	279713.22[1]	483135.30[2]	22003.02	4424.45	$812,298.89
						TOTAL	$1,095,068.72

1. Includes $88,605.68 for"Egg Crate" gas distribution devices and $188,421.79 for platforms in hoppers
2. Performed by CE, contract costs of $324,841.21 included
   a. Zig Zag plate adjustments
   b. "Egg Crate" installation
   c. Permanent platforms in hoppers and hopper inspections
   d. Straightening of bowed curtains (collecting plates)
   e. Ladder installation to zig zag plates.

* Employee benefits: e.g., Workmans Comp., Insurance, Payroll Taxes, etc.

TABLE 27

ESTIMATED POWER COST OF PRECIPITATOR

Item	Energy Requirement, kW	Cost/hr.[1]
Transformer rectifiers, 48	1,490	$37.25
Purge air system for high voltage bus ducts		
Heaters	425	$10.63
Blowers	37	$ .93
Ash system blowers	596	$14.90
ID Fans - incremental cost of ESP	501	$12.53
	TOTAL	$76.24

1. Assuming a power cost of 2.5¢/kWh.

TABLE 28

SUMMARY OF OPERATING COSTS

	$/yr	mills/kWh	% of Total Annual Operating Costs
Energy Cost[1]	534,300	0.0953	8.2
Normal Operating & Maintenance Cost	276,000	0.0492	4.2
Ash Handling Cost	460,900	0.0822	7.07
Sub-total	1,271,200	0.227	19.5
Capital Charges 34,940,000x.15 =	5,240,000	0.935	80.5
Total	6,511,000	1.162	100.0

1. Based on 7008 hrs/yr at full load (800 MW) - 80% load factor

OPERATING AND MAINTENANCE PROBLEMS

The Salt River Project organized a task force to discuss possible means of improving precipitator performance and to determine the reasons for the performance limitations. The task force is composed of personnel from Western Precipitation, Bechtel Corporation, Southern Research Institute, and the Salt River Project. Some of the more significant problems which have occurred with Unit 3 and which have been considered by the task force include:

1. Gas velocity distribution,
2. Air infiltration,
3. Ash buildup in hoppers,
4. Transformer rectifiers, and
5. Rapper failure.

Gas Velocity Distribution

After Unit 3 began operation and the performance of the precipitator was below the design value, the gas velocity distribution was considered to be a possible problem. The Salt River Project personnel obtained velocity distribution measurements on a number of the chambers and discovered that the velocity distribution was extremely nonuniform. With the installation of baffle plates at the edges of the zigzag plate gas distribution devices, and adjustment of the zigzag slots, the gas velocity distribution was improved to a normalized standard deviation of 17%.

After gas flow model studies were conducted by Western Precipitation, it was decided to install egg-crate gas distribution devices at the inlet of each chamber to aid in obtaining a uniform gas velocity distribution.

Air Infiltration

Leaking guillotine isolation dampers at the inlet of each chamber were considered to be the major contribution of the ambient air infiltration to Unit 3. Additional air infiltration was contributed by leaking manholes and insulator compartment doors. The replacement or addition of gasket materials helped alleviate the majority of these problems.

Ash Buildup in Hoppers

The major maintenance problem with Unit 3 has been high ash buildup in the hoppers which results in shorted fields, buckled plates and broken wires. The malfunction of the Nuva feeders, due to mechanical failures or clogging by foreign objects, results in high ash levels. A major maintenance problem following chamber shutdown has been access to the bottom of the

high-voltage frames and collection plates. To alleviate this problem, hopper platforms have been installed to allow easy access to the wires and plates.

In an effort to detect ash buildup problems before the ash level reaches the collecting plates, hopper-level indicators* have been experimented with and have operated satisfactorily. The installation of hopper-level indicator is planned at the Navajo Station and should result in fewer maintenance charges and higher reliability for the precipitator.

Transformer Rectifier

Only minor problems have been encountered with the high-voltage system. There have been no electrical failures of the TRs, but the following have required maintenance after the problem was discovered.

- Gaskets had to be changed on the low-voltage bushings of 3 TR sets after they began leaking pyranol.
- The low-voltage bushing cable termination was changed from a clamp type connector to a crimp type connector. Due to overheating, the clamp type connector would not remain tight on the cable.
- The metering resistor from the TR set low-voltage bushing terminal box was relocated to the AVC cabinets in the control room due to overheating of the resistor.
- Sparking in bus ducts - infiltration of ambient air on rainy days resulted in sparking in some of the bus ducts.

Rapper Failure

Failure of the impact rappers and controllers has been the cause of maintenance associated with the rapping system. Maintenance on the rapping system was reduced by installing 1) improved rapper wear rings, 2) flexible coil connectors to the rappers, and 3) improved rapper control power relays. A different rapper control was tested and considered to be superior because: 1) it has demonstrated reliability, in that for over five months operation has occurred with no problems, 2) it is easier to set rapper impact than on present controller, and 3) it is an updated control. An additional maintenance item associated with the rapping system is the repair or replacement of rapper seal boots which have leaked.

---

*K-Ray hopper level indicators.

A major preventive maintenance effort by SRP has kept maintenance problems to a minimum. Work is performed on the Nuva feeders, rappers, insulator compartment ventilation system, and TR sets on a weekly basis. Constant tuning and observation of precipitator performance accounts for quick recognition and service of problem areas.

Reliability

Although the precipitator has not operated reliably with regard to its design efficiency, it has operated reliably from a mechanical standpoint. Table 29 presents the percent of available on-time for each chamber from July 1, 1976 to July 1, 1977, excluding unit overhaul. As discussed earlier, the major cause for ESP down-time has been high ash buildups in the hoppers due to malfunctioning Nuva feeders. As a result of the preventive maintenance program established by the Salt River Project and the system modifications, the reliability of the precipitator is expected to increase over that experienced during the past years.

Modifications

The modifications to Unit 3 precipitator have been performed in an effort to improve precipitator performance and reduce maintenance problems which have occurred. The majority of the modifications were completed prior to Southern Research Institute's test of Unit 3 and are as follows:

- Rapper Optimization

  The rapper controls were rewired to separate the wire and plate rappers from the same programming card and to lengthen the time between raps, especially for the last fields.

  A more reliable and versatile rapper controller will replace the original controls as they fail.

- Hopper Ash-Level Detectors

  Ash-level indicators have been studied and will be placed on each hopper in an effort to reduce ESP internal damage and down time.

- Platforms Within the Hoppers

  Platforms were installed in each hopper to allow access to the bottom of the collecting plates and high-voltage discharge frames in order to reduce maintenance time associated with high ash buildups and wire failures.

TABLE 29

ESP CHAMBER AVAILABILITY

Chamber	% Available[1]
1	96.8
2	94.3
3	100.0
4	100.0
5	100.0
6	100.0
7	97.1
8	98.7
9	98.5
10	100.0
11	97.2
12	100.0
13	99.6
14	98.9
15	98.6
16	96.9

1. Excluding unit overhaul.

- Gas Distribution Systems

  Installation of side plates of the zigzag gas distribution devices was a necessary and early modification. Extensive work on adjusting the zigzag plates was done by SRP. The installation of egg-crate distribution devices and ladders for access to the distribution devices was completed in 1977.

- Changed Low-Voltage TR Connectors

  The low-voltage bushing-cable termination connectors were changed from the clamp type connector to a crimp type connector due to overheating of the clamp type connector.

- Relocation of Metering Resistors

  The metering resistors of the TR set low-voltage bushing terminal box were relocated to the automatic voltage control cabinets in the control room due to failure of the resistor caused by overheating.

DESCRIPTION AND ESTIMATED COSTS OF AN IMPROVED PRECIPITATOR

The preceding section of this report has indicated the rationale for the recommended hot-side design specific collecting area of 93.9 $m^2/(m^3/sec)$ (477 $ft^2/1000$ acfm). Based on a gas flow of 824 dsm^3/sec (16 times the outlet value for Chamber 8), the estimated total plate area required for the recommended SCA at approximately 350°C is 206,200 m^2 (2.217 x 10^6 ft^2). The estimated cost of this design was computed as follows:

- Cost in 1977 dollars assigned to the precipitator installation, excluding the I.D. fan incremental costs and the ash handling system costs, was calculated on a dollar per unit area basis.

- The total plate area of 206,200 m^2 was used to calculate the cost of the enlarged unit.

- The original cost of the ash handling system (1977 basis) was scaled upward and added to the cost calculated for the enlarged unit, along with the incremental I.D. fan charges.

The above procedure results in a total estimated capital cost of $60,440,000, or $75.5/kW, based on 800 MW generating capacity. No retrofit charges are included in the estimating procedure, since the objective is to estimate the cost of the improved design in 1977 dollars for a new installation. The

additional cost of the added collecting surface clearly predominates over the cost of the previously discussed mechanical improvements.

Comparison of Hot- and Cold-Side Designs

A comparison of hot- vs cold-side designs for the Navajo Station precipitators is necessarily based on certain assumptions regarding the required plate area and the design details of the installation. The estimated plate area requirements were generated as described previously, and the basic geometrical configurations of the recommended designs were arbitrarily chosen to be the same as the existing installation. Table 30 contains the recommended design parameters for one hot-side and two cold-side conditions at Navajo. The enlarged hot-side unit represents an increase in plate area of 83% over the existing unit. The added collecting surface is expected to provide an adequate safety margin to allow the design efficiency to be achieved in the presence of the dust layer effects that limit operating voltages which were observed during the test program.

The capital costs of the existing hot-side design were compared with those obtained from a recent cost model published by Research Cottrell, Inc.[17] This cost model provides installed cost for precipitators on a flange-to-flange basis, and gives a value of $\$123/m^2$ ($\$11.4/ft^2$) for the existing design. From Table 23 the sum of precipitator costs, labor and subcontracts, insulation, and electrical equipment costs gives $\$165/m^2$ ($\$15.3/ft^2$). This value is in reasonable agreement with the Research Cottrell model, since a portion of the electrical and insulation costs in Table 23 was for items not included in the flange-to-flange model. These data imply that the total cost of the entire precipitator installation and associated equipment at Navajo is about 2.5 times the unit area installed cost of the precipitator. For the recommended hot-side design in Table 30, the Research Cottrell model gives about 42% of the total estimated precipitator ash handling, duct work, and auxiliary equipment costs.

The estimated cost of the cold-side units was computed as follows:

- The installed unit area cost, including ductwork and auxiliaries but excluding the ash handling system costs, of a cold-side unit was computed from recent data[18] as $\$133/m^2$ ($\$12.34/ft^2$) and used as a basis for calculating the cold-side precipitator costs.

- A scaled value of the Navajo system ash handling costs, and the I.D. fan incremental costs were added to the expense for the precipitator installation to obtain the estimated costs.

TABLE 30

RECOMMENDED DESIGN PARAMETERS FOR IMPROVED PERFORMANCE

Condition	Hot-Side - Peabody Coal[1]	Cold-Side - Peabody Coal[1]	Cold-Side - Utah Coal[1]
Gas flow, am^3/sec	2,194	1,571	1,571
Gas flow, acfm	4,649,000	3,329,000	3,329,000
Temperature, °C	350	150	150
Electrical fields in direction of gas flow	8	8	8
Collecting length, m	14.63	14.63	14.63
Collecting height, m	9.15	9.15	9.15
Area/chamber, m^2	9,369	9,369	9,369
No. of chambers	22	22	28
Total collecting area, m^2	2.062×10^5	2.062×10^5	2.623×10^5
Gas velocity, m/sec	1.36	0.976	0.767
Specific collecting area, $m^2/(m^3/sec)$	93.9	131	167
ft^2/1000 acfm	477	666	848
Avg. kV } Model Inputs	29.0	25.8	23.8
Avg nA/cm^2 } Model Inputs	40	9.9	2.0
Collection efficiency, %			
Design minimum	99.50	99.50	99.50
Expected	99.70	99.77	99.75
Dust resistivity, ohm-cm	5×10^9	8.5×10^{10}	7.0×10^{11}
Capital cost estimates (1977)			
Total ESP system	$\$61.44 \times 10^6$	$\$41.92 \times 10^6$	$\$52.1 \times 10^6$
$/kW at 800 MW	$76.8	$52.40	$65.13
$/$ft^2$	$27.7	$18.90	$18.46
RC Model, flange-to-flange, Installed, $/$ft^2$	11.7	9.7	9.4

1. Based on indicated dust resistivity values.

The cold-side Research Cottrell cost model gives a value of $\$104/m^2$ and $\$102/m^2$ ($\$9.66/ft^2$ and $\$9.44/ft^2$) for the suggested cold-side design in Table 30. The Research Cottrell model thus indicates that the hot-side units are about 20% more expensive on a unit area and flange-to-flange basis. The total installation estimates in Table 30, however, indicate that the hot-side installation is about 50% more expensive than the cold-side on a unit area basis. Total cost for the two systems will, of course, depend upon the relative plate areas and design details for the ductwork.

REFERENCES

1. Johnson, J. W., G. I. Clinard, L. G. Felix, and J. D. McCain. A Computer-based Cascade Impactor Data Reduction System. EPA-600/7-78-042, March, 1978.

2. Liu, B. Y. H., and D. Y. H. Pui. On the Performance of the Electrical Aerosol Analyzer. J. Aerosol Science, 6, pp. 249-64 (1975).

3. Nichols, G. B. Techniques for Measuring Fly Ash Resistivity. EPA-650/2-74-079, August, 1974.

4. Bickelhaupt, R. E. Measurement of Fly Ash Resistivity Using Simulated Flue Gas Environments. EPA-600/7-78-035, March, 1978.

5. Lisle, E. S., and J. D. Sensenbaugh. Combustion 36(1),12 (1965).

6. Smith, W. B., and R. R. Wilson, Jr. Development and Laboratory Evaluation of a Five-Stage Cyclone System. EPA-600/7-78-008, January, 1978.

7. Cahill, T. A., et al. Monitoring of Smog Aerosols with Elemental Analysis by Accelerator Beams. National Bureau of Standards Special Publication 422, issued August, 1976.

8. Hoel, Paul G. Introduction to Mathematical Statistics, 3rd Ed., John Wiley and Sons, Inc., New York. p. 276.

9. Marlow, W. H., P. C. Reist, and G. A. Dwiggins. Aspects of the Performance of the Electrical Aerosol Analyzer under Non-Ideal Conditions. J. Aerosl Sci. 1976, Vol. 7, p. 457.

10. Ensor, D.S., et al. Evaluation of a Particulate Scrubber on a Coal Fired Utility Boiler. EPA-600/2-75-074, 1975.

11. Ensor, D. S., R. G. Hooper, and R. W. Scheck. Determination of the Fractional Efficiency, Opacity Characteristics, Engineering and Economic Aspects of a Fabric Filter Operating on a Utility Boiler. Electric Power Research Institute Report No. EPRI FP-297. November 1976.

12. Leutert, G., and B. Böhlen. The Spatial Trend of Electric Field Strength and Space Charge Density in Plate Type Electrostatic Precipitators. STAUB. 32(7), July, 1972.

13. Gooch, J. P., J. R. McDonald, and S. Oglesby, Jr. A Mathematical Model of Electrostatic Precipitation. EPA-650/2-75-037, April, 1975.

14. McDonald, J. R., W. B. Smith, H. W. Spencer, and L. E. Sparks. A Mathematical Model for Calculating Electrical Conditions in Wire-Duct Electrostatic Precipitation Devices. J. Appl. Phys., 48(6): 2231-2246, 1977.

15. McDonald, J. R., and J. P. Gooch. Report in preparation to the Environmental Protection Agency under Contract No. 68-02-2193.

16. Gooch, J. P., and G. H. Marchant, Jr. Electrostatic Precipitator Rapping Reentrainment and Computer Model Studies. Electric Power Research Institute, Final Report Draft, EPRI Contract RP413-1, Task 1.1 and 1.3, August, 1977.

17. Bubenick, David V. Economic Comparison of Selected Scenarios for Electrostatic Precipitators and Fabric Filters. J. of the Air. Pollution Control Assoc., 28(3), March, 1978, p. 279.

18. Stearns-Roger, Incoporated. Engineering Analysis of the Neal Station Unit No. 3 Cold Side Electrostatic Precipitators, prepared for Meterology Research Incorporated, August, 1977.

APPENDICES

Appendix 1	Description of Methods
Appendix 2	Impactor Substrate Weight Changes for Blank Runs
Appendix 3	Voltage-Current Data
Appendix 4	Size-Dependent Elemental Concentration Data

APPENDIX 1

DESCRIPTION OF METHODS

MASS MEASUREMENT SYSTEM

Mass measurements were conducted at the inlet and outlet sampling locations as outlined in EPA Method 17.[1] The main difference between EPA Method 17 and the EPA Method 5 is the location of the particulate filter in the stack. With this arrangement, a thimble-shaped filter (Figure 1-1) is used to sample high mass concentrations and a conventional, disk-shaped, filter is used for low mass concentrations. The advantage of this system is that the particles are trapped before they enter the probe and a probe wash is not required. A condenser and gas cooler are still required between the probe and the gas metering system. The pitot tube, pump, and other parts of the system are similar to the EPA Method 5 Sampling Train that is shown in Figure 1-2. The thimble-filter system has often been used in engineering tests to evaluate the performance of a control device. In general, this system is easier to use than the EPA Method 5 Sampling Train. The main advantages are the elimination of the probe wash routine and greater flexibility in the placement and mounting of the larger and bulkier components of the system, especially the impinger box, that is available when the rigid probe-filter/impinger box connection is eliminated. If a ceramic thimble is used, the technique is sometimes referred to as the "ASME Method" (American Society of Mechanical Engineers). Calculation of mass concentrations from the data obtained with this sampling system were performed using standard methods as those found in Reference (1).

CASCADE IMPACTORS

Cascade impactors were used to obtain particle mass and particle size distribution entering and leaving the electrostatic precipitator for the diameter range 0.5 to 10 μm.

Particle separation by size interval takes place within cascade impactors by passing the sample gas stream sequentially through a series of dry impingement type inertial classifiers. The classifiers operate by impingement of the aerosol stream as an air jet against a plate, causing the gas in the jet to sharply change direction and flow around the plate. Because of inertia, particles leave the flow streamlines and are deposited on the plate. Each impingement stage in the series operates at a higher impingement velocity (or as a higher energy separator) than the previous stage. Depending on the desired sampling rate and jet velocities the stages may contain single or multiple jets.

---

1. Environmental Protection Agency. Determination of Particulate Emissions from Stationary Sources (In-stack Filtration Methods). Federal Register 43(37):7584, February 23, 1978.

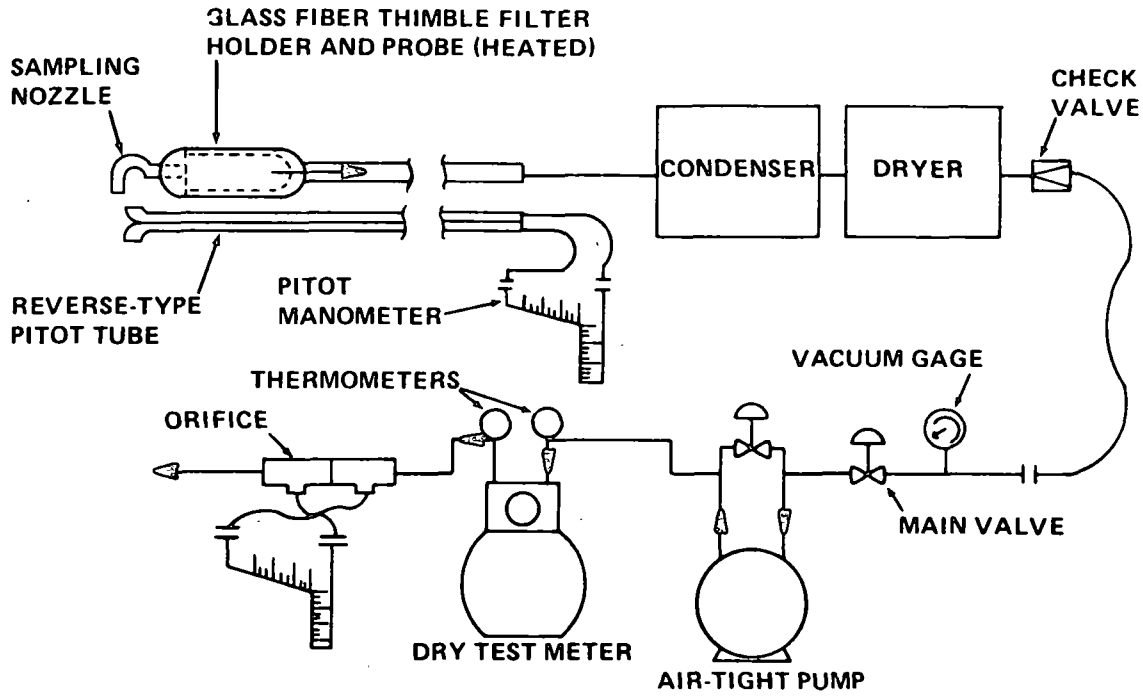

Figure 1-1. Arrangement for Mass Concentration Measurements with Thimble-shaped Filters

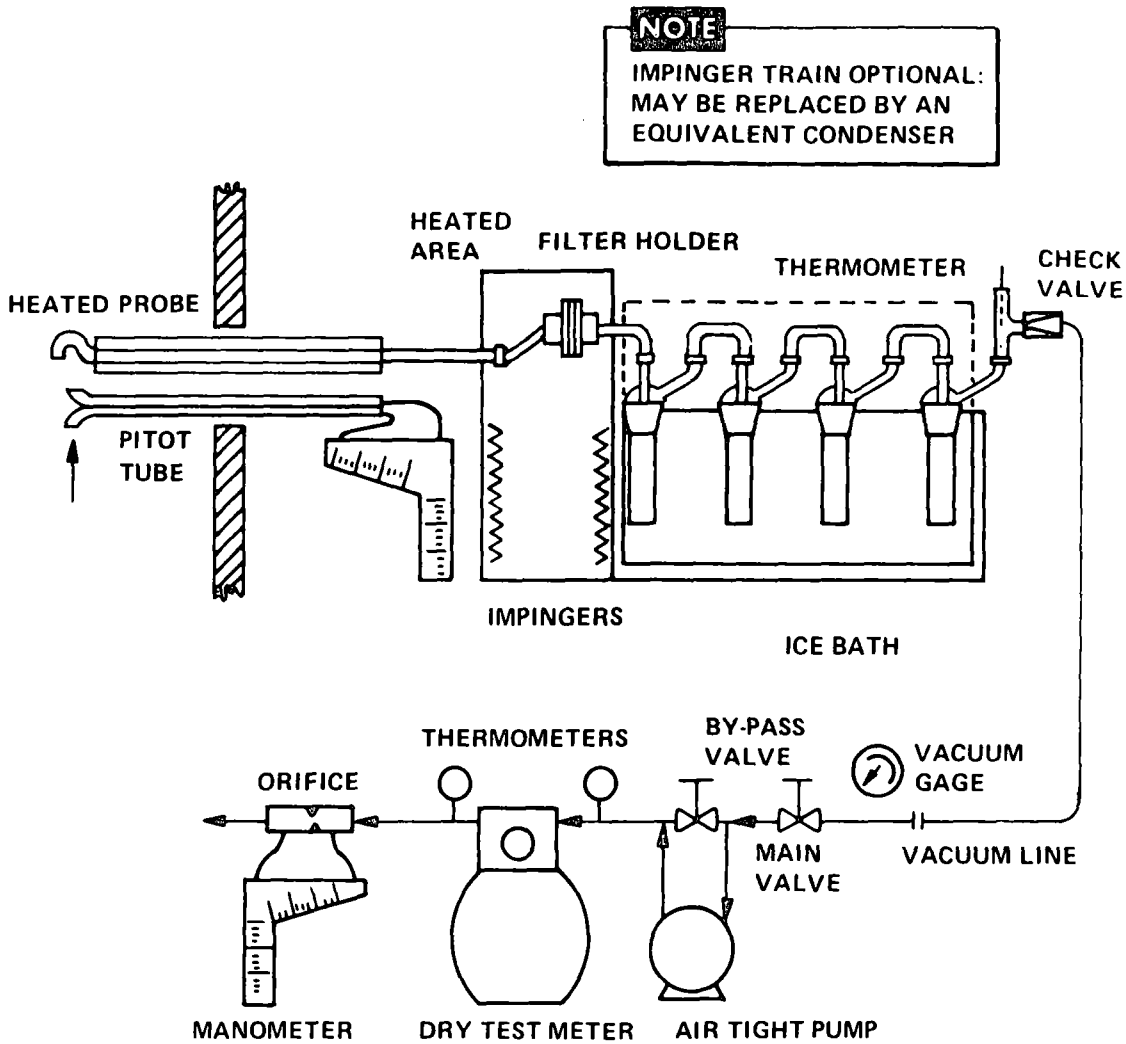

Figure 1-2. Particulate Sampling Train

A typical single-jet impactor is the Brink impactor which operates at a flow rate of about 1.18×10^{-5} m^3/sec (0.025 cfm), while typical multijet impactors are the Andersen and University of Washington impactors which operate at flow rates of about 2.36×10^{-4} m^3/sec (0.5 cfm). By operating the impactors in situ, uncertainties due to probe losses are avoided. However, the impactors must operate at a constant flow rate in order to maintain the various size fractionation diameters of the stages at fixed values. Thus even though traverses are made, isokinetic sampling cannot be maintained. Instead, a suitable flow rate and nozzle diameter are chosen which will best approximate isokinetic sampling over the traverse area.

During the test program modified Brink impactors were used at the inlet sampling locations and Andersen Mark III impactors were used at the outlet sampling locations. Reeve Angel 934 AH glass fiber substrate material which had been acid washed and conditioned in situ was used in each impactor during the test program. Sampling procedures as outlined by Harris[2] were followed.

Once the impactor stage weights were obtained, data reduction procedures as outlined below were followed.

1. Stage weights were corrected for "blank" weight gains.

2. Cut points for the individual stages for each impactor were calculated based on calibration studies conducted in the laboratory using polystyrene latex beads for sizes smaller than 2.0 μm diameter and ammonium fluorescein particles for particle diameters from 2 to 8 μm diameter. Glass fiber substrates were in place for the calibration studies.

3. Impactor runs were arranged in groups in an appropriate manner for the test program.

4. The data were then used as input to a computer program[3] which calculates the size distribution and fractional efficiencies.

---

2. Harris, D. Bruce. Procedures for Cascade Impactor Calibration and Operation in Process Streams. Environmental Protection Technology Services, EPA-600/2-77-004, January 1977.

3. Johnson, J. W., G. I. Clinard, L. G. Felix, and J. D. McCain. A Computer-based Cascade Impactor Data Reduction System. EPA-600/2-78-0242, March 1978.

A detailed description of the data reduction program is available in the EPA publication, "A Computer-based Cascade Impactor Data Reduction System."[3] A brief outline of the operations performed by the program is given below.

1. Individual impactor runs are fit with a series of segmented polynomials (spline fit) which are continuous at the points of overlap in the first derivative with respect to particle size.

2. The "spline fits" for all runs are arranged in the groups desired.

3. The polynomials are differentiated to obtain values of dM/dLOGD at fixed particle sizes. All particle diameters are "Stokes diameter", defined as the diameter of a sphere having the same density which exhibits aerodynamic behavior identical to the particle of interest. Average density values are used which are obtained from helium pycnometer determinations.

4. Average values of dM/dLOGD are calculated for the fixed particle sizes from the members of each group, and an outlier analysis is performed. If the analysis results in certain values being discarded, a new average is computed without the outliers. Fifty percent confidence intervals are then computed.

5. The averaged values of dM/dLOGD are ratioed to calculate penetration values at the fixed particle diameters. Fifty percent confidence intervals for the penetrations are also calculated.

6. The functions determined by the averaged dM/dLOGD values are integrated to obtain corresponding cumulative distributions.

7. The program then plots the size distributions and the penetrations in the desired format.

Page 117 presents the computer printout for one of the Andersen impactors which was operated during the test series and the data reduced using the computer program referenced above. The remainder of the impactor data from this test program is available through the Fine Particle Emissions Information System, in care of Mr. Gary L. Johnson, Special Studies Staff (MD-63), Industrial Environmental Research Lab, Environmental Protection Agency, Research Triangle Park, N.C. 27711.

Table 1-1 contains the calibration constants in the form of $\sqrt{\Psi}$ for each of the impactors used in the test program.

INGSO-5 7-13-77 2,3,4,5,6,7,1 2304 OUTLET SAMPLE ANDERSEN MODEL III STACK SAMPLER NUMBER = 619

IMPACTOR FLOWRATE = 0.308 ACFM IMPACTOR TEMPERATURE = 623.0 F = 328.3 C SAMPLING DURATION = 126.00 MIN

IMPACTOR PRESSURE DROP = 0.1 IN. OF HG STACK TEMPERATURE = 623.0 F = 328.3 C

ASSUMED PARTICLE DENSITY = 2.41 GM/CU.CM. STACK PRESSURE = 24.69 IN. OF HG MAX. PARTICLE DIAMETER = 32.0 MICROMETERS

GAS COMPOSITION (PERCENT) CO2 = 13.86 CO = 0.00 N2 = 73.14 O2 = 4.20 H2O = 8.80

CALC. MASS LOADING = 5.1378E-03 GR/ACF 1.3776E-02 GR/DNCF 1.1757E+01 MG/ACM 3.1524E+01 MG/DNCM

IMPACTOR STAGE	S1	S2	S3	S4	S5	S6	S7	S8	FILTER
STAGE INDEX NUMBER	1	2	3	4	5	6	7	8	9
D50 (MICROMETERS)	10.77	10.43	6.37	4.22	2.45	1.18	0.62	0.27	
MASS (MILLIGRAMS)	2.60	0.69	0.23	0.11	1.67	1.77	2.95	2.15	0.75
MG/DNCM/STAGE	6.43E+00	1.71E+00	5.69E-01	2.72E-01	4.13E+00	4.38E+00	7.30E+00	5.32E+00	1.85E+00
CUM. PERCENT OF MASS SMALLER THAN D50	79.88	74.54	72.76	71.90	58.98	45.28	22.45	5.80	
CUM. (MG/ACM) SMALLER THAN D50	9.39E+00	8.76E+00	8.55E+00	8.45E+00	6.93E+00	5.32E+00	2.64E+00	6.82E-01	
CUM. (MG/DNCM) SMALLER THAN D50	2.52E+01	2.35E+01	2.29E+01	2.27E+01	1.86E+01	1.43E+01	7.08E+00	1.83E+00	
CUM. (GR/ACF) SMALLER THAN D50	4.10E-03	3.83E-03	3.74E-03	3.69E-03	3.03E-03	2.33E-03	1.15E-03	2.98E-04	
CUM. (GR/DNCF) SMALLER THAN D50	1.10E-02	1.03E-02	1.00E-02	9.91E-03	8.12E-03	6.24E-03	3.09E-03	8.00E-04	
GEO. MEAN DIA. (MICROMETERS)	1.86E+01	1.06E+01	8.16E+00	5.19E+00	3.21E+00	1.70E+00	8.53E-01	4.06E-01	1.89E-01
DM/DLOGD (MG/DNCM)	1.36E+01	1.25E+02	2.66E+00	1.52E+00	1.74E+01	1.38E+01	2.62E+01	1.45E+01	6.16E+00
DN/DLOGD (NO. PARTICLES/DNCM)	1.68E+06	8.32E+07	3.88E+06	8.63E+06	4.16E+08	2.23E+09	3.34E+10	1.72E+11	7.29E+11

NORMAL (ENGINEERING STANDARD) CONDITIONS ARE 21 DEG C AND 760MM HG.

SQUARE ROOTS OF PSI BY STAGE	0.305	0.430	0.410	0.385	0.342	0.370	0.352	0.272
HOLE DIAMETERS BY STAGE (CENTIMETERS)	0.1621	0.1263	0.0946	0.0757	0.0581	0.0355	0.0258	0.0245

TABLE 1-1

$\sqrt{\Psi_{50}}$ Values for Cascade Impactor Stages

	Stage	0	1	2	3	4	5	6	7	8
Andersen	229		.305	.430	.410	.385	.328	.319	.364	.283
Andersen	231		.305	.430	.410	.385	.332	.313	.365	.280
Andersen	583		.305	.430	.410	.385	.341	.320	.331	.274
Andersen	619		.305	.430	.410	.385	.342	.370	.352	.272
Andersen	627		.305	.430	.410	.385	.344	.335	.339	.278
Brink	A	.322	.322	.338	.345	.258	.317	.229		
Brink	B	.322	.322	.349	.330	.302	.345	.175		
Brink	C	.322	.322	.351	.388	.330	.350	.273		
Brink	D	.322	.322	.346	.354	.297	.337	.226		

Stage 1 through 4 of the Andersen impactor and stages 1 through 3 of the Brink impactor were calibrated with ammonium fluorescein while stages 5 through 8 of the Andersen impactors and 4 through 6 of the Brink impactors were calibrated with polystyrene latex spheres. During the calibration of each impactor stage, glass fiber substrates were in place.

ELECTRICAL AEROSOL ANALYZER (EAA)

A Thermo-Systems Inc. Model 3030 Electrical Aerosol Analyzer (EAA) was used at the inlet and outlet sampling locations to determine concentration vs. size information in the diameter range of 0.01 to 0.3 μm. This system is shown in Figure 1-3. The EAA operates by placing a known charge on the particles and precipitating the particles under closely controlled conditions. Size selectivity is obtained by varying the electric field in the precipitator section of the mobility analyzer. Charged particle mobility is monotonically related to particle size in the operating regime of the instrument (0.01 to 0.3 μm).

The instrument used for field work by SRI personnel had been slightly modified for ruggedness and convenience. A set screw was installed on the Flow Straightener Cylinder to prevent the spring-loaded electrical contacts from vibrating loose (recent production units of the EAA incorporate this modification), the electrometer connectors were replaced with push-on, quick-disconnect circular connectors, and a "compression tube fitting" assembly connected to the sample inlet allows the Sheath Air Flow and Sample Air Flow to be drawn from separate locations. Output of the EAA was recorded both manually (in digital form) and on a chart recorder (Hewlett Packard Model 7100B, Electric Write).

Data Reduction Procedures

Once the equipment has been set up as shown schematically in Figure 1-4, the flows are adjusted through the sample orifice and the dilution air orifice, to obtain the desired dilution factor. The EAA is placed in a manual scan mode and the current readings for each channel are recorded with a strip chart recorder. Manual control allows run times of from two to five minutes in each of the nine channels. This allows one to average out rapid source fluctuations. At the beginning of each day the internal calibration points and flows through the EAA are checked, as described in the instrument manual. These are also periodically rechecked throughout the day.

The theory of operation and basic equations for the EAA have been given by Liu et al[4] and calibration of the Model 3030 EAA has been done by Liu and Pui[5] which revises the previous calibration. Table 1-2 shows these revised calibration constants in a data reduction format. The calibration by Liu suggested the use of a calibration matrix; however, typical source fluctuations in

---

4. Liu, B.Y.H., K. T. Whitby, and D.Y.H. Pui. A Portable Electrical Aerosol Analyzer for Size Distribution Measurements of Sub-Micron Aerosols. Presented at the 66th Annual Meeting of the Air Pollution Control Association, Paper No. 73-283 (June 1973).

5. Liu, B.Y.H., and D.Y.H. Pui. On the Performance for the Electrical Aerosol Analyzer. J. Aerosol Science, 6, pp. 249-64 (1975).

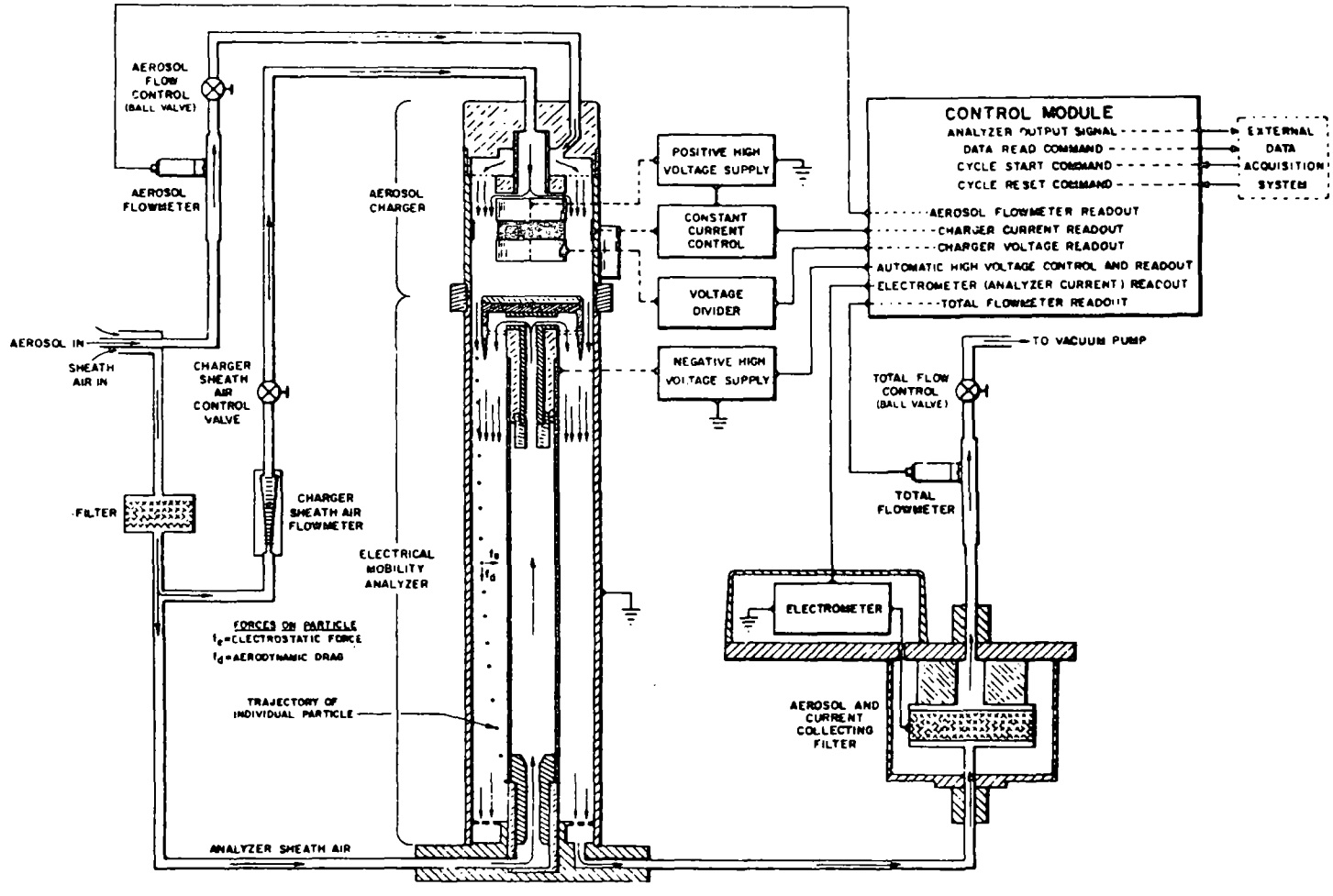

Figure 1-3. Schematic Diagram of the Electrical Aerosol Analyzer. (Liu and Piu[4])

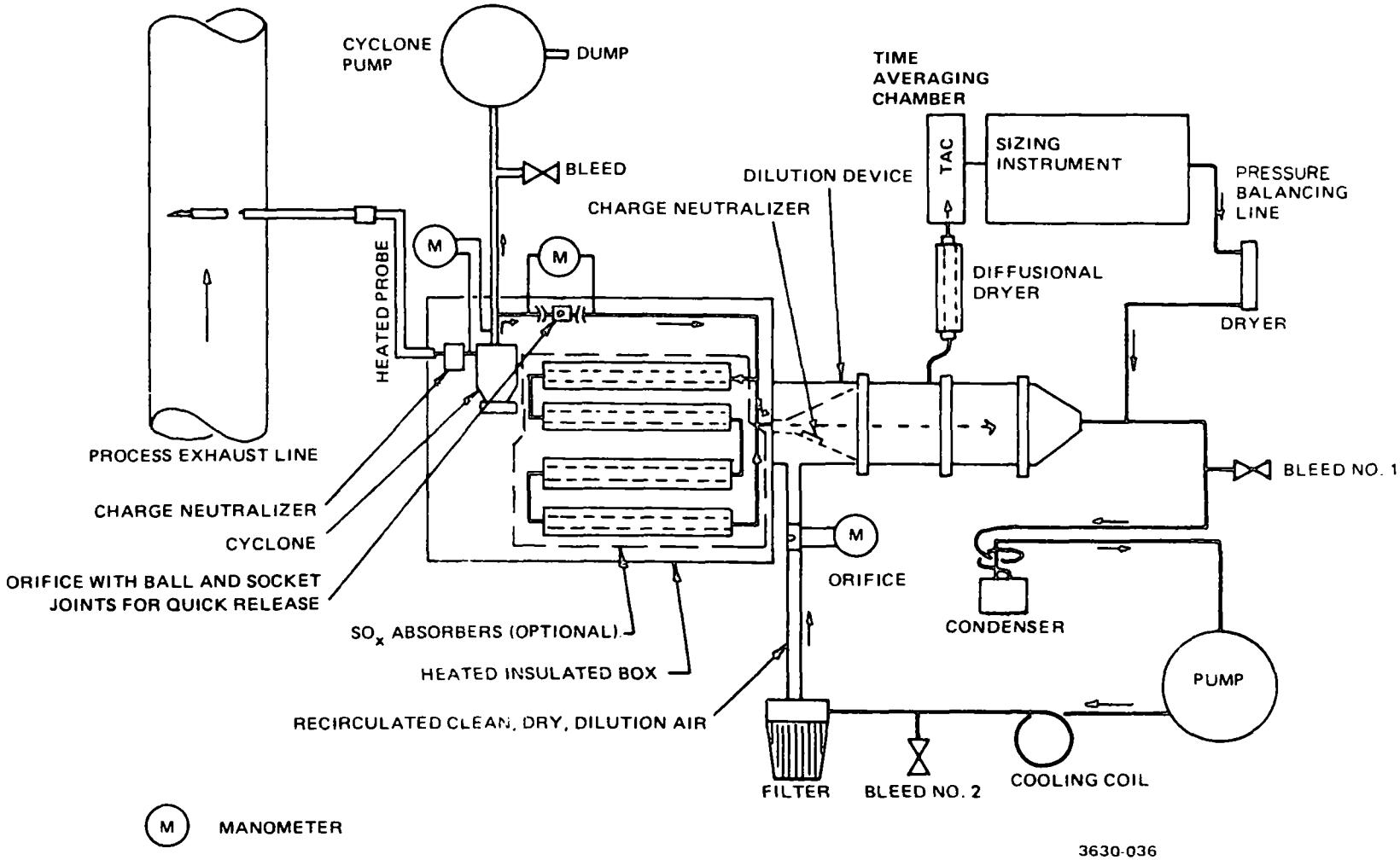

Figure 1-4. Sample Extraction-Dilution System

TABLE 1-2

EAA (Model 3030) Data Reduction Form
Concentration, Cumulative Concentration, and $\Delta N_s/\Delta LogD$ from Scan No. _____
for DF = _____

1	2	3	4	5	6	7	8	9	10	11	12
Channel No.	Collector Voltage	D_p, μm	D_{pi}, μm	$\Delta N/\Delta I$	$\Delta \log D_p$	I,pA	ΔI,pA	ΔN	ΔN_s	ΣN_s	$\Delta N_s/\Delta \log D$
3	196	0.0100				____					
			0.0133	4.76×10^5	0.250		____	___	____	___	_____
4	593	0.0178				____					
			0.0215	2.33×10^5	0.165		____	___	____	___	_____
5	1220	0.026				____					
			0.0306	1.47×10^5	0.141		____	___	____	___	_____
6	2183	0.036				____					
			0.0502	8.33×10^4	0.289		____	___	____	___	_____
7	3515	0.070				____					
			0.0917	4.26×10^4	0.234		____	___	____	___	_____
8	5387	0.120				____					
			0.149	2.47×10^4	0.188		____	___	____	___	_____
9	7152	0.185				____					
			0.219	1.56×10^4	0.148		____	___	____	___	_____
10	8642	0.260				____					
			0.306	1.10×10^4	0.141		____	___	____	___	_____
11	9647	0.360				____					

industrial processes generally negate any potential advantage of such refinements. Table 1-2 is essentially self-explanatory. The heading "D_p,μm" (column 3) is the particle diameter in microns. A value of 0.0100 means that the center rod voltage is such that all particles of 0.0100 μm diameter and smaller are collected in the analyzer tube while larger particles penetrate to the current collecting filter where an electrometer measures the total current carried by the unprecipitated particles. This current represents the charges on all particles larger than 0.0100 μm. This measured current is the basic output of the Model 3030.

The fourth column (D_{pi},μm) is the geometric mean diameter of the particles represented by the current difference of two successive steps (Channel No.'s). For example, the difference in current for the 0.0100 μm cut-off and the current for the 0.0178 μm cut-off is the total current collected from particles between these sizes, or rather for a mean diameter of 0.0133 μm. The current differences are entered in column 8 headed "ΔI,pA" (picoAmps).

The fifth column gives the revised calibration factor (based on the calibration by Liu and Pui[5]) for each of the eight size bands. These factors are in units of particles per cm^3 per picoAmpere. Multiplying this size specific current sensitivity, $\Delta N/\Delta I$, (column 5) by the current difference, ΔI (column 8) gives the total number of particles, ΔN, (column 9) in units of particles by cm^3, within this size band (column 4) for the diluted aerosol. To correct for dilution and find in-stack concentrations, multiply column 9 by the dilution factor (DF) and enter the result, ΔN_s, in column 10. Columns 6 and 12 are used for $\Delta N_s/\Delta LOGD$ information calculated from the number distribution in column 10. Column 11 is used for cumulative concentrations, corrected for dilution to engineering standard (normal) conditions by a dilution factor (i.e. column 10). Engineering standard or normal conditions are defined as 21°C and 760 mm Hg pressure.

The basic data from the EAA is cumulative current for each of nine channels (column 7). One must then take the differences of the current readings for successive channels (column 8) in order to find ΔN, etc. These ΔI values are multiplied by a series of constants ($\Delta N/\Delta I_i$, DF_j) to arrive at ΔN_s (concentration in stack corrected to dry, standard conditions). While a single scan should be made at a constant dilution, different scans may be made at different dilutions. To simplify the arithmetic for each test condition, we form the product $\alpha_i = \Delta I_{i,j} \times DF_j$ and average all such inlet (outlet) products for the same size band. This average is used in Table 1-3 to calculate N_s, cumulative concentration, and $\Delta N_s/\Delta LOGD$ for each size band. When Table 1-3 is used the data reduction is as follows:

TABLE 1-3

EAA (Model 3030) Data Reduction Form
Concentration, Cumulative Concentration, and $\Delta N_s/\Delta LogD$
From Average $\bar{\alpha}$ for Condition _____

1	2	3	4	5	6	7	8	9	10
Channel No.	Collector Voltage	D_p, μm	D_{pi}, μm	$\Delta N/\Delta I$	$\Delta \log D_p$	$\bar{\alpha}$	ΔN_s	$\Sigma \Delta N_s$	$\Delta N_s/\Delta \log D$
3	196	0.0100							
			0.0133	4.76×10^5	0.250	____	____	____	_____
4	593	0.0178							
			0.0215	2.33×10^5	0.165	____	____	____	_____
5	1220	0.026							
			0.0306	1.47×10^5	0.141	____	____	____	_____
6	2183	0.036							
			0.0502	8.33×10^4	0.289	____	____	____	_____
7	3515	0.070							
			0.0917	4.26×10^4	0.234	____	____	____	_____
8	5387	0.120							
			0.149	2.47×10^4	0.188	____	____	____	_____
9	7152	0.185							
			0.219	1.56×10^4	0.148	____	____	____	_____
10	8642	0.260							
			0.306	1.10×10^4	0.141	____	____	____	_____
11	9647	0.360							

Summary of the Calculation Format

STEP 1

A. Calculate the average instrument reading (I) for each channel as obtained from the strip chart recording of channel current vs. time.

B. Calculate all dilution factors (DF_j).

STEP 2

Calculate current differences ($\Delta I_{i,j}$) from adjacent channels and average the i products ($\alpha_i = \Delta I_{i,j}$ s DF_j) for the same size band for all scans taken for the same test conditions. Calculate 90% confidence intervals for each $\bar{\alpha}_i$. Note: the i subscript denotes size and the j subscript denotes dilution setting.

STEP 3

Using α_i and Table 1-2 calculate "number concentration" (ΔN_s), "average cumulative concentration of all particles having diameter greater than the indicated size" ($\Sigma\Delta N_s$), and "$\Delta N_s/\Delta$LOGD" for each size band for each test condition.

STEP 4

Plot "Cumulative Concentration vs. Size" for each test condition.

STEP 5

Plot $\Delta N_s/\Delta$LOGD [with upper and lower (50% or 90%) confidence limits] vs. size for each test condition.

RESISTIVITY MEASUREMENT SYSTEMS

Resistivity measurements were obtained with an ASME Power Test Code 28 apparatus, and a point-to-plane probe, for conducting the laboratory and in situ measurements, respectively, as described below.

LABORATORY MEASUREMENTS

The basic conductivity cell is shown in Figure 1-5. It consists of a cup which contains the ash sample and which also serves as an electrode, and an upper electrode with a guard ring. To conform with the code, the high-voltage conductivity cell must have the same dimensions as shown, and must use electrodes constructed from 25-micron porosity sintered stainless steel.

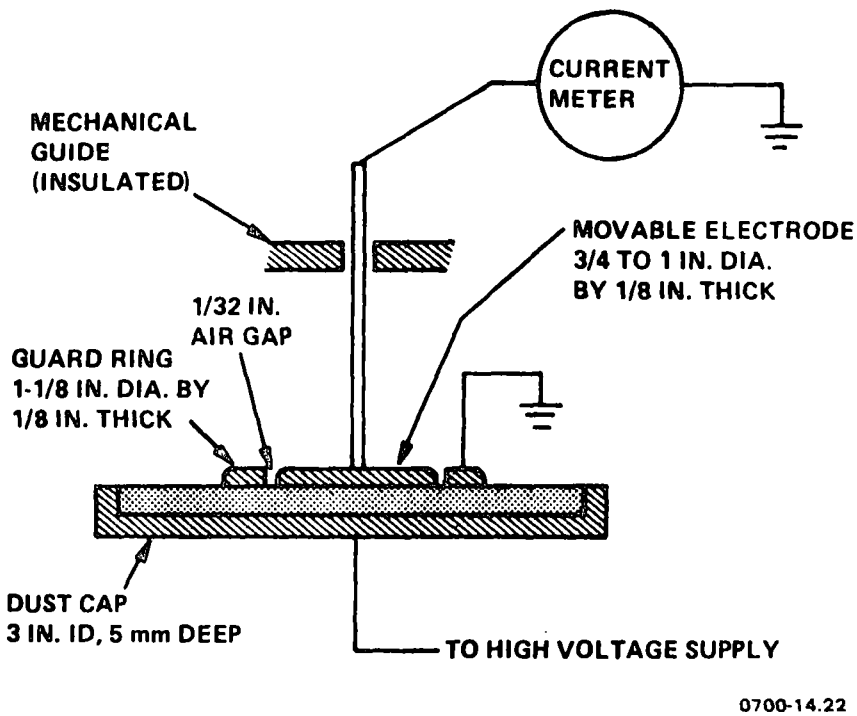

Figure 1-5. Bulk Electrical Resistivity Apparatus, General Arrangement

The movable disk electrode is weighted so that the pressure on the dust layer due to gravitational force is 10 grams per square centimeter. The nominal thickness of the dust layer is 5 millimeters. The actual thickness is to be determined with the movable electrode resting on the surface of the dust. All electrode surfaces in the region of the dust layer are to be well rounded to eliminate high electric field stresses.

The controlled environmental conditions required for the measurement of resistivity in the laboratory can be achieved by an electric oven with thermostatic temperature control and with good thermal insulation to maintain uniform internal temperature, and a means to control humidity. Humidity may be controlled by any one of several conventional means, including circulation of preconditioned gas through the oven, injection of a controlled amount of steam, use of a temperature-controlled circulating water bath, or the use of chemical solutions which control water vapor pressure. It is desirable to circulate the humidified gas directly through the dust layer; hence the reason for the porous electrodes. Figure 1-6 illustrates a set-up for resistivity measurements similar to the one presently in use in our laboratories. However, the present set-up has the capability of providing a simulated flue gas environment.

Our standard procedure for laboratory resistivity measurements can be used to obtain data from 84 to 460°C. The ash is thermally equilibrated at 460°C overnight in a dry nitrogen atmosphere. The test environment, which will consist of a mixture containing H_2O, O_2, CO_2, SO_2, and the balance N_2, is then introduced, and current is measured every ten minutes thereafter until the current increases less than 10% in a ten minute period. At this point, it is assumed that the ash and environment are reasonably equilibrated, and the oven is turned off. As the temperature decreases, the current is determined for every 30 to 40°C drop in temperature under an applied electric field.

Point-to-Plane Probe for In Situ Measurements

The point-to-plane probe is shown in Figure 1-7. The probe is inserted directly into the dust-laden gas stream and allowed to come to thermal equilibrium. The particulate sample is deposited electrically onto the measurement cell through the electrostatic action of the corona point and plate electrode. A high voltage is impressed across the point and plate electrode system such that a corona is formed in the vicinity of the point. The dust particles are charged by the ions and perhaps by free electrons from this corona in a manner analogous to that occurring in a precipitator.

The dust layer is formed through the interaction of the charged particulate with the electrostatic field adjacent to the collection plate. Thus, this device is intended to simulate the behavior of a full-scale electrostatic precipitator and to provide a realistic value for the resistivity of the dust that should be comparable to that in the actual device.

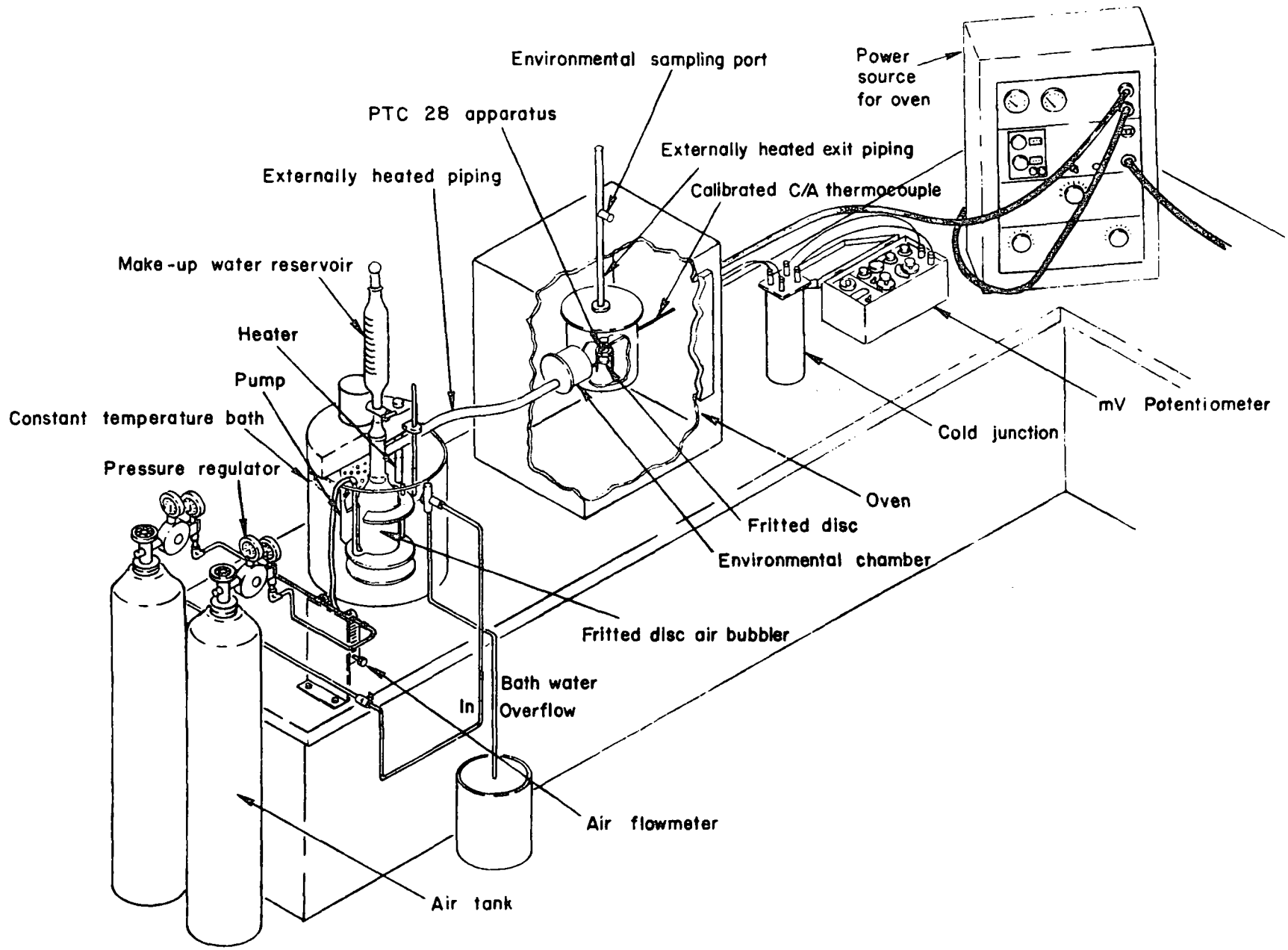

Figure 1-6. Schematic of Apparatus Set-up for Resistivity Measurements

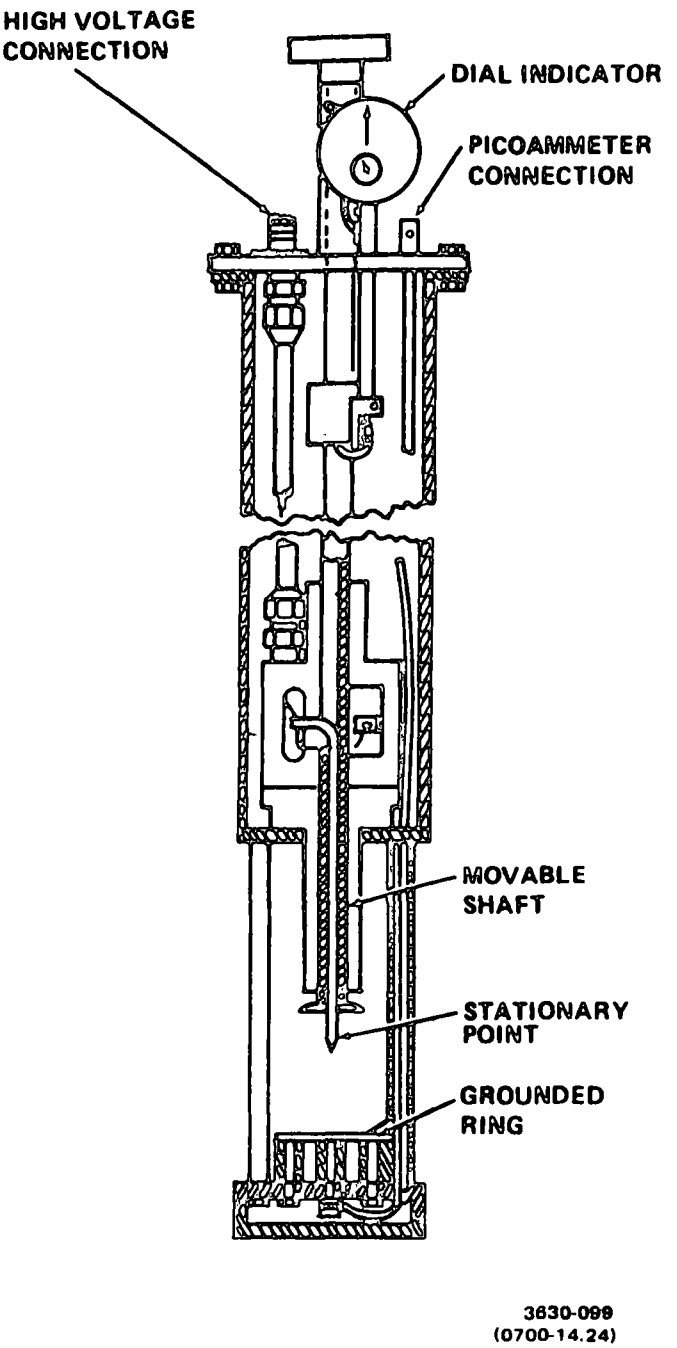

Figure 1-7. Point-to-plane resistivity probe.

In the point-to-plane technique, two methods of making measurements on the same sample may be used. The first is the "V-I" method. In this method, a voltage-current curve is obtained before the electrostatic deposition of the dust, while the collecting disc is clean. A second voltage-current curve is obtained after the dust layer has been collected. After the layer has been collected and the clean and dirty voltage-current curves obtained, the second method of making a measurement may be used. In the second method, a disc the same size as the collecting disc is lowered on the collected sample. Increasing voltages are then applied to the dust layer and the current obtained is recorded until the dust layer breaks down electrically and sparkover occurs. The geometry of the dust sample, together with the applied voltage and current, provide sufficient information for determination of the dust resistivity.

In the point-to-plane method, the voltage drop across the dust layer is determined by the shift in the voltage-vs-current characteristics along the voltage axis as shown in Figure 1-8. The situation shown is for resistivity values ranging from 10^9 to 10^{11} ohm-cm.

If the parallel disc method is used, dust resistance is determined from the voltage measured just prior to sparkover. In both methods the resistivity is calculated as the ratio of the electric field to the current density.

The practice of measuring the resistivity with increasing voltage has evolved because the dust layer behaves as a nonlinear resistor. As the applied voltage is increased, the current increases greater than that attributable to the increase in voltage. Therefore, as described in the A.S.M.E. Power Test Code Number 28 procedure, the value just prior to sparkover is reported as the resistivity.

SAMPLE CALCULATIONS FOR DATA REDUCTION OF RESISTIVITY MEASUREMENTS

After all data has been recorded for the point-to-plane resistivity probe, Figure 1-9, the resistivity can be calculated by using the following equation:

$$\rho = \frac{V}{I} \cdot \frac{A}{L}$$

where:

ρ = resistivity, ohm-cm.

V = voltage or voltage drop when calculating resistivity from the V-I method, volts.

I = current at voltage used to calculate resistivity, amps.

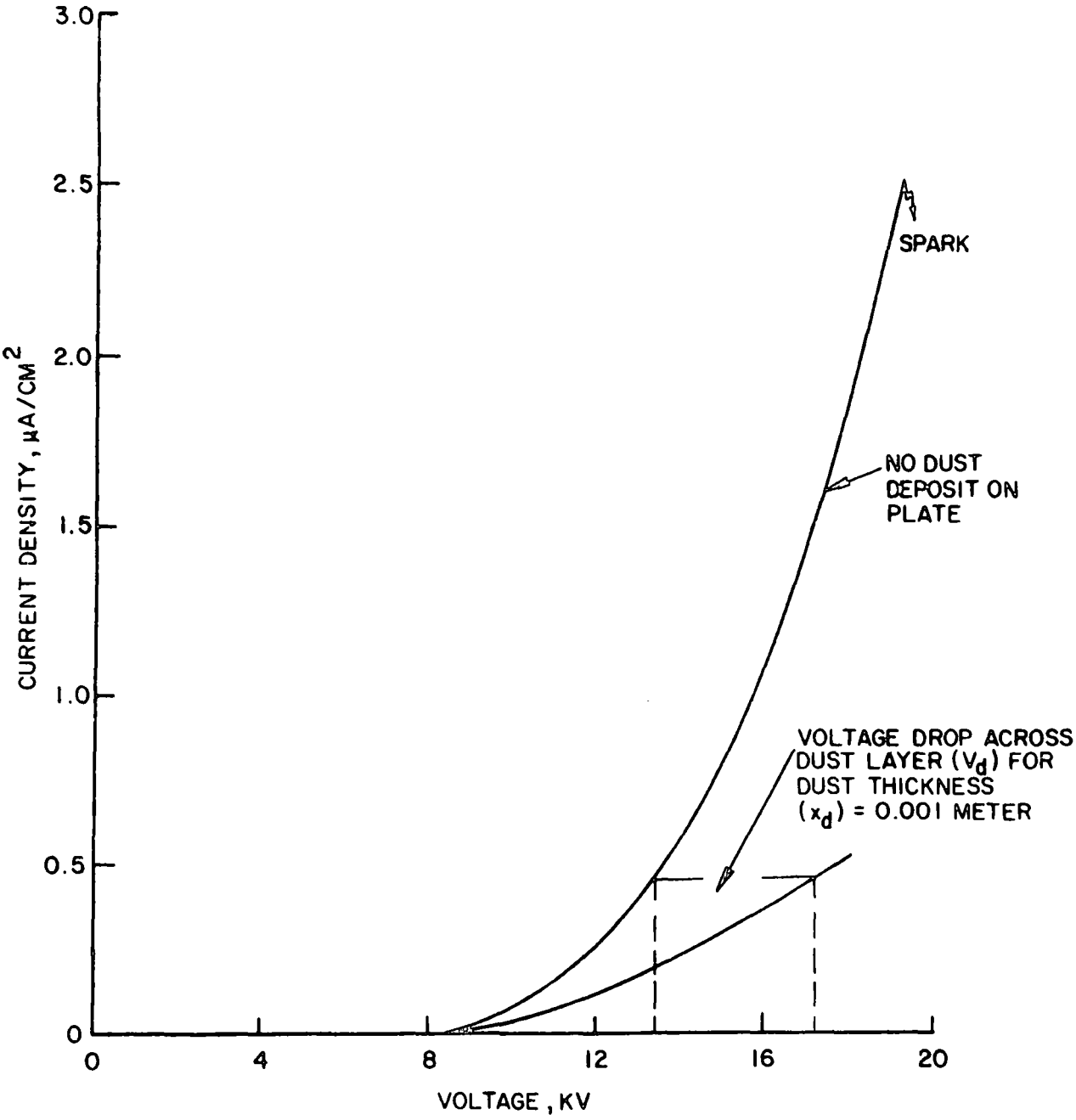

Figure 1-8. Typical voltage-current relationships for point-to-plane resistivity probe.

Area = 5 cm^2

V-I DATA		
VOLTS KV	AMPS. CLEAN	DIRTY
1		
2		
3		
4	Start	Start
5	.20 μA	.17 μA
6	.38 μA	.29 μA
7	.57 μA	.48 μA
8	.88 μA	.75 μA
9	Spark	Spark
10		
11		
12		
13		
14		
15		
16		
17		
18		
19		
20		
21		
22		
23		
24		
25		

Date May 31, 1977

Time 12:00 - 1:00

Place Coal Fired Power Plant

Temp. 655°F (346°C)

Cell Depth 1.0 mm (.1 cm)

Location Inlet Port 3

Test # 1

SPARK DATA			RESISTIVITY
VOLTS	AMPS	E = V/cm	$\rho = \frac{E \cdot A}{I}$
100	.13 μA	1000	3.8×10^{10}
200	.45 μA	2000	2.2×10^{10}
300	.81 μA	3000	1.85×10^{10}
400	1.0 μA	4000	2.0×10^{10}
500	1.2 μA	5000	2.0×10^{10}
600	1.9 μA	6000	1.6×10^{10}
700	2.4 μA	7000	1.5×10^{10}
800	2.7 μA	8000	1.5×10^{10}
900	Spark		
1000			
1100			
1200			
1300			
1400			
1500			
1600			
1700			
1800			
1900			
2000			
2100			
2200			
2300			
2400			
2500			
2600			
2700			
2800			
2900			
3000			
3500			
4000			
4500			

Figure 1-9. Resistivity Field Data Sheet

A = cross sectional area of sample, cm^2.

L = depth of the sample, cm.

From Figure 1-9, the V-I data can be graphed as in Figure 1-10, and the resistivity calculated.

V-I Data,

$$\rho = \frac{\Delta V}{I} \quad \frac{A}{L}$$

$$\rho = \frac{400V}{.5\mu A} \quad \frac{5\ cm^2}{.1\ cm}$$

$$= 4 \times 10^{10} \text{ ohm-cm.}$$

Also, from Figure 1-9, the resistivity can be calculated at each applied voltage from the spark data with the same equation.

Gas Analysis System

Flue gas constituents of oxygen and carbon dioxide were determined, entering and leaving the precipitator with commercial Orsat-type apparatus. Two Orsat-type analyzers were used to determine oxygen content of the gas entering and leaving the precipitator simultaneously.

The flue gas was sampled for SO_2 and SO_3 using a sampling technique developed under previous EPA contracts. The technique is illustrated in Figure 1-11, and is similar to one described by Lisle and Sensenbaugh.[6]

The sampling probe includes two concentric tubes with lengths of 1.2 m; the inner tube or sampling line is made of Pyrex with an interval diameter of about 7 mm, and the outer tube used for support and insulation is made of stainless steel with an external diameter of about 25 mm. The annulus between the two tubes contains an electrical heating tape around the wall of the Pyrex tube and an insulating asbestos tape around the heating tape. The end of the Pyrex tube that is inserted in the flue is packed with quartz wool to prevent particles of fly ash and H_2SO_4-H_2O condensate from entering the collection system; the other end of the Pyrex tube is fitted with a ball-and-socket joint for connection to the condenser. The condenser consists

6. Lisle, E.S., and J.D. Sensenbaugh. Combustion 36(1),12 (1965).

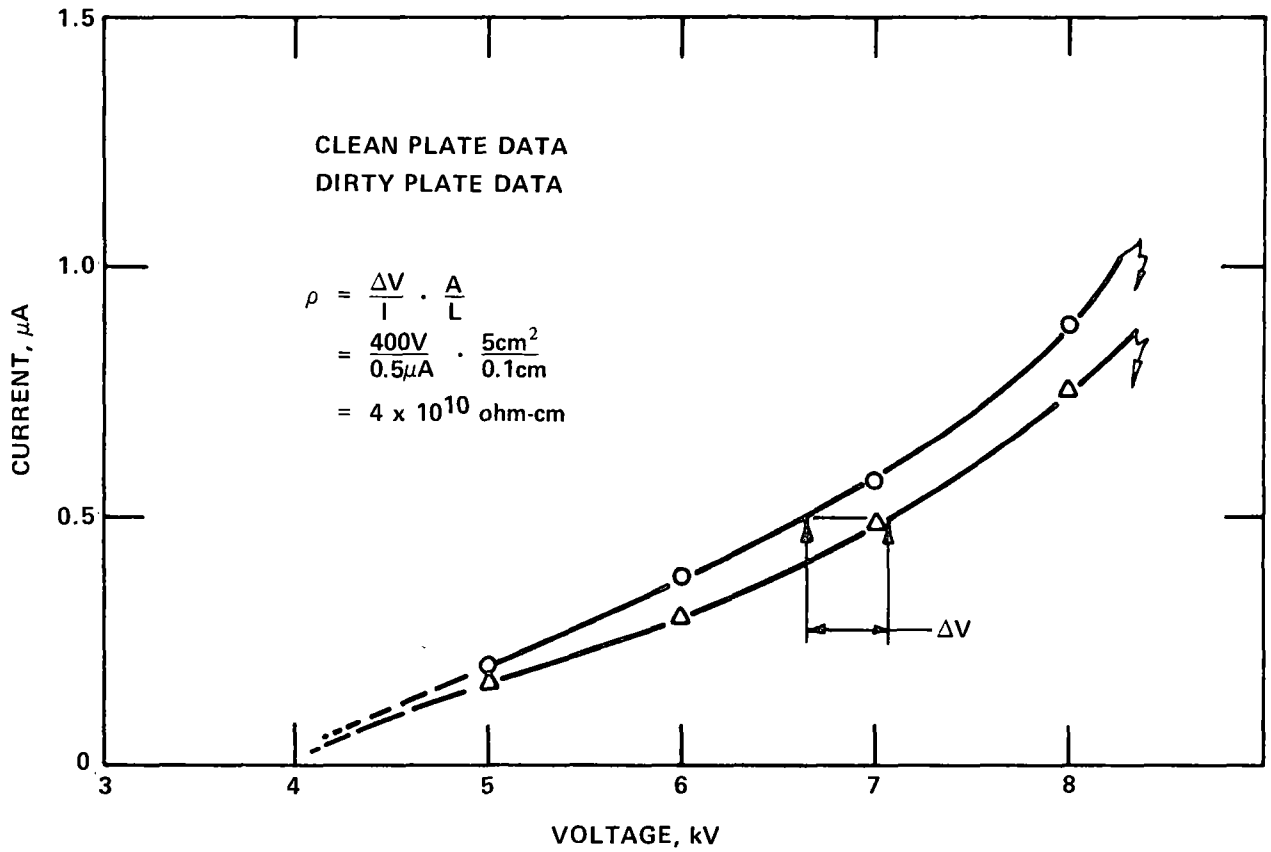

Figure 1-10. In situ V-I resistivity measurements.

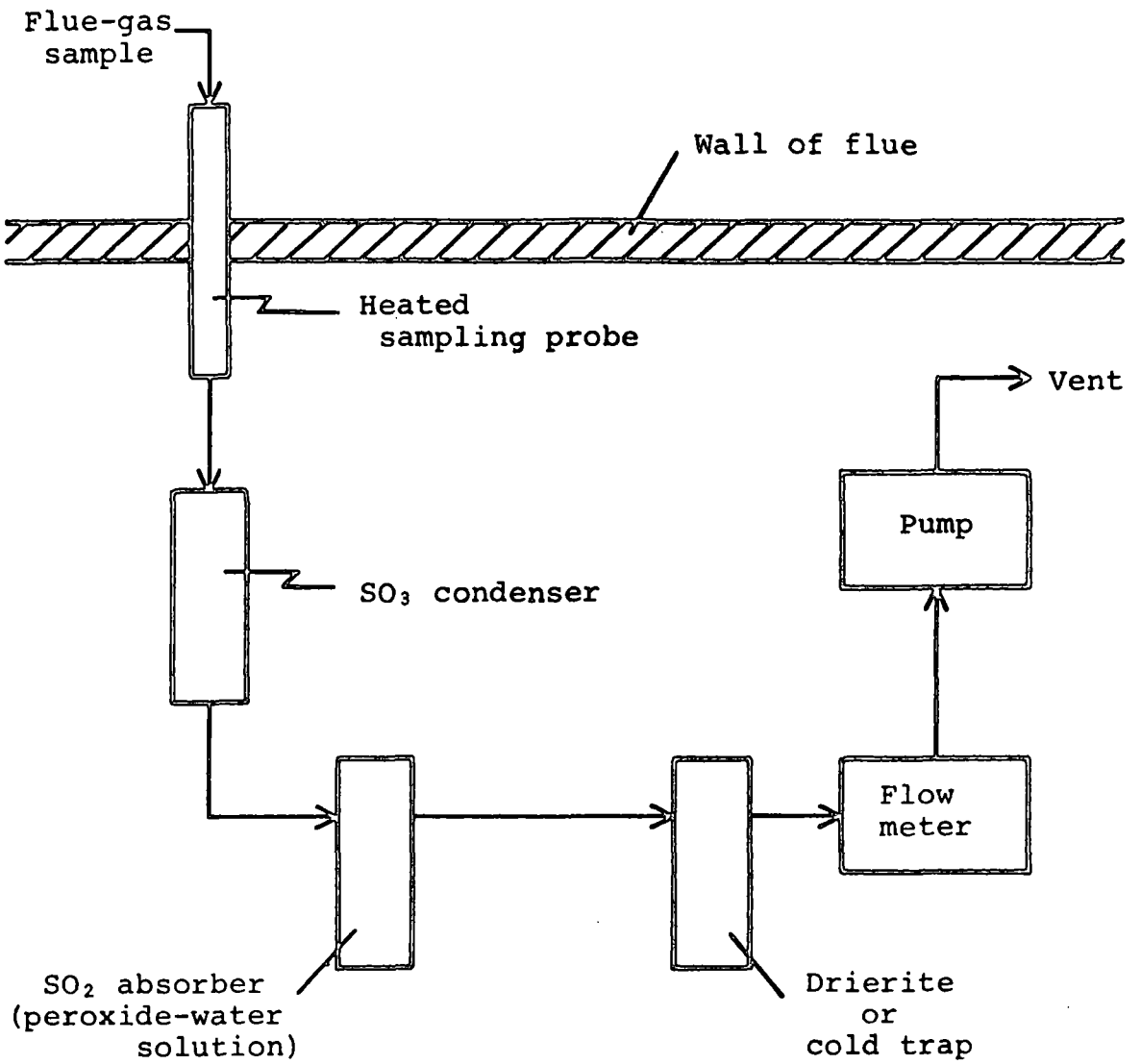

Figure 1-11. Schematic Diagram of Apparatus for Collection of SO_3 by the Condensation Method

of a helical condensation tube made from Pyrex tubing with an internal diameter of about 7 mm and an overall length of about 1 m; a spray trap consisting of a fritted-glass filter (sealed to the helix near the exit); a heated bath of ethylene glycol and water around the helix and filter; and a steel pipe fitted with an external heating tape for containing and heating the water-glycol mixture. The SO_2 scrubber is a bubbler filled with a 3% solution of H_2O_2 in water. The flow-rate indicator is a Charcoal Test Meter (product of American Meter Company) with an inlet filter of Drierite or, as an alternative, a vapor trap immersed in an ice bath. The Charcoal Test Meter registers the integral of flow rate with time and, thus, shows the total volume of dry flue gases sampled except for the relatively small volumes of SO_3 and SO_2 collected upstream. A small vacuum pump (Model 1031-V102-351 of Gast Manufacturing Corporation) is used for sampling flue gases at an approximate rate of 2 l/min for a period of about 20 min.

A titration method was used for determination of SO_3 and SO_2 collected as H_2SO_4. The method is based on titration of H_2SO_4 with $Ba(ClO_4)_2$, with 4:1 mixture of isopropanol and water as the solvent and the organic dye thorin as the indicator of the end point. This titration method is sufficiently sensitive for use in determining SO_3 in flue gases at concentration down to 1 ppm with samples of reasonable volumes (40 liters). It is also sufficiently sensitive in determining the characteristically much higher concentrations of SO_2.

Water vapor content of the flue gas was determined with the use of an efficient drying agent in solid form. Experimental data obtained in the laboratory with simulated flue gas mixtures (under past EPA contracts) showed high efficiency of water vapor recovery and indicated that an accurate determination of water vapor concentration could be made with Drierite in the presence of other flue gas components.

SAMPLE CALCULATION FOR DATA REDUCTION OF GAS ANALYSIS MEASUREMENTS

After performing the necessary sampling, the data in Table 1-4 is used to calculate SO_2 and SO_3 concentration and moisture content of the flue gas.

1. Volume of gas sampled at STP (0°C, 760 mm Hg) = V_s

TABLE 1-4

SO_x DATA

Meter Temperature:	75°F (24°C)	Barometric Pressure:	659 mmHg
Sample Line Pressure Drop:	119 mmHg	Flue Gas Temperature:	640°F (330°C)
		Condenser Temperature:	5°C

Gas Meter Start:	61.6 ft^3
Gas Meter End:	63.9 ft^3
Total Sample, Vm:	2.3 ft^3
Start Sample Time:	11:00
End Sample Time:	11:30
Total Sample Time:	30 minutes

H_2O DATA

Weight of Drierite Column, before:	55.0309 g	Gas Meter Start	72.84 ft^3
Weight of Drierite Column, after:	55.3726 g	Gas Meter Stop:	73.04 ft^3
Total Weight of H_2O	.3417 g	Total Sample, Vm	.20 ft^3

Time:	2:30 p.m.
Flue Gas Temperature:	640°F (338°C)
Sample Line Pressure	33.5 mmHg
Gas Meter Temperature:	76°F (24°C)

LAB DATA

	SO_2	SO_3
Volume of Final Sample	200 ml	50 ml
Aliquot Taken	2 ml	50 ml
Net Titration Volume	4.11 ml	0.97 ml

$$V_s = V_m \times \frac{P_{bar}-P_m}{P_{std}} \times \frac{T_{std}}{T_m} \times 28.3\ \ell/ft^3$$

$$= 2.3\ ft^3 \times \frac{659-119}{760} \times \frac{273}{273+24} \times 28.3\ \ell/ft^3$$

$$= 42.5\ \ell$$

where:

V_s = volume of gas sample at STP, liters.

V_m = volume of gas sample through the dry gas meter (meter conditions), ft^3.

P_{bar} = barometric pressure, mm Hg.

P_m = meter pressure, mm Hg.

P_{std} = absolute pressure at standard conditions, 760 mm Hg.

T_{std} = absolute temperature at STP, 273°C.

T_m = dry gas meter temperature, °K.

1 ft^3 = 28.3 liters at STP.

2. Concentration of SO_2 or SO_3, ppm = C_{SOx}

$$C_{SOx} = \frac{TXN \times 11.2\ ml/meq \times 10^3\ \mu l/ml \times F}{V_s}$$

where:

C_{SOx} = concentration of SO_2 or SO_3 in parts per million.

T = titration volume of $Ba(ClO_4)_2$ solution, ml.

N = normality of $Ba(ClO_4)_2$ solution, milliequivalent/milliliter.

1 milliquivalent = 11.2 milliliters at STP

1 milliliter = 10^3 microliters (µl)

F = volume of sample/volume of aliquiot taken.

V_s = volume of gas sample at STP, liters.

and from Table 1-4,

$$C_{SO_2} = \frac{4.11 \text{ ml} \times 5.3 \times 10^{-3} \text{ meq/ml} \times 11.2 \text{ ml/meq} \times 10^3 \text{ µl/ml} \times 200/2}{42.5 \text{ l}}$$

$$C_{SO_2} = 574 \text{ µl/l (ppm)}$$

and

$$C_{SO_3} = \frac{0.97 \text{ ml} \times 5.3 \times 10^{-3} \text{ meq/ml} \times 11.2 \text{ ml/meq} \times 10^3 \text{ µl/ml} \times 50/50}{42.5 \text{ l}}$$

$$C_{SO_3} = 1.4 \text{ µl/l (ppm)}$$

In order to determine the moisture content of the flue gas, the weight of water must be converted to a vapor volume at STP and divided by the volume of gas sample plus the vapor volume. Therefore:

3.
$$Vw_{std} = M_{H_2O} \times 1.24 \text{ l/g } H_2O$$

$$= .3417\text{g} \times 1.24 \text{ l/g } H_2O = 0.42$$

$$= 0.42 \text{ l}$$

where:

Vw_{std} = volume of water vapor in the gas sample (0°C, 760 mm Hg), liters.

1.24 l/g H_2O = 22.4 l/mole/18g/mole of H_2O at 0°C and 760 mm Hg.

4.
$$Vm_{std} = Vm \times 28.3 \text{ l/ft}^3 \times \frac{P_{bar} - P_m}{P_{std}} \times \frac{T_{std}}{T_m}$$

$$= .20 \text{ ft}^3 \times 28.3 \text{ l/ft}^3 \times \frac{659-33.5}{760} \times \frac{273}{297}$$

$$= 4.28 \text{ l}$$

and

5. Moisture Content = B_{wo}

$$B_{wo} = \frac{Vw_{std}}{Vm_{std} + Vw_{std}}$$

$$B_{wo} = \frac{.42\ l}{4.28\ l + .42\ l}$$

$$= .089 \text{ or } 8.9\%$$

Five-Stage Series Cyclone System

A five-stage series cyclone system[7] which was designed and fabricated by Southern Research Institute under EPA Contract No. 68-02-2131 (Figure 1-12) was used at the inlet and outlet sampling locations sequentially to obtain size fractionated particulate for elemental analysis. The series cyclone system was used since it satisfied the specific objectives of achieving larger sampling times in high grain loading situations than may be possible with an impactor, and collecting gram quantities of size fractionated particulate for chemical analysis.

After size fractionated samples were obtained, they were sent to Crocker Nuclear Laboratory for ion-excited X-ray analysis.[8] When they were received by Crocker Nuclear Laboratory, they were deposited upon a suitable filter material and an elemental analysis determined for each.

SAMPLE CALCULATIONS FOR DATA REDUCTION OF FIVE-STAGE SERIES CYCLONE MEASUREMENTS

The data reduction technique for the cyclones follows that of the impactor data reduction as previously outlined with the major difference being the calculation of the D_{50} cut point for each cyclone.

---

7. Smith, Wallace B. and Rufus R. Wilson, Jr. Development and Laboratory Evaluation of a Five-Stage Cyclone System. EPA-600/7-78-008, January, 1978.

8. Cahill, T.A., et al. Monitoring of Smog Aerosols with Elemental Analysis by Accelerator Beams. National Bureau of Standards, Special Publication 422, issued August, 1976.

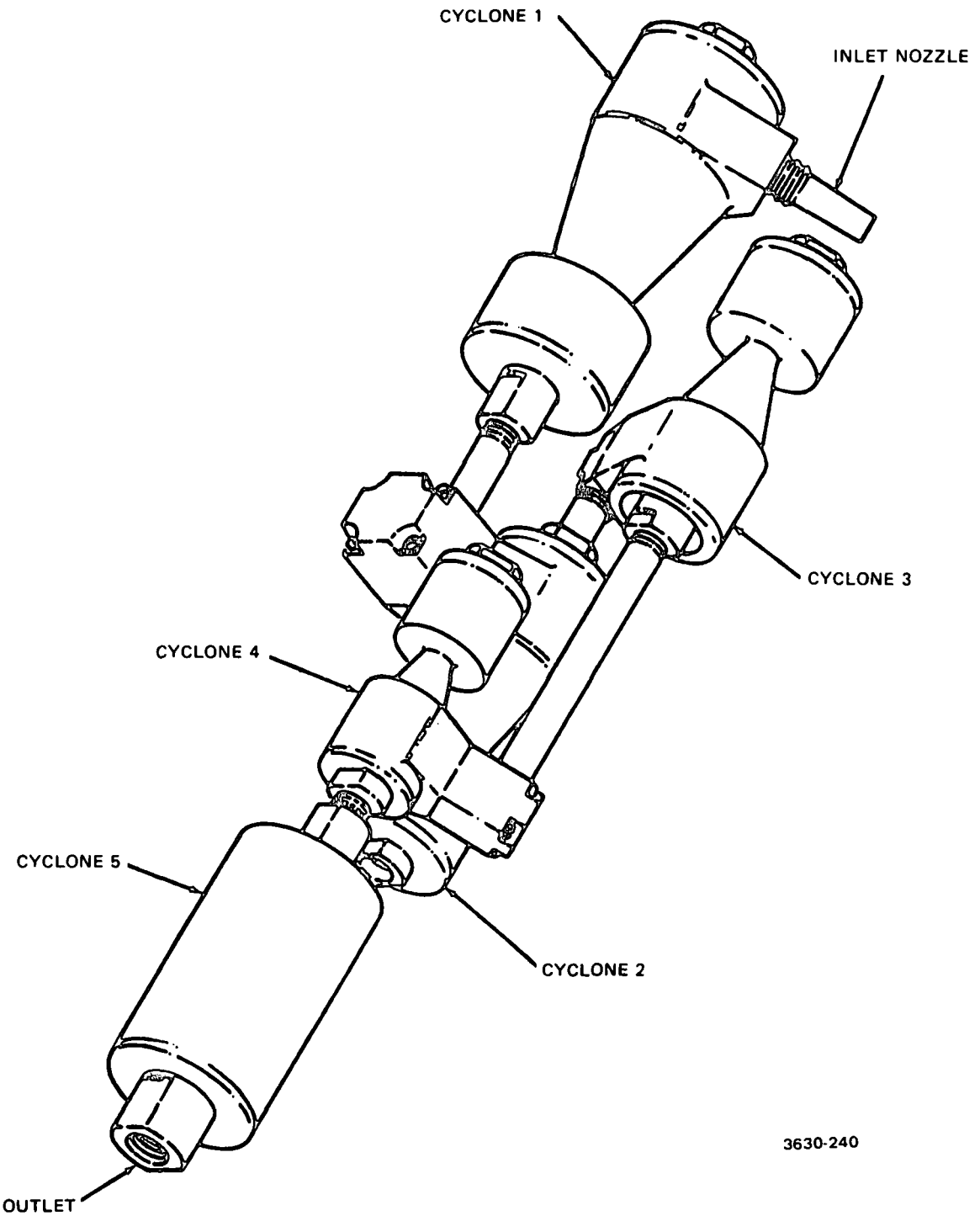

Figure 1-12. Southern Research Institute Five Series Cyclone System.

The following is a description of the procedure used in calculating the D_{50} cutpoints for the cyclones which were operated at the Navajo Generating Station under the conditions stated in Table 19 of the text.

It is assumed that changes in viscosity (temperature), flowrate, and particle density are independent of each other in affecting cyclone performance. Thus, adjustments can be made in each of these separately of the other.

Example Calculation: Cyclone 1 D_{50} for Run ID CYC 3

From Figure 1-13, the D_{50}-viscosity line is extrapolated to obtain 8.18 μm for the D_{50} of cyclone 1 at a temperature of 685°F, a particle density of 2.04 g/cm^3, and a flowrate of 1 ft^3/min. The density of the dust collected was 2.41 g/cm^3. The D_{50} varies inversely with the square root of the density for cyclones, thus:

$$\frac{D_{50}\ (\rho=2.41\ g/cm^3)}{D_{50}\ (\rho=2.04\ g/cm^3)} = \frac{\sqrt{2.04}}{\sqrt{2.41}} \qquad (1)$$

Since D_{50} for a particle density of 2.04 g/cm^3 is 8.18 μm, the D_{50} of cyclone 1 for a particle density of 2.41 g/cm^3, a temperature 685°F, and a flowrate of 1 ft^3/min is 7.53 μm. The D_{50} flowrate dependence for cyclone 1 is assumed to be

$$D_{50} = KQ^n \qquad (2)$$

where Q is flowrate in liters/min and K and n are experimental constants.

Dividing equation (2) by itself, for the two flow rate, we obtain

$$\frac{D_{50}(2.41\ g/cm^3,\ 685°F,\ 1.07\ ft^3/min)}{D_{50}(2.41\ g/cm^3,\ 685°F,\ 1.00\ ft^3/min)} = \frac{(30.30)^{-.63}}{(28.32)^{-.63}} \qquad (3)$$

where n = -.63 is an experimental value found in our laboratory calibration of cyclone 1. Equation (3) gives 7.21 μm for the D_{50} of cyclone 1 for a particle density of 2.41 g/cm^3, a temperature 685°F, and a flowrate of 1.07 ft^3/min.

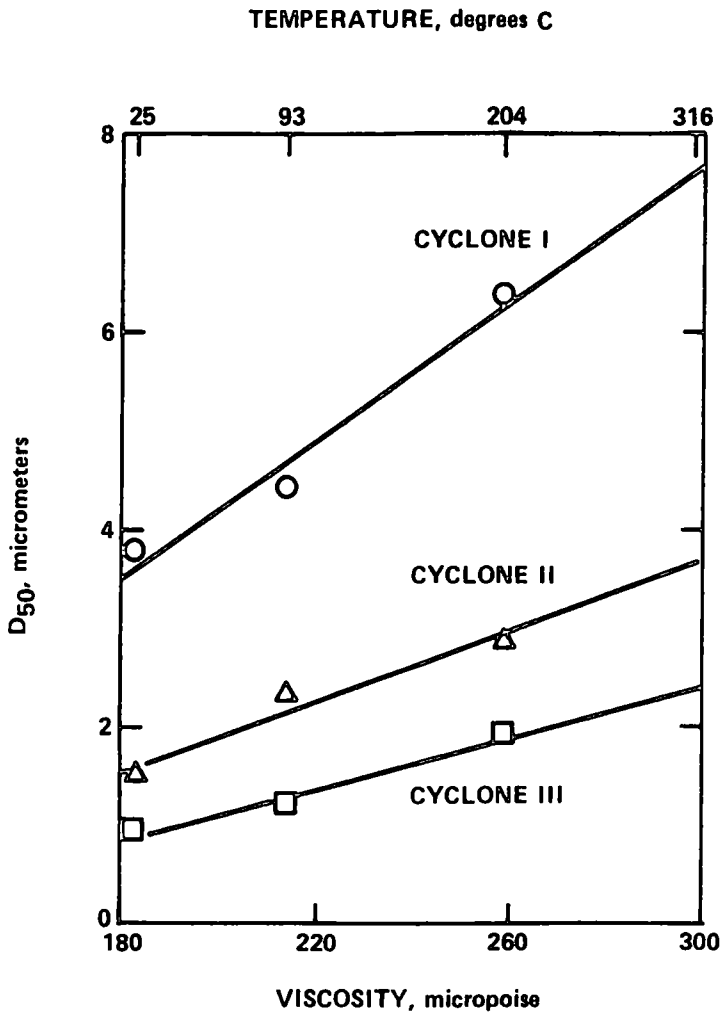

Figure 1-13. *D_{50} cut point versus viscosity for EPA-S.R.I. Cyclones I, II, and III at a flow rate of 28.3 ℓ/min, temperatures of 25, 93, and 204°C, and for a particle density of 2.04 gm/cm^3.*

Cyclone 1 D_{50} for Run IDC CYC 5

From Figure 1-13, an extrapolation of the D_{50}-viscosity curve gives 7.83 μm for the D_{50} of cyclone 1 for a temperature of 630°F, a particle density of 2.04 g/cm^3, and a flowrate of 1 ft^3/min. Equation (1) then becomes

$$\frac{D_{50}(\rho=2.41\ g/cm^3)}{7.83\ \mu m} = \frac{\sqrt{2.41}}{\sqrt{2.41}}$$

giving 7.20 μm for the D_{50} of cyclone 1 for a temperature of 630°F, a particle density of 2.41 g/cm^3, and a flowrate of 1 ft^3/min. Finally, equation (3) becomes

$$\frac{D_{50}(2.41\ g/cm^3,\ 630°F,\ 1.1\ ft^3/min}{7.20\ \mu m} = \frac{(31.15)^{-.63}}{(28.32)^{-.63}}$$

giving 6.78 μm for the D_{50} of cyclone 1 for a temperature of 630°F, a particle density of 2.41 g/cm^3, and a flowrate of 1.1 ft^3/min.

Cyclone 1 D_{50} for Run ID CYC 7

From Figure 1-13, an extrapolation of the D_{50}-viscosity curve gives 8.27 μm for the D_{50} of cyclone 1 for a temperature of 700°F, a particle density of 2.04 g/cm^3, and a flowrate of 1 ft^3/min. Equation (1) then becomes

$$\frac{D_{50}(\rho=2.41\ g/cm^3)}{8.27\ \mu m} = \frac{\sqrt{2.04}}{\sqrt{2.41}}$$

giving 7.61 μm for the D_{50} of cyclone 1 for a temperature of 700°F, a particle density of 2.41 g/cm^3, and a flowrate of 1 ft^3/min. Finally, equation (3) becomes

$$\frac{D_{50}(2.41\ g/cm^3,\ 700°F,\ 1.2\ ft^3/min}{7.61\ \mu m} = \frac{(34.55)^{-.63}}{(28.32)^{-.63}}$$

giving 6.78 μm for the D_{50} of cyclone 1 for a temperature of 700°F, a particle density of 2.41 g/cm^3, and a flowrate of 1.2 ft^3/min. The D_{50}'s for cyclone 2 and 3 are calculated exactly like the D_{50}'s for cyclone 1 but using the appropriate curve from Figure 1-13 and using n = -.70 for cyclone 2 and n = -.84 for cyclone 3.

Cyclones 4 and 5 were calibrated at only one temperature because of experimental limitations. However, the D_{50}-viscosity dependence was assumed to be linear for both of them. From the D_{50}-viscosity curves for cyclones 2 and 3 it was noticed that the D_{50}'s at 400°F were approximately twice those at 77°F. Cyclones 4 and 5 were assumed to have similar behavior, that is, that their D_{50}'s at a temperature of 400°F would be twice those at 77°F.

The D_{50}'s of cyclones 4 and 5 were estimated for a particle density of 2.04 g/cm^3, as follows:

$$\frac{D_{50}(77°F,\ 2.04\ g/cm^3,\ 1\ ft^3/min)}{D_{50}(77°F,\ 1.05\ g/cm^3,\ 1\ ft^3/min)} = \frac{1.05}{2.04}$$

From Table 1-5 (Table 3, p. 36, EPA report #EPA-600/7/78-008), for cyclone 4, the D_{50} is 0.64 μm at 1.05 g/cm^3 and 0.46 μm at 2.04 g/cm^3.

For cyclone 5, the D_{50} is 0.32 μm at 1.05 g/cm^3 and 0.23 μm at 2.04 g/cm^3.

Therefore, the D_{50} of cyclone 4 is 0.46 μm at 77°F, 2.04 g/cm^3, and 1 ft^3/min and 0.92 μm (2x0.46) at 400°F, 2.04 g/cm^3, and 1 ft^3/min. These points were plotted on the grid in Figure 1-13 and a line was drawn through them and extrapolated to 700°F. Likewise, the D_{50} of cyclone 5 is 0.23 μm at 77°F, 2.04 g/cm^3, and 1 ft^3/min, and 0.46 μm (2x0.23) at 400°F, 2.04 g/cm^3, and 1 ft^3/min. These points were plotted on the grid in Figure 1-13 and a line was drawn through them and extrapolated to 700°F. After the D_{50}-viscosity curves for cyclones 4 and 5 were plotted, the same procedure for estimating the D_{50}'s of cyclones 1, 2, and 3 could be utilized. Table 1-6 shows the D_{50}'s of each of the cyclones at each step of the procedure for all three runs.

Secondary Voltage-Current Measurements

Calibrated voltage divider resistor assemblies were attached to the high voltage bus-bar of each transformer rectifier which powered chambers 7 and 8 of the Unit #3 precipitator. Secondary voltage vs. current curves were obtained for each TR beginning with the "C" or 6th field and progressing to the "H" or 1st field.

The correct secondary voltage was obtained by multiplying the correction factor of the voltage divider times the reading of the volt-Ohm-meter.

TABLE 1-5

LABORATORY CALIBRATION OF THE FIVE-STAGE CYCLONES
D_{50} Cut Points

Cyclone		I		II		III			IV		V	
Particle Density (gm/cm^3)		2.04	1.00	2.04	1.00	2.04	1.35	1.00	1.05	1.00	1.05	1.00
Flow ℓ/min	Temperature °C	Cyclone D_{50} cut points micrometers										
7.1	25								2.5	(2.5)	1.5	(1.5)
14.2	25	5.9	(8.4)	2.4	(3.5)	(1.7)	2.1	(2.4)	1.5	(1.5)	.85	(.87)
28.3	25	3.8	(5.4)	1.5	(2.1)	.95	-	(1.4)	.64	(.65)	.32	(.32)
28.3	93	4.4	(6.3)	2.3	(3.3)	1.2	-	(1.8)				
28.3	204	6.4	(9.1)	2.9	(4.1)	1.9	-	(2.8)				

D_{50} cut points enclosed in parentheses are derived from the experimental data using Stoke's law.

TABLE 1-6

STEPS IN PROCEDURE USED TO ESTIMATE CYCLONE D_{50}'s
FOR TESTS AT
NAVAJO GENERATING STATION, PAGE, ARIZONA

Run Number	Cyclone	At Calibration Conditions 1 cfm 400°F 2.04 g/cm³	At Adjusted Temperature 1 cfm, 2.04 g/cm³ °F	At Adjusted Temperature 1 cfm, 2.04 g/cm³ D_{50}	At Adjusted Density 1 cfm, 2.41 g/cm³ D_{50}	At Adjusted Flowrate 2.41 g/cm³ cfm	At Adjusted Flowrate 2.41 g/cm³ D_{50}
CYC 3	I	6.39	685	8.18	7.53	1.07	7.2
	II	2.89	685	3.95	3.64	1.07	3.5
	III	1.94	685	2.62	2.41	1.07	2.3
	IV	.46	685	1.41	1.30	1.07	1.2
	V	.23	685	.58	.534	1.07	.50
CYC 5	I	6.39	630	7.83	7.20	1.1	6.8
	II	2.89	630	3.78	3.47	1.1	3.2
	III	1.94	630	2.49	2.29	1.1	2.1
	IV	.46	630	1.16	1.07	1.1	.96
	V	.23	630	.56	.515	1.1	.46
CYC 7	I	6.39	700	8.27	7.61	1.2	6.8
	II	2.89	700	4.00	3.68	1.2	3.2
	III	1.94	700	2.66	2.44	1.2	2.1
	IV	.46	700	1.24	1.14	1.2	.96
	V	.23	700	.59	.543	1.2	.45

APPENDIX 2

IMPACTOR SUBSTRATE WEIGHT CHANGES FOR BLANK RUNS

Table 2-1

Inlet Blanks Navajo Generating Station

Run Number Date	NGSI-3 7/12/7	NGSI-5 7/13/77	NGSI-10 7/14/77	NGSI-14 7/15/77	NGSI-18 7/16/77	NGSI-22 7/18/77	NGSI-26 7/19/77	NGSI-29 7/20/77	NGSI-33 7/21/77	NGSI-52 8/2/77	NGSI-55 8/3/77	NGSI-60 8/4/77
S0 (mg)	0.32*	0.05*	0.07	0.08	0.11*	0.04	-0.03*	0.02	0.92*	0.03	0.06*	-0.02
S1 (mg)	0.13*	0.02*	0.10	0.10*	0.08*	0.03	-0.05*	0.05	-0.13*	0.00	0.11*	0.00
S2 (mg)	0.10*	0.04*	0.06	0.08*	0.10*	0 06	0.01*	0.03	-0.69*	0.00	0.07*	0.00
S3 (mg)	0.11*	1.03*	0.06	0.10	0.23	0.04	-0.05*	0.07	0.06	0.00	0.10*	0.00
S4 (mg)	0.13*	0.30*	0.06	0.09	0.09	0.03	-0.07*	0.13	0.06	0.00	0.18*	-0.04*
S5 (mg)	0.08*	0.01*	0.07	0.15*	0.09	0.01	-0.05*	0.03*	0.01	0.00	0.49*	-0.04*
S6 (mg)	0.07*	-	-	-	-	-	-	-	-		0.06*	-0.03*
SF (mg)	0.09*	0.02*	0.09	0.15	0.15	0.08	0.23*	0.13	0.09	0.10	0.15*	0.14

i *not used in average because of copper chips or particulate detected on stage when impactor was unloaded, or test for outlier excluded stage weight.

ii. S0-S6 average together for all Brink stage runs in a test series

iii. SF average together for all Brink back-up filters in a test series

Table 2-2

Outlet Blanks Navajo Generating Station

Run Number	NGSO-3B	NGSO-4B	NGSO-11B	NGSO-14B	NGSO-20B	NGSO-28B	NGSO-33B	NGSO-36B	NGSO-40B	NGSO-54	NGSO-55	NGSO-58
Date	7/12/77	7/13/77	7/14/77	7/15/77	7/16/77	7/18/77	7/19/77	7/20/77	7/21/77	8/2/77	8/3/77	8/4/77
Nozzle (mg)	2.67	3.97	1.95	2.39	1.35	0.42	0.33	0.30	1.06	11.35	9.12	10.97
S1 (mg)	-0.26	-0.13	0.00	-0.26	0.15	-0.08	-0.84*	0.40*	-0.44	0.11*	0.41	0.25
S2 (mg)	-0.13	-0.25	-0.03	-0.15	0.06	0.33*	-1.11*	-0.49	-0.20	0.03*	0.56	0.17
S3 (mg)	0.03	0.07	-0.09	0.38*	0.04	0.04	-0.22	0.11	-0.23	0.04*	0.19	0.08
S4 (mg)	-0.32	-0.31	-0.12	-0.10	-0.07	0.12	-1.46*	-0.46	0.03	0.04*	0.25	0.72
S5 (mg)	-0.30	-0.08	0.00	-0.11	-0.02	0.01	-^ 36	-0.13	-0.47	0.06*	0.32	0.06
S6 (mg)	-0.56*	0.03	-0.06	-0.20	-0.10	0.33*	-0.88*	-0.29	-0.15	-0.06*	0.07	0.61
S7 (mg)	-0.06	-0.03	-0.06	0.18	-0.03	0.04	-0.60*	-0.36	-0.51*	0.04*	0.13	0.22
S8 (mg)	-0.22	-0.22	-0.09	-0.06	-0.10	0.34*	-0.30	-0.36	-0.74*	-0.10*	0.27	0.77
SF (mg)	0.46	-0.07	0.24	0.01	0.24	0.03	-0.02	2.55*	0.19	0.06	0.21	0.13

i. *not used in average because of filter being torn, particulate matter on stage, or outlier test excluded stage weight.
ii. nozzle average together for all runs in a test series
iii. S1-S8 average together for all runs in a test series
iv. SF average together for all runs in a test series
v. S1 correction factor is $S1_{real} \pm S1_{blank} \pm Nozzle_{real} \pm Nozzle_{blank}$

APPENDIX 3

VOLTAGE - CURRENT DATA

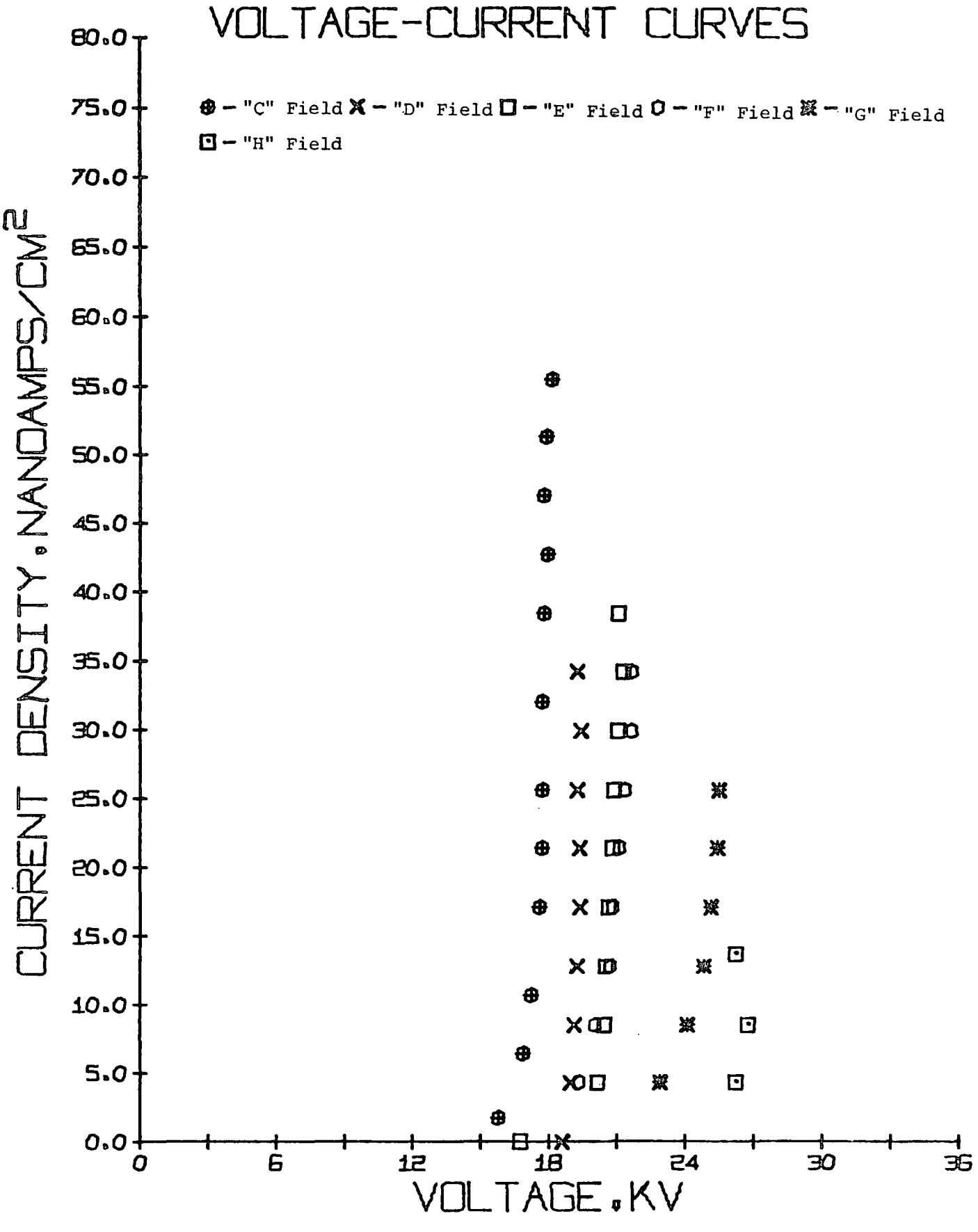

All Fields July 13-14, 1977

VOLTAGE-CURRENT CURVES

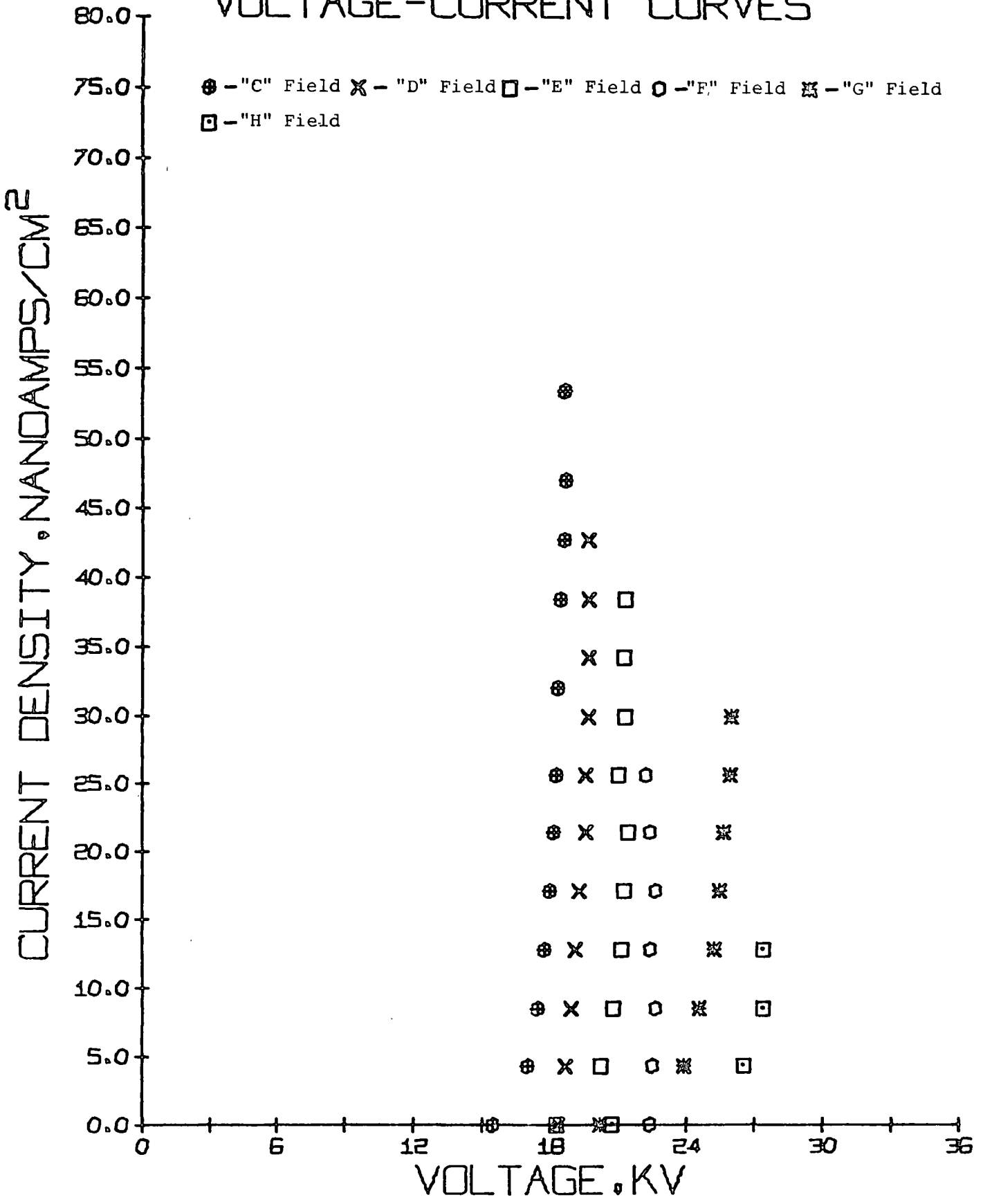

July 14-15, 1977

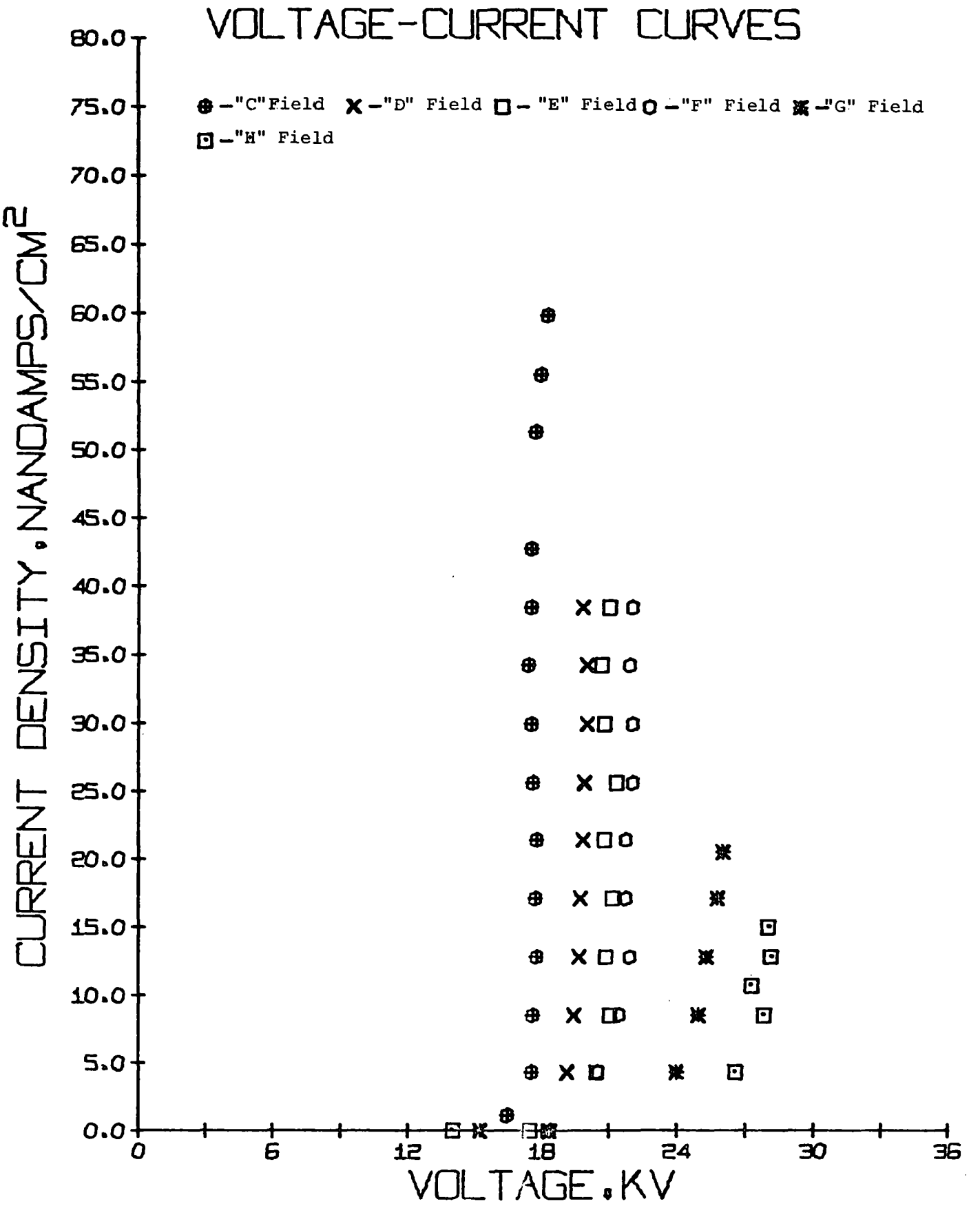

July 15-16, 1977

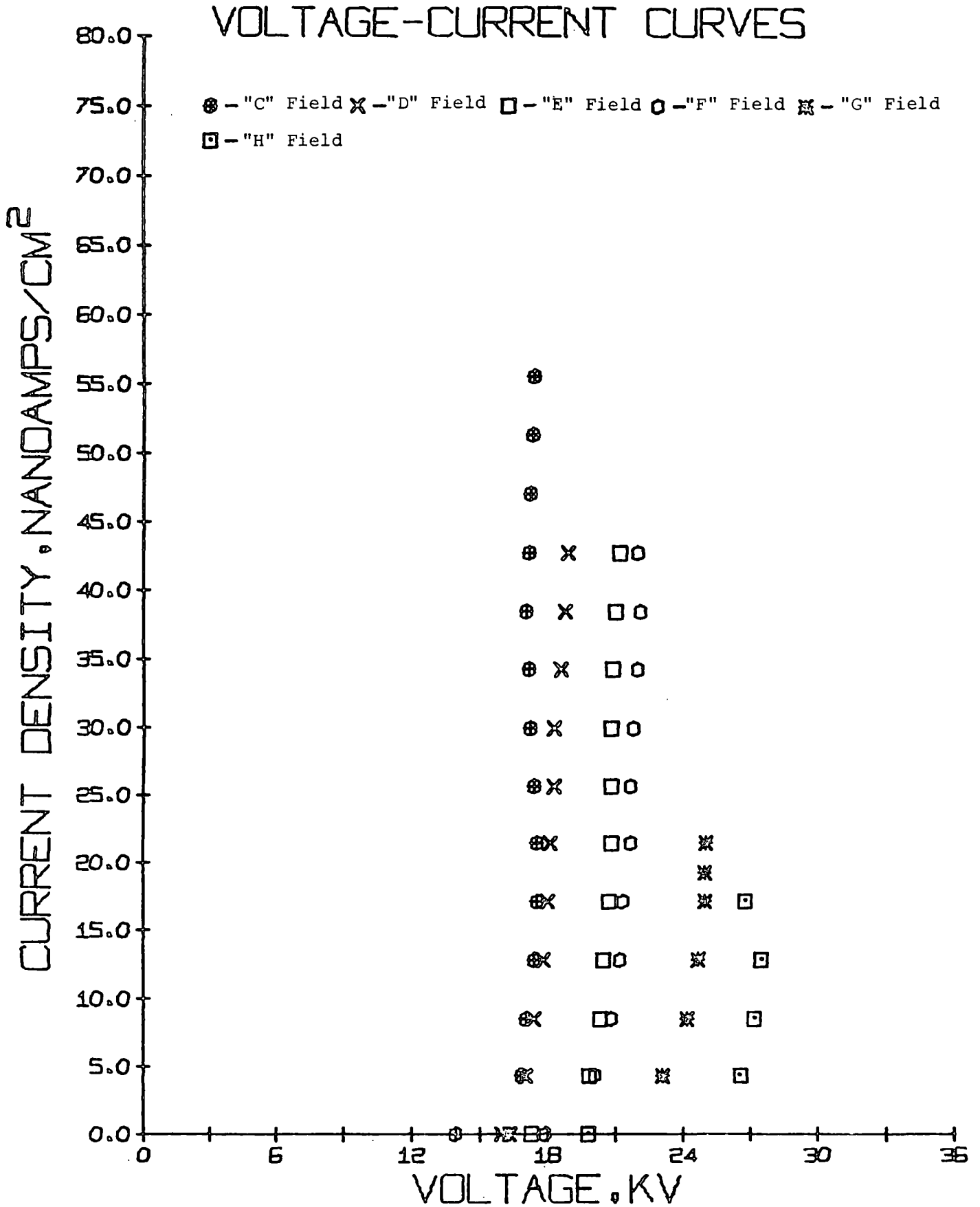

July 16-17, 1977

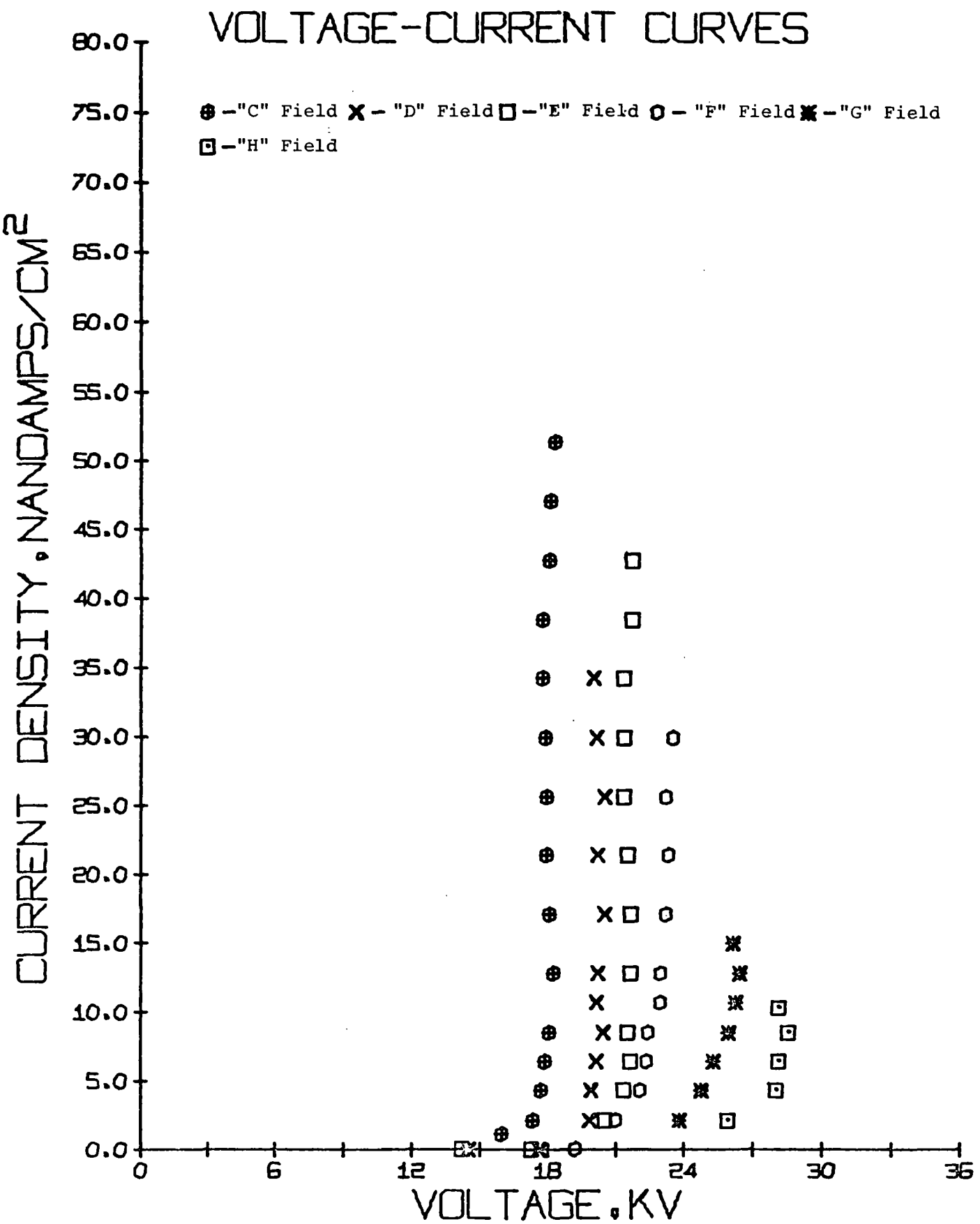

July 21-22, 1977

Panel meter readings obtained for voltage-current curves
and corrected secondary voltages as measured with voltage dividers

Chambers 7 & 8, 7/14/77, 'H' Field

Primary Voltage	Primary Current	Spark Rate	Secondary Voltage	Secondary Current	Corrected Secondary Voltage	Current Density
V	A	Sparks/ min	KV	MA	KV	nA/ cm^2
158	25	25	28	100	26.2	4.3
170	50	150	29	200	26.8	8.5
180	75	320	29	300	26.2	13.7

Chambers 7 & 8, 7/14/77, 'G' Field

140	20	--	24	100	22.9	4.3
162	48	--	25.2	200	24.1	8.5
175	65	25	26	300	24.9	12.8
180	84	75	26.5	400	25.1	17.1
190	110	200	26.8	500	25.4	21.4
195	125	350	26.5	600	25.5	25.6

Chambers 7 & 8, 7/14/77, 'F' Field

130	20	--	20.2	100	19.3	4.3
140	50	--	21.2	200	20.0	8.5
152	68	--	21.8	300	20.7	12.8
165	85	--	22	400	20.8	17.1
172	105	--	22.5	500	21.1	21.4
180	125	25	22.5	600	21.4	25.6
185	145	250	23	700	21.7	29.9
190	160	350	23	800	21.7	34.2

Panel meter readings obtained for voltage-current curves and corrected secondary voltages as measured with voltage dividers

Chambers 7 & 8, 7/14/77, 'E' Field

Primary Voltage	Primary Current	Spark Rate	Secondary Voltage	Secondary Current	Corrected Secondary Voltage	Current Density
V	A	Sparks/ min	KV	MA	KV	nA/ cm^2
85	--	--	19	--	16.7	--
130	20	--	22.5	100	20.2	4.3
140	50	--	23	200	20.4	8.5
150	67	--	23.5	300	20.5	12.8
155	80	--	23.5	400	20.6	17.1
157	105	--	23.5	500	20.8	21.4
170	125	--	24	600	20.9	25.6
175	140	--	24	700	21.1	29.9
185	160	100	24	800	21.3	34.2
185	175	200	24	900	21.1	38.4

Chambers 7 & 8, 7/14/77, 'D' Field

110	20	--	20.3	--	18.6	--
135	65	--	20.7	100	19.0	4.3
140	95	--	21	200	19.2	8.5
148	112	--	21.5	300	19.3	12.8
150	133	--	21.3	400	19.4	17.1
154	150	25	21.4	500	19.4	21.4
160	167	50	21	600	19.3	25.6
165	185	300	21.5	700	19.5	29.9
170	200	50	21.5	800	19.3	34.2

Panel meter readings obtained for voltage-current curves and corrected secondary voltages as measured with voltage dividers

Chambers 7 & 8, 7/14/77, 'C' Field

Primary Voltage	Primary Current	Spark Rate	Secondary Voltage	Secondary Current	Corrected Secondary Voltage	Current Density
V	A	Sparks/ min	KV	MA	KV	nA/ cm^2
100	--	--	18.4	40	15.8	1.7
110	20	--	19.7	150	16.9	6.4
115	55	--	20	250	17.2	10.7
135	87	--	20.2	400	17.6	17.1
140	110	--	20.4	500	17.7	21.4
145	128	--	20.5	600	17.7	25.6
150	157	--	20.5	750	17.7	32.0
155	183	--	20.7	900	17.8	38.4
160	195	50	20.8	1000	18.0	42.7
164	210	100	20.6	1100	17.8	47.0
165	228	100	21	1200	17.9	51.3
175	250	250	21.5	1300	18.1	55.5

Panel meter readings obtained for voltage-current curves and corrected secondary voltages as measured with voltage dividers

Chambers 7 & 8, 7/15/77, 'H' Field

Primary Voltage	Primary Current	Spark Rate	Secondary Voltage	Secondary Current	Corrected Secondary Voltage	Current Density
V	A	Sparks/ min	KV	MA	KV	nA/ cm^2
100	--	--	21.5	--	20.8	--
160	25	--	28.5	100	26.6	4.3
175	50	100	29.5	200	27.4	8.5
185	70	250	30	300	27.4	12.8

Chambers 7 & 8, 7/15/77, 'G' Field

100	--	--	21	--	20.2	--
150	25	--	25	100	23.9	4.3
160	45	--	26	200	24.6	8.5
175	65	--	26.5	300	25.2	12.8
185	85	--	27	400	25.5	17.1
195	105	--	27.5	500	25.7	21.4
200	125	200	27.5	600	26.0	25.6
205	140	300	28	700	26.1	29.9

Chambers 7 & 8, 7/15/77, 'F' Field

75	--	--	18	--	22.5	--
150	20	--	25	100	22.6	4.3
165	40	--	26	200	22.7	8.5
175	62	25	26.4	300	22.5	12.8
185	80	125	26.8	400	22.7	17.1
200	105	200	27.5	500	22.5	21.4
200	125	200	27	600	22.3	25.6

Panel meter readings obtained for voltage-current curves and corrected secondary voltages as measured with voltage dividers

Chambers 7 & 8, 7/15/77, 'E' Field

Primary Voltage	Primary Current	Spark Rate	Secondary Voltage	Secondary Current	Corrected Secondary Voltage	Current Density
V	A	Sparks/min	KV	MA	KV	nA/cm^2
100	--	--	20	--	18.3	--
130	25	--	23	100	20.3	4.3
145	50	--	23.5	200	20.8	8.5
150	70	--	24	300	21.2	12.8
155	80	--	24	400	21.3	17.1
165	105	--	24.5	500	21.5	21.4
168	120	25	24	600	21.1	25.6
175	135	--	24	700	21.4	29.9
178	160	50	24.5	800	21.3	34.2
185	175	250	25	900	21.4	38.4

Chambers 7 & 8, 7/15/77, 'D' Field

127	50	--	20.2	--	18.3	--
137	72	--	20.6	100	18.7	4.3
142	92	--	21	200	18.9	8.5
148	113	--	21.3	300	19.1	12.8
150	132	--	21.5	400	19.3	17.1
155	148	25	21.7	500	19.6	21.4
160	165	--	21.5	600	19.6	25.6
166	185	100	22	700	19.7	29.9
170	200	200	21.7	800	19.7	34.2
174	220	150	22	900	19.7	38.4
175	232	150	21.7	1000	19.7	42.7

Panel meter readings obtained for voltage-current curves and corrected secondary voltages as measured with voltage dividers

Chambers 7 & 8, 7/15/77, 'C' Field

Primary Voltage	Primary Current	Spark Rate	Secondary Voltage	Secondary Current	Corrected Secondary Voltage	Current Density
V	A	Sparks/ min	KV	MA	KV	nA/ cm^2
100	--	--	18	--	15.4	--
120	--	--	20	100	17.0	4.3
130	45	--	20.5	200	17.4	8.5
140	70	--	20.6	300	17.7	12.8
145	90	--	21.2	400	18.0	17.1
148	108	--	21.2	500	18.1	21.4
153	130	--	21.3	600	18.2	25.6
160	158	20	21.5	750	18.3	32.0
165	184	30	21.5	900	18.4	38.4
170	200	40	21.6	1000	18.6	42.7
173	210	100	21.8	1100	18.7	47.0
177	235	250	22	1250	18.6	53.4

Panel meter readings obtained for voltage-current curves and corrected secondary voltages as measured with voltage dividers

Chambers 7 & 8, 7/16/77, 'H' Field

Primary Voltage	Primary Current	Spark Rate	Secondary Voltage	Secondary Current	Corrected Secondary Voltage	Current Density
V	A	Sparks/ min	KV	MA	KV	nA/ cm^2
20	--	--	15	--	14.0	--
160	20	--	28.5	100	26.6	4.3
172	50	50	29.5	200	27.8	8.5
180	59	25	29.7	250	27.3	10.7
185	70	150	30	300	28.1	12.8
190	85	175	31	350	28.0	15.0

Chambers 7 & 8, 7/16/77, 'G' Field

50	--	--	15	--	15.3	--
150	20	--	25	100	24.0	4.3
165	40	25	26.4	200	25.0	8.5
178	67	--	26.5	300	25.3	12.8
185	85	150	27.5	400	25.8	17.1
190	100	250	27.4	480	26.1	20.5

Panel meter readings obtained for voltage-current curves and corrected secondary voltages as measured with voltage dividers

Chambers 7 & 8, 7/16/77, 'F' Field

Primary Voltage	Primary Current	Spark Rate	Secondary Voltage	Secondary Current	Corrected Secondary Voltage	Current Density
V	A	Sparks/ min	KV	MA	KV	nA/ cm^2
117	20	--	19.5	--	18.3	--
140	25	--	22	100	20.5	4.3
155	50	--	22.8	200	21.5	8.5
165	70	--	23	300	22.0	12.8
170	88	25	23.2	400	21.8	17.1
175	107	--	23	500	21.8	21.4
185	128	75	23.4	600	22.1	25.6
190	140	100	23	700	22.1	29.9
195	160	150	23.3	800	22.0	34.2
200	175	250	23.5	900	22.1	38.4

Chambers 7 & 8, 7/16/77, 'E' Field

90	--	--	20	--	17.5	--
130	25	--	23	100	20.4	4.3
145	50	--	23.8	200	21.1	8.5
150	65	--	24	300	20.9	12.8
160	80	--	24.5	400	21.2	17.1
165	110	25	24	500	20.8	21.4
178	125	50	24	600	21.4	25.6
175	140	50	24	700	20.8	29.9
178	155	100	24	800	20.7	34.2
180	175	300	24	900	21.1	38.4

Panel meter readings obtained for voltage-current curves and corrected secondary voltages as measured with voltage dividers

Chambers 7 & 8, 7/16/77, 'D' Field

Primary Voltage	Primary Current	Spark Rate	Secondary Voltage	Secondary Current	Corrected Secondary Voltage	Current Density
V	A	Sparks/ min	KV	MA	KV	nA/ cm^2
130	50	--	20.5	--	18.4	--
90	72	--	21.2	100	19.2	4.3
145	95	--	21.6	200	19.5	8.5
150	110	--	22	300	19.6	12.8
153	132	20	22.2	300	19.8	17.1
158	150	50	22.3	500	19.8	21.4
163	168	100	22	600	19.9	25.6
165	185	100	22.2	700	20.0	29.9
172	205	150	22.5	800	20.0	34.2
172	218	250	22.5	900	19.8	38.4

Chambers 7 & 8, 7/16/77, 'C' Field

110	--	--	19	25	16.4	1.1
122	20	--	20.4	100	17.5	4.3
130	40	--	20.5	200	17.6	8.5
140	78	--	20.8	300	17.8	12.8
144	88	--	20.8	400	17.7	17.1
148	108	--	21	500	17.8	21.4
152	128	--	21	600	17.6	25.6
154	148	--	21	700	17.5	29.9
157	163	--	20.5	800	17.4	34.2
162	183	--	20.5	900	17.5	38.4
162	195	--	20.5	1000	17.5	42.7
170	225	--	21	1200	17.7	51.3
172	240	100	21.5	1300	18.0	55.5
180	255	50-250	21.7	1400	18.3	59.8

Panel meter readings obtained for voltage-current curves and corrected secondary voltages as measured with voltage dividers

Chambers 7 & 8, 7/17/77, 'H' Field

Primary Voltage	Primary Current	Spark Rate	Secondary Voltage	Secondary Current	Corrected Secondary Voltage	Current Density
V	A	Sparks/ min	KV	MA	KV	nA/ cm^2
100	--	--	21	--	19.8	--
160	25	--	29	100	26.6	4.3
172	50	50	29.5	200	27.2	8.5
190	70	100	30.4	300	27.5	12.8
195	100	300	30	400	26.8	17.1

Chambers 7 & 8, 7/17/77, 'G' Field

50	--	--	17	--	16.3	--
145	20	--	24.5	100	23.1	4.3
160	50	--	25.3	200	24.2	8.5
170	65	50	26	300	24.7	12.8
180	85	100	26.5	400	25.0	17.1
185	95	150	26.5	450	25.0	19.2
190	110	200	27	500	25.0	21.4

Panel meter readings obtained for voltage-current curves and corrected secondary voltages as measured with voltage dividers

Chambers 7 & 8, 7/17/77, 'F' Field

Primary Voltage	Primary Current	Spark Rate	Secondary Voltage	Secondary Current	Corrected Secondary Voltage	Current Density
V	A	Sparks/ min	KV	MA	KV	nA/ cm^2
105	--	--	19.5	--	17.9	--
135	20	--	21.5	100	20.1	4.3
150	50	--	22.5	200	20.8	8.5
160	70	--	22.6	300	21.2	12.8
165	75	--	22.8	400	21.3	17.1
175	108	--	23	500	21.7	21.4
180	123	25	23.5	600	21.7	25.6
188	140	--	23	700	21.8	29.9
196	157	100	23.5	800	22.0	34.2
200	170	150	23.5	900	22.1	38.4
205	180	300	24	1000	22.0	42.7

Chambers 7 & 8, 7/17/77, 'E' Field

100	--	--	20	--	17.3
130	20	--	23	100	19.9
140	48	20	23.8	200	20.3
150	70	--	23.9	300	20.4
160	80	--	24	400	20.7
165	105	--	24	500	20.8
170	125	25	24	600	20.8
175	145	50	24	700	20.8
180	155	100	24.5	800	20.9
165	175	250	25	900	21.0
190	180		25	1000	21.2

Panel meter readings obtained for voltage-current curves and corrected secondary voltages as measured with voltage dividers

Chambers 7 & 8, 7/17/77, 'D' Field

Primary Voltage	Primary Current	Spark Rate	Secondary Voltage	Secondary Current	Corrected Secondary Voltage	Current Density
V	A	Sparks/ min	KV	MA	KV	nA/ cm^2
120	20	--	20	--	16.0	--
138	75	--	21.4	100	17.0	43.
145	95	--	21.8	200	17.4	8.5
150	115	--	22	300	17.8	12.8
152	132	--	22.3	400	18.0	17.1
157	150	25	22.2	500	18.1	21.4
162	167	--	22	600	18.3	25.6
163	182	--	21.8	700	18.3	29.9
170	200	50	22.2	800	18.6	34.2
173	218	100	22.5	900	18.8	38.4
175	228	0-500	22	1000	18.9	42.7

Chambers 7 & 8, 7/17/77, 'C' Field

65	--	--	--	--	13.9	--
125	20	--	20	100	16.9	4.3
132	50	--	20.4	200	17.1	8.5
135	70	--	20.8	300	17.4	12.8
140	88	--	21	400	17.5	17.1
145	110	--	21	500	17.5	21.4
148	128	--	20.8	600	17.4	25.6
153	148	--	20.7	700	17.2	29.9
155	165	--	20.5	800	17.2	34.2
158	182	--	20.4	900	17.1	38.4
164	200	--	20.6	1000	17.2	42.7
166	215	--	20.6	1100	17.2	47.0
170	228	--	21	1200	17.3	51.3
170	245	200	21	1300	17.4	55.5

Panel meter readings obtained for voltage-current curves and corrected secondary voltages as measured with voltage dividers

Chambers 7 & 8, 7/22/77, 'H' Field

Primary Voltage	Primary Current	Spark Rate	Secondary Voltage	Secondary Current	Corrected Secondary Voltage	Current Density
V	A	Sparks/ min	KV	MA	KV	nA/ cm^2
50	--	--	16	--	14.2	--
148	20	--	28.5	50	25.9	2.1
165	25	--	30.3	100	28.0	4.3
175	40	--	30.5	150	28.1	6.4
180	50	20-50	31	200	28.6	8.5
184	57	100-250	31.5	240	28.1	10.3

Chambers 7 & 8, 7/22/77. 'G' Field

50	--	--	16	--	14.5	--
140	10	--	25.2	50	23.8	2.1
155	25	--	26.3	100	24.8	4.3
165	28	--	27	150	25.3	6.4
172	48	20-50	27.5	200	26.0	8.5
179	55	30-75	28	250	26.3	10.7
190	70	250	28.5	300	26.4	12.8
190	73	200-400	28.5	350	26.2	15.0

Panel meter readings obtained for voltage-current curves and corrected secondary voltages as measured with voltage dividers

Chambers 7 & 8, 7/22/78, 'F' Field

Primary Voltage	Primary Current	Spark Rate	Secondary Voltage	Secondary Current	Corrected Secondary Voltage	Current Density
V	A	Sparks/ min	KV	MA	KV	nA/ cm^2
120	20	--	20	--	19.2	--
133	25	--	22	50	21.0	2.1
145	30	--	23.2	100	22.1	4.3
153	35	--	23.5	150	22.4	6.4
163	50	--	24	200	22.5	8.5
166	58	--	24.3	250	23.0	10.7
170	67	10-25	24.4	300	23.0	12.8
180	87	--	24.5	400	23.2	17.1
189	112	50-150	24.8	500	23.3	21.4
191	125	25-50	24.5	600	23.2	25.6
200	140	100-500	24.5	700	23.5	29.9

Panel meter readings obtained for voltage-current curves and corrected secondary voltages as measured with voltage dividers

Chambers 7 & 8, 7/22/77, 'E' Field

Primary Voltage	Primary Current	Spark Rate	Secondary Voltage	Secondary Current	Corrected Secondary Voltage	Current Density
V	A	Sparks/ min	KV	MA	KV	nA/ cm^2
70	--	--	20	--	17.3	--
125	20	--	23.5	50	20.5	2.1
140	25	--	25	100	21.4	4.3
147	35	--	25	150	21.6	6.4
150	50	--	25	200	21.6	8.5
160	67	--	25.2	300	21.6	12.8
166	87	--	25.3	400	21.6	17.1
170	110	--	25	500	21.6	21.4
175	123	--	25	600	21.4	25.6
180	138	20-50	25	700	21.4	29.9
185	155	50-150	25	800	21.4	34.2
190	170	150-300	25	900	21.7	38.4
195	180	50-350	25	1000	21.7	42.7

Chambers 7 & 8, 7/22/77, 'D' Field

100	10	--	20	--	17.6	--
140	65	--	22.2	50	19.8	2.1
145	75	--	22.5	100	19.9	4.3
148	87	--	22.8	150	20.1	6.4
150	95	--	23	200	20.4	8.5
150	105	--	22.6	250	20.1	10.7
154	115	--	23	300	20.2	12.8
160	132	25-100	23	400	20.5	17.1
165	150	150	22.8	500	20.2	21.4
170	170	200-450	23	600	20.5	25.6
173	185	200-300	22.6	700	20.1	29.9
180	200	450	22.7	800	20.0	34.2

Panel meter readings obtained for voltage-current curves and corrected secondary voltages as measured with voltage dividers

Chambers 7 & 8, 7/22/77, 'C' Field

Primary Voltage	Primary Current	Spark Rate	Secondary Voltage	Secondary Current	Corrected Secondary Voltage	Current Density
V	A	Sparks/ min	KV	MA	KV	nA/ cm^2
100	--	--	18	25	16.0	1.1
120	10	--	21	50	17.3	2.1
128	15	--	21.2	100	17.7	4.3
133	25	--	21.4	150	17.9	6.4
138	50	--	21.5	200	18.0	8.5
142	70	--	21.7	300	18.2	12.8
148	87	--	21.5	400	18.0	17.1
150	108	--	21.5	500	18.0	21.4
155	132	--	21.5	600	18.0	25.6
160	150	10-20	21.4	700	17.9	29.9
162	163	25-30	21.3	800	17.8	34.2
168	185	25-75	21.6	900	17.8	38.4
170	200	25-100	21.5	1000	18.0	42.7
173	214	100	21.6	1100	18.1	47.0
178	230	250-500	22.5	1200	18.3	51.3

Navajo Generating Station
Unit #3
Voltage Current Readings

Date: 8/1-2/77 Time: 03:00

Chambers 1 & 2

FIELD	DC KV	ACV	SPARK	ACA	DCMA
H	31	200	25	65	200
G	30.5	195	40	145	660
F	25.2	205	20	195	1100
E	23	182	10	180	1000
D	22.3	190	60	240	1400
C	22.3	185	35	248	1430

Chambers 3 & 4

FIELD	DC KV	ACV	SPARK	ACA	DCMA
H	31.8	195	50	95	340
G	31	210	75	130	620
F	26.5	200	50	190	1020
E	23.5	190	25	195	1080
D	22	190	35	240	1320
C	20.5	180	20	240	1300

Chambers 5 & 6

FIELD	DC KV	ACV	SPARK	ACA	DCMA
H	30	180	20	50	200
G	30	200	75	65	280
F	27	175	60	70	360
E	25	180	45	95	440
D	22.5	180	25	160	850
C	21.5	170	30	180	910

Chambers 7 & 8

FIELD	DC KV	ACV	SPARK	ACA	DCMA
H	30	190	35	100	360
G	26.5	205	45	140	740
F	22.5	200	20	198	1060
E	23.5	190	20	200	1050
D	21.0	175	15	250	1135
C	21	175	15	250	1400

Chambers 9 & 10

FIELD	DC KV	ACV	SPARK	ACA	DCMA
H	30	190	40	40	180
G	32	220	30	80	400
F	25.5	200	25	180	960
E	24	200	80	165	1020
D	23.5	190	55	245	1475
C	21.5	180	35	250	1575

Chambers 11 & 12

FIELD	DC KV	ACV	SPARK	ACA	DCMA
H	30.5	190	80	35	160
G	31.75	225	65	85	430
F	27	210	40	160	1020
E	25.5	205	10	195	1050
D	22.5	200	20	250	1420
C	21.5	185	10	253	1380

Chambers 13 & 14

FIELD	DC KV	ACV	SPARK	ACA	DCMA
H	31	200	120	40	160
G	33	220	35	70	320
F	27.5	205	35	160	960
E	24.5	200	20	192	980
D	23	190	25	247	1400
C	22.25	183	20	250	1450

Chambers 15 & 16

FIELD	DC KV	ACV	SPARK	ACA	DCMA
H	30.5	200	35	35	180
G	31	220	40	75	340
F	26	200	35	183	920
E	24	190	30	170	900
D	23.5	190	45	248	1425
C	22	165	10	250	1520

Navajo Generating Station
Unit #3
Voltage Current Readings

Date: 8/2-3/77 Time: 23:45

Chambers 1 & 2

FIELD	DC KV	ACV	SPARK	ACA	DCMA
H	33.5	205	45	50	200
G	32	200	20	150	580
F	26.5	210	50	185	1060
E	24	185	10	190	1000
D	23.5	195	25	250	1400
C	23	190	10	247	1425

Chambers 3 & 4

FIELD	DC KV	ACV	SPARK	ACA	DCMA
H	34	195	20	70	250
G	33	210	50	145	530
F	28	205	60	175	940
E	24.5	195	50	180	1100
D	22.5	190	20	242	1350
C	21.5	185	30	240	1350

Chambers 5 & 6

FIELD	DC KV	ACV	SPARK	ACA	DCMA
H	32	185	40	40	140
G	31.5	205	70	60	260
F	27.5	190	60	80	330
E	25	175	30	90	400
D	23	180	40	165	850
C	21.5	180	50	190	1000

Chambers 7 & 8

FIELD	DC KV	ACV	SPARK	ACA	DCMA
H	32.5	190	30	55	240
G	28.5	218	30	130	680
F	23.5	210	50	165	980
E	25	190	25	175	720
D	22.5	178	15	235	1100
C	22	180	40	245	1275

Chambers 9 & 10

FIELD	DC KV	ACV	SPARK	ACA	DCMA
H	32.5	200	50	30	150
G	33.5	220	70	85	410
F	26.5	210	105	175	930
E	25	200	30	180	1030
D	24.5	195	30	250	1500
C	22	180	60	245	1450

Chambers 11 & 12

FIELD	DC KV	ACV	SPARK	ACA	DCMA
H	31.5	195	50	30	140
G	33	225	50	65	340
F	28.5	215	45	135	710
E	27	210	30	150	900
D	24.5	205	30	250	1400
C	22	190	20	250	1350

Chambers 13 & 14

FIELD	DC KV	ACV	SPARK	ACA	DCMA
H	32	200	100	30	140
G	32.5	220	60	45	200
F	30	200	30	140	720
E	26	210	25	175	940
D	24	195	25	240	1350
C	23	190	30	250	1450

Chambers 15 & 16

FIELD	DC KV	ACV	SPARK	ACA	DCMA
H	32.5	200	40	30	130
G	33.5	230	50	70	315
F	27	200	50	170	900
E	25.5	200	30	190	1000
D	24.0	195	10	245	1400
C	22.5	170	15	250	1500

Navajo Generating Station
Unit #3
Voltage Current Readings

Date: 8/2-3/77 Time: 02:00

Chambers 1 & 2

Field	DC KV	ACV	SPARK	ACA	DCMA
H	33.5	205	100	70	360
G	32	200	115	150	560
F	26	200	130	160	960
E	24	180	170	170	900
D	23	190	125	220	1200
C	23	185	200	200	1100

Chambers 3 & 4

Field	DC KV	ACV	SPARK	ACA	DCMA
H	35	210	120	75	260
G	33.5	220	160	100	440
F	27	195	300	140	640
E	24	195	170	180	1000
D	22	190	180	230	1200
C	21	180	200	230	1200

Chambers 5 & 6

FIELD	DC KV	ACV	SPARK	ACA	DCMA
H	32	180	170	40	130
G	32	200	165	60	250
F	29	200	190	90	420
E	26	180	215	100	450
D	23	180	160	170	900
C	22	180	150	190	1000

Chambers 7 & 8

FIELD	DC KV	ACV	SPARK	ACA	DCMA
H	33	200	100	65	300
G	29	220	210	150	740
F	24	210	180	185	980
E	25.5	200	130	210	1120
D	33	180	300	240	1000
C	22	185	45	250	1400

Chambers 9 & 10

FIELD	DC KV	ACV	SPARK	ACA	DCMA
H	32.5	200	130	40	200
G	34.5	230	150	100	440
F	26	210	220	170	900
E	25	210	140	170	1000
D	24	200	120	235	1500
C	22	180	170	255	1550

Chambers 11 & 12

FIELD	DC KV	ACV	SPARK	ACA	DCMA
H	32	200	130	40	140
G	34	240	125	100	500
F	29	220	160	170	940
E	27	210	80	190	1020
D	23	205	40	250	1400
C	22	190	20	250	1380

*Chambers 13 & 14

FIELD	DC KV	ACV	SPARK	ACA	DCMA
H	32	205	150	50	160
G	35	235	120	75	360
F	30	220	140	160	860
E	26	210	90	195	1030
D	24	190	140	230	1300
C	23	190	40	250	1450

Chambers 15 & 16

FIELD	DC KV	ACV	SPARK	ACA	DCMA
H	31.5	200	80	40	140
G	33.5	230	80	110	440
F	27	205	55	190	1060
E	25	180	210	150	840
D	24	200	50	250	1400
C	22.5	170	30	250	1500

*13 & 14 - Main heaters out

Navajo Generating Station
Unit #3
Voltage Current Readings

Date: 8/2-3/77 Time: ∿04:00

Chambers 1 & 2

FIELD	DC KV	ACV	SPARK	ACA	DCMA
H	33	215	100	90	400
G	32	210	90	145	720
F	26	210	80	200	1100
E	23.5	185	140	190	1000
D	23	190	220	240	1400
C	23	190	100	250	1450

Chambers 3 & 4

FIELD	DC KV	ACV	SPARK	ACA	DCMA
H	35	215	145	80	300
G	33.5	220	120	145	740
F	27	205	140	190	1000
E	24	195	100	200	1100
D	22	190	110	240	1350
C	21	185	140	240	1300

Chambers 5 & 6

FIELD	DC KV	ACV	SPARK	ACA	DCMA
H	31	180	110	45	180
G	31	205	200	60	260
F	28	195	220	110	500
E	25	185	190	130	580
D	23	180	125	170	850
C	21.5	180	180	200	1150

Chambers 7 & 8

FIELD	DC KV	ACV	SPARK	ACA	DCMA
H	32	200	150	75	320
G	28	210	210	135	700
F	23	205	110	200	1100
E	25	190	130	200	1020
D	22	170	130	240	1000
C	22	180	80	250	1400

Chambers 9 & 10

FIELD	DC KV	ACV	SPARK	ACA	DCMA
H	32	200	120	50	200
G	34	230	220	100	450
F	22	210	90	195	1000
E	25	210	20	195	1120
D	24	200	100	250	1450
C	22	180	100	250	1550

Chambers 11 & 12

FIELD	DC KV	ACV	SPARK	ACA	DCMA
H	32	200	140	50	180
G	33	230	130	100	500
F	28	220	120	170	1000
E	26	210	50	195	1040
D	23	200	110	250	1450
C	22	190	20	250	1400

Chambers 13 & 14

FIELD	DC KV	ACV	SPARK	ACA	DCMA
H	32	210	180	50	200
G	34	230	170	85	380
F	29	210	130	135	800
E	25	200	70	195	1040
D	24	200	140	250	1400
C	23	190	100	250	1450

Chambers 15 & 16

FIELD	DC KV	ACV	SPARK	ACA	DCMA
H	31.5	210	90	50	200
G	32.5	230	120	115	500
F	27	200	240	175	840
E	25	200	100	190	1000
D	24	195	80	250	1450
C	27.5	170	50	250	1900

Navajo Generating Station
Unit #3
Voltage Current Readings

Date: 8/3-4/77 Time: 23:00

Chambers 1 & 2

FIELD	DC KV	ACV	SPARK	ACA	DCMA
H	35.5	225	110	85	360
G	33.5	215	130	145	620
F	28	220	125	190	1060
E	25	190	155	195	980
D	24.5	210	120	235	1400
C	23.5	195	50	250	1450

Chambers 3 & 4

FIELD	DC KV	ACV	SPARK	ACA	DCMA
H	26.5	175	230	90	400
G	35	230	125	125	570
F	29	215	75	200	1100
E	26	200	80	200	1100
D	23.5	200	140	250	1350
C	22	190	120	240	1350

Chambers 5 & 6

FIELD	DC KV	ACV	SPARK	ACA	DCMA
H	33	200	100	60	200
G	33	225	140	75	340
F	29	210	125	145	740
E	26.5	200	120	165	800
D	24	200	200	235	1300
C	27.5	190	110	240	1300

Chambers 7 & 8

FIELD	DC KV	ACV	SPARK	ACA	DCMA
H	33.5	210	120	105	420
G	30	220	125	150	760
F	25.2	220	50	200	1100
E	26	205	40	205	1120
D	23.5	190	90	250	1150
C	22.5	185	70	250	1400

Chambers 9 & 10

FIELD	DC KV	ACV	SPARK	ACA	DCMA
H	33.5	205	110	40	200
G	35.5	240	170	120	480
F	27	220	150	190	960
E	26.5	220	140	195	1100
D	25	205	120	250	1550
C	22.5	190	180	250	1500

Chambers 11 & 12

FIELD	DC KV	ACV	SPARK	ACA	DCMA
H	33	215	140	40	180
G	35	240	130	120	600
F	30	230	180	175	960
E	27.5	220	130	185	1010
D	24	210	230	240	1400
C	22.2	195	130	250	1400

Chambers 13 & 14

FIELD	DC KV	ACV	SPARK	ACA	DCMA
H	33	215	160	45	200
G	35	240	110	85	480
F	31	230	200	180	1000
E	27	210	110	170	940
D	24.5	200	210	245	1400
C	23	190	100	250	1450

Chambers 15 & 16

FIELD	DC KV	ACV	SPARK	ACA	DCMA
H	32.5	210	150	40	180
G	34.5	240	160	90	460
F	28	210	120	185	1020
E	26.5	200	210	185	1000
D	24.5	200	60	240	1400
C	21	260	60	190	1800

Navajo Generating Station
Unit #3
Voltage Current Readings

Date: 8/3-4/77 Time: 03:00

Chambers 1 & 2

FIELD	DC KV	ACV	SPARK	ACA	DCMA
H	34.5	215	110	80	280
G	32.5	210	100	150	740
F	27	215	100	195	1080
E	24.5	195	90	195	1000
D	23.5	200	110	245	1400
C	23.5	190	125	250	1450

Chambers 3 & 4

FIELD	DC KV	ACV	SPARK	ACA	DCMA
H	34.5	220	125	90	380
G	34	225	110	140	640
F	28	205	210	160	1060
E	25	200	180	200	1100
D	22.5	190	130	240	1300
C	21	180	100	240	1350

Chambers 5 & 6

FIELD	DC KV	ACV	SPARK	ACA	DCMA
H	33	200	140	50	220
G	32	210	140	55	280
F	28	200	190	125	600
E	25.5	190	150	145	1020
D	23.5	200	130	205	1200
C	22	190	190	235	1300

Chambers 7 & 8

FIELD	DC KV	ACV	SPARK	ACA	DCMA
H	33	205	110	75	300
G	29	210	190	155	700
F	24.5	215	70	200	1100
E	25	200	120	200	1100
D	23	185	150	250	1150
C	22	180	60	250	1400

Chambers 9 & 10

FIELD	DC KV	ACV	SPARK	ACA	DCMA
H	33	205	90	35	180
G	34.5	235	125	110	460
F	22	215	130	190	980
E	25	205	110	195	1100
D	24	200	180	250	1550
C	22	185	180	250	1550

Chambers 11 & 12

FIELD	DC KV	ACV	SPARK	ACA	DCMA
H	32	210	130	45	240
G	34	250	130	120	580
F	30	220	280	185	1000
E	27	210	90	193	1000
D	23.5	205	220	250	1400
C	22	190	90	250	1350

Chambers 13 & 14

FIELD	DC KV	ACV	SPARK	ACA	DCMA
H	32.5	210	150	40	200
G	36	250	130	100	480
F	30	225	160	190	1000
E	26	210	90	195	1020
D	24	195	160	250	1425
C	23	185	70	250	1450

Chambers 15 & 16

FIELD	DC KV	ACV	SPARK	ACA	DCMA
H	32	210	140	35	180
G	34	240	180	110	460
F	27.5	205	260	185	1020
E	26.5	200	300	190	1040
D	24	200	90	250	1400
C	20.5	250	30	190	1800

Navajo Generating Station
Unit #3
Voltage Current Readings

Date: 8/4-5/77 Time: 23:00

Chambers 1 & 2

FIELD	DC KV	ACV	SPARK	ACA	DCMA
H	34	210	120	60	280
G	32.5	200	200	120	530
F	25.5	200	180	160	640
E	24	180	170	190	920
D	23	190	155	225	1250
C	22.5	185	125	215	1200

Chambers 3 & 4

FIELD	DC KV	ACV	SPARK	ACA	DCMA
H	35	210	150	95	330
G	33.5	210	280	120	500
F	27.5	200	210	150	750
E	24.5	190	280	180	880
D	22	190	220	220	1200
C	20.5	185	180	220	1200

Chambers 5 & 6

FIELD	DC KV	ACV	SPARK	ACA	DCMA
H	33	195	125	42	150
G	33	205	150	47	210
F	28.5	190	190	95	430
E	25.5	180	150	150	560
D	23	190	110	190	900
C	21	175	130	190	1000

Chambers 7 & 8

FIELD	DC KV	ACV	SPARK	ACA	DCMA
H	33	195	130	60	260
G	26.5	150	0	10	80*
F	25	200	120	155	740
E	25	175	110	140	800
D	22	175	175	220	900
C	22	180	120	255	1400

Chambers 9 & 10

FIELD	DC KV	ACV	SPARK	ACA	DCMA
H	31.5	190	120	45	180
G	34	210	230	42	260
F	26.5	205	200	165	880
E	25	200	210	150	800
D	23	185	170	205	1200
C	20.5	170	170	205	1200

Chambers 11 & 12

FIELD	DC KV	ACV	SPARK	ACA	DCMA
H	32	200	155	40	160
G	33	220	130	50	220
F	28	200	140	130	660
E	26.5	200	190	155	1060
D	22	190	190	220	1150
C	20.5	180	150	225	1150

Chambers 13 & 14

FIELD	DC KV	ACV	SPARK	ACA	DCMA
H	32	210	170	40	160
G	33.5	210	170	50	240
F	29.5	200	160	110	560
E	25	200	130	120	860
D	23	190	130	230	1250
C	21.5	180	190	250	1450

Chambers 15 & 16

FIELD	DC KV	ACV	SPARK	ACA	DCMA
H	32	210	120	32	180
G	32.5	220	100	65	300
F	26.5	190	160	145	730
E	25	185	150	135	700
D	23	190	185	235	1300
C	20	250	240	170	1525

* suspected field out

	FIELD	DC KV	ACV	SPARK	ACA	DCMA
back in	G	28.5	200	140	135	580

Navajo Generating Station
Unit #3
Voltage Current Readings

Date: 8/4-5/77 Time: 03:00

Chambers 1 & 2

FIELD	DC KV	ACV	SPARK	ACA	DCMA
H	33	190	130	50	220
G	32	185	130	135	560
F	26	200	150	165	720
E	23	180	130	190	1020
D	22.5	185	160	205	1050
C	22	178	220	200	1100

Chambers 3 & 4

FIELD	DC KV	ACV	SPARK	ACA	DCMA
H	34	200	170	75	260
G	33	200	185	75	360
F	27	190	190	140	700
E	24	175	320	165	800
D	21.5	185	200	210	1100
C	20	170	170	200	1050

Chambers 5 & 6

FIELD	DC KV	ACV	SPARK	ACA	DCMA
H	32	190	160	42	120
G	32	200	170	45	180
F	28	170	170	50	240
E	25	180	190	120	530
D	22.5	170	140	145	750
C	20.5	165	220	180	950

Chambers 7 & 8

FIELD	DC KV	ACV	SPARK	ACA	DCMA
H	31.5	180	170	40	160
G	26	145	0	10	70*
F	23	160	0	50	200
E	24	130	0	0	20*
D	22.5	160	200	135	400
C	21.5	175	200	200	1050

Chambers 9 & 10

FIELD	DC KV	ACV	SPARK	ACA	DCMA
H	32	200	110	45	200
G	33	210	170	50	320
F	27	200	250	145	820
E	25	200	140	160	840
D	23	185	160	200	1150
C	20.5	165	300	210	1200

Chambers 11 & 12

FIELD	DC KV	ACV	SPARK	ACA	DCMA
H	32	205	130	43	200
G	33.5	220	100	55	270
F	28.5	200	110	170	660
E	26.5	205	125	170	840
D	22	190	140	215	1150
C	20.5	180	110		

Chambers 13 & 14

FIELD	DC KV	ACV	SPARK	ACA	DCMA
H	31.5	210	180	40	180
G	35	225	125	55	220
F	29	205	160	125	640
E	25	200	170	175	900
D	23	190	230	230	1300
C	21.5	180	170	250	1500

Chambers 15 & 16

FIELD	DC KV	ACV	SPARK	ACA	DCMA
H	31	205	120	40	180
G	32.5	220	100	55	240
F	26	190	170	150	760
E	25	185	220	150	740
D	22.5	185	200	220	1200
C	20.5	250	330	170	1400

* Fields with electrical problems - E Field operating at near normal at ∿03:30, G Field remained low throughout test.

APPENDIX 4

SIZE-DEPENDENT ELEMENTAL CONCENTRATION DATA

ELEMENTAL CONCENTRATIONS IN MILLIGRAMS/DSCM/CYCLONE

CYCLONE RUN #3 CHAMBER #8, INLET 7/14-15/77

D_{50}, μm	Cyclone #	K	Ca	Ti	Ba	V	Cr	Mn	Fe	Cu
7.2	1	2.10E+01	1.52E+02	2.48E+01	9.44E-01*	2.73E+00	1.78E-01*	3.46E-01	1.28E+02	2.19E-01
3.5	2	9.91E+00	6.07E+01	9.06E+00	5.88E-01*	1.38E+00	1.06E-01*	9.19E-02*	4.78E+01	1.00E-01
2.3	3	3.40E+00	2.17E+01	3.15E+00	2.79E-01*	6.26E-01	4.89E-02*	4.29E-02*	1.72E+01	3.63E-02
1.2	4	2.15E+00	1.26E+01	1.90E+00	2.37E-01*	4.15E-01	1.90E-01	3.68E-02*	1.07E+01	2.62E-02
0.5	5	3.39E-01	2.07E+00	3.79E-01	6.43E-02*	1.11E-01	1.08E-02*	1.51E-02	1.69E+00	7.34E-03

		Zn	As	Pb	Br	Rb	Sr	Zr	Mo
7.2	1	2.97E-01	5.56E-02	8.32E-02	2.23E-02*	2.14E-01	6.37E+00	7.00E-01	1.11E-01*
3.5	2	2.14E-01	2.51E-02	7.41E-02	1.69E-02*	8.05E-02	2.15E+00	1.84E-01	5.27E-02
2.3	3	1.15E-01	3.33E-02	4.77E-02	8.57E-03*	3.03E-02	7.30E-01	5.52E-02	3.94E-02*
1.2	4	1.00E-01	1.02E-02	3.14E-02	7.42E-03*	1.45E-02	3.97E-01	3.92E-02	9.19E-02
0.5	5	1.36E-02	1.61E-03	6.66E-03	2.01E-03*	2.43E-03	7.81E-02	5.12E-03*	9.22E-03*

CYCLONE RUN #5 CHAMBER #8, OUTLET 7/18-19/77

		K	Ca	Ti	Ba	V	Cr	Mn	Fe	Cu
6.8	1	7.01E-02	5.87E-01	7.96E-02	5.93E-03*	1.70E-02	1.04E-03*	8.95E-04*	3.91E-01	9.36E-04
3.2	2	3.88E-02	3.16E-01	4.27E-02	3.40E-03*	9.26E-03	5.87E-04*	5.11E-04*	2.06E-01	3.78E-04
2.1	3	4.34E-02	3.03E-01	4.31E-02	4.46E-03*	1.02E-02	7.36E-04*	6.47E-04*	2.09E-01	7.27E-04
0.96	4	5.11E-02	3.45E-01	5.40E-02	6.40E-03*	1.41E-02	1.46E-03	9.26E-04*	2.55E-01	7.36E-04
0.46	5	7.96E-03	6.22E-02	9.72E-03	1.43E-03*	3.38E-03	2.32E-04*	2.08E-04*	4.16E-02	1.53E-04

		Zn	As	Pb	Br	Rb	Sr	Zr	Mo
6.8	1	2.28E-03	1.06E-04*	1.35E-03	1.65E-04*	5.16E-04	2.04E-02	1.30E-03	7.77E-04*
3.2	2	1.28E-03	6.31E-05*	7.40E-04	1.01E-04*	2.70E-04	1.08E-02	6.23E-04	4.73E-04*
2.1	3	1.49E-03	1.94E-04	6.38E-04	1.41E-04*	3.32E-04	9.98E-03	6.25E-04	6.40E-04*
0.96	4	2.52E-03	2.30E-04	8.42E-04	2.01E-04*	4.04E-04	1.16E-02	8.04E-04	9.40E-04*
0.46	5	4.90E-04	6.80E-05	1.49E-04	4.74E-05*	4.23E-05	2.16E-03	1.20E-04*	2.16E-04*

CYCLONE RUN #7 MAIN INLET 8/3-4/77

		K	Ca	Ti	Ba	V	Cr	Mn	Fe	Cu
6.8	1	1.17E+01	4.83E+01	1.05E+01	3.96E-01*	1.22E+00	7.49E-02*	2.04E-01	5.81E+01	8.03E-02
3.2	2	2.51E+01	8.95E+01	1.90E+01	9.92E-01*	2.36E+00	1.80E-01*	4.11E-01	1.03E+02	1.62E-01
2.1	3	1.01E+01	3.44E+01	7.68E+00	4.53E-01*	8.85E-01	8.23E-02*	1.38E-01	3.95E+01	7.45E-02
0.96	4	5.02E+00	1.64E+01	3.48E+00	3.10E-01*	6.08E-01	5.49E-02*	9.08E-02	1.84E+01	3.90E-02
0.45	5	1.78E+00	5.46E+00	1.33E+00	1.18E-01*	2.26E-01	2.12E-02*	3.37E-02	7.11E+00	1.35E-02

		Zn	As	Pb	Br	Rb	Sr	Zr	Mo
6.8	1	1.02E-01	2.21E-02	4.84E-02	9.61E-03*	1.25E-01	2.51E+00	3.93E-01	4.61E-02*
3.2	2	2.56E-01	8.09E-02	7.11E-02	2.75E-02*	2.66E-01	4.37E+00	5.56E-01	1.22E-01*
2.1	3	1.61E-01	2.39E-02	6.55E-02	1.28E-02*	9.64E-02	1.62E+00	1.58E-01	5.67E-02*
0.96	4	1.09E-01	1.22E-02	4.37E-02	9.39E-03*	4.30E-02	7.02E-01	6.40E-02	4.20E-02*
0.45	5	4.25E-02	8.49E-03	1.63E-02	3.54E-03*	1.85E-02	2.71E-01	2.12E-02	1.59E-02*

*Denotes upper limit of element not found.

ENRICHMENT RATIO/ELEMENT/CYCLONE, NORMALIZED TO Fe

CYCLONE RUN #3 CHAMBER #8, INLET 7/14-15/77

Cyclone #	K	Ca	Ti	Ba	V	Cr	Mn	Fe	Cu
1	0.792	0.934	0.858	0.184*	0.318	0.056*	0.333	1.000	0.500
2	1.000	1.000	0.844	0.316*	0.439	0.111*	0.222*	1.000	0.500
3	0.957	0.995	0.813	0.421*	0.545	0.167*	0.222*	1.000	0.500
4	0.971	0.929	0.791	0.579*	0.591	1.000	0.333*	1.000	0.500
5	0.971	0.968	1.000	1.000*	1.000	0.333*	1.000	1.000	1.000

	Zn	As	Pb	Br	Rb	Sr	Zr	Mo
1	0.222	0.000	0.250	0.000*	1.000	1.000	1.000	0.111*
2	0.444	0.500	0.500	0.000*	1.000	0.900	0.800	0.111
3	0.778	1.000	0.750	0.000*	1.000	0.860	0.600	0.222*
4	1.000	0.500	0.750	1.000*	0.500	0.740	0.800	1.000
5	0.889	0.500	1.000	1.000*	0.500	0.920	0.600*	0.556*

CYCLONE RUN #5 CHAMBER #8, OUTLET 7/18-19/77

	K	Ca	Ti	Ba	V	Cr	Mn	Fe	Cu
1	0.865	0.977	0.872	0.441*	0.531	0.500*	0.400*	1.000	0.500
2	0.671	1.000	0.889	0.500*	0.556	0.500*	0.400*	1.000	0.500
3	1.000	0.942	0.880	0.618*	0.605	0.667*	0.600*	1.000	0.750
4	0.966	0.881	0.906	0.735*	0.691	1.000	0.800*	1.000	0.750
5	0.923	0.973	1.000	1.000*	1.000	1.000*	1.000*	1.000	1.000

	Zn	As	Pb	Br	Rb	Sr	Zr	Mo
1	0.600	0.000*	0.750	0.000*	0.500	0.981	1.000	0.400*
2	0.600	0.000*	1.000	0.000*	0.500	1.000	1.000	0.400*
3	0.700	0.500	0.750	1.000*	1.000	0.906	1.000	0.800*
4	1.000	0.500	0.750	1.000*	1.000	0.868	1.000	1.000*
5	0.200	1.000	1.000	1.000*	0.500	0.981	1.000*	1.000*

CYCLONE RUN #7 MAIN INLET 8/3-4/77

	K	Ca	Ti	Ba	V	Cr	Mn	Fe	Cu
1	0.736	0.934	0.933	0.412*	0.636	0.333*	0.800	1.000	0.500
2	0.890	0.976	0.948	0.588*	0.697	0.667*	0.800	1.000	1.000
3	0.938	0.980	1.000	0.647*	0.667	0.667*	0.600	1.000	1.000
4	1.000	1.000	0.974	1.000*	1.000	1.000*	1.000	1.000	1.000
5	0.916	0.865	0.969	1.000*	0.970	1.000*	1.000	1.000	1.000

	Zn	As	Pb	Br	Rb	Sr	Zr	Mn
1	0.333	0.000	0.500	0.000*	0.667	1.000	1.000	0.500*
2	0.333	1.000	0.500	0.000*	1.000	0.977	0.714	0.500*
3	0.667	1.000	1.000	0.000*	0.667	0.953	0.571	0.500*
4	1.000	1.000	1.000	0.000*	1.000	0.884	0.429	1.000*
5	1.000	1.000	1.000	1.000*	0.667	0.884	0.429	1.000*

*Denotes upper limit of element not found.

TECHNICAL REPORT DATA (Please read Instructions on the reverse before completing)		
1. REPORT NO. EPA-600/7-78-214	2.	3. RECIPIENT'S ACCESSION NO.
4. TITLE AND SUBTITLE Performance and Economic Evaluation of a Hot-side Electrostatic Precipitator		5. REPORT DATE November 1978 6. PERFORMING ORGANIZATION CODE
7. AUTHOR(S) G. H. Marchant Jr. and J. P. Gooch		8. PERFORMING ORGANIZATION REPORT NO. SORI-EAS-78-415 3764-XXIIIDF
9. PERFORMING ORGANIZATION NAME AND ADDRESS Southern Research Institute 2000 Ninth Avenue, South Birmingham, Alabama 35205		10. PROGRAM ELEMENT NO. EHE624 11. CONTRACT/GRANT NO. 68-02-2185
12. SPONSORING AGENCY NAME AND ADDRESS EPA, Office of Research and Development Industrial Environmental Research Laboratory Research Triangle Park, NC 27711		13. TYPE OF REPORT AND PERIOD COVERED Final; 12/76 - 9/78 14. SPONSORING AGENCY CODE EPA/600/13
15. SUPPLEMENTARY NOTES IERL-RTP project officer is Leslie E. Sparks, Mail Drop 61, 919/541-2925.		

16. ABSTRACT The report gives results of measurements--to determine the overall mass and fractional collection efficiency of a hot-side electrostatic precipitator (ESP)--across 1 chamber of a 16-chambered ESP. Measurements of fractional efficiency were conducted across the entire ESP. In situ and laboratory resistivity measurements were performed, and voltage-current characteristics of the power supplies were obtained. An engineering analysis was conducted, including an estimate of the specific collecting area required for a cold-side ESP on the same boiler. Results include: (1) voltage waveforms and secondary voltage-current relationships showed characteristics similar to back-corona although fly ash resistivity was 5 x 10 to the 9th power ohm-cm at 350 C (in situ determination); (2) ESP operation was sensitive to resistivity variation in a resistivity region (2 x 10 to the 10th power to 8 x 10 to the 8th power ohm-cm from laboratory determinations) where no sensitivity was expected; (3) overall mass collection efficiency of an isolated chamber was 99.22% for a specific collection area of 52.6 sq m/(cu m/sec), average secondary voltage was 22 kV, and average secondary current density was 40 nA/sq cm; and (4) the turnkey cost of the ESP system was estimated at $34,940,000 ($44/kW) in 1977 dollars.

17. KEY WORDS AND DOCUMENT ANALYSIS		
a. DESCRIPTORS	b. IDENTIFIERS/OPEN ENDED TERMS	c. COSATI Field/Group
Air Pollution Electrostatic Precipitation Performance Evaluation Cost Analysis Fly Ash	Air Pollution Control Stationary Sources Hot-side ESP	13B 13H 05A 14A 21B
18. DISTRIBUTION STATEMENT Unlimited	19. SECURITY CLASS (This Report) Unclassified 20. SECURITY CLASS (This page) Unclassified	21. NO. OF PAGES 192 22. PRICE

EPA Form 2220-1 (9-73)